



UNIVERSITY OF  
TECHNOLOGY SYDNEY

# **Developing Constitutive Model to Simulate Behaviour of Cement Treated Clay Composite Capturing Effect of Cementation Degradation**

A thesis in fulfilment of the requirement  
for the award of the degree

**Doctor of Philosophy**

from

**University of Technology Sydney (UTS)**

by

**Lam Dinh Nguyen, BEng, BBus, MEng**

School of Civil and Environmental Engineering  
Faculty of Engineering and Information Technology

July 2016

## **CERTIFICATE OF ORIGINAL AUTHORSHIP**

I certify that the work in this thesis has not previously been submitted for a degree nor has it been submitted as part of requirements for a degree except as fully acknowledged within the text.

I also certify that the thesis has been written by me. Any help that I have received in my research work and the preparation of the thesis itself has been acknowledged. In addition, I certify that all information sources and literature used are indicated in the thesis.

---

*Lam Dinh Nguyen*

*Date:*

## DEDICATION

This thesis is deeply dedicated to the following people:

*To my respective parents, Dinh Son Nguyen & Bach Hue T. Nguyen*

For their sacrifices, endless love, hard work and inspiration

*To my wonderful wife, Kim Ngan Huynh*

For her constant love, supports and caring

*To my lovely daughters, Amy & Helen Thien Nguyen*

For bringing joy and hope

## ABSTRACT

Stabilising soft clays with cement has become an effective ground modification method to improve the properties of the soft soils. However, laboratory experiments have shown that the cementation of clay gradually diminishes as the mean effective yield stress increases, due to the degradation of cementation bonds. Furthermore, the shear strength of cement treated clay is influenced by the shear degradation induced by the shear deformation, particularly at the post-peak state where a significant shear deformation and consequently breakage of cementation bonds occur. Moreover, a typical stress-strain relationship shows brittle failure behaviour of the soil treated with cement where the shear strength decreases rapidly after the peak strength state. Hence, in recent years, the inclusion of fibre into soil treated with cement has become increasingly popular to overcome the challenge of the unfavourable brittle behaviour of the cement treated soil. The soil treated with cement and fibre, referred to as the improved soil composite or the fibre reinforced cemented soil (FRCS) shows significant increase in ductility due to the bridging effects provided by the fibre during compression. However, when the accumulation of deviatoric straining becomes very large, the fibre failure due to pull-out or breakage occurs. Hence, an effective constitutive model is required to capture the effect of fibre and its failure mechanism on the behaviour of the fibre reinforced cement treated soil.

In this study, a constitutive model and its extended version were developed to simulate the behaviour of cement treated clay with or without fibre reinforcement, respectively. The proposed models include the formulation of the modified mean effective stress considering the effect of cement and fibre inclusion, together with the cementation degradation and fibre failure due to volumetric and shear deformation. A non-linear failure envelope was also formulated to merge with the Critical State Line (CSL) of the reconstituted soil mixture at high mean effective stresses in order to capture the cementation degradation and ruptured fibres. The special characteristics of the proposed models include a non-associated plastic potential function derived from a modified energy dissipation equation with the parameter  $\alpha$ . When  $\alpha = 0$  is adopted, the proposed models become associated with the yield surface being identical to the plastic potential surface. In addition, a general stress-strain relationship including the hardening and the softening processes to simulate the pre-and-post peak states of the treated clay

was also proposed. When the effects of cement and fibre are absent, together with  $\alpha = 0$ , the proposed models return to the Modified Cam Clay model.

Furthermore, a series of undrained and drained triaxial tests were conducted and the results were reported on the natural Ballina clay treated with different cement contents (i.e. 10%, 12% and 15%) and the artificial Kaolin clay treated with 5% cement under various loading conditions (confining pressures ranging from 50 kPa to 800 kPa) in order to study the effect of cementation and its degradation on the behaviour of the cement treated clay. The performance of the proposed model for the cement treated clay was evaluated by comparing the model predictions with the new experimental results in this study and existing case studies available in the literature. It has been evident that many researchers focus on the addition of fibre into sand, soft clay, and sand treated with cement, whereas the behaviour of soft clay treated with fibre and cement requires further investigations. Therefore, an extensive experimental program was carried out to determine how the fibre and cement contents affect the behaviour of cement treated clay with fibre reinforcement. Numerous triaxial tests were conducted and reported on the cement treated Ballina clay with 0.3% and 0.5% fibre contents while the results for the Kaolin clay treated with 5% cement and differing fibre contents (i.e. 0.1% and 0.5%) under various loading conditions were also included. In addition, the micro-structure of the Ballina clay with or without treatments were analysed using the SEM images for the pre-and-post shearing stages. The experimental results were used for the verification of the extended version of the proposed model for the improved soil composite.

The laboratory results indicated that the combined effects of cementation and fibre reinforcement increase the shear strength and ductility of the treated soft clay. Under triaxial conditions the peak shear strength of soft clay treated with cement and fibre increases dramatically due to the formation of cementation bonds and the bridging effect provided by the fibres, and the brittleness caused by the cementation bonds breaking also improves significantly due to the inclusion of fibre. However, when shearing at a high mean effective yield stress, the cementation bonds break and the fibre ruptures due to the plastic deviatoric strain which caused major cracks to appear within the sample. By capturing the main features of the cement treated clay with or without fibre reinforcement, the proposed model provides reliable predictions that agree well with the experimental results.

## ACKNOWLEDGEMENT

My PhD journey has been quite challenging and frustrating as well as enjoyable and rewarding experiences. During this candidature period, supports and encouragements have never been absence. I would like to take this opportunity to express my sincere thanks and appreciations to those who made this thesis possible.

First of all, I owe my deepest gratitude to my principal supervisor, Dr Behzad Fatahi, and my co-supervisor, A/Prof Hadi Khabbaz for their continuous supports related to the research as well as other aspects in my life, also for their guidance, time, patience, and leadership. Since the start of my study, I have learnt and developed many important skills, including technical and inter-personal, from their ideas, critical review of this thesis, knowledge and motivation which encourage me to overcome many difficulties to achieve this milestone.

Secondly, the supports and guidance from the soil laboratory manager, Mr Antonio Reyno, and other laboratory staff members are greatly appreciated for helping me accomplish the experiments. Also, I would like to thank the science laboratory manager, Katie McBean, for her time and supports in completing the microstructure analysis. Moreover, I would like to show my gratitude to Dr Thu Minh Le and Dr Babak Azari for their valuable advices and contributions. It is a pleasure for me to express my appreciation to many of my colleagues for an enjoyable and friendly working environment.

During my study, the financial supports from the University of Technology Sydney (UTS) and the Faculty of Engineering and Information Technology (FEIT), as well as the Australian Postgraduate Awards (APA) from the Australian Government are immensely acknowledged.

Lastly, I am hugely indebted to my family for their supports, unconditional love and guidance. My parents taught me many aspects of life including the importance of education, integrity and responsibility. My wife and two beautiful daughters are always there to bring love, joy and caring which motivate and encourage me to reach this point. Moreover, I am also grateful to my brother for his time and supports during my study.

# LIST OF PUBLICATIONS

## Published Journal Papers

Nguyen, L.D., Fatahi, B. and Khabbaz, H. 2014. A constitutive model for cemented clays capturing cementation degradation, *International Journal of Plasticity*, 56: 1-18.

Nguyen, L. and Fatahi, B. 2016. Behaviour of clay treated with cement & fibre while capturing cementation degradation and fibre failure–C3F Model. *International Journal of Plasticity*, 81: 168-195.

## Conference Papers

Nguyen, L., Fatahi, B. and Khabbaz, H. 2013. Predicting behaviour of cemented clay considering strength reduction due to high confining pressure. *GeoMontreal 2013*, Canadian Geotechnical Society, Montreal, Canada, pp. 1-6.

Nguyen, L., Fatahi, B. and Khabbaz, H. 2014. Modelling behaviour of cemented clay capturing cementation degradation. *Geotechnical Special Publication*, American Society of Civil Engineers (ASCE), pp. 168-177.

Nguyen, L., Fatahi, B. and Khabbaz, H. 2016. A novel model to simulate behaviour of cement treated clay under compression and shear. *GeoChina 2016, Geotechnical Special Publication*, American Society of Civil Engineers (ASCE)

Nguyen, L., Fatahi, B. and Khabbaz, H. 2016. Predicting the behaviour of fibre reinforced cement treated clay. *International Conference on Transportation Geotechnics 2016*, Guimarães, Portugal.

## TABLE OF CONTENT

<b>ABSTRACT</b>	<b>IV</b>
<b>ACKNOWLEDGEMENT</b>	<b>VI</b>
<b>LIST OF PUBLICATIONS</b>	<b>VII</b>
<b>TABLE OF CONTENT</b>	<b>VIII</b>
<b>LIST OF FIGURES</b>	<b>XIV</b>
<b>LIST OF TABLES</b>	<b>XXII</b>
<b>LIST OF SYMBOLS</b>	<b>XXIII</b>

<b>Chapter 1 Introduction</b> .....	<b>1</b>
1.1. Overview .....	1
1.2. Statement of Problem.....	4
1.3. Research Objectives and Scope .....	5
1.4. Thesis Organisation.....	7
<b>Chapter 2 Literature Review</b> .....	<b>9</b>
2.1. Introduction.....	9
2.2. Behaviour of Cement Treated Soil.....	10
2.2.1. Hardening Mechanisms.....	10
2.2.2. Formation of Structure and Effect of Cementation Degradation.....	12
2.2.2.1. The Formation of Structure .....	12
2.2.2.2. Effect of Cementation Degradation.....	16
2.2.3. Engineering Properties of Cement Treated Clay .....	18
2.2.3.1. Unconfined Compression Strength (UCS).....	18
2.2.3.1.1. Factors Affecting the Unconfined Compressive Strength.....	20
2.2.3.1.1.1. Effect of Cement Content .....	20

2.2.3.1.1.2.	Effect of Curing Time.....	21
2.2.3.1.1.3.	Effect of Water Content.....	23
2.2.3.1.1.4.	Effect of Different Types of Soil .....	24
2.2.3.2.	One Dimensional Compressibility Behaviour.....	26
2.2.3.2.1.	Effect of Cement Content.....	26
2.2.3.2.2.	Effect of Water Content .....	28
2.2.3.2.3.	Effect of Curing Time .....	29
2.2.3.3.	Behaviour of Cement Treated Clay Under Triaxial Compression Test	30
2.2.3.3.1.	Isotropic Compression.....	31
2.2.3.3.2.	Deviatoric Stress-Strain Relationship .....	32
2.2.3.3.3.	Undrained Stress Path .....	36
2.2.3.3.4.	Excess Pore Water Pressure .....	38
2.2.4.	Existing Constitutive Models for Cement Treated Clay.....	40
2.2.4.1.	Critical State Soil Mechanics .....	40
2.2.4.2.	Review of Modified Cam Clay Model .....	42
2.2.4.3.	Existing Constitutive Models Based on Single Yield Surface .....	45
2.2.4.4.	Existing Constitutive Models Based on Bounding Surface Plasticity Theory .....	49
2.2.4.5.	Failure Envelope of Cement Treated Clay.....	51
2.3.	Behaviour of Fibre Reinforced Soil With or Without Cement .....	53
2.3.1.	General.....	53
2.3.2.	Engineering Properties of Fibre Reinforced Soil With or Without..... Cement .....	55
2.3.2.1.	Unconfined Compression Strength (UCS) Test.....	55
2.3.2.2.	Direct Shear Test.....	59
2.3.2.3.	Consolidation Behaviour.....	62
2.3.2.4.	Triaxial Behaviour.....	63
2.3.2.5.	Failure Mechanisms .....	66

2.3.2.5.1.	Soil-Fibre Interaction .....	67
2.3.2.5.2.	Failure Envelope of Fibre Reinforced Soil.....	69
2.3.2.6.	Existing Constitutive Models for the Fibre Reinforced Soil .....	70
2.4.	Summary .....	73
<b>Chapter 3 Developing New Constitutive Models Capturing Cementation</b>		
	<b>Degradation &amp; Fibre Failure .....</b>	<b>77</b>
3.1.	General .....	77
3.2.	Development of the Proposed Constitutive Model for Cement Treated clay .....	79
3.2.1.	Modified Mean Effective Stress.....	80
3.2.2.	Compressibility Behaviour.....	82
3.2.3.	Proposed Failure Envelope .....	87
3.2.4.	Elastic Deformation .....	91
3.2.5.	Proposed Yield Function.....	92
3.2.6.	Plastic Energy Dissipation Equation.....	94
3.2.7.	Flow Rule and Plastic Potential Function .....	96
3.2.8.	Virgin Yielding Behaviour.....	99
3.2.9.	Modified Mean Effective Stress Including Shear Degradation .....	100
3.2.10.	General Stress-Strain Relationship .....	105
3.2.11.	Softening Behaviour.....	105
3.3.	Extended Constitutive Model for Cement Treated Clay with Fibre .....	
	Reinforcement .....	107
3.3.1.	General Quantities of Stress and Strain .....	107
3.3.2.	Modified Mean Effective Stress for FRCS .....	107
3.3.3.	Compressibility Behaviour of FRCS .....	108
3.3.4.	Extended Failure Envelope for FRCS.....	110
3.3.5.	Extended Yield Function for FRCS .....	113
3.3.6.	Extended Plastic Energy Dissipation Equation for FRCS .....	116

3.3.7.	Elastic Deformation of FRCS .....	118
3.3.8.	Extended Plastic Potential Function for FRCS .....	118
3.3.9.	Virgin Yielding Behaviour of FRCS.....	121
3.3.10.	Modified Mean Effective Stress while Considering the Effect of Shear ... Deformation .....	122
3.3.11.	General Stress-Strain Relationship for FRCS .....	125
3.4.	Summary .....	127
<b>Chapter 4 Laboratory Experiments &amp; Results .....</b>		<b>129</b>
4.1.	General .....	129
4.2.	Sample Preparation .....	130
4.3.	Experimental Program .....	135
4.3.1.	Unconfined Compression Strength (UCS) Tests .....	137
4.3.2.	Scanning Electron Microscopy (SEM) .....	138
4.3.3.	Triaxial Compression Apparatus .....	139
4.4.	Experimental Results .....	142
4.4.1.	Scanning Electron Microscopy (SEM) .....	142
4.4.1.1.	SEM Image Analysis for the Cement Treated Clay.....	142
4.4.1.2.	SEM Image Analysis for the Improved Clay Composite.....	144
4.4.2.	Unconfined Compression Strength (UCS) Test Results .....	147
4.4.3.	Results of Triaxial Compression Tests .....	151
4.4.3.1.	Triaxial Test Results of Cement Treated Ballina Clay .....	151
4.4.3.1.1.	Isotropic Compressibility of Cement Treated Ballina Clay.....	151
4.4.3.1.2.	Undrained Stress Path.....	155
4.4.3.1.3.	Stress-Strain Relationship and Excess Pore Water Pressure Response .....	160
4.4.3.1.4.	Behaviour of Cement Treated Clay in Drained Triaxial Conditions	167
4.4.3.2.	Triaxial Test Results of Improved Ballina Clay Composite .....	173

4.4.3.2.1.	Isotropic Compressibility of Improved Ballina Clay Composite ..	173
4.4.3.2.2.	Undrained Stress Path .....	174
4.4.3.2.3.	Stress-Strain Relationship .....	177
4.4.3.2.4.	Excess Pore Water Pressure Response .....	180
4.4.3.3.	Triaxial Test Results of Treated Kaolin clay .....	185
4.4.3.3.1.	Isotropic Compressibility of Improved Kaolin Clay Composite ...	185
4.4.3.3.2.	Undrained Stress Path .....	188
4.4.3.3.3.	Stress Strain Relationship and Excess Pore Water Pressure Response .....	193
4.5.	Summary .....	201
<b>Chapter 5 Model Verification and Discussion</b> .....		<b>203</b>
5.1.	General .....	203
5.2.	Estimation of Model Parameters .....	204
5.3.	Proposed Model Verification .....	206
5.3.1.	Cement Treated Ballina Clay .....	206
5.3.1.1.	Isotropic compressibility .....	206
5.3.1.2.	Undrained Triaxial Compression .....	210
5.3.1.3.	Drained Triaxial Compression .....	217
5.3.2.	Improved Ballina Clay Composite .....	222
5.3.2.1.	Isotropic compressibility for FRCS (Ballina clay composite) .....	222
5.3.2.2.	Undrained Triaxial Compression for FRCS ( Ballina clay composite)..... .....	224
5.3.3.	Improved Kaolin Clay Composite .....	231
5.3.3.1.	Isotropic Compressibility for FRCS (Kaolin clay composite) .....	231
5.3.3.2.	Undrained Triaxial Compression for FRCS (Kaolin clay composite) .....	234
5.3.4.	Further Verification for the Cement Treated Clay .....	242
5.4.	Summary .....	253

<b>Chapter 6 Conclusions and Recommendations</b> .....	256
6.1. Summary .....	256
6.2. Conclusions .....	259
6.3. Recommendations for Future Studies .....	262
<b>References</b> .....	264
APENDIX A .....	275
APENDIX B .....	277

## LIST OF FIGURES

Figure 2.1: SEM image of untreated clay at 5,000 magnification (Kamruzzaman et al. 2009) .....	14
Figure 2.2: SEM image of 10% cement treated clay at 28 day curing at 5,000 magnification (Kamruzzaman et al. 2009).....	15
Figure 2.3: SEM image of Naticoke clay treated with 8.7% cement at 15,000 magnification (Sasanian 2011).....	15
Figure 2.4: SEM image at shear band of 10% cement treated sample under confining pressure of 1000 kPa at 28 days curing (Kamruzzaman et al. 2009).....	18
Figure 2.5: Effect of cement content on UCS of the un-treated and treated Bangkok soft clays at 28 days curing (after Uddin et al. 1997) .....	19
Figure 2.6: Effect of cement content and curing time on the UCS of cement treated clay (after Uddin et al. 1997).....	22
Figure 2.7: Effect of curing time on the UCS of treated clay with differing cement content (after Endo 1976).....	22
Figure 2.8: Effect of remoulding water content on UCS of treated clay at differing curing period (after Lorenzo and Bergado 2006).....	24
Figure 2.9: Effect of different types of Singapore marine clay treated with 20% cement in UCS test (after Tan et al. 2002) .....	25
Figure 2.10: Effect of cement content in one-dimensional consolidation of treated clay at 28 days curing in $e - \log \sigma v'$ plane (after Kamruzzaman et al. 2009).....	27
Figure 2.11: Effect of water content in one-dimensional consolidation of 15% cement treated clay in $e - \log \sigma v'$ plane (after Lorenzo and Bergado 2006).....	28
Figure 2.12: Effect of curing time in one-dimensional consolidation of 30% cement treated clay in $e - \log \sigma v'$ plane (after Kamruzzaman et al. 2009).....	29
Figure 2.13: Effect of cement content on the isotropic compressibility behaviour of cement treated clay in $e - \ln p'$ plane (after Horpibulsuk et al. 2004) .....	32
Figure 2.14: Deviatoric stress-strain relationship of un-treated and 9% cement treated samples in $q - \varepsilon q$ plane below the initial yield stress (after Horpibulsuk et al. 2004) ..	33
Figure 2.15: Deviatoric stress-strain relationship of un-treated and 6% cement treated samples in $q - \varepsilon q$ plane (after Horpibulsuk et al. 2004) .....	34
Figure 2.16: Effect of cement content on $q - \varepsilon q$ relationship of treated clay at 1000 kPa confining pressure and 28 day curing (after Kamruzzaman et al. 2009) .....	35
Figure 2.17: Undrained stress paths of un-treated and 6% cement treated sample in $p' - q$ plane (after Horpibulsuk et al. 2004) .....	36
Figure 2.18: Effect of confining pressure on $q - p'$ relationship of treated clay with 10% cement content and 28 days curing (after Kamruzzaman et al. 2009).....	37
Figure 2.19: Effect of confining pressure on excess pore water pressure response (in $u - \varepsilon a$ plane) of treated clay with 10% cement and 28 days curing (after Kamruzzaman et al. 2009).....	39
Figure 2.20: Effect of cement content on pore water pressure response of treated clay at confining pressure of 1000 kPa and 28 days curing (after Kamruzzaman et al. 2009) ..	39

Figure 2.21: Critical State Concept: (a) in $v - \ln p'$ plane, (b) in $p' - q$ plane (after Yu 2006) .....	41
Figure 2.22: Schematic diagram of the failure state line including the effect of cementation in (a) $p - q$ plane and (b) $e - \ln(p + pr)$ plane (after Kasama et al. 2000) .....	46
Figure 2.23: Schematic diagram of the SCC model for cement treated clay in (a) $e - \ln p'$ plane and (b) $p' - q$ plane (after Horpibulsuk et al. 2010).....	47
Figure 2.24: Schematic diagram of the S3-SKH in triaxial stress space (after Baudet and Stallebrass 2004) .....	51
Figure 2.25: Failure envelope for artificially cemented Indian marine clay.....	52
Figure 2.26: Effect of increasing fibre content on the UCS of fibre reinforced clay with differing fibre length (after Jiang et al. 2010).....	56
Figure 2.27: Effect of fibre content on the UCS of 4% cement treated sand reinforced with fibre (after Park 2011).....	57
Figure 2.28: Effect of increasing fibre length on the UCS of fibre reinforced clay with differing fibre content (after Jiang et al. 2010) .....	58
Figure 2.29: Stress-strain behaviour of sand reinforced with different fibre contents under vertical normal stress = 250 kPa (after Shao et al. 2014) .....	60
Figure 2.30: Comparison between unreinforced and fibre reinforced fly ash sample in direct shear test at differing vertical normal stress (after Kaniraj and Havanagi 2001) .	60
Figure 2.31: Comparison between un-reinforced and 1% fibre reinforced sand in direct shear test under differing vertical normal stresses (after Yetimoglu and Salbas 2003)..	62
Figure 2.32: Stress-strain behaviour of polyamide fibre reinforced fine sand with differing fibre concentration (after Michalowski and Cermák 2003).....	64
Figure 2.33: Effect of fibre content on the energy absorption capacity of the 3% cement treated sand (after Hamidi and Hooresfand 2013) .....	66
Figure 2.34: Effect of water content on the pull-out load of a single fibre in reinforced soil (after Tang et al. 2010).....	69
Figure 2.35: Failure envelope of 2% fibre reinforced fine sand at differing aspect ratio (after Ranjan et al. 1996).....	70
Figure 2.36: Failure envelope of fibre reinforced soil (after Maher and Gray 1990) .....	71
Figure 2.37: Shear strength envelope of fibre reinforced soil in discrete framework (after Zornberg 2002).....	73
Figure 3.1. Schematic diagram of isotropic compression of the cement treated clay.....	83
Figure 3.2. The prediction of proposed model on the compressibility of cemented Ottawa clay.....	86
Figure 3.3: The prediction of proposed model on the compressibility of 6% cemented Ariake clay .....	87
Figure 3.4: Proposed failure envelope prediction of 3% lime treated Indian Marine clay .....	91
Figure 3.5. The effect of increasing parameter $Cc$ on the proposed yield surface.....	93
Figure 3.6. The effect of increasing hardening parameter $p'_0$ on the proposed yield surface for cement treated clay .....	93

Figure 3.7. The effect of hardening parameter $p_0'$ on the proposed plastic potential surface .....	98
Figure 3.8. The effect of variation of $\alpha$ on the proposed plastic potential.....	98
Figure 3.9: Schematic diagram of deconstructurisation .....	102
Figure 3.10: Effect of increasing parameter $\omega$ on destructuring process.....	102
Figure 3.11: Effect of increasing parameter $b$ on degradation process.....	103
Figure 3.12. The proposed failure envelope for cement treated clay.....	104
Figure 3.13: Isotropic compression of the fibre improved cement treated clay.....	110
Figure 3.14: Schematic diagram of the proposed failure envelope.....	113
Figure 3.15: The effect of variation of hardening parameter $p_0'$ on the yield surface	115
Figure 3.16: The proposed yield surface with variations of $C_c$ .....	115
Figure 3.17: Variation of $p_0'$ on the size of the proposed yield surface.....	120
Figure 3.18: Variation of $\alpha$ on the proposed plastic potential function.....	120
Figure 3.19: Schematic diagram of strength reduction due to cementation degradation and fibre failure .....	125
Figure 4.1: Location of Ballina in the map (courtesy of Google Maps) .....	130
Figure 4.2: Location of the natural Ballina clay .....	131
Figure 4.3: Polypropylene fibre adopted in this study (the illustrated scale is in cm)..	134
Figure 4.4: Sample preparation stages: (a) sample moulded in slipt cylindrical mould, (b) wrapped in vinyl plastic wrap, (c) demoulded sample after 24 hours, (d) placed in curing bath.....	135
Figure 4.5: Unconfined compression strength (UCS) test setup.....	138
Figure 4.6: (a) Triaxial test setup used in this study; (b) Schematic diagram of the triaxial cell.....	141
Figure 4.7: SEM images of the un-treated Ballina clay at $2 \mu m$ with the magnification of 5000 .....	143
Figure 4.8: SEM images of the 10% cement treated Ballina clay at $2 \mu m$ with the magnification of 5000 .....	143
Figure 4.9: SEM images of the 10% cement treated Ballina after shearing at 800 kPa at $2 \mu m$ with a magnification of 5000.....	144
Figure 4.10: SEM image of the improved Ballina clay (15% cement content and 0.3% fibre content) before triaxial test at 1500 magnification.....	145
Figure 4.11: SEM image of the improved Ballina clay (15% cement and 0.3% fibre) after shearing at 800 kPa (taken at the shear band) at 1000 magnification.....	146
Figure 4.12: SEM image of the improved Ballina clay (15% cement content and 0.3% fibre content) after shearing at 800 kPa (taken at shear band) at 2500 magnification..	146
Figure 4.13: UCS results of the Ballina clay treated with differing cement contents (10%, 12% and 15%) .....	148
Figure 4.14: UCS results of 15% cement treated Ballina clay reinforced with increasing fibre contents (0.3% and 0.5%).....	150
Figure 4.15: Effect of fibre and cement inclusion on the brittleness index of natural Ballina clay in an unconfined compression condition .....	150

Figure 4.16: Results of isotropic compression tests of Ballina clay treated with different cement contents .....	152
Figure 4.17: Undrained stress paths of natural Ballina clay .....	155
Figure 4.18: Undrained stress paths of Ballina clay treated with 10% cement.....	156
Figure 4.19: Stress paths of Ballina clay treated with 12% cement.....	157
Figure 4.20: Stress paths of Ballina clay treated with 15% cement.....	158
Figure 4.21: Effect of increasing cement content on the peak shear strength of the Ballina clay treated with cement in undrained triaxial conditions .....	159
Figure 4.22: Stress-strain relationships of natural Ballina clay .....	160
Figure 4.23: Excess pore water pressure response of natural Ballina clay .....	161
Figure 4.24: Stress-strain relationship of Ballina clay treated with 10% cement .....	162
Figure 4.25: Excess pore water pressure response of Ballina clay treated with 10% cement .....	163
Figure 4.26: Stress strain relationship of Ballina clay treated with 12% cement .....	164
Figure 4.27: Excess pore water pressure responses of Ballina clay treated with 12% cement .....	165
Figure 4.28: Stress strain relationship of Ballina clay treated with 15% cement .....	166
Figure 4.29: Excess pore water pressure responses of Ballina clay treated with 15% cement .....	166
Figure 4.30: Drained stress paths of the Ballina clay treated with 10% cement.....	167
Figure 4.31: Stress-strain relationship of the Ballina clay treated with 10% cement in drained condition.....	168
Figure 4.32: Failure behaviour of the 10% cement treated Ballina clay at $p'_0 = 800$ kPa in: (a) drained and (b) undrained triaxial condition .....	169
Figure 4.33: Drained stress paths of Ballina clay treated with 12% cement.....	170
Figure 4.34: Stress-strain relationship of the Ballina clay treated with 12% in drained condition.....	171
Figure 4.35: Drained stress paths of the Ballina clay treated with 15% cement.....	171
Figure 4.36: Stress-strain relationship of the Ballina clay treated with 15% cement in drained condition.....	172
Figure 4.37: Results of isotropic compression tests on Ballina clay treated with 15% cement and different fibre contents (0%, 0.3% and 0.5%) .....	174
Figure 4.38: Undrained stress paths of the 15% cement treated Ballina clay and improved with fibre (fibre contents: 0%, 0.3% and 0.5%) in $p' - q$ plane .....	176
Figure 4.39: Effect of increasing fibre content on the peak shear strength of the improved Ballina composite .....	176
Figure 4.40: Stress-strain relationship of the 15% cement treated Ballina clay and improved with fibre (fibre contents: 0%, 0.3% and 0.5%) in $\varepsilon q - q$ plane. ....	178
Figure 4.41: Effect of increasing fibre content on the brittleness index of the cement treated Ballina clay.....	179
Figure 4.42: Failure of the 15% cement treated Ballina clay and reinforced with: (a) 0% fibre, (b) 0.3% fibre, (c) 0.5% fibre, in undrained shearing at $p_0' = 800$ kPa.....	180

Figure 4.43: Excess pore water pressure response of Ballina clay treated with 15% cement and improved with fibre (fibre contents: 0%, 0.3% and 0.5%).....	181
Figure 4.44: Stress paths of Ballina clay treated with 15% cement and 0.3% fibre .....	182
Figure 4.45: Stress-strain relationship of Ballina clay treated with 15% cement and 0.3% fibre.....	182
Figure 4.46: Excess pore water pressure response of Ballina clay treated with 15% cement and 0.3% fibre.....	183
Figure 4.47: Stress paths of Ballina clay treated with 15% cement and 0.5% fibre .....	183
Figure 4.48: Stress-strain relationship of Ballina clay treated with 15% cement and 0.5% fibre.....	184
Figure 4.49: Excess pore water pressure response of Ballina clay treated with 15% cement and 0.5% fibre.....	184
Figure 4.50: Results of isotropic compression test on Kaolin clay treated with 15% cement and different fibre content (0%, 0.3% and 0.5%).....	186
Figure 4.51: Undrained stress paths of the Kaolin clay .....	188
Figure 4.52: Undrained stress paths of the Kaolin clay treated with 5% cement .....	189
Figure 4.53: Undrained stress paths of the Kaolin clay treated with 5% cement and 0.1% fibre .....	190
Figure 4.54: Undrained stress paths of the Kaolin clay treated with 5% cement and 0.5% fibre .....	191
Figure 4.55: Effect of cement and fibre reinforcement on the peak shear strength of the improved Kaolin clay.....	192
Figure 4.56: Stress-strain relationship of the un-treated Kaolin clay.....	194
Figure 4.57: Stress-strain relationship of the Kaolin clay treated with 5% cement.....	194
Figure 4.58: Excess pore water pressure response of the un-treated Kaolin clay.....	195
Figure 4.59: Excess pore water pressure response of the Kaolin clay treated with 5% cement .....	195
Figure 4.60: Stress-strain relationship of the Kaolin clay treated with 5% cement and 0.1% fibre.....	196
Figure 4.61: Stress-strain relationship of the Kaolin clay treated with 5% cement and 0.5% fibre.....	197
Figure 4.62: Excess pore water pressure response of the Kaolin clay treated with 5% cement and 0.1% fibre.....	198
Figure 4.63: Excess pore water pressure response of the Kaolin clay treated with 5% cement and 0.5% fibre.....	199
Figure 4.64: Effect of fibre reinforcement on the brittleness index of the improved Kaolin clay .....	200
Figure 5.1: Simulation of isotropic compression of 10% cement treated Ballina clay.	209
Figure 5.2: Simulation of isotropic compression of Ballina clay treated with different cement content (i.e. 10%, 12% and 15%) .....	209
Figure 5.3: Predicted stress paths of undrained triaxial tests of 10% cement treated Ballina clay.....	211

Figure 5.4 Predicted stress paths of undrained triaxial tests of 12% cement treated Ballina clay.....	211
Figure 5.5: Predicted stress paths of undrained triaxial tests of 15% cement treated Ballina clay.....	212
Figure 5.6: Predicted stress-strain curves of undrained triaxial tests of 10% cement treated Ballina clay.....	213
Figure 5.7: Predicted stress-strain curves of undrained triaxial tests of 12% cement treated Ballina clay.....	213
Figure 5.8: Predicted stress-strain curves of undrained triaxial tests of 15% cement treated Ballina clay.....	214
Figure 5.9: Simulated reduction in structure strength due to cementation degradation of 10% cement treated Ballina clay.....	214
Figure 5.10 Predictions on the excess pore water pressure response of the Ballina clay treated with 10% cement.....	216
Figure 5.11: Predictions on the excess pore water pressure response of the Ballina clay treated with 12% cement.....	216
Figure 5.12: Predictions on the excess pore water pressure response of the Ballina clay treated with 15% cement.....	217
Figure 5.13: Predicted stress path of drained triaxial tests of 10% cement treated Ballina clay.....	218
Figure 5.14: Predicted stress path of drained triaxial tests of 12% cement treated Ballina clay.....	218
Figure 5.15: Predicted stress path of drained triaxial tests of 15% cement treated Ballina clay.....	219
Figure 5.16: Predicted stress-strain curves of drained triaxial tests of 10% cement treated Ballina clay.....	220
Figure 5.17: Predicted stress-strain curves of drained triaxial tests of 12% cement treated Ballina clay.....	221
Figure 5.18: Predicted stress-strain curves of drained triaxial tests of 15% cement treated Ballina clay.....	221
Figure 5.19: Predictions on the isotropic consolidation test result of the Ballina clay treated with 15% cement and fibre contents of 0%, 0.3% and 0.5%. .....	224
Figure 5.20: Predictions on the stress path curves of the Ballina clay treated with 15% cement and 0.3% fibre.....	226
Figure 5.21: Predictions on the stress path curves of the Ballina clay treated with 15% cement and 0.5% fibre.....	227
Figure 5.22: Effect of increasing isotropic consolidation pressure $p_0'$ on the yield surface of the Ballina clay treated with 15% cement and 0.5% fibre. ....	228
Figure 5.23: Predictions on the stress strain relationship of the Ballina clay treated with 15% cement and 0.3% fibre .....	228
Figure 5.24: Predictions on the stress strain relationship of the Ballina clay treated with 15% cement and 0.5% fibre .....	229

Figure 5.25: Predictions on the excess pore water pressure response of the Ballina clay treated with 15% cement and 0.3% fibre .....	230
Figure 5.26: Predictions on the excess pore water pressure response of the Ballina clay treated with 15% cement and 0.5% fibre .....	230
Figure 5.27: Predictions on the isotropic consolidation test result of the improved soil composite .....	232
Figure 5.28: Predictions on the stress path of the Kaolin clay treated with 5% cement .....	236
Figure 5.29: Predictions on the stress path of the improved Kaolin composite with 5% cement and 0.1% fibre.....	236
Figure 5.30: Predictions on the stress path of the improved Kaolin composite with 5% cement and 0.5% fibre.....	237
Figure 5.31: Predictions on the stress-strain relationship of the Kaolin clay treated with 5% cement.....	238
Figure 5.32: Predictions on the stress strain relationship of the improved Kaolin composite with 5% cement and 0.1% fibre.....	238
Figure 5.33: Predictions on the stress strain relationship of the improved Kaolin composite with 5% cement and 0.5% fibre.....	239
Figure 5.34: The effect of shear deformations on the contribution of cement and fibre reinforcement to the improved Kaolin composite.....	240
Figure 5.35: Predictions on the excess pore water pressure response of the Kaolin clay treated with 5% cement.....	241
Figure 5.36: Predictions on the excess pore water pressure response of the improved Kaolin composite with 5% cement and 0.1% fibre.....	241
Figure 5.37: Predictions on the excess pore water pressure response of the improved Kaolin composite with 5% cement and 0.5% fibre.....	242
Figure 5.38: Predictions on the stress path curves of the Aberdeen soil admixed with 5% cement.....	245
Figure 5.39: Predictions on the stress strain of the Aberdeen soil admixed with 5% cement.....	245
Figure 5.40: Predictions on the excess pore water pressure response of the Aberdeen soil admixed with 5% cement.....	246
Figure 5.41: Predictions on the isotropic consolidation test result of the Ariake clay treated with 6% cement.....	247
Figure 5.42: Predictions on the stress path curves of the Ariake clay treated with 6% cement.....	248
Figure 5.43: Predictions on the stress strain of the Ariake clay treated with 5% cement.....	248
Figure 5.44: Predictions on the excess pore water pressure response of the Ariake clay treated with 6% cement.....	249
Figure 5.45: Predictions on the stress path curves of the Singapore clay treated with 10% cement.....	250

Figure 5.46: Predictions on the stress strain of the Singapore clay treated with 10% cement. ....	251
Figure 5.47: Predictions on the excess pore water pressure response of the Singapre clay treated with 10% cement.....	251

## LIST OF TABLES

Table 2.1. Properties of three different type of soft Singapore clays (after Tan et al. 2002) .....	25
Table 4.1: Properties of adopted clay samples.....	132
Table 4.2: Average properties of the adopted fibre.....	134
Table 4.3: Experimental program in this study .....	136
Table 4.4: Summary of results of undrained triaxial tests of the treated Ballina clay ..	153
Table 4.5: Summary of results of undrained triaxial tests of the treated Kaolin clay ...	187
Table 5.1: Model values for cement treated Ballina clay.....	207
Table 5.2: Model values for the improved Ballina clay composite .....	223
Table 5.3: Model values for the improved Kaolin clay composite .....	233
Table 5.4: Model values for the cement treated clays.....	244

# LIST OF SYMBOLS

## Abbreviations

CSL	Critical State Line
CD	Consolidated-Drained triaxial test
CU	Consolidated-Undrained triaxial test
ELDPC	Enterprise Level Pressure/Volume Controllers
FRCS	Fibre Reinforced Cemented Soil
LVDT	Linear Variable Displacement Transducer
MCC	Modified Cam Clay
MSCC	Modified Structured Cam Clay
PWPT	Pore Water Pressure Transducer
SEM	Scanning Electron Microscopy
SCC	Structured Cam Clay
UCS	Unconfined Compression Strength

## Greek notations

$\alpha$	non dimensional parameter
$\beta$	Cementation degradation parameter due to mean effective stress
$\varepsilon_1$	Axial strain
$\varepsilon_3$	Radial strain
$\dot{\varepsilon}$	Strain rate adopted for triaxial tests
$\varepsilon_f$	Strain level at failure
$\varepsilon_{peak}$	Strain level at peak stress
$\varepsilon_{res}$	Strain level at residual stress
$\kappa$	Swelling or recompression index
$\lambda$	Compression index
$\eta$	Stress ratio
$\eta^*$	Modified stress ratio
$\nu$	Poisson's ratio

$\omega$	Cementation degradation parameter due to shear deformation
$\psi$	Derivative of $p'_0$ with respect to $p'$
$\sigma_1$	Total axial stress
$\sigma'_1$	Axial effective stress
$\sigma_3$	Total radial stress
$\sigma'_3$	Radial effective stress
$\sigma_f^p$	Plastic stress limit of the fibre
$\delta_{sf}$	Frictional component between fibre and soil matrix
$\xi$	Correlation factor for the effect of cementation to the shear strength

### Latin notations

$A$	Derivative of $p'_\Omega$ with respect to $p'$
$a_{sf}$	Adhesive component between fibre and soil matrix
$B$	Derivative of $p'_f$ with respect to $q$
$b$	Cementation degradation parameter due to shear deformation
$C_c$	Shear strength contributed by cementation when $p' = 0$
$C_f$	Shear strength contributed by fibre
$d_f$	Diameter of the fibre
$d_v$	Total volumetric strain increment
$d_v^e$	Elastic volumetric strain increment
$d_v^p$	Plastic volumetric strain increment
$d_\varepsilon$	Total plastic deviatoric strain increment
$d_\varepsilon^e$	Elastic deviatoric strain increment
$d_\varepsilon^p$	Plastic deviatoric strain increments
$dW_{in}$	Internal plastic energy per unit volume
$d\lambda$	Non-negative plastic multiplier
$\Delta s$	Effect of soil fabric
$\Delta u$	Excess pore water pressure
$\Delta u_{max}$	Maximum excess pore water pressure
$e$	Void ratio of the soil
$f$	Yield function

$G'$	Shear modulus
$g$	Plastic potential function
$I_B$	Brittleness index
$l_f$	Length of the fibre
$M$	Slope of failure envelope of reconstituted soil composite
$m$	Fibre degradation parameter due to shear deformation
$n$	Fibre degradation parameter
$p$	Total mean stress
$p'$	Mean effective stress
$p'_f$	Describing the effect of fibre
$p''_f$	Fibre degradation due to plastic deviatoric strain
$p'^*$	Modified mean effective stress
$p^*_{crit}$	Critical mean effective stress
$p'^*_0$	Modified mean effective stress on the yield surface when $q = 0$
$p'_0$	Hardening parameter – mean effective stress on the yield surface when $q = 0$
$p'_{0,i}$	Initial mean effective yield stress
$p'_{\Omega}$	$p'$ (tension) when $q = 0$ , describing the effect of cementation
$p''_{\Omega}$	Cementation degradation due to plastic deviatoric strain
$p'_{\Omega,i}$	Describing the beneficial effect of cementation
$q$	Deviatoric stress
$q_c$	Critical deviatoric stress
$q_{peak}$	Peak shear strength
$q_{res}$	Residual shear strength
$t_f$	Time to failure
$u$	Pore water pressure
$u_{max}$	Maximum pore water pressure

# Chapter 1

## Introduction

---

### 1.1. Overview

The demand for construction over soft soil is generally higher due to dramatic growth in population and economic activities around the world. Weak soils such as soft clays are prevalent around lakes and coastal environments where poor ground condition is often encountered. The problems with soft soil include high compressibility, low strength and low permeability which present a tremendous challenge for the construction and design engineers. Therefore, these sites should be improved by suitable ground improvement techniques in order to perform satisfactorily under applied structural loads. Over the years, deep soil mixing and cement stabilisation techniques have proven to be effective ground improvement methods where in-situ soils are mixed with cement to improve the properties of the soft soils. The improved ground condition generally has lower compressibility, higher strength and greater permeability. According to Porbaha (1998), deep soil mixing method offers several advantages such as increasing speed of construction, achieving the design strength, enhancing reliability, utilising the resources and effective in various applications, which have been reported by a number of researchers (Ando et al. 1995; Jasperse and Ryan 1992; Neff 1996; Tatsuoka et al. 1997). Moreover, this technology can be employed in conjunction with the use of shallow foundations, instead of deep foundations, the costs of which may be prohibitive in low-budget road, pavement, slope protection, and building projects.

The importance of understanding the engineering properties of the improved ground treated with cement, results in a growing interest among researchers over the past few decades. A large number of experimental tests in the laboratory and the field were conducted to study the behaviour of the cement treated soil (e.g. Balasubramaniam et al. 1998; Bergado et al. 1996; Hayashi et al. 2002; Kamruzzaman et al. 2009; Kitazume et al. 2002; Lee et al. 2005; Uddin et al. 1997; Yin 2001). The effect of cementation is to increase the shear strength and reduce the compressibility of the soft clay due to the formation of cementation bonds within the soil matrix (Kamruzzaman et al. 2009; Lo and Wardani 2002; Uddin et al. 1997). In isotropic compression condition, the initial yield stress of the cement treated clay increases with cement content as compared to that of the un-treated soil at the same void ratio which is owing to the effect of cement inclusion as suggested by Miura et al. (2001) and Lade and Overton (1989). However, the void ratio of cement treated clay decreases significantly in isotropic consolidation and triaxial conditions, when subjected to a high mean effective yield stress (or effective confining pressure), particularly beyond the initial yield stress. In undrained triaxial condition, the peak shear strength of the cement treated clay has been observed to be higher than that of the un-treated clay. Additionally, laboratory experiments have shown that the cementation of clay gradually diminishes as the mean effective stress increases, due to the degradation of cementation bonds (Kamruzzaman et al. 2009). Furthermore, when the peak shear strength of the cement treated clay is obtained, softening process occurs resulting to a significant drop in strength due to the crushing of cementation bonds with increasing deviatoric strains (Suebsuk et al. 2010). The undrained stress path during the softening process directs toward and stays on the Critical State Line (CSL) at the residual strength state indicating a complete removal of the cementation bonds. At this stage, the behaviour of the soft clay treated with cement is similar to that of the un-treated clay.

With a significant reduction in the strength at the post-peak state, the cement treated clay behaves as a brittle material as reported by a number of researchers (Lorenzo and Bergado 2006; Panda and Rao 1998; Porbaha et al. 2000). This unfavourable behaviour due to the inclusion of cement presents a challenge for the construction and design engineers as well as the contractors in implementing the cement stabilisation technique. Therefore, in recent years, research activities have focused on improving the material ductility of the soft soil or cement treated soil by including the

geosynthetics such as fibre and geotextile within the soil-cement mixture (Casagrande et al. 2006; Consoli et al. 2009b; Michalowski and Čermák 2002; Park 2011). According to Maher and Ho (1994) and Tang et al. (2007) and based on a number of laboratory experiments, the usage of fibre has been proven to be an effective and reliable treatment to the soft soil. The peak and particularly the residual shear strengths of soft soil, including both cohesive and cohesionless soils increase due to the bridging effect provided by the fibre (Maher and Ho 1994; Michalowski and Čermák 2003; Tang et al. 2007). However, majority of the previous research activities are on the effect of fibre reinforcement on sand, clay and cement treated sand while the behaviour of fibre reinforced cement treated clay, referred to as the improved soil composite or FRCS, is rarely found in the literature. A few researchers such as Cai et al. (2006), Tang et al. (2010) and Fatahi et al. (2012) suggested that the residual shear strength of the cement treated clay increases significantly due to the effect of fibre reinforcement. Moreover, the brittle failure of the cement treated clay changes to more ductile failure by mixing the fibre into the soil-cement matrix. In addition, the effect of fibre failure on the behaviour of the improved clay composite requires further investigation. Zornberg (2002) and Ranjan et al. (1996) characterised the failure of fibre as pull-out or rupture depending on the level of the applied confining pressure compared to the critical confining pressure. In particular, the breakage of fibre may occur under confining pressure higher than the critical confining pressure as the frictional resistance exceeds the fibre breakage capacity (Zornberg 2002).

## 1.2. Statement of Problem

The importance of the soil cementation and its degradation has resulted in the development of a number of constitutive models, based on different plasticity theories to simulate the behaviour of the cement treated clay. In particular, the existing constitutive models fall into two main categories, namely a single yield surface and a bounding surface, both following the concept of the Critical State Soil Mechanics. For example, constitutive models developed by Kasama et al. (2000), the Structured Cam Clay (SCC) model developed by Horpibulsuk et al. (2010) and the Modified Structured Cam Clay (MSCC) model proposed by Suebsuk et al. (2010) are based on a single yield surface while the bounding surface plasticity theory is adopted in the proposed models by Baudet and Stallebrass (2004) and Kavvadas and Amorosi (2000). However, there are a number of drawbacks in the existing constitutive models for the cement treated clay which are discussed in details in Chapter 2. Most importantly, the peak shear strength of the cement treated clay is often over-predicted which can lead to unrealistic simulation. As suggested by Lade and Overton (1989) and Uddin et al. (1997), the beneficial contribution of the cementation to the shear strength of the cement treated clay reduces with increasing mean effective yield stress or effective confining pressure due to significant breaking of cementation bonds at the pre-shear stage. Hence, the failure envelope of the cement treated clay should merge with the Critical State Line (CSL) as the mean effective stress continues to increase. The existing constitutive models such as SCC and MSCC chose to ignore this effect by adopting the linear failure envelope for the cement treated clay. Besides the mean effective yield stress, the effect of shear degradation on the pre-and-post peak strength state should be included in any constitutive models for the cement treated clay. The MSCC model proposes two separate equations to describe the diminishing effect of the cementation bonds induced by shear deformation while a unique single equation is preferable to simulate the smooth transition between the peak and the residual strength states. Furthermore, the existing constitutive models simulate the softening behaviour of the cement treated clay adopting the negative hardening rule, which cannot properly capture the complex mechanisms involved during the post peak state as suggested by Zhu et al. (2010).

The use of fibre reinforcement to improve the ductility of the cement treated clay becomes increasingly popular. Moreover, previous studies have focused mainly on the effect of fibre inclusion on clay, sand and cement treated sand. Hence, conducting the experimental program to study the behaviour of the improved clay composite, particularly under the triaxial compression tests is necessary. In addition, the effect of fibre reinforcement in the improved soil composite under isotropic consolidation remains limited. While the previous studies have indicated that the peak and the residual shear strength values of the improved clay composite under unconfined compression strength (UCS) test increase due to the fibre reinforcement, the effect of increasing mean effective stress to the shear strength requires further investigation. Furthermore, the mean effective stress and the deviatoric strain play important roles on the failure of the fibre which consequently affects the shear strength of the treated clay.

A constitutive model to simulate the behaviour of the fibre reinforced cement treated clay is required, since the existing constitutive models have been developed for fibre reinforced soil, excluding cementation such as the models proposed by Diambra and Ibraim (2014), Ranjan et al. (1996) and Zornberg (2002). The constitutive model for the improved clay composite should consider the combined effects of cement and fibre, together with their degradations including cementation degradation and fibre failure. The model predictions should provide reliable simulation of the realistic behaviour of the improved clay composite which can be recommended to practitioners.

### **1.3. Research Objectives and Scope**

The key objective of the present study is to propose a constitutive model for the cement treated clay with or without fibre reinforcement under different loading conditions. The beneficial and diminishing effects of cementation and fibre inclusion need to be collaboratively simulated. The model parameters should be readily estimated so that practicing engineers can adopt the model for complex designs. The proposed model takes the limitations from existing models into consideration. With reference to the existing models and knowledge obtained from literature review, several concepts and ideas are conceptualised to form a predictive model. Furthermore, the proposed

constitutive model includes the important features required to predict the behaviour of the treated clay, providing reliable predictions. This study comprises of the following parts:

- Developing a constitutive model to simulate the behaviour of cement treated clays, incorporating the beneficial effect of cementation and its degradation, particularly at high effective confining pressures.
- Developing an extended version of the proposed model to include the effect of fibre reinforcement, together with fibre failure.
- Conducting laboratory experiments on the soft clay treated with various cement contents and under different confining pressures. The purpose of the experimental program is to enhance the understanding of the pre-and-post peak state of the cement treated clays, including the effect of cement content and confining pressure on the cementation degradation rate. Moreover, the experimental results are used to verify the proposed model.
- Further verifying the proposed model for the cement treated clay using several case studies available in the literature.
- Conducting laboratory experiments on the cement treated soft clay reinforced with various fibre contents to investigate the factors influencing the behaviour of improved clay composite under triaxial compression condition. Moreover, the performance of the extended version of the proposed model can be verified against the experimental results.

It should be noted that, the scope of the present study is limited to the behaviour of the cement treated clay under compression; in other words this study only focuses on the shear strength of the improved clay (and not tensile strength). Furthermore, the main aim of the proposed models is to capture the behaviour of the treated clay at high confining pressures, particularly beyond the initial yield stress where plastic deformations occur causing significant breakage of cementation bonds and fibre failure.

The specific objectives of the present study can be summarised as follows:

- Providing accurate and reliable prediction tools to simulate the behaviour of cement treated clay with or without fibre reinforcement.

- Measuring the performance of the proposed models.
- Investigating the combined effects of cement and fibre inclusion under different loading conditions in the laboratory.

## 1.4. Thesis Organisation

This thesis consists of six chapters which can be organised as follows:

- Chapter 1 provides a brief introduction regarding the behaviour of the cement treated clay with or without fibre reinforcement. Moreover, the statement of the problem, the objectives and the scope of this study are also presented in this chapter.
- Chapter 2 presents a comprehensive literature review on the engineering properties of the cement treated clay with or without fibre reinforcement and their behaviour under different testing conditions. In addition, the existing constitutive models to simulate the soil behaviour are also discussed in details.
- Chapter 3 proposes a new constitutive model to simulate the behaviour of the cement treated clay considering the effect of cementation and its degradation. Furthermore, the proposed model is extended to predict the behaviour of the fibre reinforced cement treated clay considering the combined effects of cement and fibre, together with their degradations. Important features of the proposed models including the non-associated plastic flow rule, the modified energy dissipation equation, the non-linear failure envelope and the general stress-strain relationship for the pre-and-post peak stress states are provided and discussed in details.
- Chapter 4 reports the experimental program and the results from the tested samples in this study. This includes the unconfined compression strength (UCS) tests, the isotropic consolidation tests, a series of drained and undrained triaxial compression tests and the scanning electron microscope (SEM) image analysis. The experiments are carried out on two types of soft clay, including the natural Ballina clay and the artificial Kaolin clay, treated with various cement and fibre contents. Moreover, the combined effects of cementation and fibre, together with their

degradations to the shear strength of the improved clay composite with or without fibre reinforcement are discussed in details.

➤ Chapter 5 provides the simulation results of the proposed models in Chapter 3 by comparing their predictions with the experimental results reported in Chapter 4, including the cement treated Ballina clay and Kaolin clay with or without fibre reinforcement. It can be noted that, an extended version of the proposed model is used to simulate the behaviour of the fibre reinforced cement treated clay. Moreover, this chapter also presents the model predictions for the existing case studies available in the literature for further verification of the proposed model.

➤ Chapter 6 summarises the thesis, together with the conclusions and recommendations for future research.

# Chapter 2

## Literature Review

---

### 2.1. Introduction

With the growth of cities and industries, suitable sites, which can be used without some ground modification, are becoming increasingly scarce. Moreover, the cost of replacing soft soils with high quality material has dramatically increased. The design engineers have various options in dealing with problematic soils such as bypassing the poor soil, replacing it with superior soil, redesigning the structure for the poor condition or improving the soil properties by compaction, inclusion of geosynthetics or mixing soil with materials such as cement, lime, gypsum and fly ash among other ground modification techniques. The latter option can be used for surface improvement, such as road and rail subgrade improvement, or in deep soil mixing or jet grouting technologies, which are soil improvement approaches, mixing in situ soil with strengthening agents.

Cement is one of the strengthening agents used to stabilise soft soil, while others such as lime, gypsum and fly ash can also be used. Cement stabilisation involves mixing in-situ soil with cement to form soil-cement column which has been adopted in Deep Soil Mixing (DSM) technology. Cement can be injected into the soil in dry powder or slurry form, which can be classified as dry or wet mixing method, respectively. Cement stabilisation technique is particularly suitable for granular and

clayey soils, which have low plasticity index (Sariosseiri 2008). The soil-cement stabilisation technique has been employed widely to improve the embankment foundation, or to support the excavations in form of retaining walls or to prevent loose ground from liquefaction (Chai and Carter 2011). According to Porbaha (1998), the cement treated clay generally has higher strength, lower permeability and controlled deformation as compared to the un-treated soft soil. The properties of the cement treated clay are improved mainly due to the chemical reaction between cement and the soil particles to enhance the structure of the soil-cement matrix (Kamruzzaman et al. 2006). However, the cement treated soil becomes more brittle as compared to the un-treated soil due to addition of cement. The behaviour of cement treated soil is observed to be similar to over-consolidated soil as the effect of cement changes the un-treated soil from the normally-consolidated condition to the over-consolidated state (Bergado et al. 1996). Hence, the brittle behaviour of cement treated soil is unfavourable as the strength suddenly drops to the residual strength (Consoli et al. 1999; Lorenzo and Bergado 2004). It can be noted that the addition of cement increases the tensile capacity of the soft soil (Das and Dass 1995; Porbaha et al. 2000), but the main focus of this study is on the shear strength of the cement treated soil. Thus, in the following sections, the engineering properties of cement treated soil and its behaviour under different conditions are reviewed. Moreover, the existing constitutive models to simulate the behaviour of cement treated soil are reviewed and discussed.

## **2.2. Behaviour of Cement Treated Soil**

### **2.2.1. Hardening Mechanisms**

According to Porbaha (1998), stabilising agents known as “binders”, can be produced in dry or slurry form prior to mixing with soil. The improvement is mainly due to the chemical interaction between soil and cement. As proposed by Diamond and Kinter (1965) and confirmed by several other researchers such as Chew et al. (2004), Kamruzzaman et al. (2006) and Porbaha (1998), the three major categories of reactions, expected in the process of mixing a stabiliser with clay, are: (i) dehydration process, (ii)

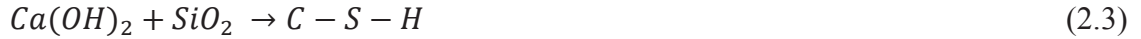
ion exchange or flocculation and (iii) pozzolanic reaction. Fang (2006), Lorenzo and Bergado (2006), and Prusinski and Bhattacharja (1999) explained that the hydration process occurs rapidly when cement is mixed with pore water of the soil to form primary cementitious products such as hydrated calcium silicates ( $C_2SH_x$ ,  $C_3S_2H_x$ ), hydrated calcium aluminates ( $C_3AH_x$ ,  $C_4AH_x$ ) and hydrated lime  $Ca(OH)_2$ , where C, S, A and H stand for Calcium ( $CaO$ ), Silicate ( $SiO_2$ ), Aluminate ( $Al_2O_3$ ) and water ( $H_2O$ ), respectively. According to Prusinski and Bhattacharja (1999), the hydrated calcium silicates (C-S-H) and hydrated calcium aluminates (C-A-H) play the most important role as they provide structure in the soil matrix, which consequently improves the strength of the soil. The following chemical formulations describe the primary hydration reactions (Bergado et al. 1996; Prusinski and Bhattacharja 1999):



Moreover, according to Lea (1956), while the hydrated lime is deposited in a separate crystalline solid phase, the formation of above mentioned hydrated calcium aluminates and hydrated calcium silicates are the main cementing products. During hardening, the cement particles interact with the adjacent cement grains to form a hardened matrix, encasing soil particles (Bergado et al. 1996).

The second process involves the cation exchange, followed by flocculation of soil-cement particles. The bivalent calcium ion ( $Ca^{2+}$ ) released from the hydrated lime, causes hydration of cement which subsequently rises the pH value of pore water in the soil (Fang 2006). It should be noted that, high pH value is important for further pozzolanic reactions. With cation exchange, flocculation of fine clay particles occurs, forming larger aggregate of clay particles. The cement hydrates (hydrated calcium silicates (C-S-H) and hydrated calcium aluminates (C-A-H)) serves as bridges and provides bonding between aggregates of clay particles through cementation (Prusinski and Bhattacharja 1999). Furthermore, the cementing products result in the dissociation of calcium ions which then react with silica and alumina in the soil to form pozzolanic products (Diamond et al. 1963; Lorenzo and Bergado 2006). This secondary cementing products, stabilising the soil and increasing the strength of treated soil with time, is also

reported by Porbaha et al. (2000). The basic pozzolanic reactions are given below as (Prusinski and Bhattacharja 1999):



### **2.2.2. Formation of Structure and Effect of Cementation Degradation**

The main aim of the inclusion of cement is to improve the strength and reduce the compressibility characteristics of soft clay, owing to the formation of cementation bonds (Ismail et al. 2002; Kamruzzaman et al. 2009; Lo and Wardani 2002; Tremblay et al. 2001; Uddin et al. 1997). The structure of soil-cement matrix plays a critical role in the strength improvement of the cement treated clay. The formation of structure results to a stronger soil-cement matrix and higher cementation bond strength, subsequently an increase in strength of the cement treated clay. The effect of cementation varies depending on a number of factors such as cement content, water content, curing time and based soil mineralogy. However, when the cement treated clay is subjected to various types of loadings, the effect of cementation degrades due to the breakage of cementation bonds, causing micro-and-macro cracks. Moreover, in constitutive modelling, it is important to investigate the effect of structure and its degradation at macro and micro-structural levels. The following section describes the process of structure formation and the degradation of cementation during loading of the cement treated clay.

#### **2.2.2.1. The Formation of Structure**

Baudet and Stallebrass (2004), with reference to Mitchell and Soga (1976), mentioned that the structure of a soil consists of two components, namely fabric and bonding. The fabric component refers to the soil particles arrangement while the

bonding describes the forces between soil particles. As mentioned in Section 2.1, due to the chemical reaction between cement and clay particles, large particle clusters form strongly bonded structure within the cement treated clay matrix. According to the description of structure provided by Baudet and Stallebrass (2004), the fabric component of clay structure refers to the stable arrangement within the structure of treated clay and remains unaffected by any cementation degradation, as confirmed by Kamruzzaman et al. (2009) and Suebsuk et al. (2010). Moreover, the bonding component is strengthened by the formation of cementation bonds which can be destroyed via loading. According to Huang and Airey (1998) and Rotta et al. (2003), the structure of naturally cemented soils possesses anisotropic properties due to various geological processes creating cementation bonds. However, the degree of anisotropy in cemented soils is reduced as a result of cementation degradation as suggested by Suebsuk et al. (2010). Naturally cemented soils often have variable densities and degrees of cementation presenting difficulties in studying the fundamental behaviour without disturbing the cementation. To overcome such difficulties, many researchers such as Kamruzzaman et al. (2009), Rotta et al. (2003) and Suebsuk et al. (2010) used artificially cemented soils in their studies. Moreover, Huang and Airey (1998) reported that the properties of artificially cement treated soils are comparable to naturally cemented soils. Furthermore, the variation of mechanical properties of artificially cemented soils can be reasonably considered to be isotropic, as suggested by Suebsuk et al. (2010). Cotecchia and Chandler (2000) further suggested that the level of bonding, geological history, creep and post deposition bonding could contribute to the structure of the clay.

The effects of cementation on the pre-and-post failure behaviours of cement treated clays can be observed at microstructural level through X-ray diffraction (XRD) and scanning electron microscopy (SEM) images. Kamruzzaman et al. (2009) explained the structuration (formation of structure due to cementation) and destructuration (due to cementation degradation) phenomena by analysing SEM images of Singapore marine clay treated with different cement contents. Figures 2.1 and 2.2 display the SEM images of un-treated Singapore marine clay and clay treated with 10% cement at 28 day curing time, respectively. They mentioned that while the untreated clay exhibits an open type of microstructure, with thin and flat clay particles spreading over a large area, the cemented clay shows evidence of flocculated structure with large treated particle

clusters interspersed by large openings. At the same time, while the flocculated structure becomes more evident as the cement content increases, the platy shape of the structure becomes less evident as also observed by Locat et al. (1990) and Yang et al. (2013). Moreover, Sasanian (2011), during analysing SEM images of Nanticoke clay treated with 8.7% cement, observed the formation of precipitated crystals and bonded contacts between clay particles during the process of cementation, as displayed in Figure 2.3. Furthermore, according to observations on naturally structured soils, Yin et al. (2009) explained that the surface forces such as electrostatic and chemical forces attract clay particles and pull them together to form particle-clusters. The clusters continue to grow in size until their weight, due to gravitation is larger than the inter-particle surface forces. At this time, the clusters stop growing in size and interact with each other mainly through mechanical forces.

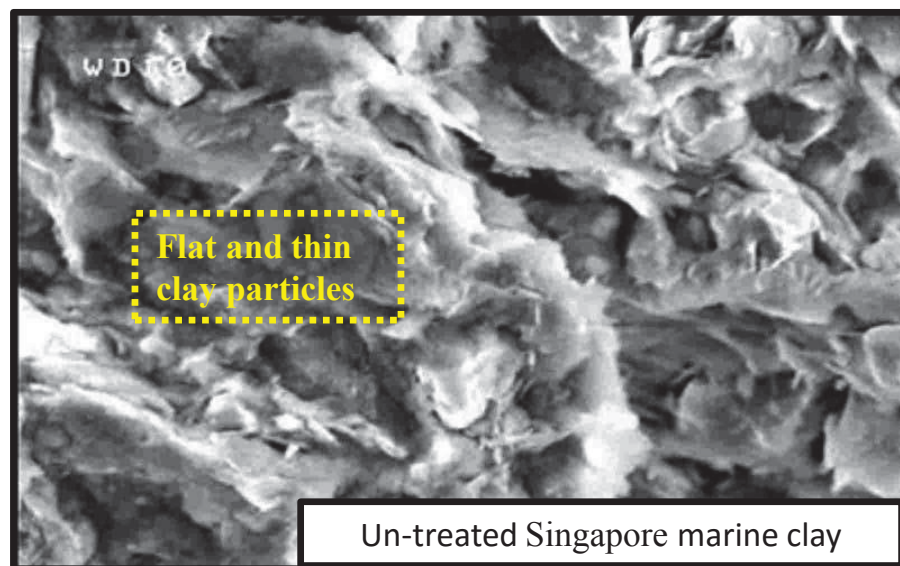


Figure 2.1: SEM image of untreated clay at 5,000 magnification (Kamruzzaman et al. 2009)

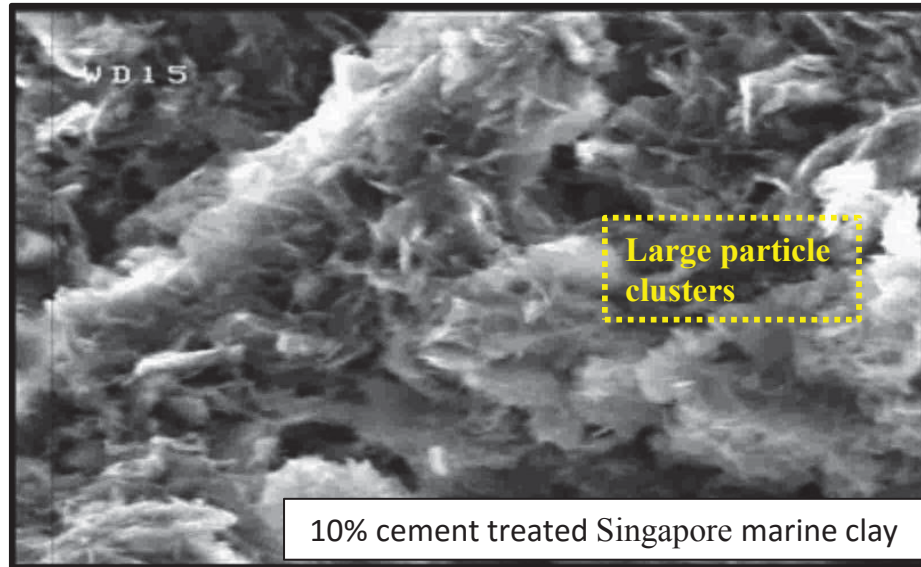


Figure 2.2: SEM image of 10% cement treated clay at 28 day curing at 5,000 magnification (Kamruzzaman et al. 2009)

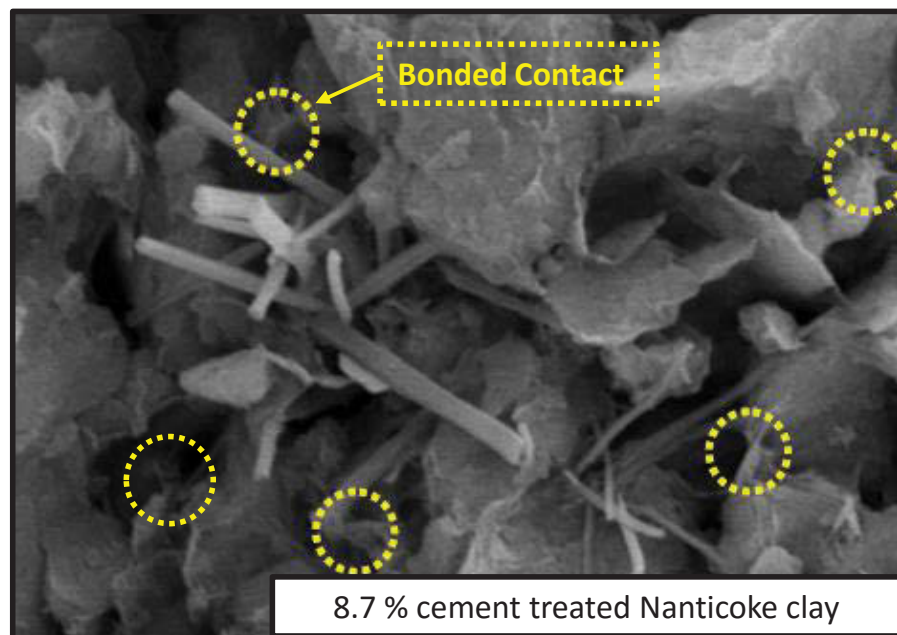


Figure 2.3: SEM image of Nanticoke clay treated with 8.7% cement at 15,000 magnification (Sasanian 2011)

### 2.2.2.2. Effect of Cementation Degradation

Due to the effect of cementation, clay particles interact to form clusters and the creation of the soil structure becomes evident. However, the effect of cementation degradation can be observed when the sample undergoes isotropic consolidation and shearing in the triaxial tests. In the Critical State framework, it is widely accepted that the void ratio (referred to as state variable,  $e$ ) is a function of applied mean effective stress or effective confining pressure. In comparison to the natural clay, the cement treated clay needs higher mean effective stress to reach the same state variable ( $e$ ), due to the formation of the structure. Yin et al. (2009) further explained that clay is regarded as an aggregate of clusters and a representative volume of clay is deformed by compressing all clusters. Hence, the overall deformation can be described as the average deformation of local contact planes in all orientations. Moreover, void ratio is observed to change with the value of the contact number per unit volume as confirmed by SEM images from Kamruzzaman et al. (2009). Furthermore, the micro-variable (the inter-cluster parameter in cementation bonds) is reasonably considered as a function of the macro-state because the behaviour of clusters is influenced by the density or void ratio of the specimen as suggested by Yin et al. (2009). According to Kamruzzaman et al. (2009) when the cement treated sample is stressed at a high consolidation (effective confining) pressure, beyond the yield stress of the cement treated clay, plastic deformation occurs associated with cementation degradation (breaking of cementation bonds) with the change in void ratio. At this stage, the large treated particle clusters collapse with gradual reduction in the void space until there is a significant reduction of inter-aggregate pore spaces, resulting in the reduced void ratio. Furthermore, during isotropic consolidation, the clusters of clay particles are compressed and rearranged due to the increase in confining pressure that brings them closer and results to an increase in the strength (Horpibulsuk et al. 2004). Thus, the compressibility of the cement treated clay relies mainly on the arrangement or fabric of soil-cement clusters which cannot be destroyed during isotropic loading (Kamruzzaman et al. 2009).

Several researchers (e.g. Horpibulsuk et al. 2010; Liu and Carter 2002; Suebsuk et al. 2010; Yin et al. 2009) have investigated the effects of shear stresses on the cementation degradation, particularly when plastic shear deformation occurs. In

addition, Kamruzzaman et al. (2009) observed that when the treated sample is loaded or deformed under shearing, the cementation bonds gradually break under the applied pressure. Furthermore, when the treated sample is loaded beyond the peak strength, crushing of cementation bonds occurs. According to Kolovos et al. (2013), during loading, the contact forces between particles increase resulting in development of micro-cracks. It should be noted that, when micro-cracks appear, the strength of cementation bonds is gradually reduced. Furthermore, the cracks continue to extend until some stage where the edges of micro-cracks collide and larger cracks (macro-cracks) are formed. As the applied load increases, macro-cracks reach the edge of the sample leading to a failure as explained by Kolovos et al. (2013). Further explanation provided by Suebsuk et al. (2010) reveals that the destructuring process depends on the plastic strains which occur mainly after yielding due to volumetric and shear deformations. However, Horpibulsuk et al. (2004) suggested that the shear resistance induced by the cementation bonds is still present, even when the breaking of cementation bonds has occurred. Suebsuk et al. (2010) further explained that the damage to the cementation bonds caused by the shear deformation before failure is insignificant because the change in the plastic deviatoric strain associated with shearing is very small prior to the shear failure. However, for post failure state where the cementation bonds begin to be crushed, large plastic deformations occurs while the shear resistance reduces.

In Figure 2.4, the SEM image in the shear plane for 10% cement treated clay sample sheared at effective confining pressure of 1000 kPa shows negligible clusters remaining. However, as reported by Kamruzzaman et al. (2009) some small clusters still appear outside the failure plane. Therefore, it can be concluded that during isotropic consolidation, the degradation of cementation bonds may not be completed as some small clusters may still be present requiring further load to be completely crushed. In addition, the rearrangement of clay particles during loading affects the void ratio at the final critical state (Liu and Carter 2003).

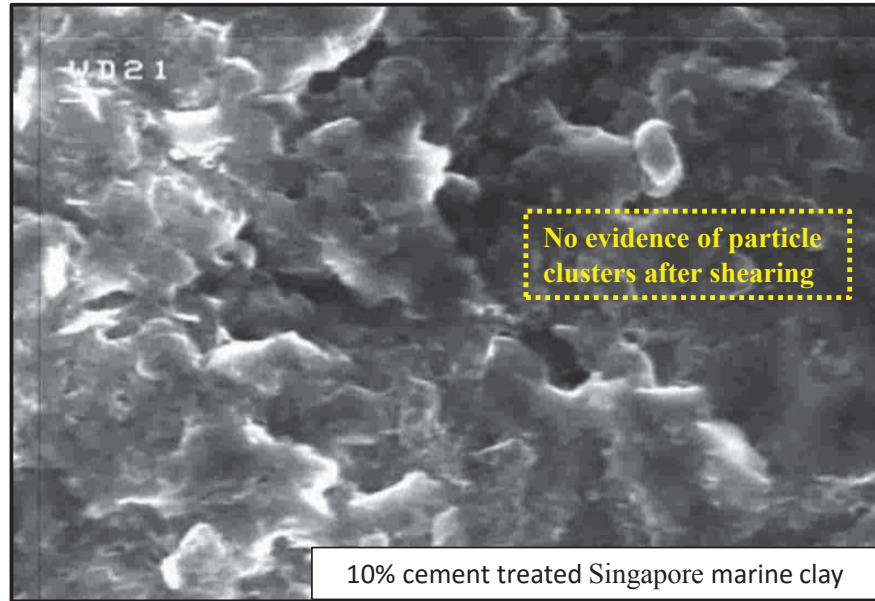


Figure 2.4: SEM image at shear band of 10% cement treated sample under confining pressure of 1000 kPa at 28 days curing (Kamruzzaman et al. 2009)

### **2.2.3. Engineering Properties of Cement Treated Clay**

In this section, the engineering properties of clay treated with cement are reviewed. They are the unconfined compressive strength, the compressibility behaviour, and the triaxial compression behaviour. Moreover, factors affecting the strength of cement treated clay, such as cement content, water content, soil type and curing time are also discussed in detail.

#### **2.2.3.1. Unconfined Compression Strength (UCS)**

Unconfined compression test is a common test to estimate the shear strength of cement treated soil. Generally, the peak shear strength of treated sample is greatly enhanced as compared to the untreated sample due to the effect of cementation bonds. Figure 2.5 displays a series of unconfined compression tests on treated Bangkok soft clays performed by Uddin et al. (1997) with differing cement contents (ranging from

0% to 40%) and compares them with the untreated sample. The stress of cement treated soil in unconfined compression tests increases dramatically to the peak unconfined compressive strength ( $q_u$ ), and then drops abruptly to the residual strength as observed by a number of researchers (Balasubramaniam et al. 1998; Lorenzo and Bergado 2006; Tan et al. 2002; Uddin et al. 1997; Yin and Lai 1998). The behaviour of cement treated soil indicates brittle behaviour through a reduction in strength at the post-peak state, which is typical of over-consolidated behaviour as suggested by Panda and Rao (1998). In contrast, the behaviour of untreated sample is typical of normally consolidated soil where the stress-strain curve approaches the state at which the axial stress remains constant for continuing strains, as observed in Figure 2.5.

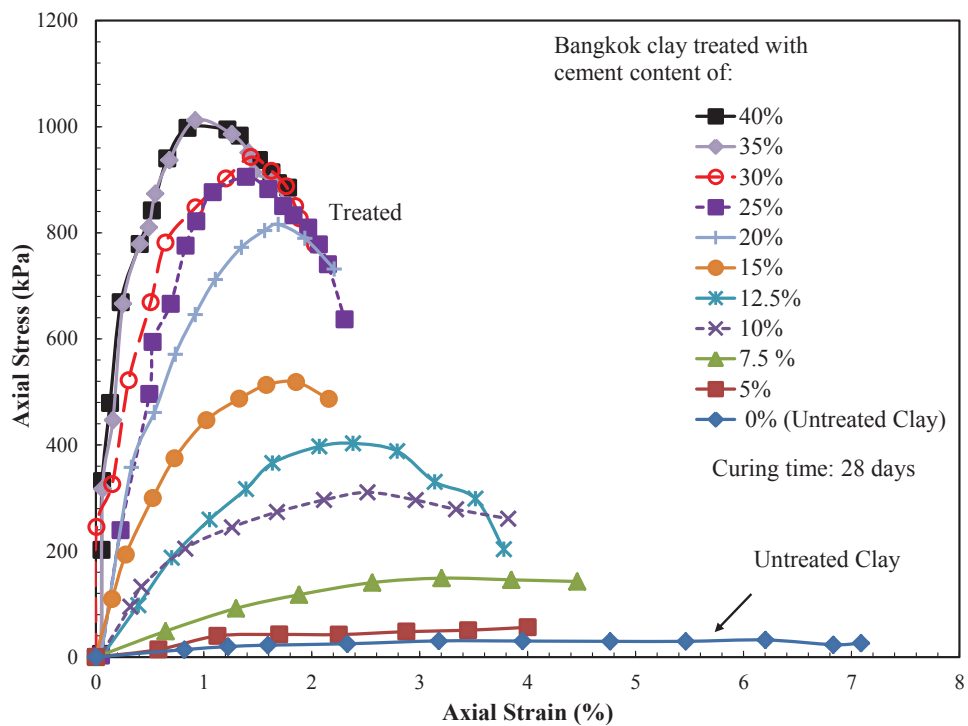


Figure 2.5: Effect of cement content on UCS of the un-treated and treated Bangkok soft clays at 28 days curing (after Uddin et al. 1997)

### **2.2.3.1.1. Factors Affecting the Unconfined Compressive Strength**

Various factors affecting the strength development of cement treated soil have been identified. Key factors are cement content, water content, curing time and type of soil (Porbaha et al. 2000; Tan et al. 2002). Other factors such as the effect of stabilising reagent and effect of curing temperature cannot be ignored. However, in the following parts, only the main factors contributing to the UCS strength of cement treated clay are discussed.

#### **2.2.3.1.1.1. Effect of Cement Content**

According to Lorenzo and Bergado (2006) and Tan et al. (2002), for a certain water content, the increase in cement content generally results to an increase in the unconfined compression strength ( $q_u$ ). Uddin et al. (1997) suggested that, the addition of cement content ranging from 10% to 20% provides the most effective cementation contribution as compared to lower cement content. As shown in Figure 2.5, for cement content below 10%, the increase in the strength is not significantly evident and  $q_u$  is not pronouncedly obtained. Moreover, the samples at a cement content below 10%, show ductile behaviour which is similar to the behaviour of un-treated clay, as also observed in the UCS tests conducted on treated Singapore marine clay by Chew et al. (2004). Furthermore, the cement content beyond 20% leads to a higher initial stiffness of the soil which results in the occurrence of failure at smaller strains. The samples with high cement content beyond 20% generally show more brittle behaviour with sudden drop in the strength at the post peak state. The brittle behaviour of the treated soil with high cement content is similar to that of highly structured or sensitive soils (Chew et al. 2004; Leroueil and Vaughan 1990). As discussed above, the increase in strength of cement treated clay is mainly due to the pozzolanic reactions which provide bonding between cement and clay particles. Furthermore, as a result of cementation bonds, stronger matrix is formed which allows the cement treated soil to sustain a higher stress as compared to un-treated clay.

### **2.2.3.1.1.2. Effect of Curing Time**

Lorenzo and Bergado (2006) suggested that curing time plays a significant role in the unconfined compressive strength development of cement treated clay since the cement hydration process and subsequently the pozzolanic reactions can further occur after a few months or years, subjected to the availability of water. As shown in Figure 2.6, it is observed that increasing the curing time (up to 24 weeks) leads to an increase in shear strength for all the cement contents (Uddin et al. 1997), as also reported by Xiao and Lee (2008). Furthermore, Kamruzzaman et al. (2009) detected that the increase in shear strength of the cement treated clay also occurs at 365 days curing time due to a significant diffusion of  $\text{Ca}^{2+}$  within the soil matrix. However, the rate of increase in shear strength due to the effect of curing time varies depending on the cement content, as observed by Chew et al. (2004) and Endo (1976). Figure 2.7 shows the effect of curing time on the compressive strength of Tokyo Bay clay treated with different cement contents (from 5% to 20%), conducted by Endo (1976). They showed that as curing time increases, the gain in strength is noticeable with cement content beyond 10%, while steady rate is observed with cement content below 10%. Overall, for a prolonged period of curing time, stronger soil matrix can develop within the soil due to continuous chemical reactions, leading to an increase in strength of the treated soil.

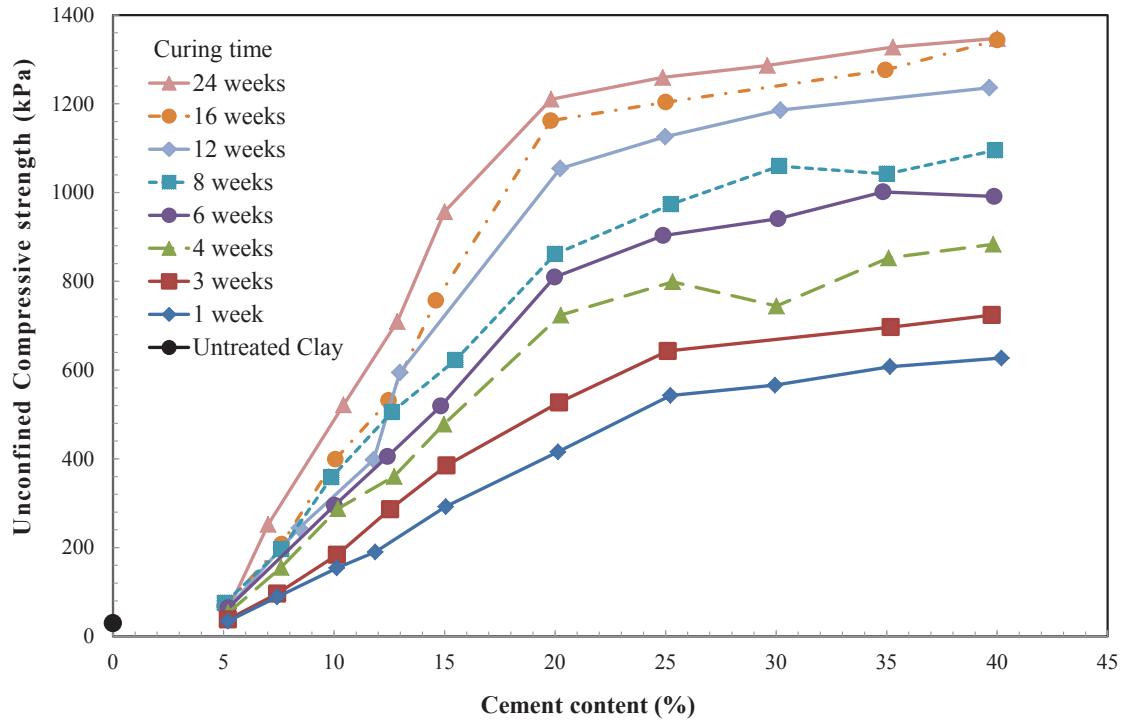


Figure 2.6: Effect of cement content and curing time on the UCS of cement treated clay (after Uddin et al. 1997)

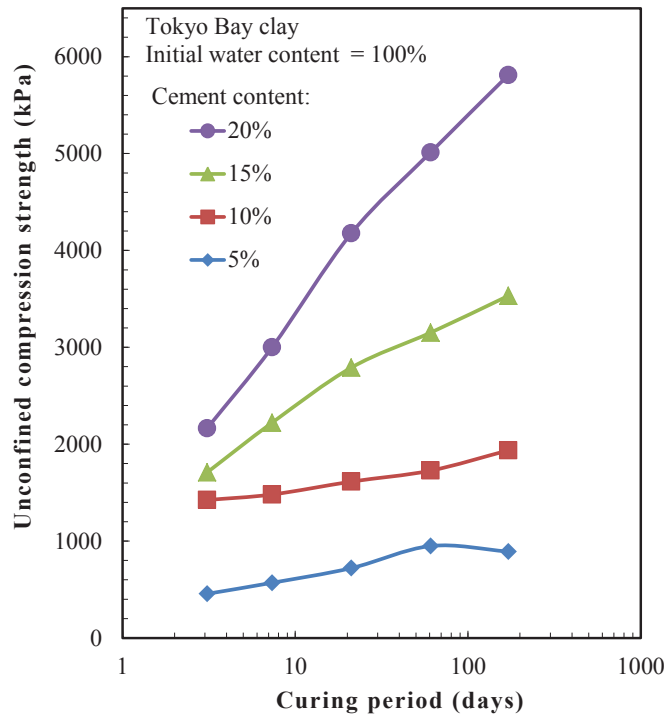


Figure 2.7: Effect of curing time on the UCS of treated clay with differing cement content (after Endo 1976)

### **2.2.3.1.1.3. Effect of Water Content**

In contrast to the effect of cement content and curing time, increasing water content in the soil-cement mixture leads to a reduction in strength of the cement treated clay, for a particular cement content and curing time, as suggested by Chew et al. (2004), Endo (1976) Porbaha et al. (2000), Tan et al. (2002), and Uddin et al. (1997). Moreover, Lorenzo and Bergado (2006) found that the UCS of cement treated clay decreases with remoulding water content well different to the liquid limit of the soil as shown in Figure 2.8. This figure compares the UCS results conducted by Lorenzo and Bergado (2006) on 10% cement treated Bangkok soft clay with differing remoulding water content where the liquid limit was measured to be 103%. The water content at the liquid limit is observed to be optimum which results in highest UCS. It can be explained that, the formation of soil-cement clusters is mainly controlled by the amount of cement required for the occurrence of chemical reactions (Lorenzo and Bergado 2004). The amount of water is consumed by the amount of cement to produce cementing products such as (C-S-H) and (C-A-H). When the soil is remoulded with water content less than the liquid limit of the soil, water is not sufficiently available for the cement hydration process. Moreover, for given cement content and the curing period, increasing the water content results in excessive amount of water in the pore space between soil-cement clusters. Thus, the treated soil matrix becomes less compacted and consequently less strength is expected.

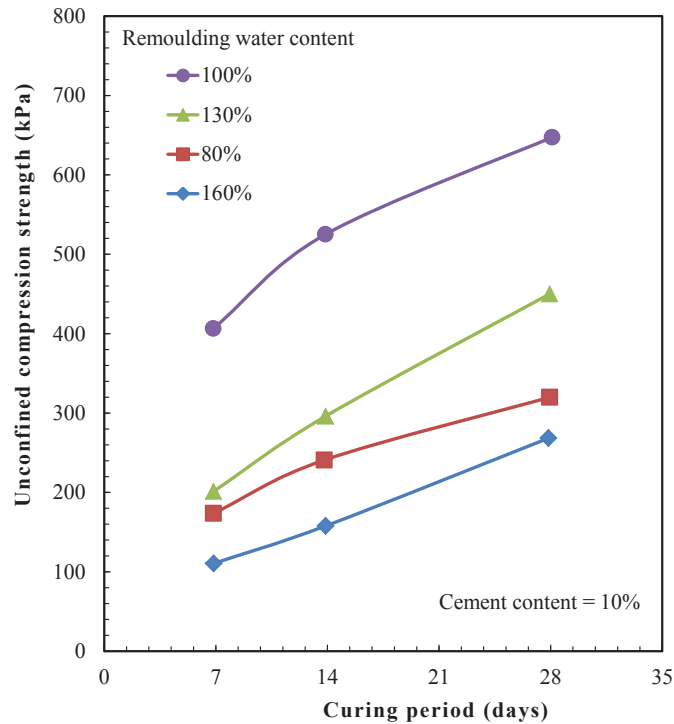


Figure 2.8: Effect of remoulding water content on UCS of treated clay at differing curing period (after Lorenzo and Bergado 2006)

#### 2.2.3.1.1.4. Effect of Different Types of Soil

According to Porbaha et al. (2000), properties of treated soil are greatly influenced by the physical and chemical properties of the base soil, such as pH of pore water, organic content, grain size distribution, water content, Atterberg limits and type of clay minerals. In particular, Porbaha et al. (2000) and Chew et al. (2004) reported that, kaolinite is more reactive with pozzolanic reactions than illite due to poor crystallinity of illite. Moreover, the process of cement hydration may be decelerated in soils with high organic or sulphates content (Porbaha et al. 2000). However, a finding from a series of unconfined compression tests conducted on three different types of Singapore clays treated with cement by Tan et al. (2002), suggested that the clay with higher organic content, sulphate content and pH value (e.g Eunost clay) attained the highest strength as compared to other clays at the same water content, cement content and curing time. The properties of different types of clays in the study by Tan et al.

(2002) is summarised in Table 2.1 while the results from UCS test on these clays treated with 20% cement is displayed in Figure 2.9.

Table 2.1. Properties of three different type of soft Singapore clays (after Tan et al. 2002)

Properties	Eunos	City Hall	Singapore Art Centre (SAC)
Specific gravity	2.61	2.61	2.62
Natural water content	66.23	61.52	57.62
Liquid limit	71.89	65.12	72.63
Plastic limit	31.89	30.03	30.82
Organic content	2.09	1.66	1.37
Chloride content	0.38	0.3	1.10
Sulphate content	1.70	1.60	0.92
pH	7.4	7.4	6.5

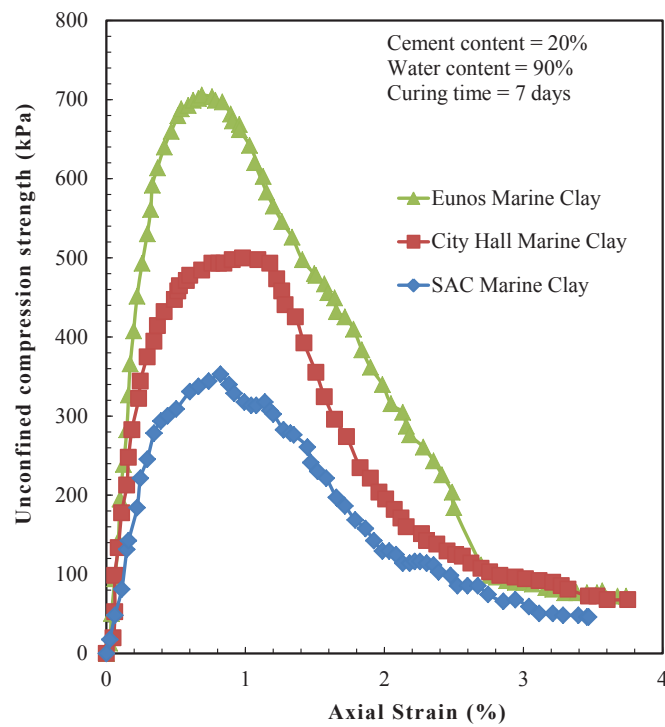


Figure 2.9: Effect of different types of Singapore marine clay treated with 20% cement in UCS test (after Tan et al. 2002)

### **2.2.3.2. One Dimensional Compressibility Behaviour**

The consolidation characteristics of the cement treated clay are normally used for settlement analysis. Oedometer consolidation test is a common test to determine the yield stress, compression indices, and reduction in the void ratio as the consolidation pressure increases. In this section, the compressibility behaviour of cement treated clay is discussed together with various factors affecting the yield stress (or apparent pre-consolidation pressure) such as cement content, water content and curing time.

#### **2.2.3.2.1. Effect of Cement Content**

Kamruzzaman et al. (2009) performed a series of oedometer consolidation tests on both treated and untreated samples as shown in Figure 2.10. The samples were treated with a range of cement contents varying from 5% to 50% to investigate the effect of cementation on the consolidation behaviour of cement treated clay, particularly the pre-consolidation pressure. At low cement contents (e.g. 5%), the effect of cementation was minimal as there is insufficient amount of cement to interact with the clay minerals to form cementitious products. When the cement content is beyond 10%, the apparent pre-consolidation pressure increases significantly due to the creation of cementation bonds, as also observed by Uddin et al. (1997) on treated Bangkok soft clay. Moreover, the pre-consolidation pressure increases with cement content due to increasing chemical interaction between cement and soil particles. Furthermore, as shown in Figure 2.10, increasing cement content leads to a reduction in the initial void ratio of the cement treated clay. Kamruzzaman et al. (2009) explained that the process of cement hydration and the pozzolanic reactions between the cement with soil particles causes a reduction in water content as cement interacts with water in the soil. Higher amount of cement increases the amount of soil-cement clusters, leading to a more compacted matrix and consequently the initial void ratio reduces.

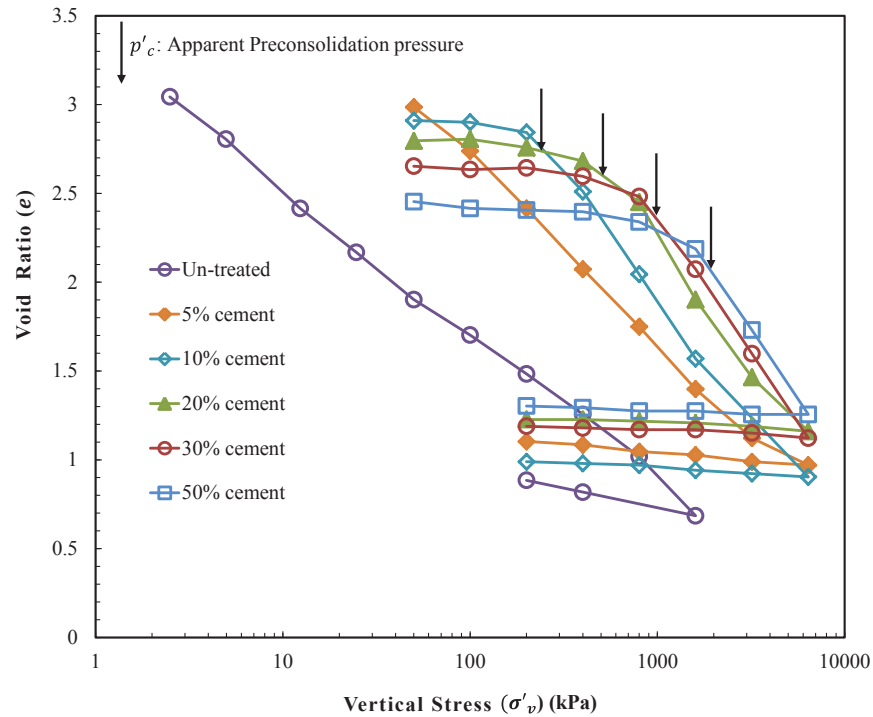


Figure 2.10: Effect of cement content in one-dimensional consolidation of treated clay at 28 days curing in  $e - \log \sigma'_v$  plane (after Kamruzzaman et al. 2009)

When the cement treated clay is stressed up to the pre-consolidation pressure, the reduction in void ratio is minimal owing to the effect of cementation bonds, so the treated sample can sustain a higher pre-consolidation than the un-treated sample, as also observed by Sasanian (2011). However, beyond the pre-consolidation pressure, for all ranges of cement content, significant reduction in void ratio is observed as evident in Figure 2.10. Kamruzzaman et al. (2009) explained that the reduction in void ratio is due to the effect of cementation degradation or breaking of cementation bonds. Moreover, Sasanian (2011) suggested that the process of cementation degradation in cement treated clay is gradual, compared to sudden reduction in naturally bonded clay due to the uniform formation of cementation bonds in the soil-cement matrix. Additionally, Lorenzo and Bergado (2006) suggested that increasing cement content generally results to an increase in the compression index and a decrease in the swelling index as the cement treated clay stiffens.

### 2.2.3.2.2. Effect of Water Content

Figure 2.11 displays one dimensional compression tests performed by Lorenzo and Bergado (2006) on soft Bangkok clays treated with 15% cement content and different remoulding water contents ranging from 100 to 200%. As observed in Figure 2.11, increasing water content results in an increase in after-curing void ratio of cement treated clay, leading to a decrease in the yield stress (Lorenzo and Bergado 2006). Lorenzo and Bergado (2004) explained that the amount of cementitious products formed due to the effect of cementation is governed mainly by the amount of cement, while the role of water is to facilitate this process. Thus, for a certain amount of cement content, excessive amount of water results in loosely packed matrix which leads to a reduction in the apparent cohesion and the yield stress.

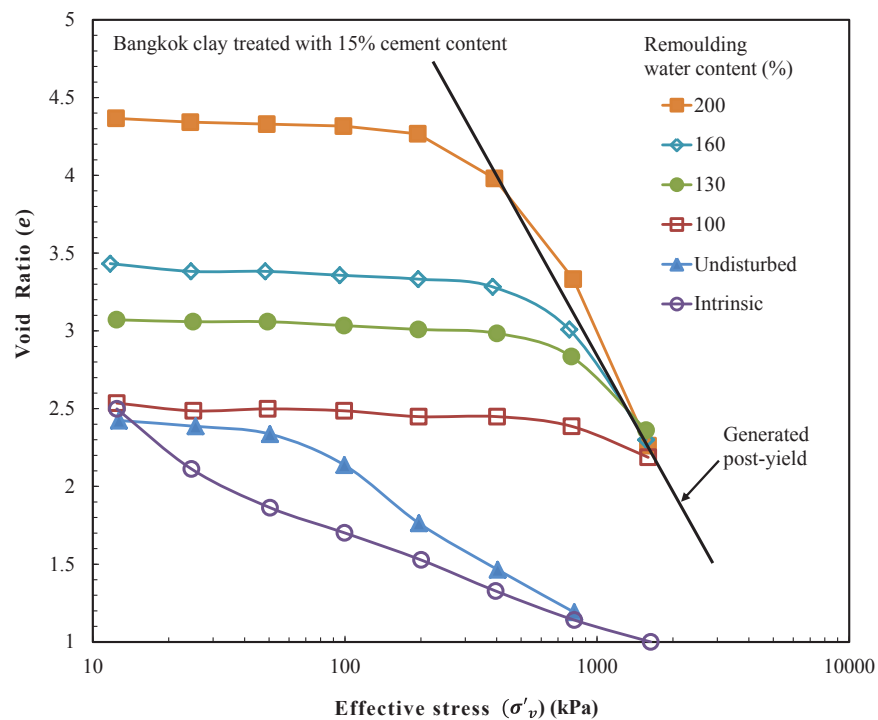


Figure 2.11: Effect of water content in one-dimensional consolidation of 15% cement treated clay in  $e - \log \sigma'_v$  plane (after Lorenzo and Bergado 2006)

### 2.2.3.2.3. Effect of Curing Time

Figure 2.12 shows the effect of increasing curing time on the void ratio and the yield stress of Singapore marine clay treated with 30% cement content (Kamruzzaman et al. 2009). Generally, the yield stress increases with the increase in curing time, in agreement with findings made by Miura et al. (2001) and Uddin et al. (1997). For curing time of 365 days, the preconsolidation pressure is significantly higher than the corresponding values for the samples cured for 28 days only. This suggested that the pozzolanic reaction can take place even up to 365 days. Moreover, the after-curing void ratio reduces as the curing period increases due to the prolonged pozzolanic reactions and the formation of soil-cement clusters.

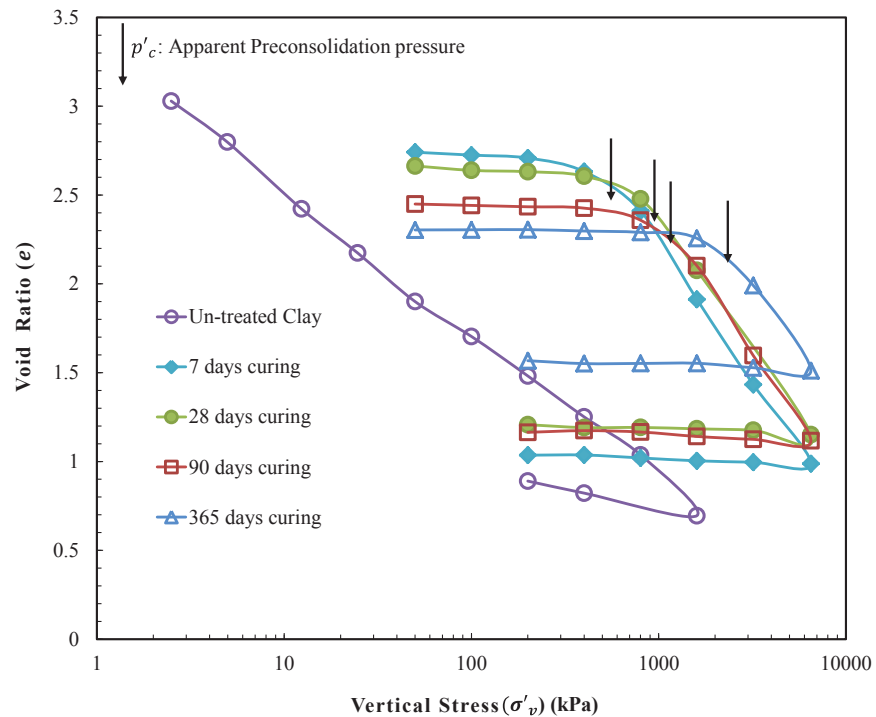


Figure 2.12: Effect of curing time in one-dimensional consolidation of 30% cement treated clay in  $e - \log \sigma'_v$  plane (after Kamruzzaman et al. 2009)

### **2.2.3.3. Behaviour of Cement Treated Clay Under Triaxial Compression Test**

A number of researchers have studied extensively the behaviour of cement treated clays under triaxial conditions, such as Horpibulsuk et al. (2004), Lorenzo and Bergado (2006), Panda and Rao (1998), Sariosseiri and Muhunthan (2009), Uddin et al. (1997), and Yin (2001). The behaviour of cement treated clay is influenced by a number of factors such as effective confining pressure, cement content and curing time as identified by Uddin et al. (1997). Similar to the UCS of cement treated clay, cement content and curing time are the two main parameters controlling the hardening effect of cement treated clay in triaxial compression condition. The effect of increasing cement content and curing time will generally lead to the increase in peak strength of cement treated clay as suggested by Lorenzo and Bergado (2006), Porbaha et al. (2000) and Uddin et al. (1997).

Confining pressure is also an important parameter influencing the behaviour of treated clay (Uddin et al. 1997). As reported by Lorenzo and Bergado (2006), the experimental results from triaxial test show that increasing confining pressure leads to the increase in the deviatoric stress at failure, while this is more significant in higher cement contents. Unlike the ductile behaviour of non-treated soil, the treated soils generally exhibit more brittle behaviour as the stress state approaches the peak strength state and then drop to the residual strength at the post-peak state (Lorenzo and Bergado 2006; and Porbaha et al. 2000). This indicates that the cement treated clay behaviour is similar to over-consolidated soil while the cement treated clay is more structured due to chemically induced cementation (Panda and Rao 1998; and Yin 2001). However, as in triaxial compression test, the effect of confining pressure is quite complex and important. Therefore, it is necessary to discuss the behaviour of cemented clays, using the isotropic compression behaviour, deviatoric stress-strain relationship and the stress path evaluation from available triaxial test results.

### 2.2.3.3.1. Isotropic Compression

A number of laboratory studies under isotropic compression condition on the cement treated clay have indicated that the yield stress of the cement treated clay increases significantly as compared to the un-treated clay (Horpibulsuk et al. 2010; Horpibulsuk et al. 2004; Kamruzzaman et al. 2009). For example, Figure 2.13 displays an isotropic compression results on Ariake clay treated with different cement contents at 180% water content (Horpibulsuk et al. 2004). The mean effective yield stress of the Ariake clay treated with 9% cement content was measured to be 220 kPa while a significant increase in the yield stress was observed when 18% cement content was used (i.e. 1800 kPa). According to Kamruzzaman et al. (2009), the increase in yield stress of cement treated clay is owing to the inclusion of cement, as also suggested by Miura et al. (2001) and Lade and Overton (1989). As illustrated in Figure 2.13, increasing cement content leads to an increase in the yield stress. Due to the formation of soil-cement clusters within the treated soil matrix, the sample is able to sustain a higher yield stress as compared to the un-treated soil at the same void ratio. Furthermore, as explained by Lade and Overton (1989), the high stiffness of the cement treated clay restricts the compressibility during consolidation, leading to the increase in the yield stress.

When the cement treated sample is isotropically compressed up to the initial yield stress, the void ratio changes minimally as observed in Figure 2.13. At this stage, only elastic deformation occurs and the sample is assumed to travel on the swelling/recompression line of the un-treated clay. According to Suebsuk et al. (2010), the volumetric strain of the cement treated clay up to the yield stress is negligible, therefore the cement treated clay can possess a higher void ratio as compared to the reconstituted clay at the same confining pressure in this range. However, as the sample is subjected to increasing confining pressure beyond the initial yield stress, the void ratio reduces significantly. Kamruzzaman et al. (2009) explained the reduction of void ratio at this stage is due to the breaking of cementation bonds as the large particle clusters collapse and the pore space between the clusters reduces significantly. Hence, at this stage, the compressibility of the cement treated clay relies mainly on the fabric component of the soil-cement clusters which cannot be destroyed during isotropic

loading. Furthermore, as soil-cement clusters are compressed during isotropic compression, the effect of confining pressure moves the clusters closer together, thus a higher strength of cement treated clay, in comparison to the un-treated clay at the same void ratio is achieved (Horpibulsuk et al. 2004).

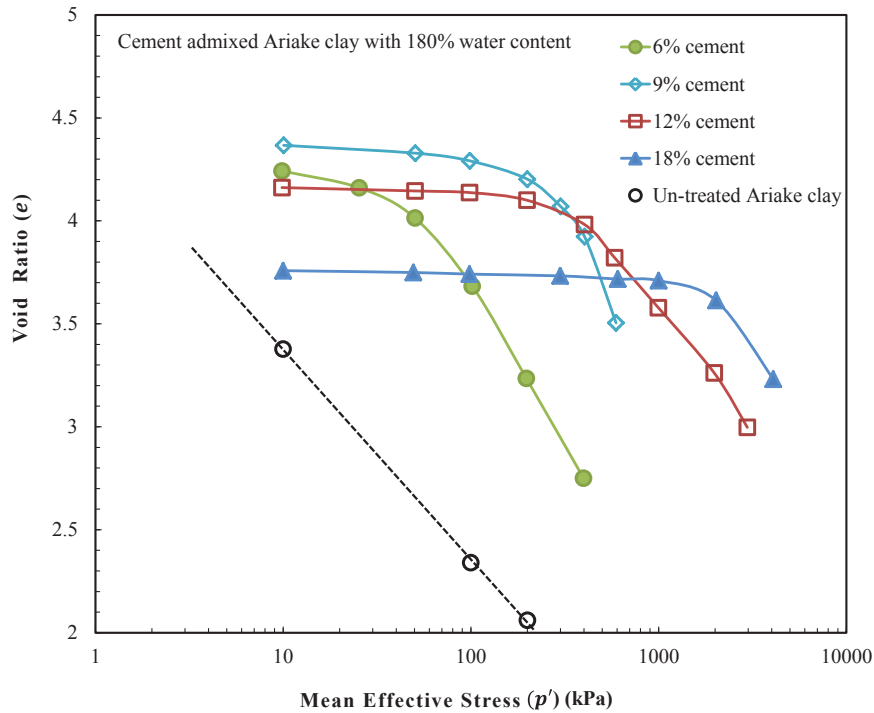


Figure 2.13: Effect of cement content on the isotropic compressibility behaviour of cement treated clay in  $e - \ln p'$  plane (after Horpibulsuk et al. 2004)

### 2.2.3.3.2. Deviatoric Stress-Strain Relationship

Figure 2.14 shows a deviatoric stress-strain relationship of Ariake clay treated with 9% cement content at high initial water content of 180% and at various effective confining pressures lower than mean effective yield stress ( $p'_y = 220$  kPa) (Horpibulsuk et al. 2004). Similar to UCS test, the deviatoric stress under triaxial compression test increases to the peak value and then drops to residual strength value. The peak strength of treated clays is significantly higher than that of untreated samples due to the effect of cementation bonds as observed in Figure 2.14. However, the peak shear strength of all

samples with increasing confining pressures is almost the same. According to Horpibulsuk et al. (2004), the effect of confining pressure, below the mean effective yield stress, is not significant as the state of stress is still within the state boundary surface or the yield surface. Thus, this indicates that when the stress state is within the yield surface, the effect of cementation on the peak deviatoric stress plays a more important role as confirmed by Lorenzo and Bergado (2006).

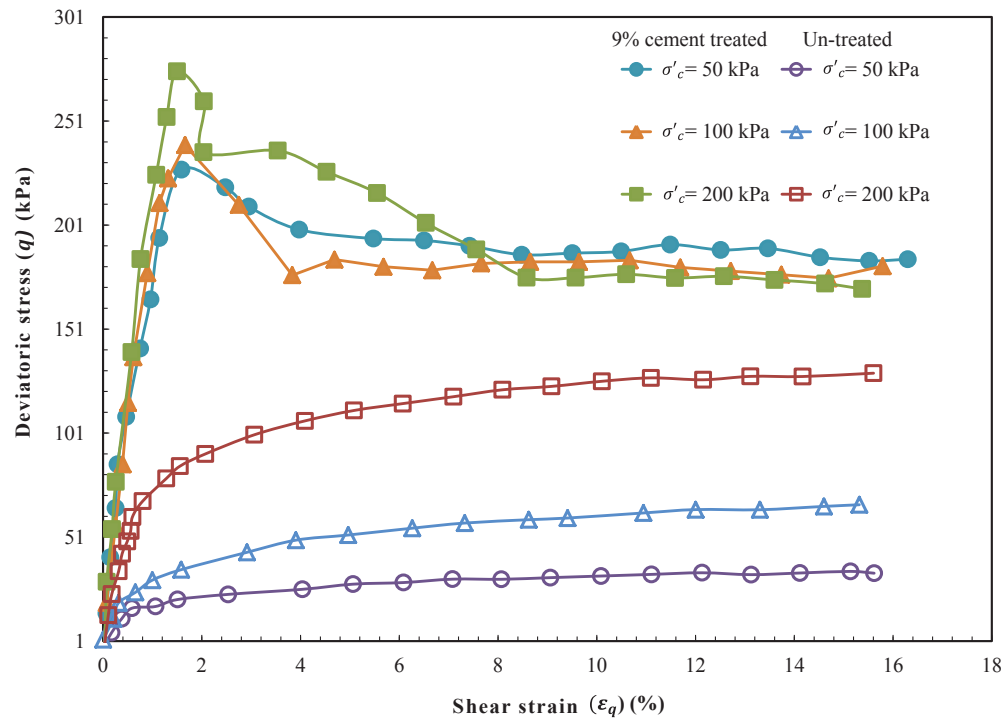


Figure 2.14: Deviatoric stress-strain relationship of un-treated and 9% cement treated samples in  $q - \varepsilon_q$  plane below the initial yield stress (after Horpibulsuk et al. 2004)

Furthermore, Horpibulsuk et al. (2004) also studied the effect of cementation when the effective confining pressure is higher than the mean effective yield stress. As indicated in Figure 2.15, the peak deviatoric stress of cement treated clay is significantly higher than that of the untreated clay due to the effect of cementation bonds. Moreover, as the effective confining pressure increases, the peak shear strength of cement treated clay increases. Horpibulsuk et al. (2004) explained that increasing confining pressures during consolidation brings the soil-cement clusters closer and the soil matrix becomes

compacted as the void ratio reduces, leading to an increase in shear strength of cement treated clay. Moreover, Lorenzo and Bergado (2006) suggested that the peak deviatoric strength of cement treated clay is governed by the bond strength between soil and cement clusters. Furthermore, Kamruzzaman et al. (2009) analysed that, the peak deviatoric stress increases with confining pressure which is due to the volume change during consolidation. At high confining pressure, high volume change is observed owing to the breaking of cementation bonds. However, as shown in Figure 2.15, at the same effective confining pressure, the deviatoric stress of both cement treated and un-treated clay is almost the same at residual values. This indicates that the effect of cementation bonds is completely destroyed during post peak state, thus the behaviour of cement treated clay is identical to that of un-treated clay at this stage.

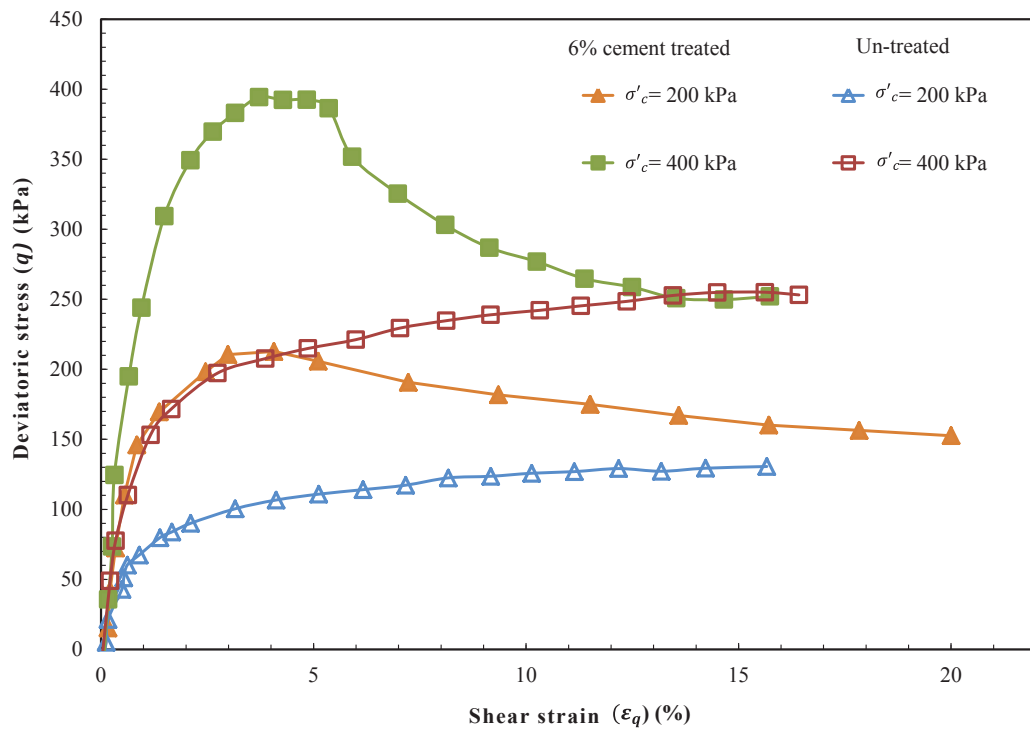


Figure 2.15: Deviatoric stress-strain relationship of un-treated and 6% cement treated samples in  $q - \epsilon_q$  plane (after Horpibulsuk et al. 2004)

Additionally, increasing the effect of curing time leads to an increase in the peak shear strength and subsequently a notable strain softening in the post peak state. As a result of pozzolanic reactions for a prolonged curing period, stronger soil-cement matrix are formed within the clay structure which allows the cement treated sample to sustain a higher stress. In a similar way, increasing cement content results to the formation of higher cementation bonds, thus higher bond strength provides an increase in the peak shear strength. However, a greater strain softening is observed with increasing cement content as shown in Figure 2.16. Kamruzzaman et al. (2009) explained that this behaviour is due to the volume change during consolidation stage which is small for samples with higher cement content.

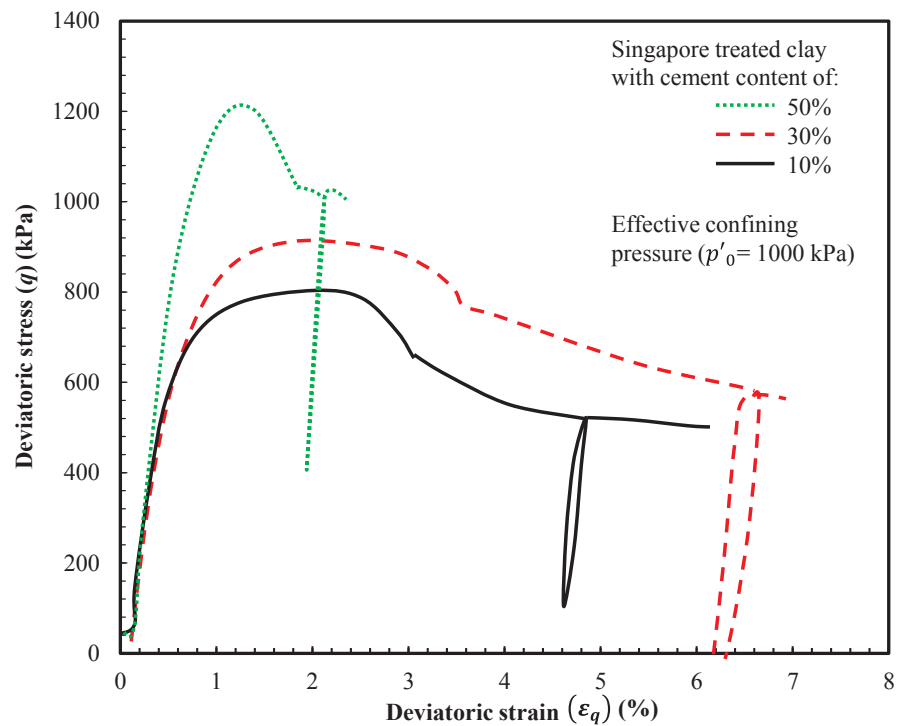


Figure 2.16: Effect of cement content on  $q - \epsilon_q$  relationship of treated clay at 1000 kPa confining pressure and 28 day curing (after Kamruzzaman et al. 2009)

### 2.2.3.3.3. Undrained Stress Path

Typical characteristics of undrained stress paths of the Ariake clays treated with 6% cement are shown in Figure 2.17 (Horpibulsuk et al. 2004). The undrained stress path of the cement treated clay is similar to that of un-treated clay which moves to the left indicating elasto-plastic behaviour. The path continues to seek the peak strength, which passes the Critical State Line (CSL) of un-treated clay. After the peak strength is obtained, the stress path drops to the residual value due to the destructuring of soil-cement clusters and travels on the Critical State Line of un-treated clay. It is observed that, the failure state of cement treated clays occurs at higher deviatoric stress, above the critical state of un-treated samples. However, the residual strength of the treated clay and un-treated clay is almost identical, suggesting that the effect of cementation is completely removed. Furthermore, Horpibulsuk et al. (2004) based on the test results also found that, the cohesion increases with the increase in cement content. Thus, the effect of cementation increases the undrained shear strength, cohesion and enhance the friction angle at failure of the treated clay, as mentioned by Kasama et al. (2000).

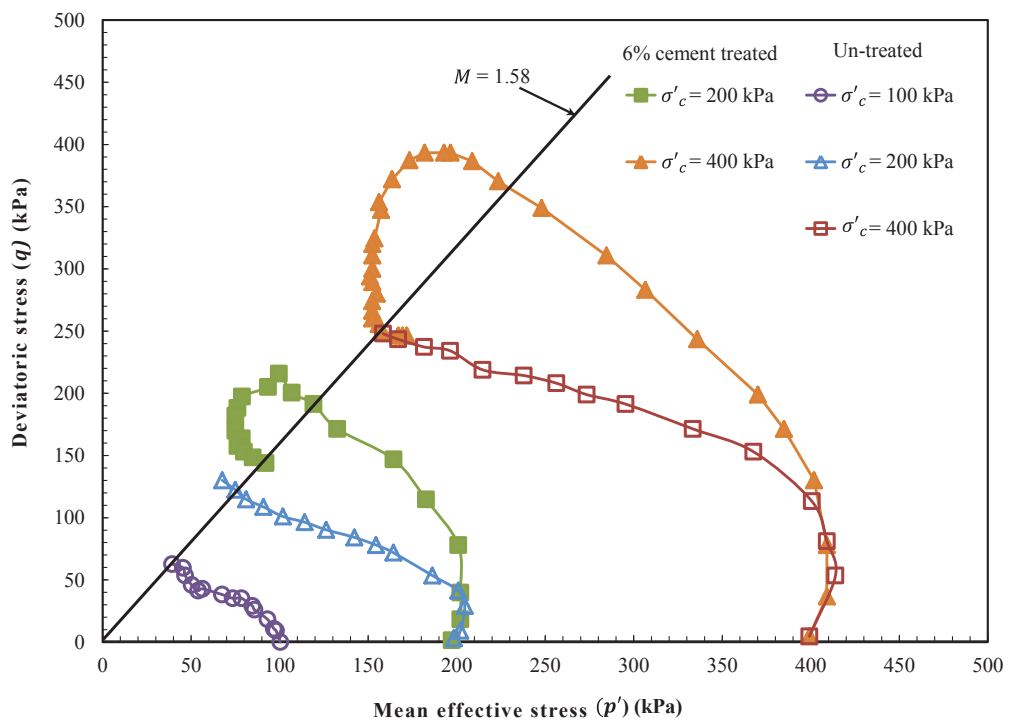


Figure 2.17: Undrained stress paths of un-treated and 6% cement treated sample in  $p' - q$  plane (after Horpibulsuk et al. 2004)

Furthermore, to investigate the behaviour of cement treated clay at higher confining pressures in undrained triaxial conditions, the undrained stress path of 10% cement treated Singapore marine clay with various effective confining pressures is shown in Figure 2.18 (Kamruzzaman et al. 2009). As observed in this figure, for effective confining pressure from 300 – 1000 kPa, which is beyond the initial yield stress ( $p'_y=220$  kPa), the deviatoric stress goes above the Critical State Line (CSL) of un-treated clay, indicating that while breakage of cementation bonds occurs during consolidation, the effect of cementation still remains at shearing stage. When the peak shear strength is obtained, softening occurs as the stress paths move toward the Critical State Line of un-treated clay, due to the crushing of cementation bonds (Suebsuk et al. 2010). In the other hand, when the sample is subjected to shearing with low confining pressure (50-100kPa), less than the initial yield stress, the stress path rises vertically upward, almost parallel to the  $q$ -axis, indicating that the sample was still within the yield surface. Therefore, the effective confining pressure plays an important role on the strength of cement treated clay as the strength increases with confining pressure (Kamruzzaman et al. 2009).

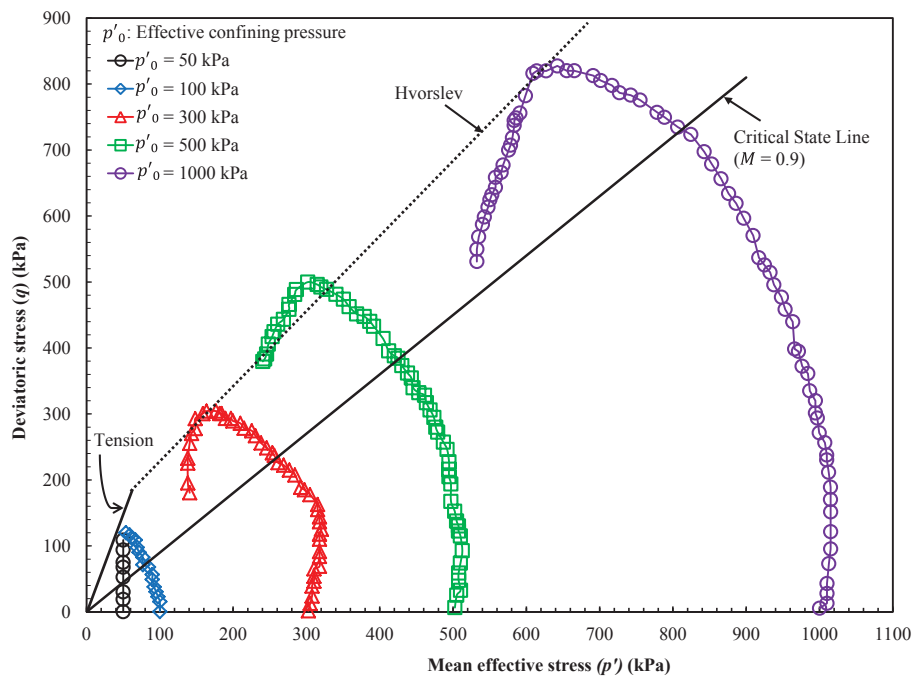


Figure 2.18: Effect of confining pressure on  $q - p'$  relationship of treated clay with 10% cement content and 28 days curing (after Kamruzzaman et al. 2009)

#### **2.2.3.3.4. Excess Pore Water Pressure**

In undrained triaxial shearing, excess pore water pressure is generated, leading to the peak deviatoric stress at low strain level, as compared to higher deviatoric stress at high strain level in drained triaxial shearing (Porbaha et al. 2000). According to Kamruzzaman et al. (2009), increasing confining pressure results to an increase in excess pore water pressure, as displayed in Figure 2.19. At low confining pressures (from 50-100 kPa), the generation of positive excess pore water pressure is small as the sample is sheared at the confining pressure less than the yield stress. On the other hand, when shearing at high confining pressure beyond the yield stress, significant positive excess pore water pressure is generated. At high confining pressure, the excess pore water pressure rises to the peak and then reduces as the sample is undergoing the softening process, reaching the residual strength. This behaviour of the cement treated clay is similar to the lightly over-consolidated soil, as suggested by Kamruzzaman et al. (2009). Furthermore, it is observed that the treated samples show higher excess pore water pressure with increasing curing time and cement content (Figure 2.20). This is due to the effect of cementation and stronger cementation bonds formed at prolonged curing period (Kamruzzaman et al. 2009).

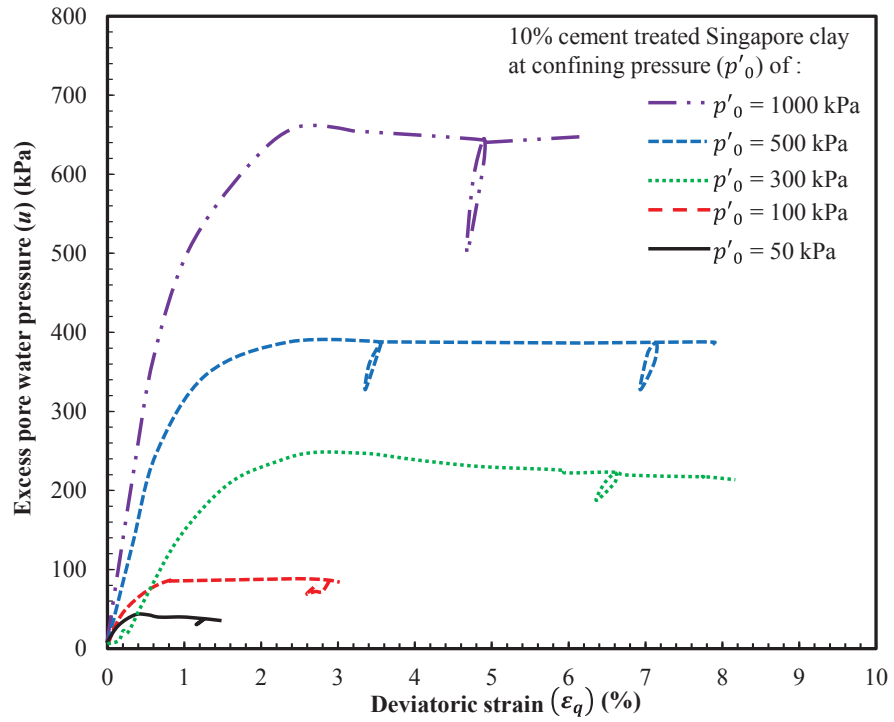


Figure 2.19: Effect of confining pressure on excess pore water pressure response (in  $u - \varepsilon_a$  plane) of treated clay with 10% cement and 28 days curing (after Kamruzzaman et al. 2009)

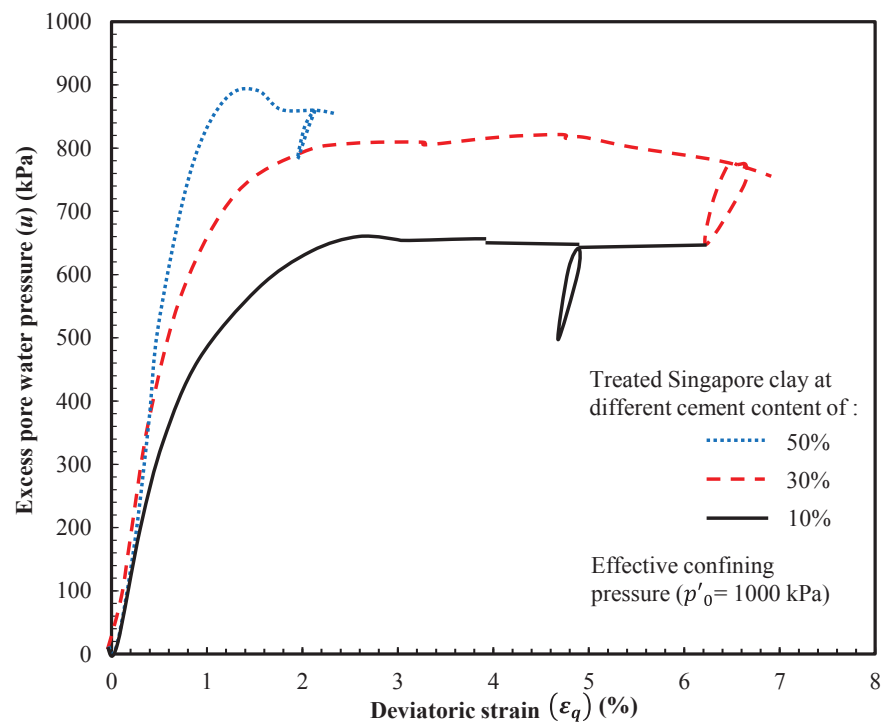


Figure 2.20: Effect of cement content on pore water pressure response of treated clay at confining pressure of 1000 kPa and 28 days curing (after Kamruzzaman et al. 2009)

## 2.2.4. Existing Constitutive Models for Cement Treated Clay

A number of laboratory experiments on the effect of cementation have resulted in several constitutive models for cement treated clays (Horpibulsuk et al. 2010; Kasama et al. 2000; Liu and Carter 2002; Yasufuku et al. 1997). Moreover, the importance of cementation degradation has also led to the advancement of constitutive models to simulate the behaviour of the cement treated clays and the influence of structure, such as those models developed by Baudet and Stallebrass (2004), Kavvadas and Amorosi (2000) and Suebsuk et al. (2010). In this section, the concept of Critical State Soil Mechanics is described, including discussion on a particular example of elastic-plastic model, i.e. Modified Cam Clay (MCC) model. Furthermore, important contributions of the existing constitutive models to simulate the behaviour of cement treated clay are discussed in detail. It should be noted that the existing constitutive models presented in this section can be classified into two main groups, according to their adopted plasticity theories, namely a single yield surface and a bounding surface concept.

### 2.2.4.1. Critical State Soil Mechanics

In the book “Critical State Soil Mechanics”, Schofield and Wroth (1968) defined the Critical State Concept as:

“The kernel of our ideas is the concept that soil and other granular materials, if continuously distorted until they flow as a frictional fluid, will come into a well-defined critical state determined by two equations:

$$q = Mp \tag{2.5}$$

$$\Gamma = v + \lambda \ln p \tag{2.6}$$

where constants  $M$ ,  $\Gamma$ , and  $\lambda$  represent basic soil-material properties, the parameters  $q$ ,  $p$ , and  $v$  are defined in due course.”

The parameters  $q$ ,  $p$ , and  $v$  are the deviatoric stress, mean effective stress and specific volume, respectively which enable the description of the Critical State Line (CSL) as shown in Figure 2.21 .

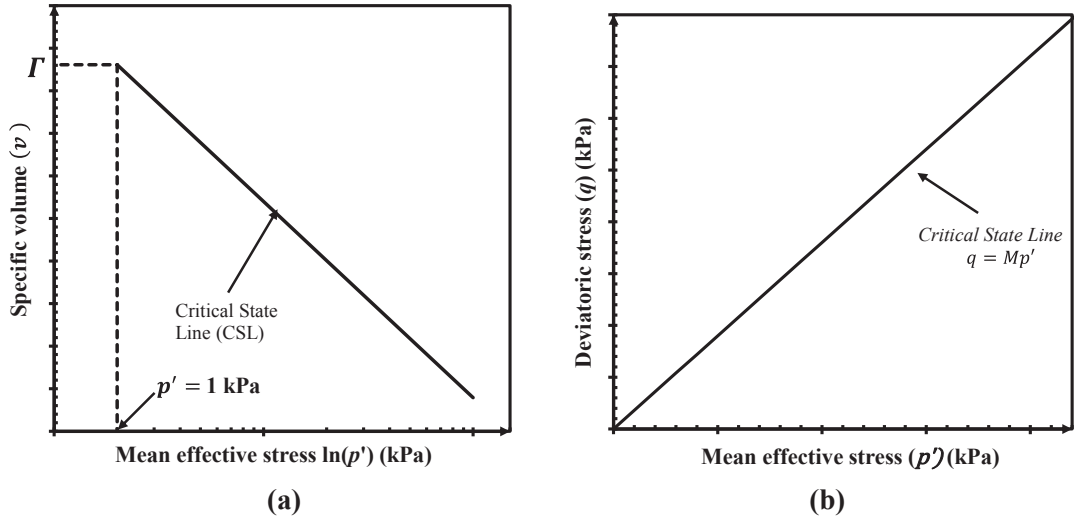


Figure 2.21: Critical State Concept: (a) in  $v - \ln p'$  plane, (b) in  $p' - q$  plane (after Yu 2006)

Yu (2006), referenced to Schofield and Wroth (1968), further explained that the yielding of soils occurs with constant volume and stresses at the critical state, so the behaviour of soil is regarded as frictional fluid. Hence, the elastic and plastic volumetric strain increments are zero since there are no volume changes and constant stress at the critical state. Moreover, the soil will approach a unique critical state line (Figure 2.21), regardless of stress path and the initial condition. The general concept of critical state was supported by various experimental results conducted on different types of soils, such as sand and natural clay (Allman and Atkinson 1992; Been et al. 1991; Novello and Johnston 1995; and Wood 1990).

In case of a triaxial test, the mean effective stress ( $p$ ) and deviatoric stress ( $q$ ) are described to follow the critical state concept as follows:

$$p = \frac{(\sigma'_1 + 2\sigma'_3)}{3} \quad (2.7)$$

$$q = \sigma'_1 - \sigma'_3 \quad (2.8)$$

Furthermore, the volumetric strain ( $\varepsilon_p$ ) and the deviatoric strain ( $\varepsilon_q$ ) take the following form:

$$\varepsilon_p = \varepsilon_1 + 2\varepsilon_3 \quad (2.9)$$

$$\varepsilon_q = \frac{2(\varepsilon_1 - \varepsilon_3)}{3} \quad (2.10)$$

where  $\sigma'_1$  and  $\sigma'_3$  are the axial and the radial effective stress, respectively, and  $\varepsilon_1$  and  $\varepsilon_3$  are the axial and the radial strain, respectively.

#### **2.2.4.2. Review of Modified Cam Clay Model**

The original Cam Clay Model was developed by Roscoe et al. (1963) while the Modified Cam Clay (MCC) model was proposed by Roscoe and Burland (1968). Models developed within the Cam clay families were examples of an elasto-plastic model which established the existence of the yield surface. For any stress excursion inside the yield surface, only elastic response occurs. When the stress state of the soil reaches the yield surface, the response is a combination of elastic and plastic. Moreover, the change in size of the yield surface in Cam Clay models was assumed to be related to the change in volume only, hence it was classified as volumetric hardening models. Wood (1990) suggested that the change in size of the yield surface or hardening rule can be related as a combination of volumetric and distortional effects. The MCC model is widely adopted in numerical simulation and its main difference to the original Cam Clay is the formulation of the yield surface. Hence, the MCC model is discussed in this section.

According to Wood (1990), there are four aspects in developing the elastic-plastic model, including the following descriptions of:

4. Elastic deformation where recoverable deformation occurs.
5. Yield surface or a boundary in which elastic deformation can be described.

6. Plastic potential surface to describe the plastic deformation, including the magnitude and directions of the plastic volumetric and deviatoric strain increments, when the soil is yielding.
7. Hardening rule to link the components of the plastic deformation to the expansion of the yield surface.

In MCC model, the recoverable deformation in elastic region, associated with the changes in mean effective stress ( $p'$ ) and deviatoric stress ( $q$ ), is expressed as follows:

$$d\varepsilon_p^e = \frac{\kappa dp'}{vp'} \quad (2.11)$$

$$d\varepsilon_q^e = \frac{dq}{3G'} \quad (2.12)$$

where  $d\varepsilon_p^e$  and  $d\varepsilon_q^e$  are the elastic volumetric and deviatoric strain increments, respectively.  $\kappa$  is the swelling index,  $v$  is the specific volume and  $G'$  is the shear modulus.

Since the yield surface is the key ingredient in the elastic-plastic model, the MCC model assumed that the yield surface possessed an elliptical shape and took the following form:

$$f = q^2 - M^2[p'(p'_0 - p')] = 0 \quad (2.12)$$

where,  $p'_0$  represents the size of the yield surface and  $M$  is the slope of the Critical State Line (CSL).

Moreover, it was assumed that the plastic potential function ( $g$ ) and the yield surface function ( $f$ ) are identical, hence the model follows an associated flow, obeying the normality condition. Then, the flow rule, defining the direction of the plastic strains vector which is normal to the yield locus, can be derived as:

$$\frac{d\varepsilon_p^p}{d\varepsilon_q^p} = \frac{M^2 - \eta^2}{2\eta} \quad (2.13)$$

where  $d\varepsilon_p^p$  and  $d\varepsilon_q^p$  are the plastic volumetric and deviatoric strain increments, respectively. The stress ratio ( $\eta$ ) is defined as  $\eta = q/p$ .

The soil material in MCC model was assumed to be isotropic, hence it followed the normal compression line in  $p' - v$  plane. Then the hardening rule took the following form:

$$\frac{dp'_0}{d\varepsilon_p} = \frac{vp'_0}{\lambda - \kappa} \quad (2.14)$$

The following general equations to describe the total volumetric and deviatoric strains are as follows:

$$d\varepsilon_p = \frac{1}{v} \left[ \frac{\lambda dp'}{p'} + (\lambda - \kappa) \frac{2\eta d\eta}{(\eta^2 + M^2)} \right] \quad (2.15)$$

$$d\varepsilon_q = \frac{dq}{3G'} + \left( \frac{\lambda - \kappa}{v} \right) \left[ \frac{dp'}{p'} + \frac{2\eta d\eta}{(\eta^2 + M^2)} \right] \left( \frac{2\eta}{M^2 - \eta^2} \right) \quad (2.16)$$

Modified Cam Clay model has been adopted to simulate the behaviour of normally consolidated cohesive soils (i.e. clays) reasonably well by comparing the model predictions with experimental results. Moreover, the model was implemented in numerical modelling of many applications such as embankment or road foundation. However, some limitations of MCC model has been identified by Yu (2006). As MCC model adopted a strain hardening yield surface, the stress at failure of soft soil is significantly overestimated, particularly on the left of the Critical State Line (CSL) in  $p' - q$  plane. Moreover, the associated plastic flow rule used in the MCC model cannot capture the behaviour of loose sand or undisturbed clay in undrained test where the sample reaches the peak shear strength prior to approaching the Critical State. In addition, the MCC model is unable to model the experimental results conducted on granular materials, including softening in dense sands and the response in very loose sand in undrained condition. Gens and Potts (1988) further suggested that models developed in Critical State framework was more suitable and limited to saturated clay while poor performance in modelling over-consolidated clay in the left side of CSL was generally observed.

### 2.2.4.3. Existing Constitutive Models Based on Single Yield Surface

Kasama et al. (2000) extended the Critical State concept to develop a constitutive model for cement treated clays by introducing the cementation effect into the energy dissipation equation within the Critical State framework. They modified the mean effective stress to include the effect of cementation to the shear strength of the cement treated clay, which results in extending the stress domain. The effect of cementation was introduced to the plastic energy dissipation equation by Kasama et al. (2000) as follows:

$$dWin = p^* \sqrt{(dv^p)^2 - Xdv^p d\varepsilon^p + (Md\varepsilon^p)^2} - p_r dv^p \quad (2.17)$$

where,  $p^* = p + p_r$ . The parameter  $p_r$  represents the effect of cementation at  $q = 0$ . The term  $Xdv^p d\varepsilon^p$  is described as the soil dilatancy dependent coupling term

Moreover, Figure 2.22 (a) shows the effect of cementation to the failure state in  $p - q$  plane while Figure 2.22 (b) presents the failure state line of the un-treated soil (slope  $\lambda$ ) and the cement treated clay (slope  $\lambda^*$ ) in  $e - \ln(p + p_r)$  plane. In this model, the failure state line of the cement treated clay was assumed to be parallel to the Critical State Line (CSL) of the un-treated clay in  $p - q$  plane which intercepted the  $q$  - axis at a certain value and met the  $p$  - axis at  $p_r$ . Furthermore, the failure line of the cement treated clay in  $e - \ln(p + p_r)$  plane was linear and approached the failure line of the untreated clay at high confining pressure. This model only provided the description of the effect of cementation to the peak shear strength, while in the post peak state this model did not describe the effect of cementation degradation and the softening process.

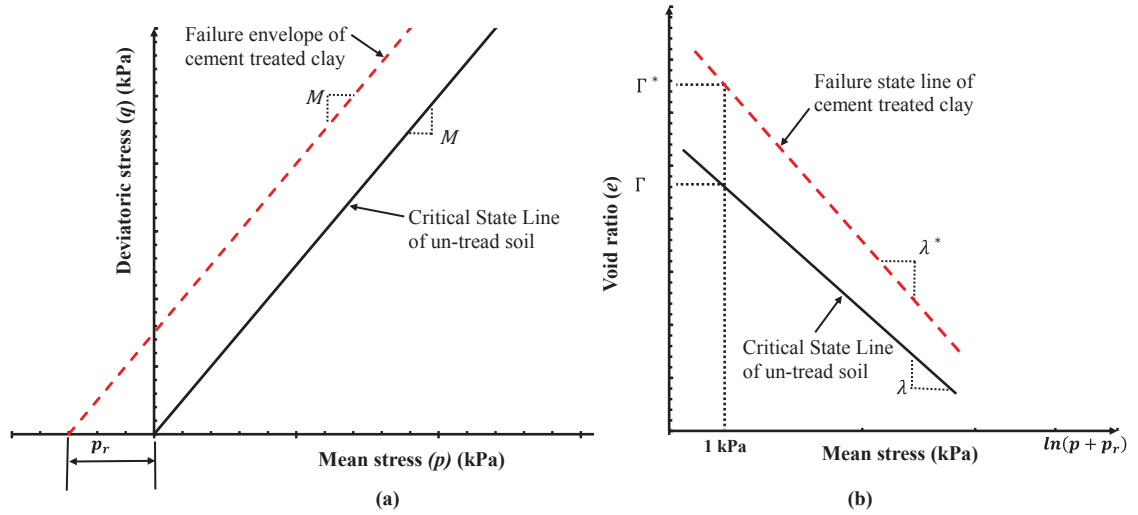


Figure 2.22: Schematic diagram of the failure state line including the effect of cementation in (a)  $p - q$  plane and (b)  $e - \ln(p + p_r)$  plane (after Kasama et al. 2000)

Horpibulsuk et al. (2010) simulated the behaviour of cemented clays via the framework of the Structured Cam Clay (SCC) model developed by Liu and Carter (2002) and the basis of the Modified Cam Clay (MCC) model. Their constitutive model extended the SCC model for cement treated clay by modifying the mean effective stress, while the effect of cementation was considered to reinforce the mean effective stress (Horpibulsuk et al. 2010). The modified mean effective stress ( $\bar{p}$ ) in the proposed model was presented as follows:

$$\bar{p} = p' + C/M \quad (2.18)$$

where,  $C$  is the contribution of cementation to the shear strength.

In this model, the effect of cementation in  $e - \ln p'$  plane was considered as an increase in the virgin yielding stress ( $p'_{y,i}$ ) and the additional void ratio ( $\Delta e$ ) obtained from the effect of cementation. When the mean effective stress increases beyond  $p'_{y,i}$  the void ratio of the cement treated clay reduces approaching the Isotropic Compression Line (ICL) of the reconstituted soil-cement mixture as the cementation bonds gradually break, as shown in Figure 2.23 (a). Part of the cementation bonds which cannot be completely destroyed during isotropic compression was presented by the parameter  $c$ , when  $p' \rightarrow \infty$ .

The equations to describe the yield surface and the virgin yielding behaviour were modified to include the effect of cementation. Figure 2.23 (b) describes the yield surface of the proposed model in elliptical shape, considering the effect of cementation as the size of the yield surface expands. In Figure 2.23 (b),  $p'_0$  and  $p'_s$  represent the size of the equivalent and the structural yield surface, respectively. The failure envelope of the extended SCC model has been assumed to be parallel to that of untreated clay and shifted by a certain intercept ( $C/M$ ), which characterises the effect of cementation similar to the model proposed by Kasama et al. (2000). Moreover, the softening process was simulated, considering the crushing of cementation bonds at the post peak state. When complete removal of the cementation bonds occurs ( $C = 0$ ), the stress state of the cement treated clay was assumed to travel on the failure line of the reconstituted soil-cement mixture in the proposed model (Horpibulsuk et al. 2010).

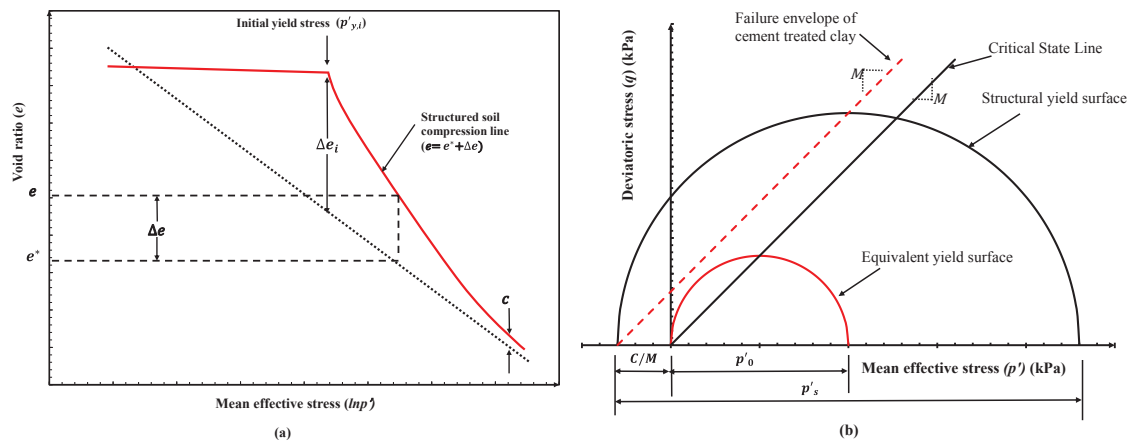


Figure 2.23: Schematic diagram of the SCC model for cement treated clay in (a)  $e - \ln p'$  plane and (b)  $p' - q$  plane (after Horpibulsuk et al. 2010)

Furthermore, the constitutive models by Kasama et al. (2000) and Horpibulsuk et al. (2010) assumed an associated plastic potential function while Shen et al. (2012) explained that the volumetric strains and the transition process from compressibility to dilatancy are only correctly described by a non-associated model for clayey material as also suggested by Yuanming et al. (2010). Although these existing models provide a conceptual framework for the development of an appropriate constitutive model capturing the behaviour of cement treated clays, the effect of cementation degradation due to the increase in the confining pressure has not been captured in these models, particularly in the post peak state.

The Modified Structured Cam Clay (MSCC) model was developed by Suebsuk et al. (2010). In this model, the structure of the cement treated clay degrades due to the volumetric and shear deformations. During the shear deformation, the reduction of structure strength ( $p'_b$ ) involved cementation degradation prior to failure state and the crushing of cementation bonds at the post peak state which was linked to the plastic deviatoric strain ( $\varepsilon_d^p$ ). Suebsuk et al. (2010) proposed a modified mean effective stress ( $\bar{p}$ ) that incorporated shear degradation for pre-and-post peak states as follows:

$$\bar{p} = p' + p'_{b0} \exp(-\varepsilon_d^p) \quad (\text{for pre-peak state}) \quad (2.19)$$

$$\bar{p} = p' + p'_{b,f} \exp[-\xi(\varepsilon_d^p - \varepsilon_{d,f}^p)] \quad (\text{for post-peak state}) \quad (2.20)$$

where  $p'_{b0}$  is the structure strength at initial state and  $p'_{b,f}$  is the structure strength at peak state.  $\varepsilon_{d,f}^p$  is the plastic deviatoric strain at peak state and  $\xi$  is the destructuring index (Suebsuk et al. 2010).

However, during consolidation, the effect of cementation degradation beyond the initial yield stress was formulated in this model by reducing the additional void ratio created by cementation, similar to the proposed model by Horpibulsuk et al. (2010). Furthermore, this reduction in the void ratio is controlled by a destructuring index, which is a model fitting parameter. Furthermore, the cementation degradation due to shearing influences the shear strength and the peak and residual strength of cement treated clays, so the effect of shear degradation presents a challenge for simulating the softening behaviour (post peak state) of cement treated clays. Moreover, the MSCC model presented two different shear degradation equations for pre-and-post peak states, while a unique relationship correlating the cementation degradation to the deviatoric strain is desirable and it can be applicable in all stress states. Although the SCC (Horpibulsuk et al. 2010) and MSCC (Suebsuk et al. 2010) models can simulate the hardening behaviour of the cement treated clay up to the peak state, they used negative hardening rule for the post peak state. Zhu et al. (2010) suggested that softening behaviour at the post peak state involves complex physical mechanisms which cannot be simulated simply by adopting negative hardening rule.

#### **2.2.4.4. Existing Constitutive Models Based on Bounding Surface Plasticity Theory**

Previous section discussed the existing constitutive models, based on a single yield surface concept similar to the Modified Cam Clay model. Although these constitutive models can describe a general behaviour of cement treated soil, poor performance in elastic region was often observed. According to Yu (2006), when a single yield surface concept is adopted, the elastic deformation is over-predicted. Moreover, a gradual transition from the elastic to the plastic state is observed in experiments while a sudden transition is predicted using a concept of single yield surface. Hence, several plasticity theories, including a multi-surface plasticity theory (Mroz et al. 1981) and a bounding surface plasticity theory (Dafalias and Herrmann 1982), were developed to better describe the behaviour of soil, particularly the smooth transition from the elastic to the plastic state and cyclic behaviour (Yu 2006). According to Prevost (1982), the multi-surface plasticity theory adopted the concept of nested yield surfaces associated with a field of plastic moduli. When loading increases, the stress point on the current yield surface approaches the next yield surface with changing in size. When the stress point reaches the outermost yield surface, referred to as bounding (limit) surface, failure occurs. Moreover, the bounding surface plasticity theory adopted only two surfaces, namely the loading surface and the bounding (limit) surface. The intermediate surfaces used in the multi surface plasticity theory were replaced by an interpolation function developed in the bounding surface plasticity theory. Prevost (1982) suggested that the bounding plasticity theory requires less effort in simulating soil behaviour, compared to the multi surface plasticity theory. However, the bounding plasticity theory is more suitable to a specific type of materials while the multi surface plasticity theory allows for a wider range of material since the hardening laws can be adjusted (Prevost 1982).

Furthermore, many constitutive models have been developed based on the concept of multi surface and bounding surface theories to simulate the behaviour of cement treated soil. Kavvadas and Amorosi (2000) proposed a constitutive model for structured soil adopting a plastic yield envelope and a bond strength envelope. While the plastic yield surface is associated with plastic yielding, the bond strength envelope,

or the bounding surface in plasticity theory, refers to the stress states with structure degradation. The bounding surface expands in size to accommodate the effect of structure. However, the effect of structure degradation was linked to the plastic volumetric and deviatoric strains with different proportions. As suggested by Baudet and Stallebrass (2004), adequate experimental results are required to determine the appropriate proportions while the proposed model by Kavvadas and Amorosi (2000) estimates the relative proportions based on parametric studies.

In addition, Suebsuk et al. (2011) proposed a constitutive model for cement treated soil based on the bounding surface plasticity theory, referred to as MSCC-B model, adopting many above mentioned features in the MSCC model such as the yield surface, plastic potential function and destructuring law. As observed in the verification of the proposed model, although the proposed model captured the peak shear strength reasonably well, the post peak state was not well simulated as significant cementation degradation occurred at this stage.

Baudet and Stallebrass (2004) proposed a Sensitivity Three Surface Kinematic Hardening (S3-SKH) model, based on a Sensitivity framework by Cotecchia and Chandler (2000), to simulate the behaviour of naturally structured soil, including structure degradation. In this model, the natural state boundary surface consisted of the history and yield surfaces in which their size changed with the plastic volumetric and the shear strain. When the natural state boundary surface intersected with the elastic wall in  $p' - q$  plane, sensitivity or bounding surface is formed. The three surfaces in this model are shown in Figure 2.24. In this model, the effect of structure was described as sensitivity which enlarges the bounding surface while the damage strain is adopted to simulate the degradation of structure during compression and shearing. The damage strain ( $d\varepsilon^d$ ) was linked directly to the plastic volumetric ( $d\varepsilon_v^p$ ) and shear strain ( $d\varepsilon_q^p$ ) increments in the following manner:

$$d\varepsilon^d = \sqrt{(d\varepsilon_v^p)^2 + (d\varepsilon_q^p)^2} \quad (2.21)$$

In Figure 2.24,  $sp'_0$  is the size of the sensitivity surface,  $Tsp'_0$  and  $TSSp'_0$  represent the size of the history surface and the yield surface with centre at  $p'_a$  and  $p'_b$ ,

respectively. Furthermore, the destructuration law was also proposed, incorporating the effect of structure (sensitivity) with reducing effect of damage strain. The damage strain proposed in Equation (2.21) assumed that the volumetric and deviatoric deformations are equally important which is unrealistic as the plastic shear strain causes significant deformation to the soil, compared to the plastic volumetric strain, as suggested by Tsoi (2005).

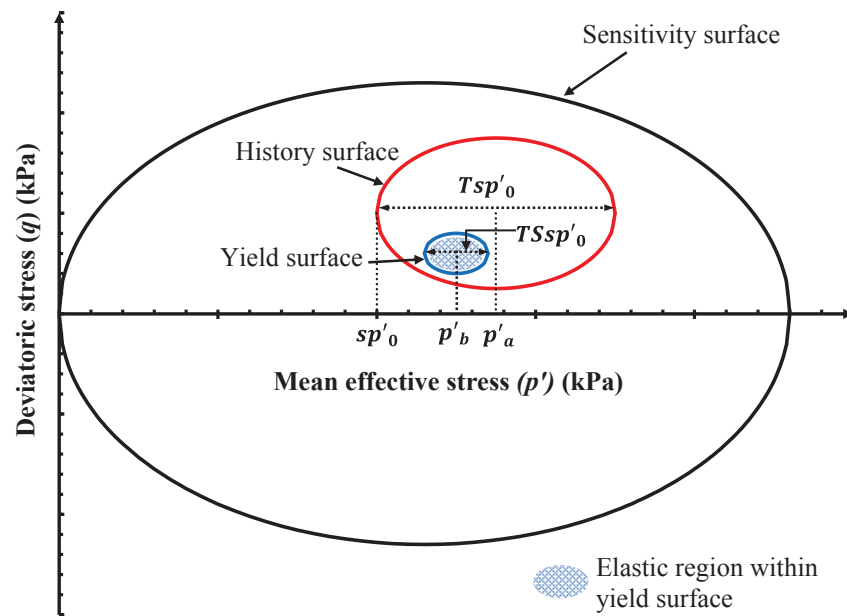


Figure 2.24: Schematic diagram of the S3-SKH in triaxial stress space (after Baudet and Stallebrass 2004)

#### 2.2.4.5. Failure Envelope of Cement Treated Clay

Moses et al. (2003) has indicated that the behaviour of cement treated clay depends on the strength of cementation, and the bond strength depends upon the stress level within the soil, and other factors such as strain parameter and type of loading. The cementation increases the friction angle and the cohesion of the soil and the cement treated clay behaves like over-consolidated soil at low confining pressures. Moreover, Lade and Overton (1989) and Uddin et al. (1997) suggested that as the mean effective stress increases, the beneficial effect of cementation to the shear strength of cement

treated clays decreases due to the development of micro-cracks and cementation degradation, hence, the cementation degradation parameters should depend on the level of mean effective stress. This dependency reduces the peak strength significantly as the soil structure is progressively changed. As a result, the failure envelope of the cement treated clay in  $p' - q$  plane gradually merges with the Critical State Line of reconstituted soil-cement mixture as the mean effective stress continues to increase as observed by Lo and Wardani (1999), Moses et al. (2003) and Panda and Rao (1998). Furthermore, Uddin et al. (1997) observed that the apparent over-consolidation ratio of the soil is reduced as the beneficial effect of cementation is diminished under sufficiently high confining pressures.

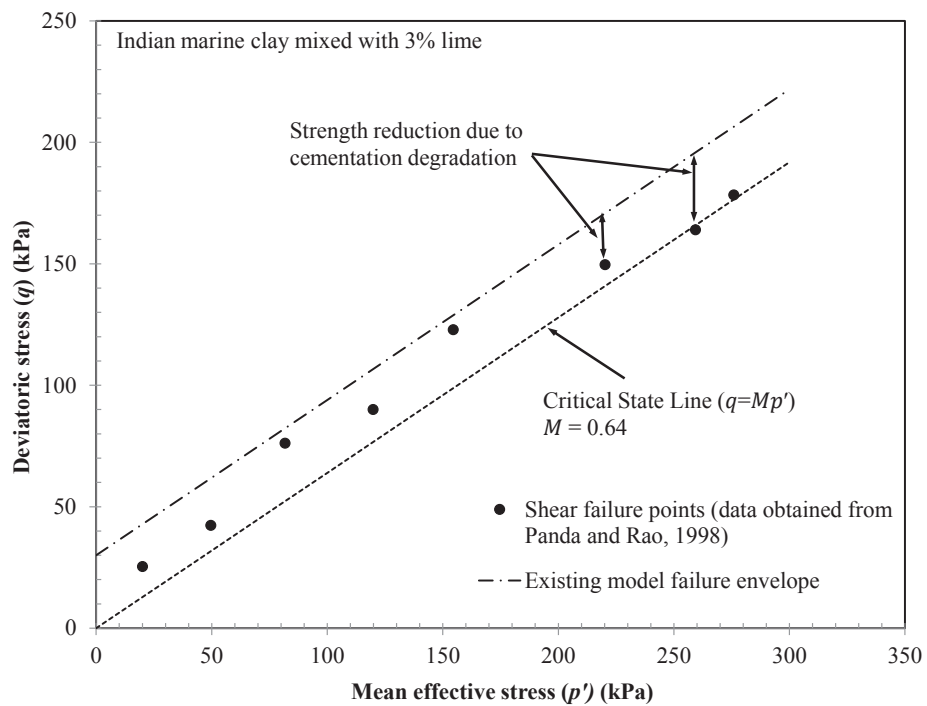


Figure 2.25: Failure envelope for artificially cemented Indian marine clay

Figure 2.25 displays the triaxial test results on Indian marine clay mixed with 3% hydrated lime. The results clearly indicated that a collection of failure points of cement treated clay forms a non-linear failure envelope, which is not parallel to the Modified Cam Clay failure envelope ( $q = Mp'$ ). For the sake of simplicity, the existing constitutive models, including the model developed by Kasama et al. (2000), the

Structured Cam Clay (SCC) model (Horpibulsuk et al. 2010; Liu and Carter 2002) and MSCC model (Suebsuk et al. 2010), assumed a linear failure line parallel to that of reconstituted soil. In other words, these constitutive models ignore the reduction in the strength of the cement treated clay due to degradation of cementation bonds as a result of confining pressure increase.

## **2.3. Behaviour of Fibre Reinforced Soil With or Without Cement**

### **2.3.1. General**

With increasing growth in population and economic activities, the construction over soft or weak soils becomes dramatically popular, leading to various ground modification techniques to improve the properties of the soft soil. Over the years, deep soil mixing is proven to be an effective soft ground improvement technique where in-situ soil is mixed with cement or lime to improve the strength and the compressibility characteristic of the base soil (Horpibulsuk 2001; Kamruzzaman et al. 2006; Porbaha 1998; Topolnicki 2004; Uddin et al. 1997; Yin 2001). The contribution of cement to the behaviour of soft soil has been extensively investigated by a number of researchers such as Chew et al. (2004), Horpibulsuk et al. (2004), Lorenzo and Bergado (2004) and Tan et al. (2002). The formation of cementation bonds due to chemical interaction between cement and soil particles lead to an increase in the strength and restrict the compressibility of the cement treated clay, as compared to the un-treated soil (Kamruzzaman et al. 2009; Lorenzo and Bergado 2006; and Uddin et al. 1997). However, with the addition of cement the unfavourably brittle behaviour at the post peak state increases significantly as the cement treated soil suddenly drops to the residual strength after failure, as reported by Lorenzo and Bergado (2006), Panda and Rao (1998), Porbaha et al. (2000) and Yin (2001). Moreover, the cementation degradation (breaking of cementation bonds) due to the volumetric and deviatoric strains also contributes towards the brittle behaviour of the cement treated clay.

In recent years, the usage of geosynthetics such as fibre, geogrid or geotextile has been employed as an effective and reliable reinforcement to the soft soil (Maher and Ho 1994; Tang et al. 2007). According to Tang et al. (2007), the fibres offer the ease of randomly mixing with soft soil and hence, enhancing the potential weakness planes, in comparison to geogrid or geotextile, as also suggested by Jiang et al. (2010). Moreover, numerous studies to investigate the effect of fibre inclusion in soft soil or cement treated soil have been carried out by many researchers such as Cai et al. (2006), Consoli et al. (2010), Diambra et al. (2013), Jiang et al. (2010), Li and Ding (2002), Maher and Ho (1994), Maher and Gray (1990) and Tang et al. (2010). The contribution of fibre improves the overall performance of soft soil by increasing the peak shear strength and enhancing the residual strength of both cohesive and cohesionless soil, as reported by Maher and Ho (1994) for the fibre improved Kaolinite clay, or Michalowski and Cermák (2003) and Ranjan et al. (1996) for sand improved with synthetic and natural fibres. Recently, Botero et al. (2015) reported the effect of fibre inclusion in improving the ductility of silty clay using polyethylene terephthalate, a recycled fibre from plastic waste such as plastic bottles and containers.

Additionally, the addition of fibre reinforcement into cement treated soil has increasingly become popular to improve the strength and most importantly the ductility of the cement treated soils. Researchers such as Consoli et al. (2010), Hamidi and Hooresfand (2013) and Park (2009), based on experimental results on fibre reinforced cement treated sand, have concluded that the brittleness of cement treated soil is improved significantly due to the effect of fibre reinforcement. Most previous studies only investigated how the inclusion of fibre affected cement treated and un-treated cohesionless soils, while studies on the behaviour of cement treated clayey soils improved with fibre are limited which few researchers such as Cai et al. (2006), Chen et al. (2015), Fatahi et al. (2012) and Tang et al. (2007) focused on this area. It was found that, the peak and the residual strengths of the cement treated clay improve due to the addition of the fibre (Cai et al. 2006; and Tang et al. 2007). In addition, according to Fatahi et al. (2013), the shrinkage properties, both axial and radial strains, of Kaolin clay decreases with higher cement and fibre content. Moreover, various factors affecting the improvement in the strength of the treated clay include the fibre type, fibre length and the content of fibre and cement, as suggested by Chen et al. (2015). For example, the contribution of polypropylene fibre in the strength of the cement treated clay is more

pronounced as compared to steel and carpet fibre (Fatahi et al. 2012). Furthermore, Tang et al. (2007) explained that the inclusion of fibre into the compacted matrix of soil-cement clusters, formed by the cement hydration and pozzolanic reactions, increases the load transfer between the matrix and the fibre, preventing further cracks within the improved soil during loading. In addition, while the soft soil is weak or unable to carry any tension forces, the tensile strength of the un-treated and cement treated soil can be improved considerably due to the inclusion of fibre (Divya et al. 2013; Fatahi et al. 2012). However, the main aim of this study focuses on the shear strength of the treated soil. In other words, the engineering properties of the treated soil are considered under compression only. Therefore, in this section, the behaviour of the fibre reinforced soil with or without cement is comprehensively discussed, including the behaviour under Unconfined Compression Strength (UCS) test, odometer test, pull-out strength test, isotropic consolidation test, and under triaxial compression test. Furthermore, factors affecting the strength of the improved soil, including the effect of fibre length, fibre type and fibre content, are also discussed in detail. It should be noted that, the fibre reinforced soil stabilised with cement is hereafter referred to as the improved soil composite or the FRCS while the term “fibre reinforced soil” remains for the fibre stabilised soil without cement.

## **2.3.2. Engineering Properties of Fibre Reinforced Soil With or Without Cement**

### **2.3.2.1. Unconfined Compression Strength (UCS) Test**

A number of researchers such as Cai et al. (2006), Consoli et al. (2010), Kaniraj and Havanagi (2001), Maher and Ho (1994), Park (2009) and Tang et al. (2007) have conducted the Unconfined Compression Strength (UCS) tests to investigate the effect of fibre mixed with soft soil and cement. The experimental results reported that the inclusion of fibre increases the peak and the residual shear strength of the improved material. As closely observed by Maher and Ho (1994), based on the unconfined compression strength (UCS) test results conducted on Kaolinite clay treated with fibre,

increasing fibre content leads to an increase in the peak shear strength and the residual strength of the fibre reinforced clay. However, with the analysis on the UCS of clayey soil treated with polypropylene fibre, Jiang et al. (2010) discovered that the shear strength of the fibre reinforced soil increases with the increase in fibre content, followed by a decrease with further increase in fibre content, as shown in Figure 2.26.

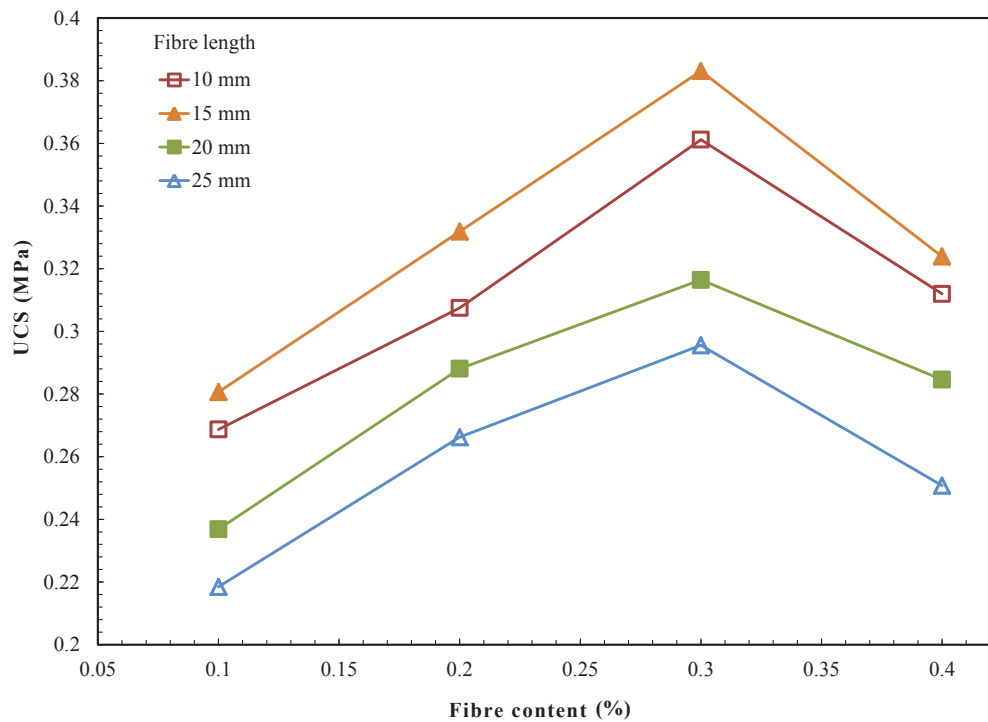


Figure 2.26: Effect of increasing fibre content on the UCS of fibre reinforced clay with differing fibre length (after Jiang et al. 2010)

Additionally, for the improved soil composite, Consoli et al. (2010) observed that the inclusion of fibre on the cement treated sand increases the peak strength and the residual strength and improve the ductility at residual strain as compared to high brittleness in the cement treated soil as also observed by many other researchers (Cai et al. 2006; Fatahi et al. 2012; Hamidi and Hooresfand 2013; and Park 2009). In addition, for the fibre reinforced sand stabilised with cement, Consoli et al. (1999) suggested that increasing fibre content results in an overall improvement of the behaviour of the improved soil. As shown in Figure 2.27, the UCS values of the 4% cement treated sand

reinforced with different fibre contents (ranges from 0% to 1%) increase with fibre content (Park 2011). Park (2011) suggested that, the effect of increasing fibre content on the cement treated sand is similar to the effect of increasing confining pressure in the cement treated sand without fibre reinforcement under triaxial condition as the horizontal deformation of the specimen is restricted due to the fibre.

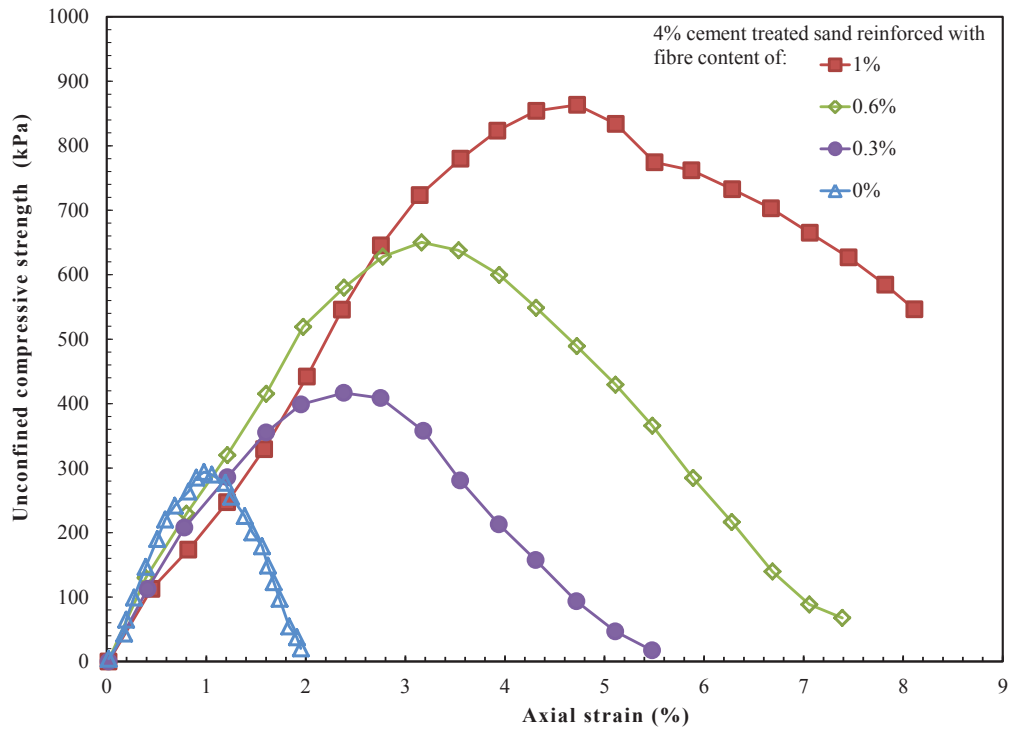


Figure 2.27: Effect of fibre content on the UCS of 4% cement treated sand reinforced with fibre (after Park 2011)

While most of the studies have focused on the effect of fibre reinforcement on soil or cement treated sand (Consoli et al. 2004; Maher and Ho 1993; Park 2009), preliminary studies on the behaviour of the improved soft clay composite have been carried out by Cai et al. (2006) and Tang et al. (2007). According to the UCS results on the improved clay composite conducted by Tang et al. (2007), increasing fibre content leads to an increase in the strength due to an increase in the frictional resistance at the interface between the soil-cement matrix and the fibre. Moreover, Cai et al. (2006) suggested that the improved soil composite shows strain softening ductile behaviour as compared to strain hardening behaviour of fibre improved soil and brittle behaviour of

cement treated soil at residual state, in line with results reported by Kaniraj and Havanagi (2001) and Consoli et al. (1999).

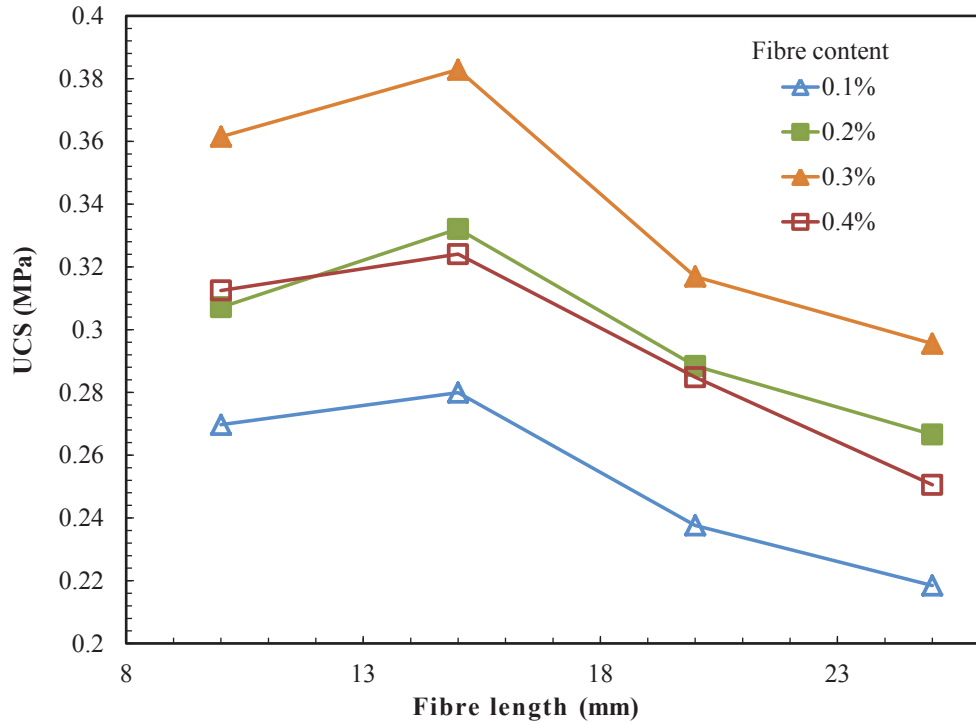


Figure 2.28: Effect of increasing fibre length on the UCS of fibre reinforced clay with differing fibre content (after Jiang et al. 2010)

Furthermore, the effect of fibre length or aspect ratio (length/diameter) plays a significant role in the shear strength of the reinforced soil composite with or without cement. For fibre reinforced clay, Jiang et al. (2010) observed that, at a same fibre content, increasing fibre length increases the peak shear strength at first, then followed by a rapid reduction when the fibre length continues to increase, as shown in Figure 2.28. Similarly, Maher and Ho (1994) reported that, while the effect of increasing fibre length significantly improves the ductility or energy absorption, the contribution of the fibre to the UCS may not be beneficial. It is explained that, for a given fibre content, increasing fibre length reduces the number of single fibre, consequently the effectiveness of fibre reinforcement decreases (Jiang et al. 2010). Moreover, Maher and Ho (1994) further explained that, when fibre is randomly distributed in the soil, the probability of the longer fibre crossing the potential weak plane is less, comparing to using shorter fibres.

### 2.3.2.2. Direct Shear Test

The direct shear test is commonly conducted to obtain the stress-strain relationship, together with the shear strength parameters (i.e. the cohesion ( $c$ ) and the friction angle ( $\phi$ )), of the improved material under different normal stresses (Gray and Ohashi 1983; Kaniraj and Havanagi 2001; Shao et al. 2014; Yetimoglu and Salbas 2003). In particular, Gray and Ohashi (1983) conducted the direct shear tests on the fibre reinforced sand with fibre orientated perpendicularly to the shear plane to investigate the effect of fibre reinforcement on the behaviour of the fibre reinforced sand. The experimental results showed that, at a given normal stress, increasing fibre content leads to an increase in the peak shear strength and less strength reduction at the post peak state, consequently the material ductility is significantly improved due to the addition of fibre. Gray and Ohashi (1983) further observed that the addition of longer fibres into the sand increases the shear strength, however there is no further effect when the fibre length continues to increase, similar to the findings by Jiang et al. (2010).

Moreover, Shao et al. (2014) analysed a ring shear test results conducted on the randomly distributed fibre improved sand and showed that the peak and the residual shear strengths of the improved soil increases with increasing fibre content and vertical normal stresses. As shown in Figure 2.29, at a given normal stress, increasing fibre content from 0% to 0.9% increases the peak shear strength of the reinforced sand notably. Shao et al. (2014) explained that the increase in the shear strength with increasing fibre contents is mainly due to the interlocking effect between the fibre and the soil matrix. As observed in Figure 2.29, the un-reinforced sand displays a rise up to the peak shear strength, followed by a reduction as the shearing continues. In the other hand, the shear strength of the fibre reinforced sand gradually increases and maintains steadily at large shear strains, indicating ductile behaviour. Moreover, it is observed that, the effect of fibre inclusion is more pronounced at large shear strains, compared to insignificant effects at small strains, which is consistent with the findings by Casagrande et al. (2006), Consoli et al. (2007) and Heineck et al. (2005).

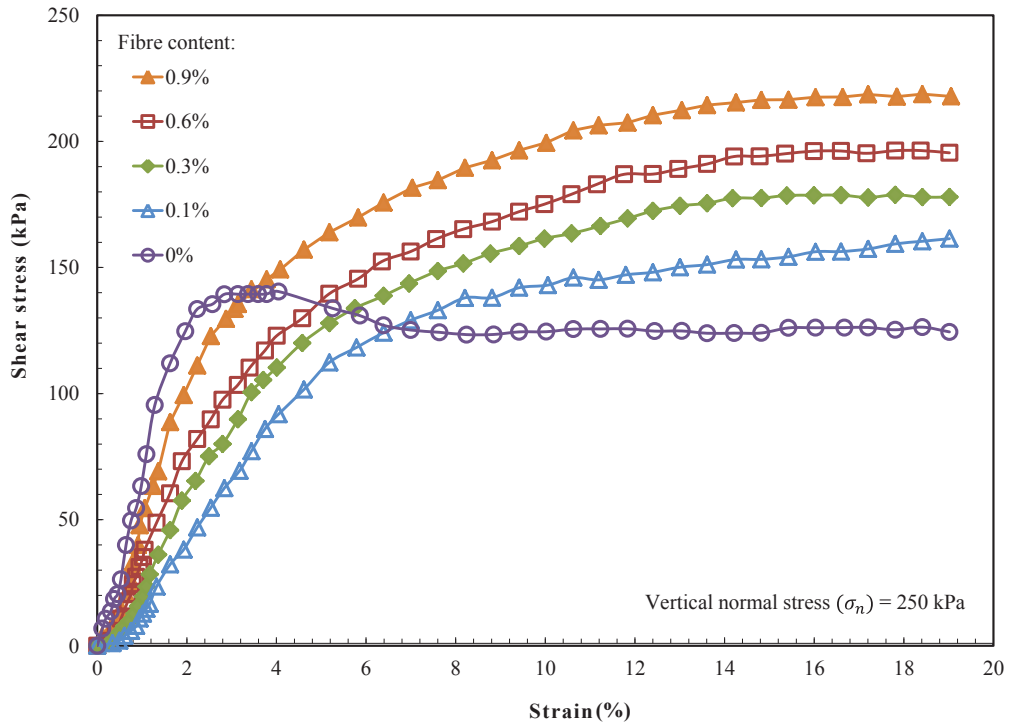


Figure 2.29: Stress-strain behaviour of sand reinforced with different fibre contents under vertical normal stress = 250 kPa (after Shao et al. 2014)

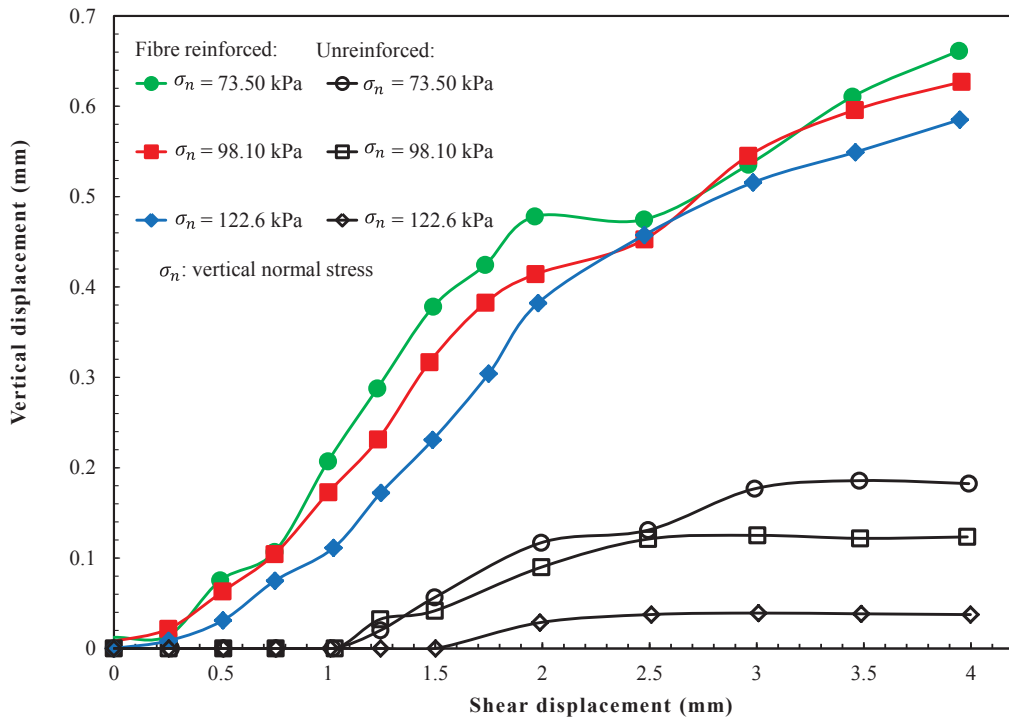


Figure 2.30: Comparison between unreinforced and fibre reinforced fly ash sample in direct shear test at differing vertical normal stress (after Kaniraj and Havanagi 2001)

Additionally, Kaniraj and Havanagi (2001) investigated the effect of fibre reinforcement in sandy silt mixed with fly ash under the direct shear apparatus, and reported a pronounced increase in the vertical displacement owing to the effect of fibre inclusion, as depicted in Figure 2.30. Moreover, the peak shear strength of the fibre reinforced soil is generally higher, compared to that of the un-reinforced soil, for all vertical normal stresses, which is also consistent with the experimental results by Shao et al. (2014). Furthermore, the fibre reinforced soil reaches the peak shear strength at higher shear strain, indicating the contribution of fibre to the material ductility.

However, Yetimoglu and Salbas (2003), based on the direct shear tests conducted on sand reinforced with randomly distributed polypropylene fibre under different vertical normal stresses (i.e. 100, 200 and 300 kPa), reported that the peak shear strength of the fibre reinforced sand increases mainly due to increasing vertical normal stress while the contribution of fibre to the shear strength is insignificant. Gray and Ohashi (1983) and Kaniraj and Havanagi (2001) reported the increase in the peak shear strength due to the fibre inclusion, Yetimoglu and Salbas (2003) explained the difference in their experimental findings, owing to the properties of the soil, type of fibre and different testing conditions. Furthermore, Figure 2.31 exhibits that, the effect of fibre inclusion mainly improves the ductile behaviour as the reduction in shear strength decreases and the friction angle increases at the post peak state, similar to the findings by Gray and Ohashi (1983) and Shao et al. (2014).

Additionally, the shear strength parameters, i.e. the friction angle and the cohesion, of the fibre reinforced soils increase with fibre content (Anagnostopoulos et al. 2014). Furthermore, a number of researchers such as Consoli et al. (2009a), Gao and Zhao (2012), Kumar et al. (1999) and Yetimoglu and Salbas (2003) explained that, while the increase in the friction angle is due to the friction between fibre and soil particles being mobilised during shearing, the stretching of the fibres contributes to an increase in the cohesion, consequently improving the material ductility.

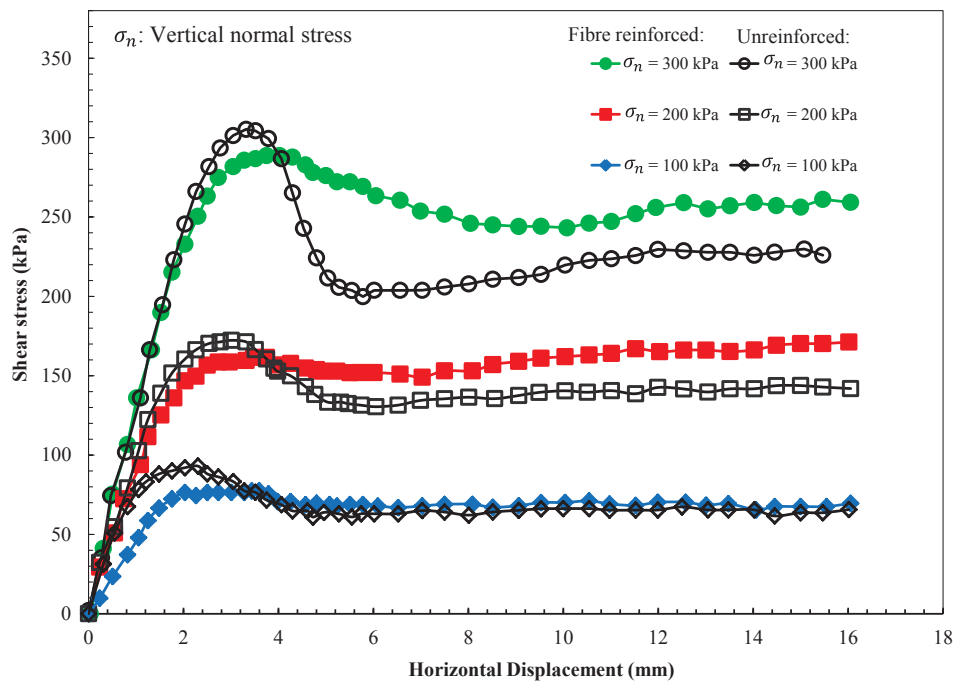


Figure 2.31: Comparison between un-reinforced and 1% fibre reinforced sand in direct shear test under differing vertical normal stresses (after Yetimoglu and Salbas 2003)

### 2.3.2.3. Consolidation Behaviour

Research results on the compressibility behaviour of the fibre improved cement treated clay remain limited and controversial. For the fibre improved sand, Consoli et al. (2005) observed that as the mean effective stress increases, the fibre improved sand samples come to a unique normal compression line (NCL) which is located above the NCL of the un-improved sand sample at the same effective stress. On the other hand, Michalowski and Čermák (2002) suggested that the inclusion of fibre has no effect under compression, similar to the findings by Diambra and Ibraim (2014). Furthermore, Ling and Tatsuoka (1994) explained that the tensile resistance provided by the fibre plays no role under isotropic compression as the fibre is compressed in all directions.

#### 2.3.2.4. Triaxial Behaviour

Over the years, many researchers have conducted triaxial compression tests to study the behaviour of the reinforced soil composite (Consoli et al. 1999; Hamidi and Hooresfand 2013; and Zornberg 2002). However, much of the previous studies were performed on fibre reinforced soil without cement stabilisation (di Prisco and Nova 1993; Diambra et al. 2013; Maher and Gray 1990; Michalowski and Cermák 2003; and Ranjan et al. 1996). Some aspects of fibre inclusion, including fibre type, aspect ratio, content, are discussed in the following parts.

Generally, the increase in the peak shear strength of the fibre reinforced soil depends on the fibre content, aspect ratio and the type of fibre. At a given fibre content, higher aspect ratio shows higher strength as compared to un-treated soil (Consoli et al. 1999; Maher and Gray 1990; Ranjan et al. 1996; and Zornberg 2002). Moreover, under triaxial compression, the shear strength of the fibre reinforced sand increases with the fibre content, as suggested by Michalowski and Cermák (2003). Although the initial stiffness of the fibre reinforced soil reduces with increasing fibre content, this effect depends on the type of fibre. For example, for soil reinforced with synthetic fibre, such as polypropylene and polyamide, the reduction in the initial stiffness is more pronounced than the corresponding values when steel fibres are adopted.

With increasing fibre content, larger shear strains are expected at failure, as shown in Figure 2.32. Moreover, the peak shear strength of the fibre reinforced soil increases with confining pressure, for all fibre contents, aspect ratios and fibre types, as observed by Maher and Gray (1990), Michalowski and Cermák (2003), and Ranjan et al. (1996). Furthermore, Michalowski and Čermák (2002) investigated the effect of fibre orientation on the shear strength of the fibre reinforced sand. Under triaxial compression, when the fibre is placed vertically, the effectiveness of the fibre is null, compared to the largest contribution when fibre is positioned horizontally crossing the plane of weakness. Moreover, due to the inclusion of fibre, the residual shear strength and the ductility of the fibre reinforced soil are improved, compared to the un-reinforced soil, as displayed in Figure 2.32. The effect of fibre reinforcement to the shear strength of the reinforced soil is explained due to the interaction between fibre and soil particles (Michalowski and Cermák 2003).

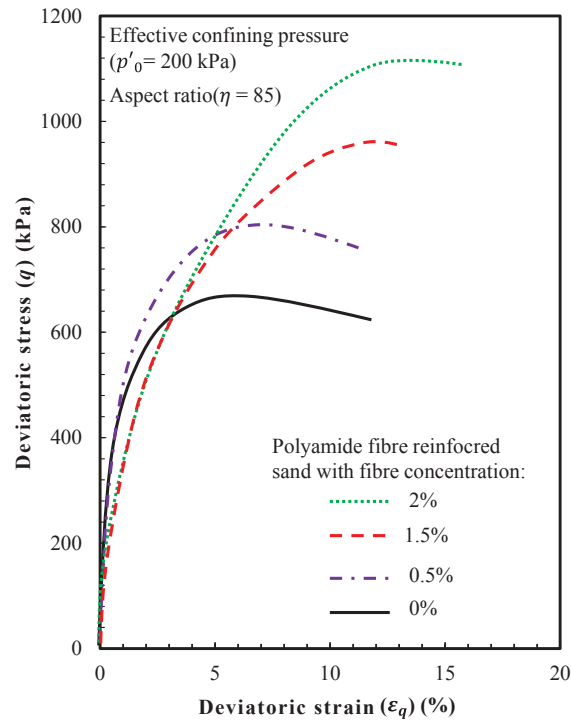


Figure 2.32: Stress-strain behaviour of polyamide fibre reinforced fine sand with differing fibre concentration (after Michalowski and Cermák 2003)

In addition, a few researchers such as Freilich et al. (2010), Li and Ding (2002) and Zornberg (2002), conducted triaxial compression tests to study the effect of fibre inclusion on the soft clay. Zornberg (2002) stated that the effect of increasing fibre content and the effective confining pressure lead to an increase in the peak shear strength, similar to the observations by Michalowski and Cermák (2003) for the fibre improved sand. Moreover, Li and Ding (2002) based on the experimental results conducted on silty clay treated with fibre under triaxial cyclic loading, concluded that a number of factors, including fibre content, confining pressures and the repetition of loading, affect the elastic shear modulus of the fibre reinforced clay. Freilich et al. (2010), based on the deformation of the un-reinforced and fibre reinforced clay, observed that while the un-reinforced clay exhibits a shear plane developed within the sample, the deformation of the fibre reinforced clay is observed to be bulging. The difference in deformation is mainly due to the inclusion of fibre, which improves the material ductility. Furthermore, the excess pore water pressure response of the fibre

reinforced soil is generally higher than the un-reinforced soil (Freilich et al. 2010). Li (2005) explained that the effect of fibre is to distribute the applied stresses within the soil, so the contractive tendency of the fibre soil mixture increases as higher amount of soil particles is under compression.

Although study on the behaviour of soil treated with fibre and cement under triaxial compression is becoming more popular, many researchers have focused on cement treated sand with fibre (Consoli et al. 2004; and Hamidi and Hooresfand 2013), while the extent of conducting triaxial tests on clay treated with cement and fibre is very limited. The behaviour of soil treated with fibre and cement is more ductile, compared to the brittle behaviour in cement treated soil without fibre, as observed by Consoli et al. (1999). For a given fibre content, the effect of fibre reinforcement in cement treated soil is affected by the cement content which is less effective when higher cement content is used (Consoli et al. 2009b). Moreover, Hamidi and Hooresfand (2013), based on the triaxial tests performed on sand treated with cement and different polypropylene fibre contents, suggested that the peak and the residual shear strengths of the improved soil composite increase with fibre content, relative density and effective confining pressures. Furthermore, the initial stiffness reduces when fibre is added to the cement treated soil (Consoli et al. 1999), as also observed by Michalowski and Cermák (2003) on the fibre reinforced soil without cement. In addition, Hamidi and Hooresfand (2013) reported that the energy absorption capacity of the cement treated sand increases with fibre content and relative density at different confining pressures owing to the elongation of the fibre enhancing greater energy absorption, as shown in Figure 2.33.

Furthermore, Consoli et al. (2004) conducted a series of drained triaxial tests on cement treated sand reinforced with different types of fibres (namely polyester, glass and polypropylene fibres), and observed that the increase in the peak and the residual strengths due to the effect of fibre depends on the type and nature of the fibre. For example, the inclusion of polypropylene fibre into cement-soil matrix reduces the shear strength at failure, while the use of polyester fibre provides negligible increase in the shear strength. In addition, the failure mode of the improved soil composite also depends on the type and nature of the fibre. Consoli et al. (2004) observed that while polypropylene fibre improves the brittleness of the cement treated soil significantly, the

inclusion of polyester and glass fibre has a slight effect on the failure mode of the improved soil composite.

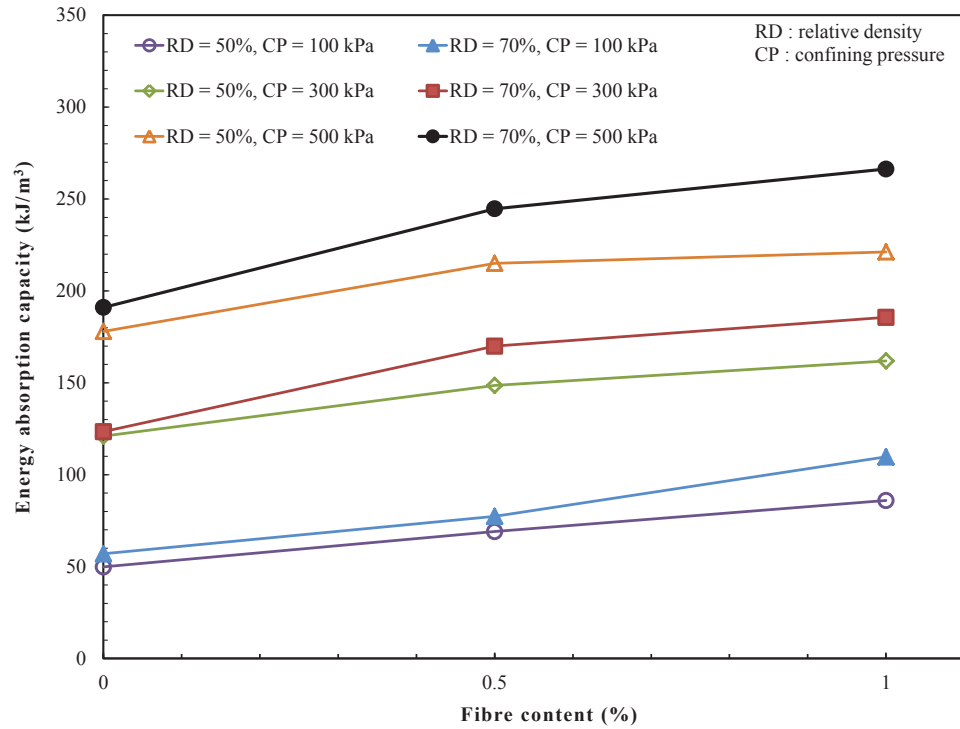


Figure 2.33: Effect of fibre content on the energy absorption capacity of the 3% cement treated sand (after Hamidi and Hooresfand 2013)

### 2.3.2.5. Failure Mechanisms

It is important to investigate the failure characteristics of the improved soil composite at macro and micro level. The addition of cement allows for the formation of cementation bonding and the interlocking forces which increase the strength, cohesion and internal friction angle of the soil (Cai et al. 2006). Moreover, the effect of fibre inclusion into the cement treated soil further increases the cohesion and interfacial forces between soil particles and fibre, which is beneficial to the shear strength, particularly at the post peak state. At macro level, as observed by Cai et al. (2006), the un-treated soil exhibits the strain softening ductile failure while the addition of cement

into the un-treated soil shows the complete brittle failure. Moreover, soil reinforced with fibre shows strain hardening ductile behaviour. The inclusion of fibre into the cement treated soil clearly shows significant increase in ductility; hence the behaviour of the cement treated soil changes from complete brittle to ductile by adding fibre. Furthermore, experimental observations show smaller cracks in the improved soil composite with increasing fibre content, compared to large cracks developed in the cement treated soil without fibre reinforcement (Cai et al. 2006; Tang et al. 2007). As also observed by Consoli et al. (2003), the addition of fibre prevents further formation of tension cracks in the cement treated sample, thus the material ductility is significantly improved. The following sections address the failure mechanisms of the fibre reinforced soil with or without cement stabilisation, including discussion on the interaction between soil matrix and fibre at micro-structural level and the failure envelope.

#### **2.3.2.5.1. Soil-Fibre Interaction**

The structure of soil at microscopic level can be examined using the Scanning Electron Microscope (SEM) images. As described by Cai et al. (2006), in analysing the SEM images of un-treated clay, cement treated clay and fibre reinforced clay with or without cement, the formation of cementation bonding makes the soil matrix denser with smaller pore space between the aggregated particles, compared to larger pore space with big packets of soil in the un-treated and fibre reinforced clay. For fibre reinforced clay, since the fibre has strong resistance to tension during shearing enhancing the friction between fibre and soil particles, increase in strength is observed. Moreover, for fibre reinforced clay treated with cement, the total effective contact area increases due to smaller pore space between the particles, hence the effect of fibre reinforcement is more effective in fibre reinforced clay with cement, compared to without cement treatment (Cai et al. 2006).

A study by Tang et al. (2007) on the interface morphologies of improved soil composite at the microstructural level (SEM images) revealed that the fibre is restrained from moving by the surrounding cementitious products formed by the chemical interaction between the particles of soil and the cement. This means the soil matrix is

tightly packed and the load transfer from the soil matrix to the fibre becomes more efficient due to the inclusion of fibre and cement. As loading begins, the normal stresses acting on the fibre increase the pull out resistance as well as the friction and interlocking forces at the interface. However during loading, small cracks are formed within the soil matrix as the cementation bonds gradually break. At this stage the fibre is mobilised as frictional and interlocking forces are distributed along the length of the fibre, such that large cracks appear within the soil matrix at failure and tensile resistance from the fibre increases the connection between the fibre and cementitious products preventing the development of any further cracks. Thus, brittle failure of the cement treated soil becomes more ductile due to the bridging effects provided by the fibre reinforcement. Furthermore, based on a pull-out test on a single fibre surrounded by the cemented clay, Tang et al. (2010) suggested that when shearing occurs, the pull out resistance provided by the fibre increases to a peak and then drops to a residual constant value as the fibre is progressively pulled out from the surrounding soil-cement matrix.

Moreover, factors such as water content, cement content and dry density influence the shear strength of the fibre reinforced clay with cement (Tang et al. 2010). For example, increasing dry soil density and cement content results in an increase in the peak and residual shear strength of the improved material due to smaller pore space between soil particles. In contrast, the effect of increasing water content reduces the peak and residual shear strength as well as the peak strain, as shown in Figure 2.34. Fredlund and Rahardjo (1993) explained that the matrix suction and the effective stress within the soil particles decreases with an increase in water content. Furthermore, the interfacial friction and the bond strength between fibre and the surrounding soil-cement clusters reduce when more water is added, similar to the corresponding behaviour for the cement treated clay without fibre reinforcement (Tang et al. 2010).

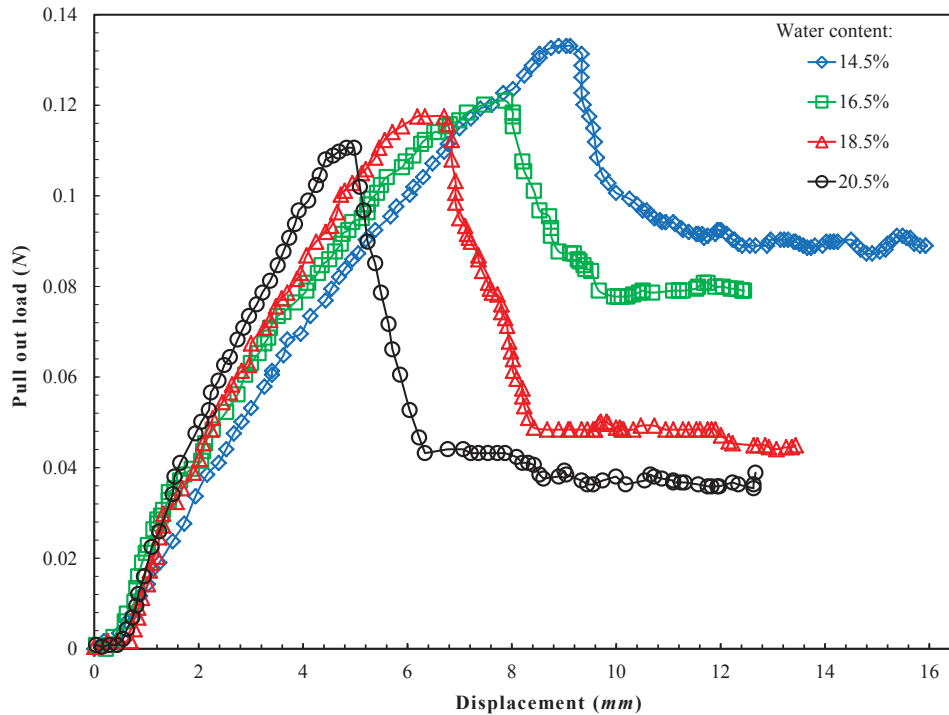


Figure 2.34: Effect of water content on the pull-out load of a single fibre in reinforced soil (after Tang et al. 2010)

### 2.3.2.5.2. Failure Envelope of Fibre Reinforced Soil

In terms of the mechanism of fibre failure, Maher and Gray (1990) observed the curve-linear failure envelope for uniformly graded round sand and bilinear failure envelope for well graded angular sand, both reinforced with fibre. Moreover, Zornberg (2002) proposed a bi-linear failure envelope in the constitutive model for fibre reinforced soil where a critical confining pressure defines the failure characteristics of the fibre. Below this critical confining pressure the failure mechanism was assumed to be due to the pull out or slippage of fibre from the soil matrix as the frictional forces between them are not fully mobilised, but once above the critical confining pressure, the frictional forces along the interface area are fully mobilised and the fibres tend to become plastic or a breakage may occur. Ranjan et al. (1996) confirmed the existence of a critical confining pressure and also observed a curvilinear failure envelope with increasing aspect ratios of the fibre in sand, as shown in Figure 2.35. Moreover, as suggested by Maher and Gray (1990), the critical confining pressure depends on a

number of factors such as fibre aspect ratio, grain shape and gradation, while fibre content has no influence on the value of the critical confining pressure. Diambra and Ibraim (2014) also suggested that after the pull-out or rupture of fibre, the ability of fibre to improve soil would be the same as un-improved soil.

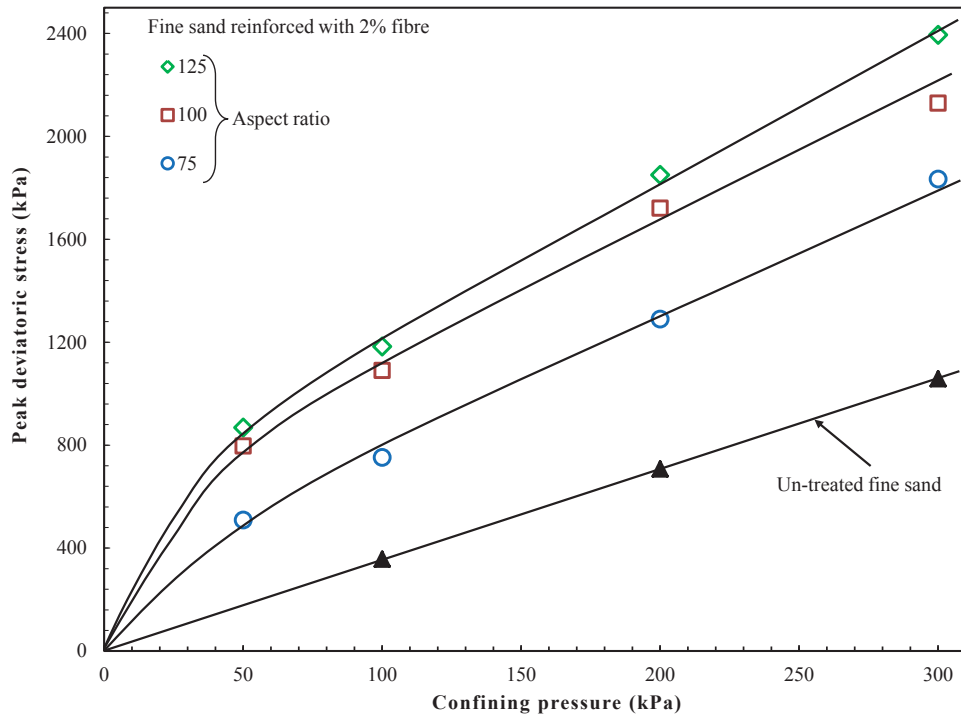


Figure 2.35: Failure envelope of 2% fibre reinforced fine sand at differing aspect ratio (after Ranjan et al. 1996)

### 2.3.2.6. Existing Constitutive Models for the Fibre Reinforced Soil

The above mentioned failure mechanisms were implemented into several models to predict the behaviour of soil reinforced with fibre. Early work by di Prisco and Nova (1993) proposed a constitutive model for soil reinforced with fibre that was verified against triaxial tests carried out on sand improved with polyester fibres. This simple model simulated the contribution of fibre to an increase in the shear strength of improved soil, but the loss of strength after failure due to softening was not captured.

The model proposed by Maher and Gray (1990) for randomly distributed fibre reinforced sand has provided a tool for capturing the increase in the strength of the material due to the addition of fibre. This model adopted a force equilibrium concept and statistical analysis method in which the predicted fibre orientation, on average, was normal to the shear plane at failure. However, Ranjan et al. (1996) suggested that, for randomly distributed fibre reinforced soil, the orientation and number of fibres in any plane are problematic to determine in experiments. Moreover, the failure envelope in the proposed model was bilinear with a kink at the critical confining pressure where the fibre may yield as shown in Figure 2.36. Beyond this critical confining pressure, the linear portion of the failure envelope was assumed to follow the Mohr-Coulomb yield criterion. Hence the failure envelope required two separate equations to capture the shear strength, for pre-and-post portion of the critical confining stress which is inconvenient as the failure envelope discontinues at the critical confining pressure. Furthermore, the thickness of the shear zone is required when adopting the proposed model which is difficult to determine (Hejazi et al. 2012).

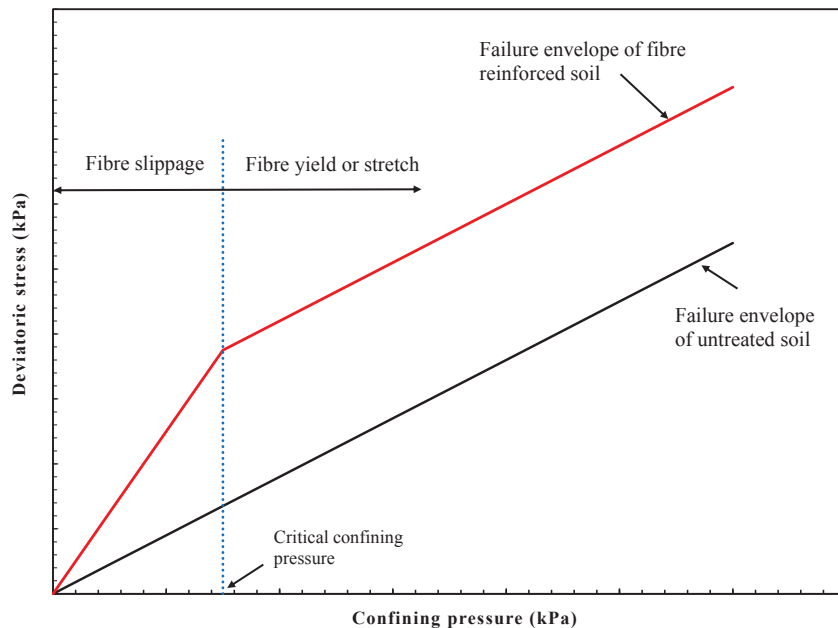


Figure 2.36: Failure envelope of fibre reinforced soil (after Maher and Gray 1990)

In addition, Ranjan et al. (1996) proposed a model using regression analysis to capture the shear strength of randomly distributed fibre reinforced sand. A curvilinear

failure envelope was adopted, while the critical confining stress was determined at the starting point of the linear portion. However, separate equations were derived for confining stress below and above the critical confining stress, while a single equation for the failure envelope is preferable. The strength at failure of the fibre reinforced sand was not well captured using the proposed model by Ranjan et al. (1996), particularly at high confining pressure where the strength reduces due to fibre degradation. Moreover, according to Hejazi et al. (2012), the model was derived using only a set of experimental results, hence the mechanisms of fibre reinforcement are not adequately captured using this model.

For cohesive soil reinforced with fibre, Diambra and Ibraim (2014) recently presented a numerical simulation under undrained triaxial conditions, using the bounding surface plasticity framework principles and the basis of a Modified Cam Clay model. Although the failure mechanisms of the fibre were considered, this model was not validated against experimental results and needed a vast amount of computational effort.

Furthermore, a discrete framework proposed by Zornberg (2002) provided a tool for predicting the shear strength of soil improved with fibre by introducing the equivalent shear strength in a bilinear failure envelope and considering the failure mechanisms governed by the pull-out or breakage of fibre, as shown in Figure 2.37. This model aimed to quantify the tensile contribution to the shear strength of the improved soil provided by the fibre. This model also adopted the critical confining stress, characterising the failure mechanisms. However, how the fibre reinforcement affected the residual strength after the soil reached a post peak state was not described. The equivalent shear strength ( $S_{eq,t}$ ) for breakage failure of the fibre was derived by Zornberg (2002) as follows:

$$S_{eq,t} = c_{eq,t} + (\tan\phi)_{eq,t}\sigma_n \quad (2.22)$$

where,  $c_{eq,t}$  and  $(\tan\phi)_{eq,t}$  are the cohesion and frictional components of the equivalent shear strength when the confining stress ( $\sigma_n$ ) is higher than the critical stress.

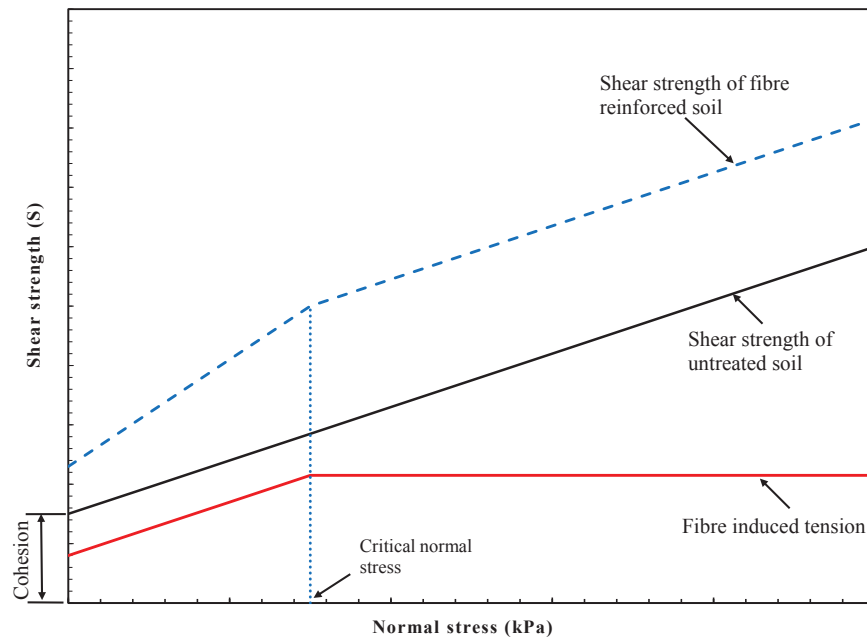


Figure 2.37: Shear strength envelope of fibre reinforced soil in discrete framework (after Zornberg 2002)

## 2.4. Summary

This chapter has described the behaviour of cement treated clay under the unconfined compression strength (UCS) tests, the oedometer consolidation tests and the triaxial compression tests. As a summary, the engineering properties of the cement treated clay depend on the effect of various factors such as the cement content, the water content, the curing time, the type and mineralogy of clay. In general, the strength of cement treated clay is significantly improved owing to the formation of cementation bonds within the soil-cement matrix. As a result of chemical reactions between the cement and the clay particles, particularly the cement hydration process and the pozzolanic reactions, the formation of cementitious products provides bonding between aggregates of clay particles which stabilise the soil and increase the strength of treated soil with time. Hence, at certain water content, higher cement content and longer curing period result to an increase in the strength of cement treated clay as higher pozzolanic products are formed at a prolonged period, subjected to availability of water. In contrast,

increasing water content reduces the strength of cement treated clay as the pore space between treated soil matrix increases and the matrix becomes less compacted.

Moreover, compared to the un-treated clay, the initial yield stress of the cement treated clay increases with cement content and curing time. In triaxial compression condition, the effect of confining pressure plays an important role on the behaviour of cement treated clay. Due to the formation of cementation bonds, the treated soil can attain a higher yield stress as compared to the un-treated soil at the same void ratio in isotropic compression. However, as the confining pressures continue to increase beyond the initial yield stress, the void ratio reduces as the soil-cement clusters collapse and the cementation bonds begin to break. At sufficiently high pressure, significant breakage of cementation bonds occurs and the compressibility of the treated clay depends mainly on the effect of fabric. Furthermore, during shearing stage, the shear strength of the cement treated clay increases with cement content and confining pressure. Compared to the un-treated clay under the same confining pressure, the cement treated clay attains a higher strength above the Critical State Line of the un-treated clay due to the effect of cementation. However, at high confining pressures, significant cementation degradation diminishes the contribution of cementation, consequently reduces the peak shear strength of the cement treated clay. Hence, the failure envelope of the treated clay should merge with the Critical State Line of the reconstituted soil-cement mixture to capture the effect of cementation degradation to the shear strength as confining pressure increases. Moreover, at the post peak state, crushing of cementation occurs resulting in significant plastic deformation. The strength reduces with increasing shear strain as the cement treated clay undergoes the softening process. At the residual state, cementation bonds are completely destroyed due to the accumulation of plastic shear strain. Hence, at this stage, the behaviour of cement treated clay is similar to that of the un-treated clay.

Furthermore, it is observed that the cement treated clay exhibits brittle behaviour as the sample increases to the peak strength then suddenly drops to the residual strength while the un-treated clay shows ductile behaviour with strain hardening. Volumetric and deviatoric strains during isotropic compression and shearing stages cause breaking of cementation bonds which attributes to the unfavourably brittle behaviour of the cement

treated clay. Thus, this chapter further reviewed the effect of fibre inclusion into the cement treated clay to improve the material ductility.

The main aim of adding fibre into the cement treated clay is to provide the bridging effect between the soil-cement clusters since the fibre has strong resistance to tension during the shearing stage. Due to fibre reinforcement, the applied load is transferred efficiently from the tightly packed matrix formed by cementitious products to the fibre body. At high stress level, the fibre is fully mobilised as the frictional and the interlocking forces between fibre and the soil-cement clusters increase preventing further cracks developed within the matrix caused by the cementation degradation. Hence, the shear strength of the improved soil composite increases particularly at the post peak state. The inclusion of fibre changes the brittle behaviour of the cement treated clay to a more ductile behaviour.

In addition, the effectiveness of fibre reinforcement depends on a number of factors such as the fibre content, fibre length, the orientation of fibre, the type of fibre and the confining pressure. Generally, the strength of the improved soil composite increases with the fibre content and the confining pressure. Moreover, at a given fibre content, increasing the fibre length contribute to the increase in the strength at first followed by a reduction in strength with further increase in the fibre length. Furthermore, in the triaxial compression condition, the fibre is most effective when it is placed horizontally crossing the weak plane while the effect of fibre is null when it is placed vertically.

The failure mechanisms of the fibre are assumed due to pull-out or breakage which are characterised by the critical confining stress. Below this critical stress level, the frictional forces between the fibre and the soil matrix are not mobilised, so the failure mode is assumed to be due to pull-out. However, when the fibre is stressed beyond the critical stress, the fibre becomes plastic and rupture may occur due to the frictional force being fully mobilised. When the fibre is ruptured, the effect of fibre reinforcement is diminished, so the behaviour of the improved soil composite would be similar to that of the un-treated soil.

Several constitutive models were developed to simulate the behaviour of the cement treated clay and the fibre reinforced soil. However, the constitutive models for

cement treated clay assumed the linear failure envelope paralleled to the Critical State Line which ignoring the effect of cementation degradation during consolidation to the peak shear strength, particularly at high confining pressures. In addition, many constitutive models adopted the negative hardening rule to simulate the softening behaviour of the cement treated clay which did not capture complex mechanisms involved. Moreover, the constitutive models for fibre reinforced soil assumed a bilinear failure envelope with a kink at the critical confining stress which required separate equations for pull-out and breakage failure modes.

Majority of the previous studies focused on the behaviour of fibre reinforced sand with or without cement, while the extent of studies on the behaviour of fibre reinforced clay with cement remains limited. Moreover, a constitutive model is required to simulate the combined effects of cement and fibre reinforcement for the improved clay composite. Thus, the following chapters further investigate the behaviour of cement treated clay with or without fibre reinforcement under various confining pressures adopting the triaxial tests conducted at UTS Geotechnical Engineering laboratory. Furthermore, constitutive models are developed for the cement treated clay with or without fibre reinforcement, considering the effect of cementation degradation and fibre failure mechanisms.

# Chapter 3

## Developing New Constitutive Models Capturing Cementation Degradation & Fibre Failure

---

### 3.1. General

The importance of cementation degradation has resulted in the advancement of constitutive models to simulate the behaviour of the cement treated clays and the influence of structure, such as those models developed by Kavvadas and Amorosi (2000), Baudet and Stallebrass (2004) and Kasama et al. (2000). More recently, some constitutive models such as the Structured Cam Clay (SCC) model by Horpibulsuk et al. (2010), and the Modified Structured Cam Clay (MSCC) model developed by Suebsuk et al. (2010), have provided a framework for developing a constitutive model where the mean effective stress is modified to include the effect of cementation. However, these constitutive models contain a number of drawbacks which were elaborated in Section 2.4.

Moreover, a number of models have also been developed to simulate the inclusion of fibre in soil, such as the discrete framework proposed by Zornberg (2002) and Diambra and Ibraim (2014). However, these models only focused on the behaviour

of soil improved with fibre, and did not consider the cementation and subsequent degradation of the soil structure. Diambra and Ibraim (2014) also suggested that after the pull-out or rupture of fibre, the ability of fibre to improve soil would be the same as un-improved soil. Thus the contribution made by fibre to the shear strength and failure mechanisms of the improved material, including its pre-and-post peak states are necessary to develop constitutive models. Furthermore, the author has not been aware of any constitutive models developed for clay treated with cement and reinforced with fibre.

Therefore, based on the fundamentals of Critical State Soil Mechanics and Modified Cam Clay model, a constitutive model is proposed to simulate the behaviour of the cement treated clay, considering the effect of cementation and its degradation due to the mean effective stress and the shear deformation. The modified mean effective stress was improved to include the effect of cementation degradation such that as the mean effective stress increases, the contribution of cementation to the modified mean effective stress decreases, representing the cementation bonds breaking. Moreover, the formulation of modified mean effective stress includes the shear degradation depending on the plastic deviatoric strain.

Furthermore, the proposed model for the cement treated clay was extended to simulate the behaviour of the fibre reinforced cemented clay (FRCS), hereafter referred to as the improved soil composite. This model considers the failure mechanism of the improved soil composite that consists of the pull-out or breakage mechanisms in the fibre and the cementation degradation due to increasing plastic volumetric and deviatoric strains. Moreover, the mean effective stress was modified to incorporate the contribution made by the fibre and cement, together with their degradations. The special characteristics of the proposed models in this study include the non-associated plastic potential function derived from a modified plastic energy dissipation equation and the non-linear failure envelope to capture the effects of cementation degradation with or without fibre failures on the peak strength of cement treated clays due to the mean effective stress and deviatoric strain.

This chapter presents the development of the constitutive model for cement treated clay in Section 3.2 while Section 3.3 provides a description of the extended version of the proposed model for the fibre reinforced cemented clay (FRCS).

## 3.2. Development of the Proposed Constitutive Model for Cement Treated clay

In this study the MCC model stress and strain quantities used for a conventional triaxial test (Roscoe and Burland 1968) are adopted as follows:

- The mean effective stress ( $p'$ ), the deviatoric stress ( $q$ ), and the stress ratio ( $\eta$ ) are given by:

$$p' = \frac{\sigma'_1 + 2\sigma'_3}{3} \quad (3.1)$$

$$q = \sigma'_1 - \sigma'_3 \quad (3.2)$$

$$\eta = \frac{q}{p'} \quad (3.3)$$

- The volumetric strain increment ( $d_v$ ) and the deviatoric strain increment ( $d_\varepsilon$ ) are defined as follows:

$$d_v = d\varepsilon_1 + 2d\varepsilon_3 \quad (3.4)$$

$$d_\varepsilon = \frac{2(d\varepsilon_1 - d\varepsilon_3)}{3} \quad (3.5)$$

where  $\sigma'_1$  and  $d\varepsilon_1$  are the axial effective stress and the axial strain increment, respectively, and  $\sigma'_3$  and  $d\varepsilon_3$  are the radial effective stress and the radial strain increment, respectively.

The key aim of stabilising soft soils with cement is the formation of cementation bonds between the particles, which improves the strength and reduces the compressibility. General Purpose Portland cement is often mixed with soils because of its economic advantage and availability. When a cement slurry is added to soil, three major chemical reactions occur between the cement and soil particles which form cementation bonds, namely i) the hydration process, ii) ion exchange or flocculation, and iii) pozzolanic reactions (Lorenzo and Bergado 2006; Porbaha et al. 2000; Sasanian 2011). The hydration process, which takes place in the space between the soil aggregates creates primary cementitious products such as hydrated calcium aluminates

and hydrated limes which form a strong matrix between the soil particles and aggregates (Lorenzo and Bergado 2006). Furthermore, since the pozzolanic reactions occur at a slower rate than the hydration process, further bonding between the primary produced cementitious products forms secondary pozzolanic products that create a bond between the particles within the aggregates. As Sasanian (2011) explained, cohesion in the soil-cement mixture increases as these cementitious products crystallise, to form a strongly bonded structure.

Naturally cemented soils often have variable densities and degrees of cementation presenting difficulties in studying the fundamental behaviour without disturbing the cementation. To overcome such difficulties, many researchers such as Rotta et al. (2003), Kamruzzaman et al. (2009) and Suebsuk et al. (2010) used artificially cement treated soils in their studies. It should be noted that Huang and Airey (1998) reported that the properties of artificially cement treated soils are comparable to naturally cemented soils. Furthermore, the variation of mechanical properties of artificially cemented soils can be reasonably considered to be isotropic (Suebsuk et al. 2010). Therefore, in order to include the effect of the structure and cementation degradation and to overcome the complexity of anisotropic effects, in this study, the material is assumed to be isotropic, while developing the constitutive model for the cement treated clay.

### **3.2.1. Modified Mean Effective Stress**

The mean effective stress affects the behaviour of cement treated clay; as Lorenzo and Bergado (2006), Porbaha et al. (2000), and Yin (2001) reported, cement treated clays are generally brittle, while increasing the mean effective stress leads to an increase in the deviatoric stress at the peak that is similar to over-consolidated soils. Moreover, the friction angle and cohesion in the soil increases due to the addition of cement, particularly at low mean effective stresses, as Lade and Overton (1989) observed, but when the mean effective stress increases in pressures beyond the yield stress, the cementation of cement treated clay decreases due to cracking and cementation degradation, as observed by Uddin et al. (1997). According to Horpibulsuk et al. (2010) and Kasama et al. (2000), cementation strengthens the mean effective

stress, thus soil treated with cement can withstand a higher yield stress than un-treated soil. Kamruzzaman et al. (2009) observed from odometer consolidation tests, carried out on treated and un-treated clays, the yield stress of cement treated clay was much higher than un-treated clay when there was more than 10% of cement. This increase in the yield stress was due to the creation of cementation bonds from chemical reactions, including the hydration and pozzolanic processes (Kamruzzaman et al. 2009; Sariosseiri 2008; Sasanian 2011). Furthermore, when cement treated clays are stressed beyond the yield stress the cementation bonds start to break as the particles of soil undergo plastic deformation. Therefore, cementation relates directly to the mean effective stress ( $p'$ ). Thus, it is convenient to introduce a function as an addition to  $p'$ , which represents the effect of cementation and its degradation. Thus, based on the framework of the Critical State Soil Mechanics and inspired by the MCC model, the modified mean effective stress ( $p'^*$ ) is proposed as follows:

$$p'^* = p' + p'_{\Omega} \quad (3.6)$$

$$p'_{\Omega} = p'_{\Omega,i} \left[ 1 + \left( \frac{p'_0 - p'_{0,i}}{\beta} \right) \right] \exp \left( - \left( \frac{p'_0 - p'_{0,i}}{\beta} \right) \right) \quad (3.7)$$

where  $p'_{\Omega}$  is a function of  $p'$  describing the effect of cementation and  $p'_{\Omega,i}$  is the parameter reflecting the beneficial effect of cementation.  $p'_0$  is the mean effective yield stress or the isotropic consolidation pressures, and  $p'_{0,i}$  is the initial mean effective yield stress on the isotropic compression line (ICL) of cement treated clay. The model fitting parameter ( $\beta$ ) influences the degradation rate of cementation due to the mean effective stress. Since a modified mean effective stress has been used, the stress ratio ( $\eta^*$ ) should also be modified as follows:

$$\eta^* = \frac{q}{p'^*} \quad (3.8)$$

Moreover, clay particles interact together through surface forces such as electrostatic and chemical forces to form particle-clusters (Yin et al. 2009) that increase in size until they weigh more than the inter-particle surface forces; the clusters then stop growing and interact mainly through mechanical forces. Kolovos et al. (2013) explained that during virgin yielding, micro-cracks develop within the clay as the contact forces between the clay clusters increase, and as they continue to extend, the mean effective

stress increases and then macro-cracks are formed when their edges collide. The cement treated clay gradually decreases in strength as a result of cementation degradation until the macro-cracks reach the edge of the sample, and finally fail. The effect of cementation bonds is captured in Equations (3.6) and (3.7) using parameter  $p'_{\Omega}$ . As the mean effective yield stress ( $p'_{o}$ ) increases,  $p'_{\Omega}$  describing the effect of cementation decreases. The micro-cracking process leading up to failure is also captured in the formulation of Equation (3.7) which  $p'_{\Omega}$  diminishes as  $p'_{o}$  approaches a sufficiently high effective pressure.

### 3.2.2. Compressibility Behaviour

Laboratory studies on the compressibility of the cement treated clays in isotropic consolidation tests indicated that the yield stress increased significantly compared to untreated clay (Horpibulsuk et al. 2010; Kamruzzaman et al. 2009). However, because the inclusion of cement results in very stiff clay, compressibility during consolidation is restricted, which leads to an increase in the yield stress Lade and Overton (1989). Figure 3.1 shows the general behaviour of cement treated clay in isotropic compression. In this figure, the isotropic compression line (ICL) of treated clay is positioned above the A-line, thus showing the contribution made by cementation ( $p'_{\Omega,i}$ ) on the increase of initial yield stress ( $p'_{o,i}$ ). The value of  $p'_{\Omega,i}$  can be calculated by the following equation:

$$p'_{\Omega,i} = p'_{o,i} - p'_d \quad (3.9)$$

where  $p'_d$  is the mean effective stress at the intersection between the ICL of the cement treated clay and the A-line, as shown in Figure 3.1. The A-line is the line parallel to the ICL of reconstituted clay (B-line) that merges with the ICL of cement treated clay when  $p' \rightarrow \infty$ .

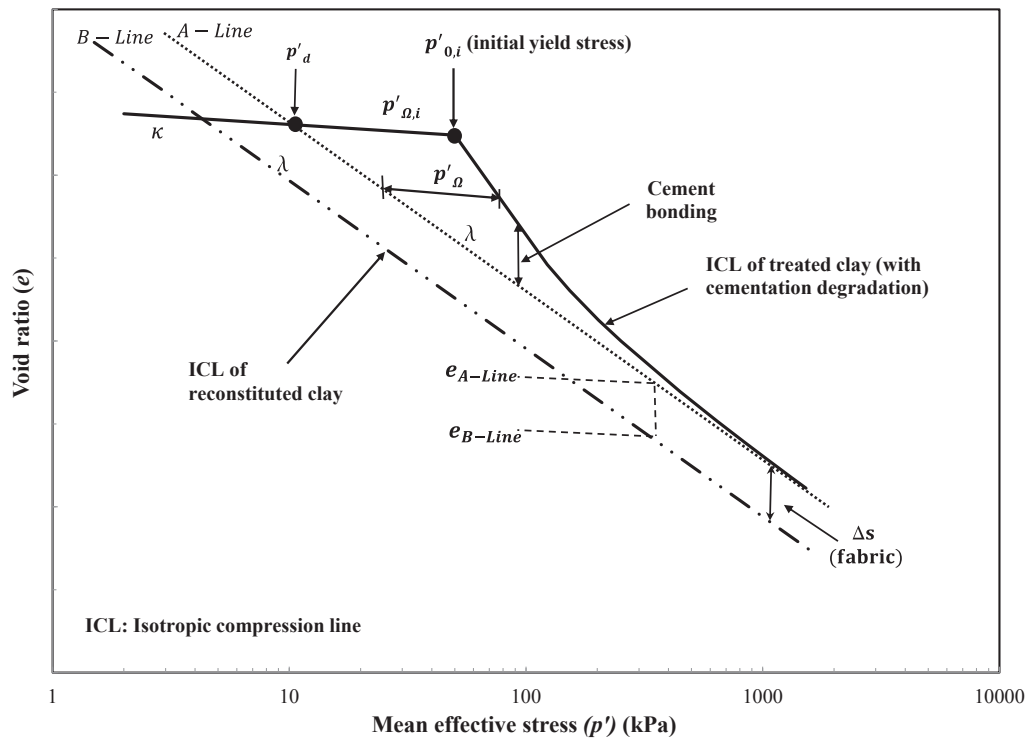


Figure 3.1. Schematic diagram of isotropic compression of the cement treated clay

The structure of cement treated clay can be defined as a combination of fabric and cementation bonding (Baudet and Stallebrass 2004), where fabric defines the arrangement between the clay particles and bonding describes the forces between these particles. The clay fabric is assumed to be a stable arrangement within the structure of clay and it is not affected by any cementation degradation (Baudet and Stallebrass 2004; Suebsuk et al. 2010), but the chemical reactions cause large clusters of particles with large openings to form within the structure of cement treated clay. According to Horpibulsuk et al. (2004), the fabric of cement treated clay includes the clusters of clay and the enclosed pore space. The effect of cementation bonds at high mean effective stresses beyond the initial yield stress is minimal because the large clusters of particles collapse and the void space between them are reduced significantly. Therefore, at this stage the compressibility of the cement treated clay relies mainly on the fabric (Kamruzzaman et al. 2009). Horpibulsuk et al. (2004) further explained that the change in orientation of particles and clusters of clay (change in fabric) during consolidation that brings them closer together stems from an increase in mean effective stresses that leads to an increase in strength, unlike the reconstituted clay at the corresponding void

ratio. According to Liu et al. (2003), the void ratio of treated clays at the final critical state depends on how the particles are rearranged during loading.

When a sample of the cement treated clay is stressed up to the initial yield stress, only elastic deformation occurs. However, according to Suebsuk et al. (2010), the volumetric strain up to the yield stress is negligible. Therefore cement treated clay in this range can have a higher void ratio than reconstituted clay at the same mean effective stress. Moreover, cementation degradation within the elastic region is negligible, and the stress state is assumed to travel along the slope of the swelling line of the reconstituted clay ( $\kappa$ ). Thus, the value of  $p'_{\Omega,i}$  in Equation (3.9) is constant prior to the initial yielding at  $p'_{0,i}$  in this region. However, beyond the yield stress where virgin yielding starts, plastic deformation associated with cementation degradation occurs, as many researchers observed (Horpibulsuk et al., 2010, Kamruzzaman et al., 2009, Suebsuk et al., 2010). Furthermore, Kamruzzaman et al. (2009) explained that the reduction in the void ratio of treated clay as the mean effective stress increases is due to the breakage of cementation bonds. As the structure of cement treated clay is damaged by the mean effective stress and the development of micro-cracks, the effect of cementation contribution ( $p'_{\Omega}$ ) gradually decreases as  $p'_0$  continued to increase. When  $p' \rightarrow \infty$  the ICL of the cement treated clay merges with the A-line; it indicates that the effect of cementation has been completely destroyed ( $p'_{\Omega} \rightarrow 0$ ).

In the proposed model the value of ( $p'_{\Omega}$ ) is formulated to decrease as the stress state of the sample progresses beyond the initial yield stress ( $p'_{0,i}$ ) to include the cementation degradation of the cement treated clay. The A-line is assumed to have the same slope ( $\lambda$ ) as the ICL of the reconstituted clay, as shown in Figure 3.1. The effect of fabric in this study refers to the additional void ratio from the ICL of reconstituted clay (B-line in Figure 3.1) to the A-line due to the reorientation of clay particles and clay clusters formed after treatment that cannot be destroyed by physical loading during isotropic compression. Thus, the effect of fabric can be expressed in the following form:

$$e_{A-line} = e_{B-line} + \Delta s \quad (3.10)$$

where  $e_{A-line}$  is the void ratio corresponding to A-line at the same mean effective stress as the reconstituted clay,  $e_{B-line}$  is the void ratio of reconstituted clay, and  $\Delta s$  is a soil

parameter that describes the additional void ratio due to the effect of fabric change from cementation.

Figure 3.2 shows the predicted compressions obtained from Equations (3.6) to (3.10) for cemented Ottawa Clay. Experimental data were obtained from isotropic compression tests conducted by Sasanian (2011). The values of  $M$ ,  $\lambda$ , and  $\kappa$  were obtained from the compression curve conducted on the reconstituted Ottawa clay, as shown in Figure 3.2. The values of model parameter  $\beta$  and  $\Delta s$  were obtained by curve fitting on the compression curve of cemented Ottawa Clay. As Figure 3.2 shows, the compression curve of cemented clay shifted to the right from the ICL of the reconstituted soil (B-line) due to cementation ( $p'_{\Omega}$ ), but beyond the initial yield stress ( $p'_{0,i} = 69.5$  kPa), the void ratio of cemented clay decreases due to cementation degradation. When the cemented clay is compressed to a high mean effective stress (e.g. 180 kPa in Figure 3.2), the cementation bonding is partially removed, but when the mean effective stress increases further, the void ratio of cement treated clay decreases significantly, indicating that most of the cementation bonds has degraded. Moreover, the  $e$  of cemented clay is still above the  $e$  of reconstituted clay ( $e \geq e_{B-line}$ ), showing how the rearrangement of clay particles affects the structure of cement treated clay, which cannot completely be destroyed. The model parameter  $\Delta s = 0.03$  indicates that in this case, the effect of fabric is insignificant, hence the prediction made by the proposed model agrees with the experimental data, particularly beyond the initial yield stress.

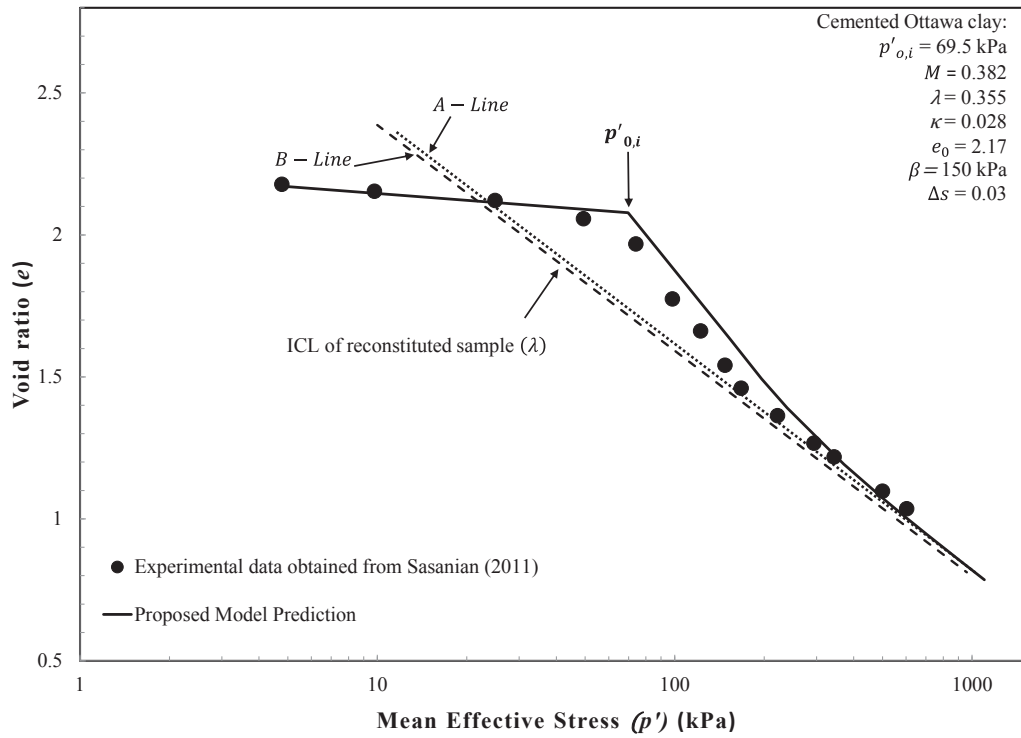


Figure 3.2. The prediction of proposed model on the compressibility of cemented Ottawa clay.

Furthermore, the effect of the fabric component on the compressibility of cement treated clay can be seen in Figure 3.3. The test data were obtained from an isotropic consolidation test on 6% cement treated Ariake clay (Horpibulsuk et al. 2004). The initial yield stress ( $p'_{0,i}$ ) occurs at 60 kPa and the initial void ratio ( $e_0$ ) is 4.37. Note that a further application of the mean effective stress beyond  $p'_{0,i}$  produces a significant drop in the void ratio of cement treated clay as the cementation bonds begin to break. The value of  $\Delta s$  in the model prediction is estimated to be 1.02, indicating that even when the cementation bonds are destroyed due to loading, the stress state at a higher mean effective stress is still well above the ICL of the reconstituted clay due to the effect of fabric change. Thus, in this case, the effect of fabric is quite significant compared to the cemented Ottawa clay ( $\Delta s = 0.03$ ). Kamruzzaman et al. (2009) explained that the effect of fabric change depends on the amount of cement because larger clay-cement clusters formed as the amount of cement increases. By considering the presence of fabric in the structure of cement treated clay, the proposed model can capture the isotropic compression of cement treated Ariake clay quite well, as shown in Figure 3.3.

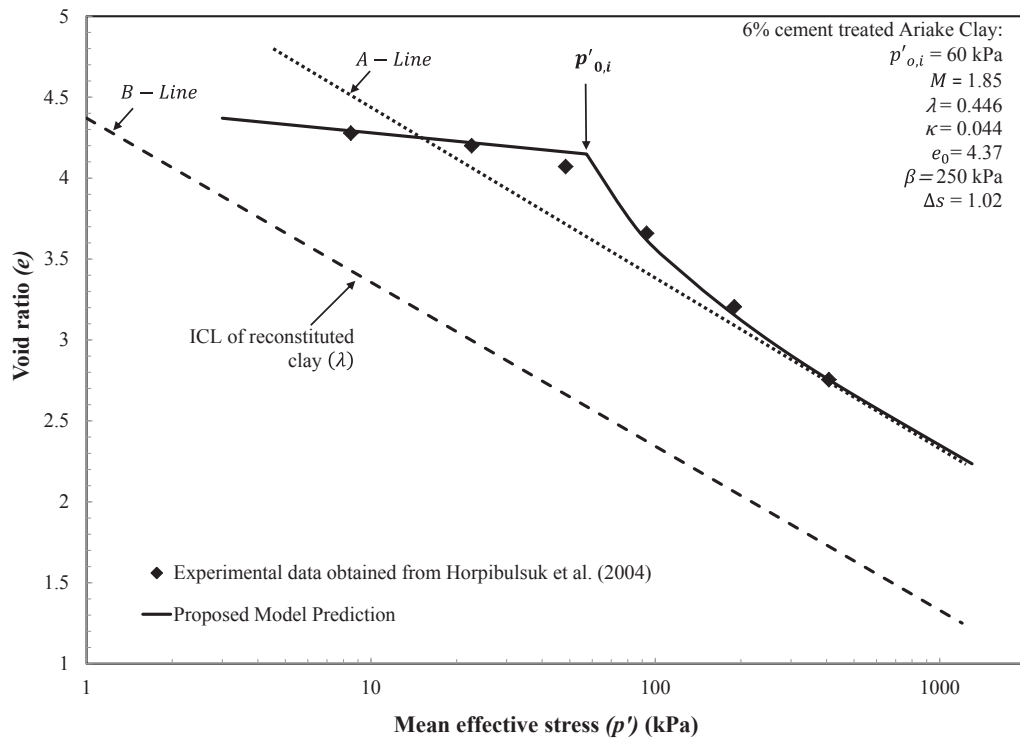


Figure 3.3: The prediction of proposed model on the compressibility of 6% cemented Ariake clay

### 3.2.3. Proposed Failure Envelope

The development of the constitutive model aims to describe the effect of cementation degradation at high effective confining pressures as it merges to the Critical State Line of reconstituted soil, while at the low effective confining pressure range, the model shows a beneficial contribution of cementation to the shear strength. Thus, it is critical to model the transition, where the effect of cementation degradation takes place. According to Kamruzzaman et al. (2009), the breakage of cementation bonds can be associated with yielding, thus indicating the occurrence of cementation degradation, as confirmed by Rotta et al. (2003). Furthermore, Shen et al. (2012) suggested that the clayey materials exhibit inelastic behaviour due to plastic deformation beyond the yield stress and the damage caused by the growth of micro-cracks. Therefore, when the mean effective stresses are lower than the yield stress, the beneficial contribution of cementation plays a dominant role on the shear strength of the cement treated clay

because the effect of cementation degradation is insignificant. However, beyond the yield stress the contribution made by cementation apparently degrades during the consolidation process that induces yielding. Suebsuk et al. (2010) and Kamruzzaman et al. (2009) suggested that destructuration occurs with the stress state on the yield surface, thus the effect of cementation degradation in the low mean effective stress range can only occur during shearing. In this proposed model the authors developed a non-linear failure envelope to capture the degradation effect of cementation. Equation (3.7) introduces the parameter  $\beta$  to capture the degradation rate that influences deformation and the peak shear strength of the cement treated clays. Moreover, this proposed failure envelope is formulated to merge with the Critical State Line (CSL) of reconstituted soil-cement mixture as the mean effective stress continues to increase, while the model still considers the effect of cementation at low stress ranges. Thus, the failure envelope takes the form of:

$$q = M[p' + \xi p'_{\Omega}] \quad (3.11)$$

where  $\xi$  is the correlation factor influencing the effect of cementation contribution to the shear strength and  $M$  is the slope of the failure envelope of the reconstituted soil-cement mixture.

Furthermore, when the mean effective stress is zero the proposed failure envelope in Equation (3.11) intersects with the vertical axis in  $p' - q$  plane at  $q = C_c$ .

where  $C_c$  represents the beneficial contribution of cementation to the shear strength when the mean effective stress is zero.

Incorporating the above condition ( $q = C_c$  when  $p' = 0$ ) into Equations (3.7) and (3.11) yields the following relationship:

$$\xi = \frac{C_c}{p'_{\Omega,1} M} \quad (3.12)$$

The model parameter  $C_c$  is associated with the contribution made by cementation to the shear strength of cement treated clay.

Combining Equations (3.6), (3.7) and (3.12) results in the modified mean effective stress as follows:

$$p'^* = p' + p'_{\Omega} \quad (3.13)$$

$$p'_{\Omega} = \frac{c_c}{\xi M} \left[ 1 + \left( \frac{p'_0 - p'_{0,i}}{\beta} \right) \right] \exp \left( -\frac{p'_0 - p'_{0,i}}{\beta} \right) \quad (3.14)$$

The substitution of  $p'_{\Omega}$  presented in Equation (3.14) into Equation (3.11) results in a non-linear failure envelope in the following form:

$$q = Mp' + C_c \left[ 1 + \left( \frac{p'_0 - p'_{0,i}}{\beta} \right) \right] \exp \left( -\frac{p'_0 - p'_{0,i}}{\beta} \right) \quad (3.15)$$

In this study, the additional strength ( $p'_{\Omega}$ ) due to the beneficial contribution of cementation to the shear strength of the soil is proposed so that as the mean effective yield stress ( $p'_0$ ) increases to a high pressure ( $p'_0 \rightarrow \infty$ ),  $p'_{\Omega}$  approaches zero, because the effect of cementation progressively diminishes. The proposed failure envelope (the peak shear strength of cement treated clay) is influenced by the cementation degradation due to the mean effective stress. Furthermore, the correlation factor ( $\xi$ ) can be estimated by comparing the triaxial shear and isotropic consolidation test results adopting Equation (3.12). It should be noted that the proposed failure envelope in Equation (3.15) will convert to the MCC model (i.e.  $q = Mp'$ ) when the cementation has no effect ( $p'_{\Omega,i} = C_c = 0$ ).

Some of the existing models such as the Structured Cam Clay (SCC) model developed by Horpibulsuk et al. (2010) and the Extended Critical State model proposed by Kasama et al. (2000), assumed that the failure envelope of cement treated clay is a straight line, parallel to, and located above the CSL of reconstituted soil-cement mixture. Consequently, the peak shear strength of cement treated clay in a higher mean effective stress range would be over-estimated because the effect of cementation degradation due to increasing the mean effective stress is not considered. As Figure 3.4 shows, the peak shear strength of Indian Marine clay treated with 3% of lime at a high mean effective stress lies almost on the CSL of reconstituted soil. There is a reduction in strength due to cementation degradation at a high mean effective stress, but the existing models (e.g. Structured Cam Clay model and Extended Critical State model) chose to ignore this effect. Thus, the proposed model aims to formulate the failure envelope in Equation (3.15) to capture the effect of cementation degradation due to the applied mean effective stress. The proposed failure envelope in Figure 3.4 in the early

stages of loading shows the effect of cementation contribution to the shear strength of cement treated clay with  $\xi = 0.73$  and  $C_c = 27.5$  kPa but the proposed failure envelope gradually approaches the CSL of the reconstituted soil as the mean effective stress continues to increase, which captures the influence of cementation degradation on the peak shear strength very well, particularly at high mean effective stresses, as shown in Figure 3.4. It should be noted that within the elastic region when the applied stress is less than the initial yield stress ( $p'_{o,i} > p'_o$ ), the cementation degradation is assumed to be negligible, and thus  $p'_{\Omega} = p'_{\Omega,i} = \frac{C_c}{\xi M}$ . Moreover, based on observations of Indian Marine clay treated with lime at a low mean effective stress (the first two data points in Figure 3.4), there are some disparities between the model predictions and the test data that can be explained by the difference in the size of the initial yield surface, i.e. the samples of cement treated clay may have the same type of minerals and structure, but the degree of structure within the samples may be different (Liu and Carter 2002). Furthermore, as Moses et al. (2003) and Panda and Rao (1998) suggested, the behaviour of cement treated clay at low mean effective stresses can be described as over-consolidated soils, and the sample strength may be affected by a long period of shear process. Furthermore, according to Moses et al. (2003), the bond strength depends not only on the stress level within the soil, but also on other factors such as the strain rate, the duration of shear process and the type of loading.

Although, there are some disparities while comparing the predicted failure envelope and experimental data for the 3% cemented Indian marine clay particularly at the low mean effective stress range, the coefficient of determination is found to be 0.96, indicating a well fitted failure envelope. Moreover, the main aim of this study is to develop a constitutive model to capture the cementation degradation which is more pronounced in higher mean effective stresses.

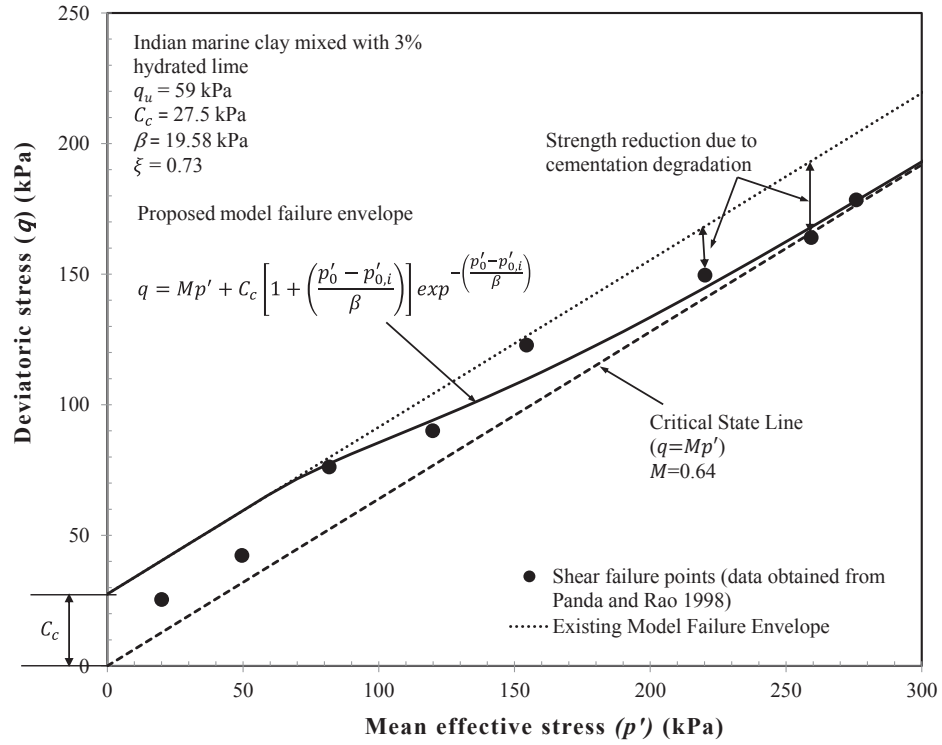


Figure 3.4: Proposed failure envelope prediction of 3% lime treated Indian Marine clay

### 3.2.4. Elastic Deformation

Elastic deformation occurs when the stress state is inside the yield surface, so Hooke's Law is used in the proposed model to describe the elastic deformation of cement treated clay, as employed by a number of researchers such as Perić and Ayari (2002), Horpibulsuk et al. (2010) and Wood (1990). On the basis of experimental observations, Horpibulsuk et al. (2010) suggested that cementation bonds increase the strength of cement treated clays in the elastic region, hence by adopting the modified mean effective stress ( $p'^*$ ), the proposed model assumes an elastic deformation (including , the elastic volumetric strain increment ( $d_v^e$ ) and the elastic deviatoric strain increment ( $d_\varepsilon^e$ )) that depends on the effect of cementation, and thus takes the following form:

$$d_v^e = \frac{\kappa}{1+e} \left( \frac{dp'^*}{p'^*} \right) \quad (3.16)$$

$$d\varepsilon^e = \frac{2\kappa(1+\nu)}{9(1-2\nu)(1+e)} \left( \frac{dq}{p'^*} \right) \quad (3.17)$$

where  $\nu$  is Poisson's ratio.

### 3.2.5. Proposed Yield Function

In this study cement treated clay is assumed to be an isotropic material possessing elastic and virgin yielding behaviour. Therefore, when the stress state of cement treated clay is on the yield surface, virgin yielding occurs and causes plastic deformation. By following the Modified Cam Clay (MCC) model, the yield function in  $p' - q$  plane can be presented as follows:

$$f = q^2 - M^2 p'^* (p'_0 - p'^*) = 0 \quad (3.18)$$

where  $p'_0 = p'_0 + p'_\Omega$ ,  $p'^*$  is the size of the yield surface where it meets the horizontal axis ( $q = 0$ ) in the  $p' - q$  plane, and  $p'_0$  is a hardening parameter that corresponds to the mean effective stress ( $p'$ ) on the yield surface when  $q = 0$ .

Yapage and Liyanapathirana (2012) suggested that cement treated clay possesses tensile strength as the size of the yield surface expands due to the effect of cementation bonding. Thus, in this proposed model,  $p'_\Omega$  is included in the size of the yield surface ( $p'^*$ ) to represent the tensile strength of cement treated clay. It should be pointed out that the critical state condition ( $\eta^* = 0$  when  $p'_0 = p'^*$ ) must be satisfied when formulating the proposed yield function. As shown in Figure 3.5, the parameter  $C_c$  affects the proposed yield surface such that increasing the value of  $C_c$  expands the yield surface due to  $p'_\Omega$  increase. As Figure 3.5 shows, when  $C_c = 0$ , the shape of the proposed yield surface is similar to the MCC model. Figure 3.6 shows the expansion in the proposed yield surface as the hardening parameter ( $p'_0$ ) increases, but as the yield surface increases in size, the value of  $p'_\Omega$  decreases accordingly due to the cementation degradation, caused by an increase in the mean effective stress.

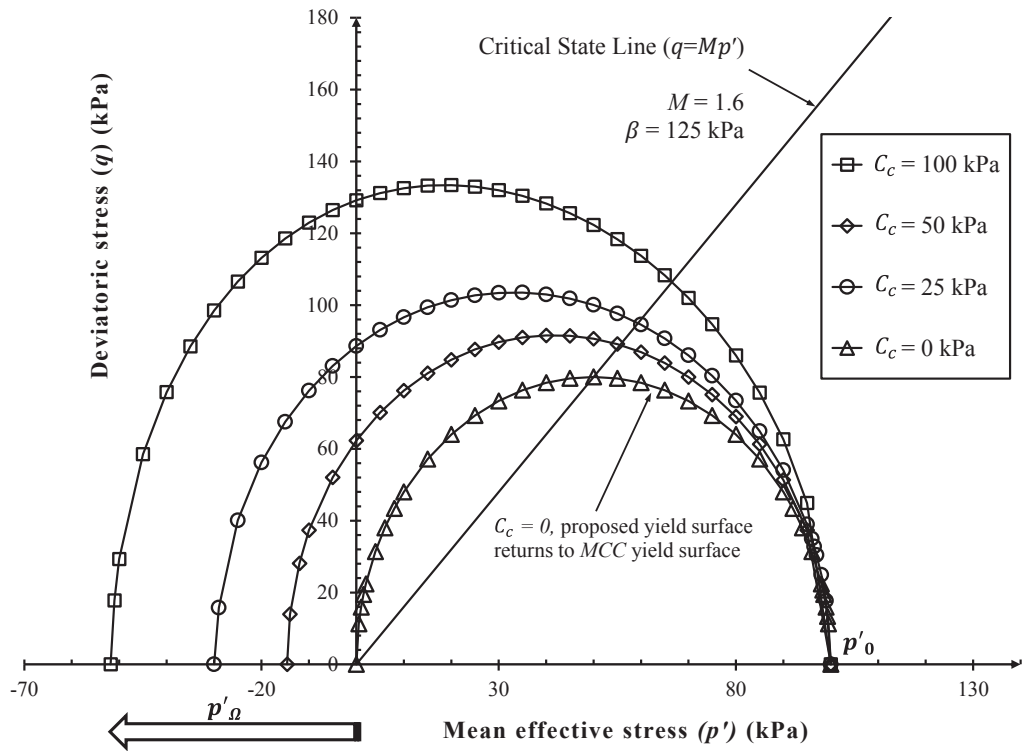


Figure 3.5. The effect of increasing parameter  $C_c$  on the proposed yield surface.

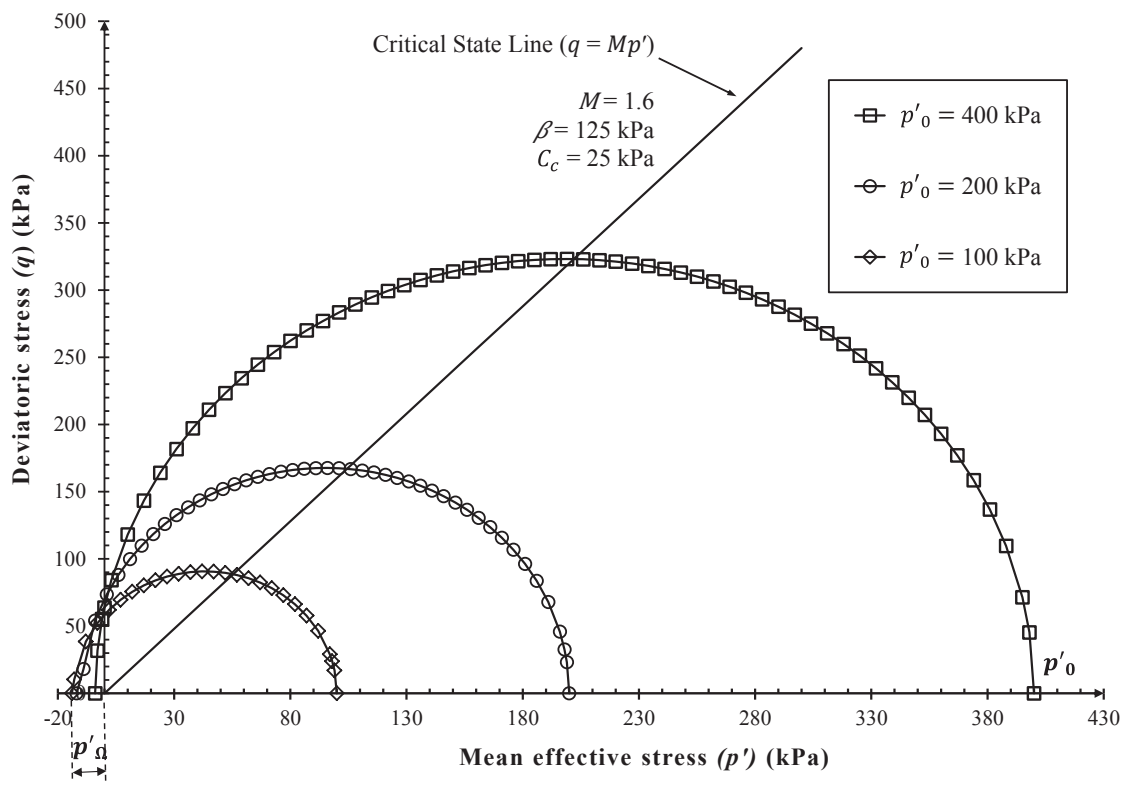


Figure 3.6. The effect of increasing hardening parameter  $p'_0$  on the proposed yield surface for cement treated clay

### 3.2.6. Plastic Energy Dissipation Equation

The internal plastic energy per unit volume ( $dW_{in}$ ) available for a soil sample to dissipate in the triaxial test under the applied mean effective stress ( $p'$ ) and the shear stress ( $q$ ), is expressed as (Wood 1990):

$$dW_{in} = p' d_v^p + q d_\varepsilon^p \quad (3.19)$$

where  $d_v^p$  and  $d_\varepsilon^p$  are the plastic volumetric strain increment and the plastic deviatoric strain increment, respectively.

MCC model assumes an expression for the dissipation of internal energy as follows (Roscoe and Burland 1968):

$$p' d_v^p + q d_\varepsilon^p = p' \sqrt{(d_v^p)^2 + (M d_\varepsilon^p)^2} \quad (3.20)$$

A more generalised equation of energy dissipation proposed by Kasama et al. (2000) is described in Equation (2.17)

The energy equation for cement treated clay proposed in this study is presented in line with the internal plastic energy dissipation and inspired by the energy dissipation expression adopted by Kasama et al. (2000), as follows:

$$p' d_v^p + q d_\varepsilon^p = (p' + \xi p'_\Omega) \sqrt{(d_v^p)^2 + (M d_\varepsilon^p)^2 + d_v^p \{X d_\varepsilon^p - Y d_v^p\}} \quad (3.21)$$

$$Y = 2\eta^* \left[ \frac{p'}{(p' + \xi p'_\Omega)} - \left( \frac{\alpha + 1}{A} \right) \right] \quad (3.22)$$

$$Y = \left[ 1 - \frac{p'^2}{(p' + \xi p'_\Omega)^2} \right] \quad (3.23)$$

It should be noted that  $\alpha$  is a non-dimensional anisotropic parameter that accounts for the balancing of deviatoric and volumetric plastic strain parameters, but

when cementation has no effect ( $C_c = 0$ ) and  $\alpha = 0$ , Equation (3.21) reduces to the MCC plastic energy dissipation equation in Equation (3.20).

For an isotropic compression case where  $q = 0$  and  $d_\varepsilon^p = 0$ , Equation (3.21) will reduce to:

$$dW_{in} = p' d_v^p \quad (3.24)$$

Moreover, on the Critical State Line where  $q = M(p' + \xi p'_\Omega)$  and  $d_v^p = 0$ , Equation (3.21) can be simplified as:

$$dW_{in} = M(p' + \xi p'_\Omega) d_\varepsilon^p \quad (3.25)$$

Since the proposed model is complex and developed based on a semi-empirical method, the proposed plastic energy dissipation equation (Equation (3.21)) is formulated depending on the simplicity of deriving the flow rules and the plastic potential function. Moreover, Equations (3.24) and (3.25) must be satisfied when choosing an appropriate expression for the plastic energy dissipation equation.

The term  $A$  in Equation (3.21) is introduced as the derivative of  $p'^*$  in Equation (3.13) with respect to  $p'$ , while  $p'_0$  is a hardening parameter that corresponds to the mean effective stress ( $p'$ ) on the yield surface when  $q = 0$ . It is convenient to express the value of  $p'_0$  as a function of  $p'$ . For the sake of a simple derivation, Equation (3.14) can be expressed in terms of  $p'$  by substituting the value of  $p'_0$  in Equation (3.18). The expression of  $p'^*$  in terms of  $p'$  can only be substituted in the yield surface function to calculate the value of  $p'_0$  in terms of  $p'$ . The value of  $p'_0$  in the yield surface function is used in the model to include the effect of cementation degradation as follows:

$$p'_0 = \frac{q^2}{M^2 \left[ p' + \frac{C_c}{\xi M} (1+K) \exp^{-K} \right]} + p' \quad (3.26)$$

$$\text{where, } K = \frac{1}{\beta} \left[ \frac{q^2}{M^2 \left( p' + \frac{C_c}{\xi M} \right)} + p' - p'_{0,i} \right] \quad (3.27)$$

The substitution of  $p'_0$  obtained from Equation (3.26) into Equation (3.14) allows for a derivation of the term  $A$  (see Equation (3.21)) to take the following form:

$$A = \frac{dp'^*}{dp'} = 1 - \frac{\Psi C_c}{\xi M \beta^2} \left[ \frac{q^2}{M^2 \left( p' + \frac{C_c}{\xi M} \right)} + p' - p'_{0,i} \right] \exp^{-\frac{1}{\beta} \left( \frac{q^2}{M^2 p'^*} + p' - p'_{0,i} \right)} \quad (3.28)$$

where  $\Psi$  is the derivative of  $p'_0$  in Equation (3.26) with respect to  $p'$  which can be presented as follows:

$$\Psi = 1 - \frac{q^2}{M^2 p'^{*2}} \left[ 1 + \frac{C_c}{\xi M \beta^2} \left( \frac{q^2}{M^2 \left( \frac{C_c}{\xi M} + p' \right)^2} - 1 \right) \left( \frac{q^2}{M^2 \left( \frac{C_c}{\xi M} + p' \right)} + p' - p'_{0,i} \right) \exp^{-K} \right] \quad (3.29)$$

### 3.2.7. Flow Rule and Plastic Potential Function

One important feature of this proposed model is the development of a non-associated plastic potential function based on an energy dissipation equation. The MCC model adopted an associated flow rule where the yield surface was the same as the plastic potential surface. However, Bousshine et al. (2001) suggested that soil materials generally exhibit a non-associated plastic flow rule because the strain parameter vectors are not normal to the yield locus. Thus, the proposed non-associated plastic potential function includes the effect of cementation and its degradation. By solving and rearranging the energy equation proposed in Equation (3.21), the relationship between  $d_v^p$  and  $d_\varepsilon^p$  can be derived as follows:

$$\frac{d_v^p}{d_\varepsilon^p} = \frac{A(M^2 - \eta^{*2})}{2\eta^*(\alpha + 1)} \quad (3.30)$$

The partial derivative of the modified stress ratio ( $\eta^*$ ) (with respect to  $p'$  and  $q$ ) can be presented in the following form:

$$d\eta^* = \frac{-qA}{p'^{*2}} dp' + \frac{dq}{p'^*} \quad (3.31)$$

Using Equations (3.30) and (3.31) and taking integration to incorporate the boundary condition ( $p' = p'_0$  when  $q = 0$ ), the plastic potential function ( $g$ ) can be derived as:

$$g = q^2(1 + 2\alpha) + M^2 p'^{*2} \left[ 1 - \left( \frac{p'_{\Omega}}{p'^*} \right)^{\left( \frac{2\alpha+1}{\alpha+1} \right)} \right] = 0 \quad (3.32)$$

The plastic potential function ( $g$ ) in Equation (3.32) can also be expressed in the following form to determine the size of the plastic potential surface ( $p'_{\Omega}$ ):

$$\frac{p'_{\Omega}}{p'^*} = \left[ \frac{q^2(2\alpha+1)}{p'^{*2}M^2} + 1 \right]^{\left( \frac{1+\alpha}{2\alpha+1} \right)} \quad (3.33)$$

The authors have selected an appropriate expression for the energy equation (Equation 3.21) for the cement treated clay to capture the effects of cementation and its degradation. In order to derive the equation for the plastic potential function, numerous mathematical procedures have been implemented. A detailed derivation of the plastic potential function is included in *Appendix A*.

Figure 3.7 shows that the plastic potential surface expands in size due to an increase in the hardening parameter  $p'_{\Omega}$ . The effect of cementation denoted by  $p'_{\Omega}$  decreases as the mean effective stress increases, thus capturing the effect of cementation degradation. Moreover, in order to evaluate the effect of  $\alpha$ , Figure 3.8 shows the shape of the plastic potential function ( $g$ ) together with variations of  $\alpha$ . With the same level of  $p'_{\Omega}$ , an increase in  $\alpha$  results in a contraction of the plastic potential surface. However, when  $\alpha = 0$ , the plastic potential function (Equation 3.32) is identical to the proposed yield surface (Equation 3.18) and consequently the proposed model satisfies the associated flow rule conditions.

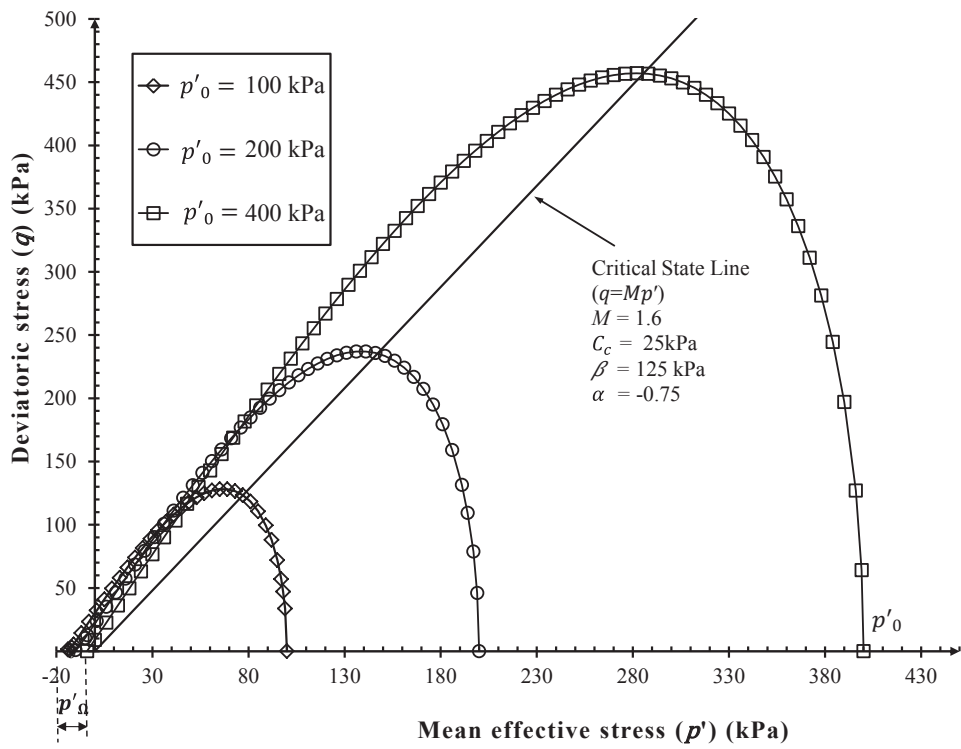


Figure 3.7. The effect of hardening parameter  $p'_0$  on the proposed plastic potential surface

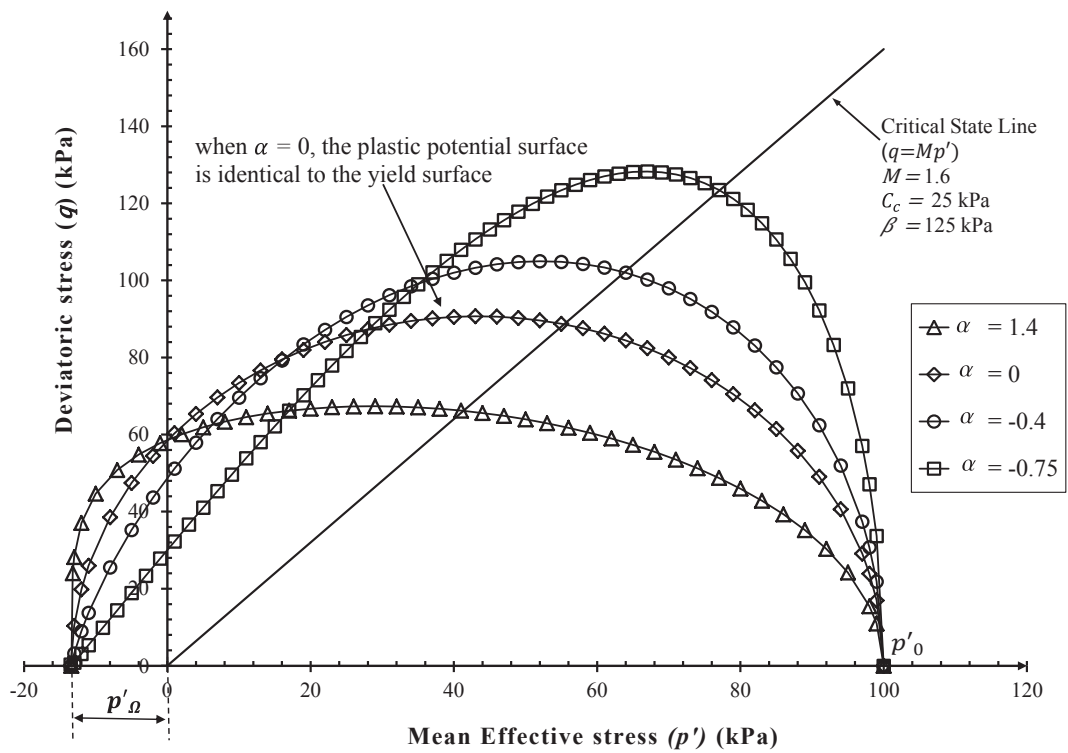


Figure 3.8. The effect of variation of  $\alpha$  on the proposed plastic potential.

### 3.2.8. Virgin Yielding Behaviour

When the stress state of cement treated clays is on the yield surface and with  $dp'_{0*} > 0$ , the virgin yielding occurs resulting in the plastic deformation. The proposed model adopts the normality rule where plastic strains are normal to the plastic potential surface. Following the framework of plasticity theory, the plastic strains can be written in the following form:

$$d_v^p = d\lambda \frac{\partial g}{\partial p'^*} \quad (3.34)$$

$$d_\varepsilon^p = d\lambda \frac{\partial g}{\partial q} \quad (3.35)$$

where  $d\lambda$  is the non-negative plastic multiplier that can be determined according to plasticity theory (Yu 2006), as follows:

$$d\lambda = \frac{-\left(\frac{\partial f}{\partial p'^*} dp'^* + \frac{\partial f}{\partial q} dq\right)}{\frac{\partial f}{\partial p'^*} \cdot \frac{\partial p'^*_{0*}}{\partial v^p} \cdot \frac{\partial g}{\partial p'^*}} \quad (3.36)$$

The proposed model assumes that the hardening parameter  $p'^*_{0*}$  depends on the plastic volumetric strain ( $d_v^p$ ), so a hardening equation is proposed in the following manner:

$$\frac{dp'^*_{0*}}{p'^*_{0*}} = \frac{(1+e)}{(\lambda-\kappa)} dv^p \quad (3.37)$$

To determine  $d_v^p$ ,  $d_\varepsilon^p$  and  $d\lambda$ , partial differentiations of yield surface function (Equation 3.18) and the plastic potential function (Equation 3.32) are calculated as follows:

$$\frac{\partial f}{\partial p'^*} = \frac{-2q^2}{M^2 p'^{*3}} + \frac{p'^*_{0*}}{p'^{*2}} \quad (3.38)$$

$$\frac{\partial f}{\partial q} = \frac{2q}{M^2 p'^{*2}} \quad (3.39)$$

$$\frac{\partial f}{\partial p'^*_{0*}} = -\frac{1}{p'^*} \quad (3.40)$$

$$\frac{\partial g}{\partial p'^*} = \frac{-2q^2(1+2\alpha)}{M^2 p'^*{}^3} + \left(\frac{2\alpha+1}{\alpha+1}\right) \frac{1}{p'^*} \left(\frac{p'^*_0}{p'^*}\right)^{\left(\frac{2\alpha+1}{\alpha+1}\right)} \quad (3.41)$$

$$\frac{\partial g}{\partial q} = \frac{2q(1+2\alpha)}{M^2 p'^*{}^2} \quad (3.42)$$

By combining Equations (3.34) to (3.42), the following equations are proposed to predict the plastic deformation, including the plastic volumetric strain increment ( $d_v^p$ ) and the plastic deviatoric strain increment ( $d_\varepsilon^p$ ):

$$d_v^p = \frac{\lambda-\kappa}{1+e} \left[ \frac{dp'^*}{p'^*} + \frac{2\eta^* d\eta^*}{M^2 \left(\frac{\eta^{*2}(2\alpha+1)+M^2}{M^2}\right)^{\left(\frac{1+\alpha}{2\alpha+1}\right)}} \right] \quad (3.43)$$

$$d_\varepsilon^p = \frac{\lambda-\kappa}{1+e} \left[ \frac{dp'^*}{p'^*} + \frac{2\eta^* d\eta^*}{M^2 \left(\frac{\eta^{*2}(2\alpha+1)+M^2}{M^2}\right)^{\left(\frac{1+\alpha}{2\alpha+1}\right)}} \right] \left[ \frac{2\eta^*(\alpha+1)}{M^2 - \eta^{*2}} \right] \quad (3.44)$$

When the effect of cementation diminishes ( $C_c = 0$ ) and  $\alpha$  is set to be 0, the proposed plastic deformation returns to that of the MCC model which is in the form of:

$$d_v^p = \frac{\lambda-\kappa}{1+e} \left( \frac{dp}{p} + \frac{2\eta d\eta}{\eta^2 + M^2} \right) \quad (3.45)$$

$$d_\varepsilon^p = \frac{\lambda-\kappa}{1+e} \left( \frac{dp}{p} + \frac{2\eta d\eta}{\eta^2 + M^2} \right) \left( \frac{2\eta}{M^2 - \eta^2} \right) \quad (3.46)$$

### 3.2.9. Modified Mean Effective Stress Including Shear Degradation

Destructurisation of cement treated clay is mainly caused by the volumetric and shear deformations (Baudet and Stallebrass 2004; Kavvas and Amorosi 2000; Suebsuk et al. 2010). According to Suebsuk et al. (2010), the structure strength of cement treated clay decreases as a result of cementation degradation. In this proposed model, the cementation degradation of cement treated clay during shearing is assumed to be related to the plastic deviatoric strain ( $\varepsilon_q^p$ ). The equation describing the

cementation degradation due to shear deformations is formulated to describe how the structure degrades, viz:

$$\frac{p''_{\Omega}}{p'_{\Omega}} = \frac{1}{1 + \omega \varepsilon_q^p \exp(\omega \varepsilon_q^p - b)} \quad (3.47)$$

where  $b$  and  $\omega$  are the soil parameters affecting the shear degradation rate and  $p''_{\Omega}$  describes the reduced effects of cementation induced by cementation degradation due to deviatoric strain. Thus, the modified mean effective stress in Equation (3.13) is altered to include the effect of degradation due to deviatoric strains as follows:

$$p'^* = p' + p''_{\Omega} = p' + \frac{\frac{c_c}{\xi M} \left[ 1 + \left( \frac{p'_0 - p'_{0,i}}{\beta} \right) \right] \exp\left(-\left(\frac{p'_0 - p'_{0,i}}{\beta}\right)\right)}{1 + \omega \varepsilon_q^p \exp(\omega \varepsilon_q^p - b)} \quad (3.48)$$

Figure 3.9 contains a schematic diagram showing a reduction in the effects of cementation ( $p''_{\Omega}$ ) due to the shear degradation of cementation. At the initial stage of shearing ( $\varepsilon_q = 0$ ), the structural strength of cement treated clay is represented by  $p'_{\Omega}$  which captures the mean effective stress during isotropic compression. When the sample is stressed inside the yield surface, only elastic deformation occurs, and hence the proposed model assumes there is no shear degradation within the elastic region, but when the stress state arrives at the yield surface, plastic shear deformation occurs due to deviatoric stress ( $d_{\varepsilon}^p > 0$ ) that reduces the effect of cementation ( $p'_{\Omega} > p''_{\Omega}$ ). As  $\varepsilon_q$  continues to increase beyond the corresponding values to the peak strength state,  $p''_{\Omega}$  suddenly decreases towards the residual value of zero, indicating that cementation is completely destroyed when  $\varepsilon_q \rightarrow \infty$ . Thus, Equation (3.48) is formulated to capture the cementation degradation due to the combined mean effective stress and deviatoric strain on the behaviour of the cement treated clays.

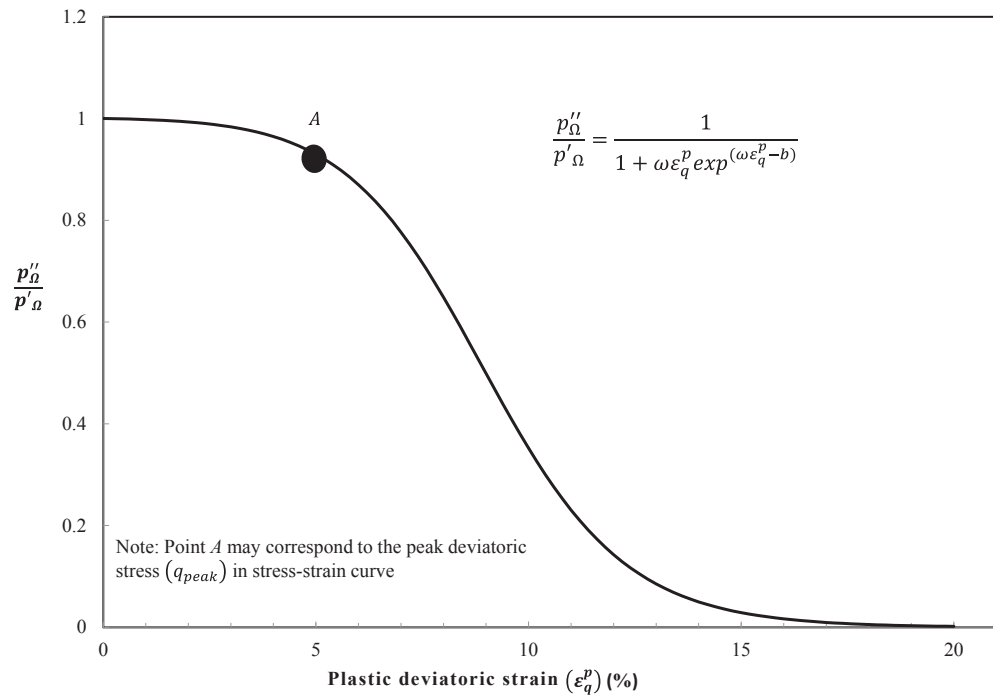


Figure 3.9: Schematic diagram of destructurisation

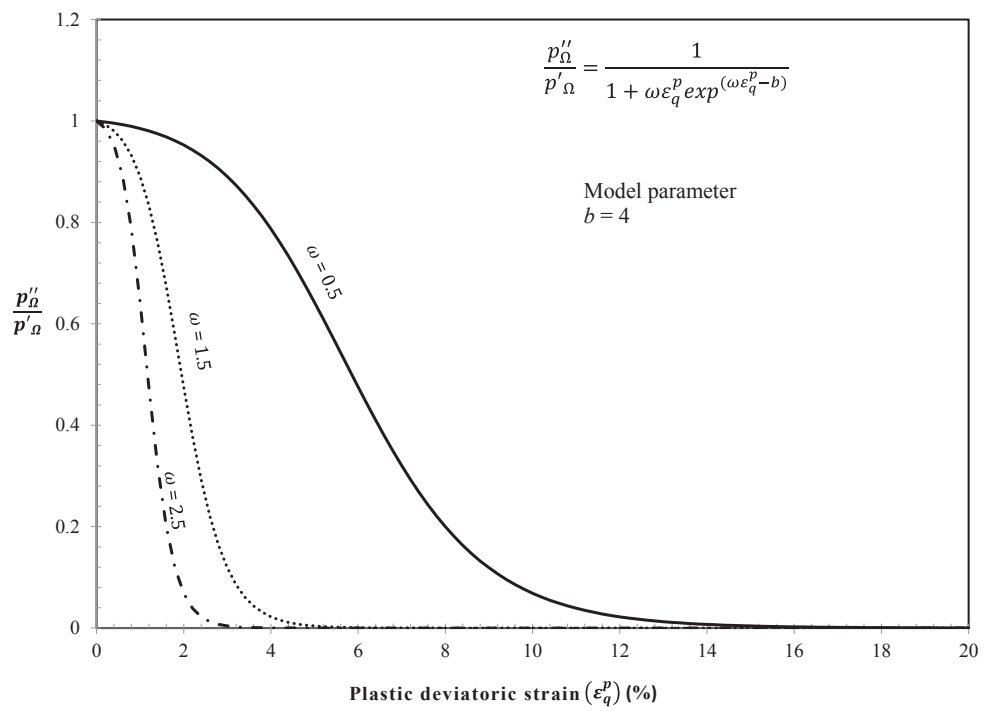


Figure 3.10: Effect of increasing parameter  $\omega$  on destructuring process

As Figure 3.10 shows, increasing parameter  $\omega$  helps to increase the rate of degradation due to shear deformation; for example, when  $\omega = 2.5$ , the rate of cementation degradation due to deviatoric strain is more than when  $\omega = 0.5$ . However, increasing parameter  $b$  shifts the cementation degradation to smaller deviatoric strains, as shown in Figure 3.11.

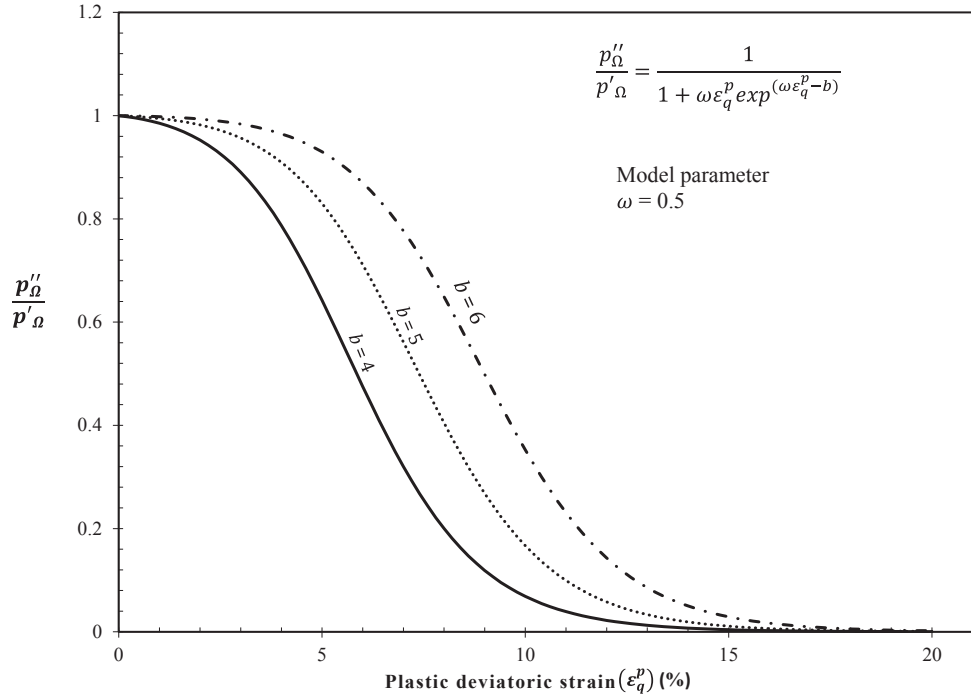


Figure 3.11: Effect of increasing parameter  $b$  on degradation process

The effect of cementation ( $p'_\Omega$ ) changes during plastic deformation because the yield surface varies in size due to the plastic volumetric strain (Equation 3.37) during drained and undrained shearing. Therefore  $p'_0$  changes and Equation (3.26) is modified to include the effect of cementation degradation due to plastic deviatoric strain:

$$p'_0 = \frac{q^2}{M^2 \left[ p' + \frac{\frac{C_C}{\xi M} (1+K) \exp^{-K}}{1 + \omega \epsilon_q^p \exp^{(\omega \epsilon_q^p - b)}} \right]} + p' \quad (3.49)$$

With the modified mean effective stress ( $p''_{\Omega}$ ) proposed in Equation (3.48), the proposed failure envelope in Equation (3.15) can be modified to include the effect of cementation degradation due to deviatoric strain, as follows:

$$q = Mp' + \frac{C_c \left[ 1 + \left( \frac{p'_0 - p'_{0,i}}{\beta} \right) \right] \exp \left( - \left( \frac{p'_0 - p'_{0,i}}{\beta} \right) \right)}{1 + \omega \varepsilon_q^p \exp(\omega \varepsilon_q^p - b)} \quad (3.50)$$

Figure 3.12 shows the proposed failure envelope (Equation 3.50) in the  $p' - q$  plane, which is located above the Critical State Line (CSL) of the reconstituted soil-cement mixture. A failure envelope is formulated such that at low mean effective stress, parameter  $C_c$  describes the beneficial contribution of cementation as shown by the intersection of the proposed failure envelope with the vertical axis at  $p' = 0$ . While the mean effective stress continues to increase to high mean effective stresses or deviatoric strains, the effect of cementation reduces as the proposed failure envelope gradually merges with the CSL of reconstituted soil-cement mixture and thus captures the effect of cementation degradation due to the mean effective stress and the deviatoric strain.

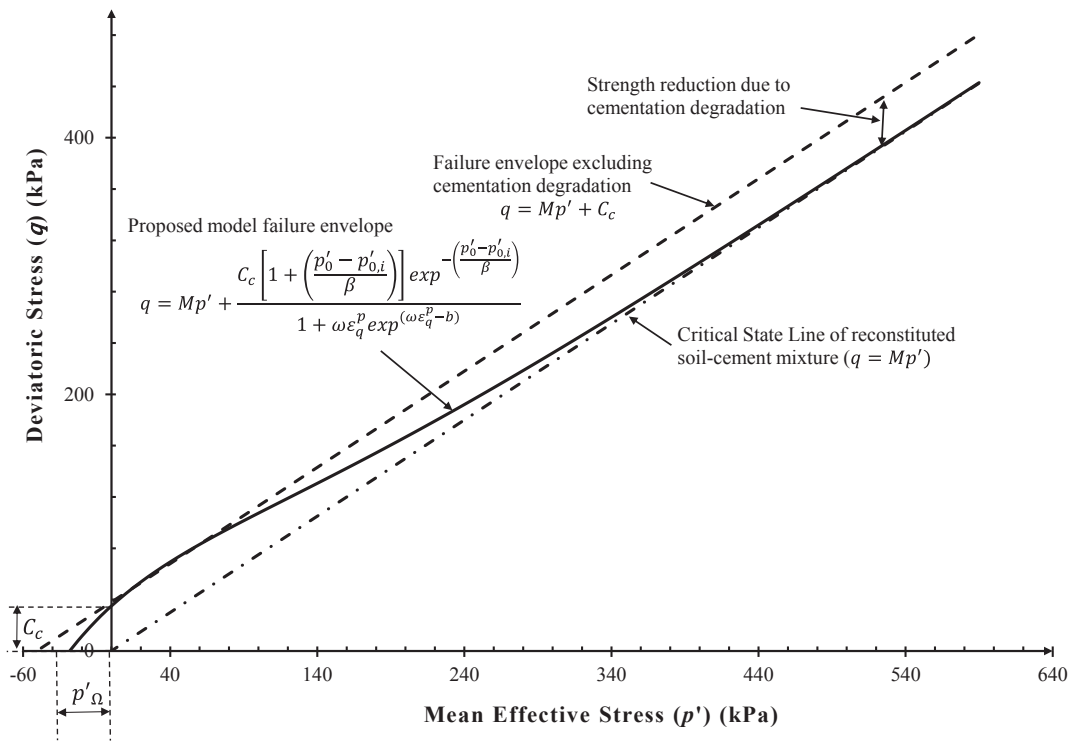


Figure 3.12. The proposed failure envelope for cement treated clay

### 3.2.10. General Stress-Strain Relationship

With the modified mean effective stress (Equation (3.48)) capturing the combined effects of cementation degradation due to mean effective stress and deviatoric strain, a general stress-strain relationship that describes the hardening process of cement treated clay can be proposed; combining Equations (3.16) and (3.43) yields the following equation to find the total volumetric strain increment ( $d_v$ ):

$$d_v = d_v^e + d_v^p = \frac{1}{1+e} \left[ \lambda \left( \frac{dp^{f*}}{p^{f*}} \right) + (\lambda - \kappa) \frac{2\eta^* d\eta^*}{M^2 \left( \frac{\eta^{*2}(2\alpha+1)+M^2}{M^2} \right)^{\frac{(1+\alpha)}{2\alpha+1}}} \right] \quad (3.51)$$

Furthermore, the total plastic deviatoric strain increment ( $d_\varepsilon$ ) can be determined by combining Equations (3.17) and (3.44) as follows:

$$d_\varepsilon = d_\varepsilon^e + d_\varepsilon^p = \frac{2\kappa(1+\nu)}{9(1-2\nu)(1+e)} \left( \frac{dq}{p^{f*}} \right) + \frac{\lambda-\kappa}{1+e} \left[ \frac{dp^{f*}}{p^{f*}} + \frac{2\eta^* d\eta^*}{M^2 \left( \frac{\eta^{*2}(2\alpha+1)+M^2}{M^2} \right)^{\frac{(1+\alpha)}{2\alpha+1}}} \right] \left[ \frac{2\eta^*(\alpha+1)}{M^2 - \eta^{*2}} \right] \quad (3.52)$$

When the stress state is increased to sufficiently high pressure and at large deviatoric strain, the contribution of cementation is diminished and  $p^{f*} \rightarrow p'$  (i.e.  $p''_\Omega \approx 0$ ). Thus the proposed stress-strain relationship is reduced to that of MCC model.

### 3.2.11. Softening Behaviour

The softening behaviour of cement treated clay occurs after they reach their peak deviatoric strength and while the stress state is still on the yield surface and  $\eta^* = M$ . Thus, theoretically, the general equations for the hardening process (Equations (3.51) and (3.52)) can be used to simulate the softening behaviour of cement treated clay. Horpibulsuk et al. (2010) explained that the transition of the stress state from peak strength to a critical state of deformation (CSL) of the cemented clay is due to the crushing of the cementation bonds, while Liu et al. (2003) suggested that its strength at

the ultimate critical state (CSL) does not depend on the structure of the soil, and the cement treated clay properties are similar to the reconstituted soil-cement mixture.

In the proposed model, it is assumed that when the stress state has reached the peak strength state, it would remain on the failure line ( $q = Mp'^*$ ), while approaching its ultimate state at the CSL, as the deviatoric strain increases. The effect of shear degradation is quite significant at this stage because there is an abrupt reduction in the effect of cementation as  $\varepsilon_q$  continues to increase, as shown in Figure 3.9. When  $\frac{p'_\Omega}{p'_\Omega} \approx 0$  as  $\varepsilon_q$  becomes very large, the effect of cementation is completely removed due to the crushing of the cementation bonds, so during the softening process, the stress state gradually approaches the CSL of the reconstituted soil-cement mixture ( $q = Mp'$ ). Therefore, Equation (3.50) can be recalled to describe the proposed softening process as follows:

$$q = Mp'^* = M \left\{ p' + \frac{c_c}{\xi M} \frac{\left[ 1 + \left( \frac{p'_0 - p'_{0,i}}{\beta} \right) \right] \exp \left( - \left( \frac{p'_0 - p'_{0,i}}{\beta} \right) \right)}{1 + \omega \varepsilon_q^p \exp(\omega \varepsilon_q^p - b)} \right\} \quad (3.53)$$

Thus,

$$dq = \frac{\partial q}{\partial p'} dp' + \frac{\partial q}{\partial p'_0} dp'_0 + \frac{\partial q}{\partial \varepsilon_q^p} d\varepsilon^p \quad (3.54)$$

### 3.3. Extended Constitutive Model for Cement Treated Clay with Fibre Reinforcement

#### 3.3.1. General Quantities of Stress and Strain

In the proposed model for the improved clay composite, the general quantities of stress and strain used in the Modified Cam Clay (MCC) model for a conventional triaxial test Roscoe and Burland (1968) were adopted which can be found in Equations (3.1) to (3.3) for the mean effective stress ( $p'$ ), the deviatoric stress ( $q$ ) and the stress ratio ( $\eta$ ), respectively. Moreover, Equations (3.4) and (3.5) were used to define the increments of volumetric strain ( $d_v$ ) and deviatoric strain ( $d_\epsilon$ ), respectively.

#### 3.3.2. Modified Mean Effective Stress for FRCS

In this study, the model considered the combined effects of fibre and cement on the behaviour of FRCS as an addition to the mean effective stress. The contribution that fibre made to the shear strength was formulated depending on the deviatoric stress, so as it increased, the frictional resistance of the fibre helped to increase the shear strength. However, there is a critical deviatoric stress level beyond which the fibre becomes plastic or broken, and this reduction in shear strength due to plastic straining or broken fibres occurs gradually when the improved soil composite exceeds the critical deviatoric stress. On the other hand, the effect that cementation degradation has on the shear strength of improved soil composite was assumed to depend on the level of mean effective stress. This means that at a low mean effective stress the improved soil composite exhibited an increase in cohesion and tensile strength due to the beneficial effect of cementation, but as the mean effective stress increased to a sufficiently high value, the effect of cementation decreases because the cementation bonds break, and the improved soil composite behaves the same as unimproved soil. Therefore, the modified mean effective stress can take the following form:

$$p'^* = p' + p'_\Omega + p'_f \quad (3.55)$$

in which the parameter ( $p'_\Omega$ ) captures the beneficial contribution made by cementation to the shear strength while considering the effect of cementation degradation due to an increasing mean effective stress. The formulation for  $p'_\Omega$  can be found in Equation (3.7).

Fibre reinforcement also improves the peak and residual shear strengths of FRCS, and helps to reduce the brittleness of the improved material. Furthermore, the effect of fibre failure resulting in a loss of strength must be considered in the formulation, so the contribution of fibre ( $p'_f$ ) in Equation (3.55) may be formulated as follows:

$$p'_f = \left(\frac{C_f}{M}\right) \frac{q}{1 + \exp^{-n(q_c - q)}} \quad (3.56)$$

where the parameter ( $C_f$ ) represents the contribution made by fibre to the strength of the improved soil composite. The fitting parameter ( $n$ ) influences the diminishing rate of the loss of strength due to the fibres either pulling out or breaking. Note that the value of ( $n$ ) depends on the type and nature of the fibre, and the parameter ( $q_c$ ) is the critical deviatoric stress in which the frictional resistance of fibre reaches its limit.

### 3.3.3. Compressibility Behaviour of FRCS

During isotropic consolidation, the yield stress of clays treated with cement increased significantly compared to untreated clays due to the effect of cementation and the creation of cementation bonding between clay particles (Horpibulsuk et al. 2010; Kamruzzaman et al. 2009; Lade and Overton 1989). When stress was applied to cement treated clay less than the initial mean effective yield stress, the structure that formed inside the clay-cement matrix allows cement treated clay to withstand a higher mean effective stress before yielding than untreated clay (Horpibulsuk et al. 2004; Kamruzzaman et al. 2006). However, as the mean effective stress increased beyond the initial yield stress, the void ratio decreased significantly as the clusters of clay collapsed and the broken cementation bonding caused plastic deformation (Horpibulsuk et al. 2013; Suebsuk et al. 2010).

Research into the compressibility of clay treated with cement and improved with fibre remains a limited and controversial topic, although Consoli et al. (2005) observed that as the mean effective stress of sand improved with fibre increased the samples arrived at a unique normal compression line (NCL) that is above the NCL of the sample of unimproved sand at the same effective stress. However, Michalowski and Čermák (2002) suggested that the inclusion of fibre had no effect under compression, which was similar to the findings made by Diambra and Ibraim (2014). Furthermore, Ling and Tatsuoka (1994) explained that the tensile resistance provided by the fibre played no role under isotropic compression because it was compressed in every direction. Therefore, in this study it was assumed that the compressibility of FRCS would follow the behaviour of clay treated with cement.

Therefore, similar to the behaviour of cement treated clay as described in Section 3.2.2, the general behaviour of improved soil composite in isotropic compression is shown in Figure 3.13 where the isotropic compression line (ICL) is located above the ICL of the reconstituted clay (B-line), emphasizing that the increase of initial mean effective yield stress at the same void ratio was due to the effect of cementation ( $p'_{\Omega,i}$ ). The A-line is positioned above and has the same slope ( $\lambda$ ) as the B-line, and it refers to the additional void ratio caused by the effect of fabric. Since the additional void ratio was sustained due to the rearrangement of clay particles and the formation of larger clusters of soil and cement, it cannot be diminished during isotropic compression, so the effect of fabric ( $\Delta s$ ) can be calculated by Equation (3.10) as in cement treated clay.

Moreover, when the stress was less than the initial yield stress ( $p'_{0,i}$ ), only elastic deformation occurred and the stress travelled along the slope of the recompression/swelling line ( $\kappa$ ) because the cementation degradation was negligible in this elastic region. Thus the value of  $p'_{\Omega,i}$  can be obtained from Equation (3.9).

However, when a sample of improved soil composite was stressed beyond  $p'_{0,i}$ , plastic deformation associated with cementation degradation occurred and micro-cracks appeared on the structure of the composite as the mean effective stress continued to increase and the void ratio decreased (Kamruzzaman et al., 2009). Furthermore, when  $p'_0 \rightarrow \infty$  then  $p'_\Omega \rightarrow 0$  and  $p'^* \rightarrow p'$ , and thus the ICL of the improved soil composite

merged with the A-line to indicate that cementation had been completely destroyed, as shown in Figure 3.13. Thus, in the proposed model the effect of cementation degradation due to the mean effective stress was captured in the formulation of  $p'_{\Omega}$  (Equation (3.7)). Since the compressibility behaviour of the FRCS is mainly governed by the effect of cementation and its degradation, it can be further elaborated in Section 3.2.2.

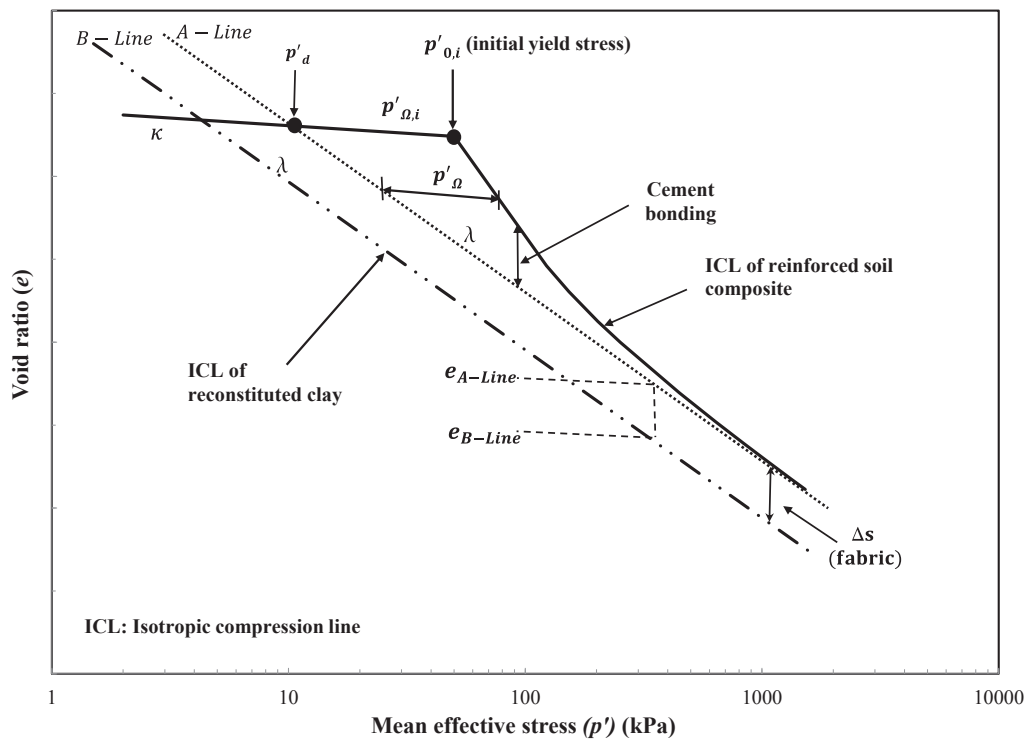


Figure 3.13: Isotropic compression of the fibre improved cement treated clay

### 3.3.4. Extended Failure Envelope for FRCS

When fibre is used as reinforcement, tensile resistance between the fibre and particles of clay occurred when the sample was subjected to deviatoric stresses. As mentioned in Section 2.3.2.5, a critical confining stress defines the failure mechanisms of the fibre (Maher and Ho, 1994), but below this level of stress, tensile resistance is not fully mobilised so the fibre tends to be pulled out of the soil matrix. However, beyond

the critical stress level, the soil matrix is densely packed and the frictional force along the length of the fibres reach their limits, so as the deviatoric stresses continue to increase, plastic straining or possible breakage of fibre may occur. Furthermore, Ranjan et al. (1996) and Zornberg (2002) confirmed this critical confining pressure ( $p_{crit}^*$ ) that characterises the failure mechanisms of fibre (i.e. pull-out or rupture), so in this study, the proposed model used the critical confining stress ( $p_{crit}^*$ ) which corresponds to  $q_c$  on the failure envelope in  $p' - q$  plane to determine the critical deviatoric stress ( $q_c$ ). Moreover,  $p_{crit}^*$  can be calculated from a given equation by Diambra and Ibraim (2014) as follows:

$$p_{crit}^* = \frac{\left(\sigma_f^p \frac{d_f}{2l_f} - a_{sf}\right)}{\tan\delta_{sf}} \quad (3.57)$$

where  $\sigma_f^p$  is the plastic stress limit of fibre,  $d_f$  and  $l_f$  are the diameter and length of the fibre, respectively. Moreover,  $a_{sf}$  and  $\delta_{sf}$  refers to the adhesive and frictional components of the interface between the fibre and soil matrix, respectively (Diambra and Ibraim, 2014).

Furthermore, cementation helps to increase the cohesion and tensile strength of the cement treated clay (Lade and Overton 1989; Sasanian 2011; Yapage and Liyanapathirana 2012), but when it was stressed beyond the initial yield stress, plastic deformation occurred that resulted in the growth of micro cracks (Shen et al., 2012). Kamruzzaman et al. (2009) and Rotta et al. (2003) explained that yielding causes the cementation bonds to break, which leads to cementation degradation; thus the contribution made by cementation decreased and so too did the strength of the FRCS.

The proposed model aimed at capturing the effect of cementation degradation and the failure mechanisms of fibre while considering the combined beneficial effects of cement and fibre. Figure 3.14 shows a schematic diagram of the proposed failure envelope of the improved soil composite. At low levels of stress the proposed failure envelope was positioned above the Critical State Line (CSL) of the reconstituted soil mixture to show how cement and fibre increased its shear strength. Below the critical mean effective stress ( $p_{crit}^*$ ), the sample reached the proposed failure line with a considerable breakage of cementation bonds and pull-out failure of the fibre, but as the stress increased beyond  $p_{crit}^*$ , there was a significant breakage of cementation bonds

and possible breakage of fibre. Furthermore, at a sufficiently high level of stress the combined effect of cement and fibre decreases and the improved soil composite behaved the same as the mixture of reconstituted soil. As Figure 3.14 shows, if the breakage of fibre is omitted the contribution made by fibre to the shear strength remains constant and the peak shear strength is overestimated. Thus, in this study, a non-linear failure envelope that merged with the Critical State Line of the reconstituted mixture of soil and cement was formulated, while considering the decreasing effects due to the breakage of cementation bonding and fibre at high levels of stress. The proposed failure envelope takes the following form:

$$q = M(p' + \xi p'_{\Omega} + p'_f) \quad (3.58)$$

where  $\xi$  is the correlating factor that influences how cementation contributes to the shear strength and  $M$  is the slope of the failure envelope of the mixture of reconstituted soil.

Additionally, considering only the effect of cementation, when the mean effective stress is zero the proposed failure envelope in Equation (3.58) intersects the vertical axis in  $p' - q$  plane at  $q = C_c$ , and the model parameter ( $C_c$ ) represents the beneficial contribution that cementation made to the shear strength of the improved soil composite.

Incorporating the above condition ( $q = C_c$  when  $p' = 0$ ) into Equations (3.7) and (3.58) yields the following relationship:

$$\xi = \frac{C_c}{p'_{\Omega,1}M} \quad (3.59)$$

Combining Equations (3.7) and (3.59) results in a modified mean effective stress as follows:

$$p'_{\Omega} = \frac{C_c}{\xi M} \left[ 1 + \left( \frac{p'_0 - p'_{0,i}}{\beta} \right) \right] e^{-\left( \frac{p'_0 - p'_{0,i}}{\beta} \right)} \quad (3.60)$$

Noted that,  $p'_{\Omega}$  in Equation (3.60) is identical to  $p'_{\Omega}$  in Equation (3.14) with change in the parameter  $C_c$  where the subscript  $c$  was adopted to characterise the contribution of cement to the shear strength of the FRCS.



(MCC) model, considers the effect of cementation and fibre reinforcement, and is presented as follows:

$$f = q^2 - (p' + p'_{\Omega} + p'_f)M^2[p'^*_{0} - (p' + p'_{\Omega} + p'_f)] = 0 \quad (3.62)$$

where  $p'^*_{0} = p'_0 + p'_{\Omega}$ , in  $p' - q$  plane,  $p'^*_{0}$  presents the size of the yield surface where it intersects the horizontal axis ( $q = 0$ ). Hence, fibre reinforcement ( $p'_f$ ) had no effect on the initial size of the yield surface due to the absence of deviatoric stress. Moreover,  $p'_0$  is the hardening parameter that corresponded to the mean effective stress  $p'$  when  $q = 0$ . It should be noted that, Equation (3.62) was modified from Equation (3.18) to include the effect of fibre inclusion ( $p'_f$ ).

Increasing the confining pressure caused the yield surface to increase in size, as shown in Figure 3.15. Due to cementation bonding, the improved soil composite developed tensile strength that is represented by  $p'_{\Omega}$  in Equation (3.60) (Yapage and Liyanapathirana, 2012), and as the hardening parameter ( $p'_0$ ) increased  $p'_{\Omega}$  decreased due to cementation degradation. Figure 3.16 also shows the effect of variations of the parameter ( $C_c$ ) on the proposed yield surface where increasing the cementation contribution ( $C_c$ ) led to an increase in  $p'_{\Omega}$ , and then the yield surface expanded in size. When  $C_c = 0$ , the effect of cementation diminished, but the yield surface of the improved soil composite had a higher peak shear strength than the MCC yield surface due to the inclusion of fibre, as shown in Figure 3.16. Note that when the cementation and fibre were not present ( $C_c = 0$  and  $C_f = 0$ ), the proposed yield surface returned to the yield surface of the MCC model, as shown in Figure 3.16.

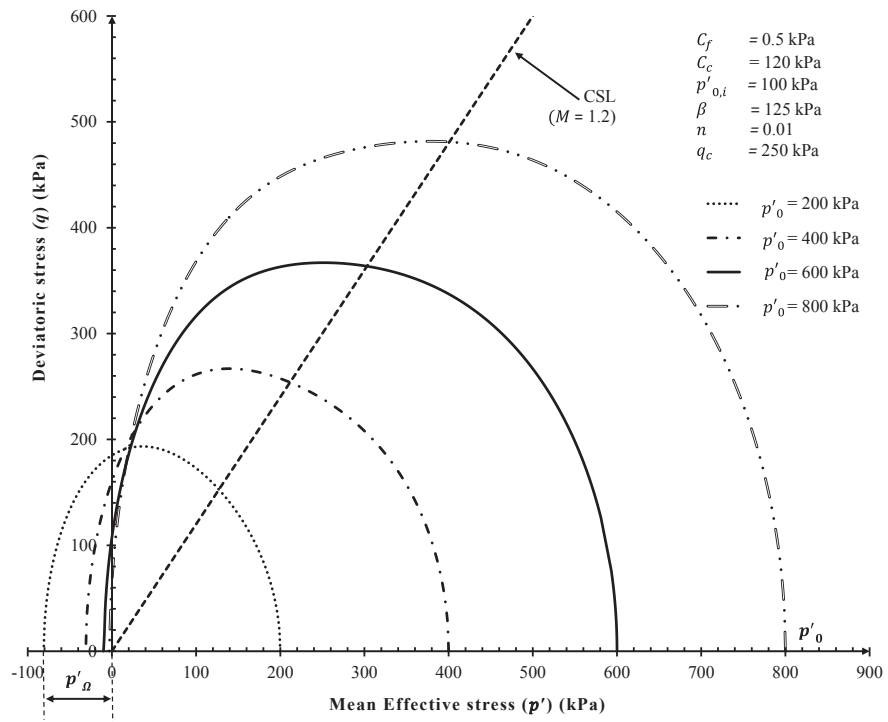


Figure 3.15: The effect of variation of hardening parameter ( $p'_0$ ) on the yield surface

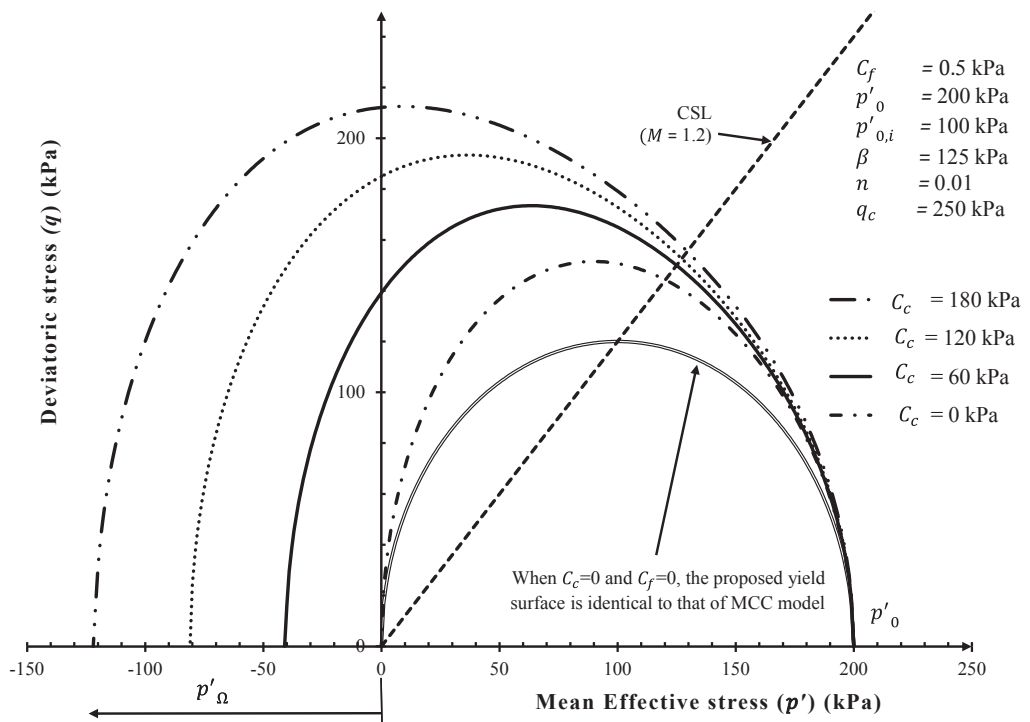


Figure 3.16: The proposed yield surface with variations of  $C_c$

### 3.3.6. Extended Plastic Energy Dissipation Equation for FRCS

According to Wood (1990), the fundamental expression for the internal plastic energy per unit volume ( $dW_{in}$ ) for a soil sample in the triaxial test can be found in Equation (3.19). Based on the Modified Cam Clay energy dissipation equation and inspired by the energy dissipation expression adopted by Kasama et al. (2000), the plastic energy dissipation equation proposed in Equation (3.21) for the cement treated clay can be modified for the FRCS to take the following form:

$$p'd_v^p + qd_\varepsilon^p = (p' + \xi p'_\Omega + p'_f) \sqrt{(d_v^p)^2 + (Md_\varepsilon^p)^2} + d_v^p \{Xd_\varepsilon^p - Yd_v^p\} \quad (3.63)$$

$$X = \left[ \frac{2\eta^* p'}{(p' + \xi p'_\Omega + p'_f)} - \frac{[2\eta^*(\alpha+1)(1-\eta^*B) + B[\eta^{*2}(1+2\alpha) + M^2]]}{1+A} \right] \quad (3.64)$$

$$Y = \left[ 1 - \frac{p'^2}{(p' + \xi p'_\Omega + p'_f)^2} \right] \quad (3.65)$$

where  $\eta^*$  is the modified stress ratio. The expression for  $\eta^*$  is taken as follows:

$$\eta^* = \frac{q}{(p' + \xi p'_\Omega + p'_f)} \quad (3.66)$$

Furthermore, the following conditions must be satisfied when formulating an appropriate expression for the plastic energy dissipation equation:

- For an isotropic compression case where  $q = 0$  and  $d_\varepsilon^p = 0$ , Equation (3.63) should decrease to:

$$dW_{in} = p'd_v^p \quad (3.67)$$

- Moreover, on the Critical State Line where  $q = M[p' + \xi p'_\Omega + p'_f]$  and  $d_v^p = 0$ , Equation (3.63) can be simplified as:

$$dW_{in} = M[p' + \xi p'_\Omega + p'_f]d_\varepsilon^p \quad (3.68)$$

Based on a semi-empirical method, the proposed energy dissipation equation introduces the non-dimensional parameter ( $\alpha$ ) that balances the deviatoric and volumetric plastic strain parameters. In Equation (3.63), the term  $A$  refers to the derivative of  $p'_\Omega$  with respect to  $p'$ , while the term  $B$  refers to the derivative of  $p'_f$  with respect to  $q$ . In order to derive an expression for the term  $A$ , the value of  $p'_0$  in Equation (3.60) is expressed as a function of  $p'$ . For simplicity, the value of  $p'_0$  in the yield surface function (Equation (3.62)) was used to include the effect of cementation degradation:

$$p'_0 = \frac{q^2}{M^2 \left[ p' + \frac{C_c}{\xi M} (1+H) \exp^{-K} + \left( \frac{C_f}{M} \right) \frac{q}{1 + \exp^{-n(qc-q)}} \right]} + p' + p'_f \quad (3.69)$$

$$\text{where } H = \frac{1}{\beta} \left\{ \frac{q^2}{M^2 \left[ p' + \frac{C_c}{\xi M} + \left( \frac{C_f}{M} \right) \frac{q}{1 + \exp^{-n(qc-q)}} \right]} + p' - p'_{0,i} \right\} \quad (3.70)$$

Substituting ( $p'_0$ ) into Equation (3.60) allows term  $A$  to be derived as follows:

$$A = \frac{dp'_\Omega}{dp'} = -\frac{C_c \psi K}{\xi \beta M} \exp \left[ \frac{-(p'_0 - p'_{0,i})}{\beta} \right] \quad (3.71)$$

where  $\psi$  is the derivative of  $p'_0$  in Equation (3.69) with respect to  $p'$  and takes the following form:

$$\psi = \frac{dp'_0}{dp'} = 1 - \frac{q^2 \left\{ 1 - \frac{C_c K}{\xi \beta M} \exp^{-K} \left[ 1 - \frac{q^2}{M^2 \left( p' + \frac{C_c}{\xi M} + \frac{C_f}{M} \frac{q}{1 + \exp^{-n(qc-q)}} \right)} \right] \right\}}{M^2 \left[ p' + \frac{C_c}{\xi M} [1+K] \exp^{-K} \right]^2} \quad (3.72)$$

Furthermore, term  $B$  in Equation (3.64) can be expressed as follows:

$$B = \frac{dp'_f}{dq} = \frac{C_f}{M [1 + \exp^{-n(qc-q)}]} \left\{ 1 - \frac{nq \exp^{-n(qc-q)}}{[1 + \exp^{-n(qc-q)}]} \right\} \quad (3.73)$$

The proposed plastic energy dissipation expression in Equation (3.63) incorporates the effect of cementation (term  $A$ ) and the effect of fibre reinforcement (term  $B$ ), and note that when  $C_c = 0$  and  $C_f = 0$ , and  $\alpha$  is set at zero, cementation and fibre have no effect and the proposed energy dissipation equation will convert to an MCC model energy dissipation equation.

### 3.3.7. Elastic Deformation of FRCS

When the stress state is within the yield surface, only elastic deformation occurs so the proposed model adopted Hooke's Law to describe the elastic behaviour of the FRCS as widely used by many researchers for soils (Horpibulsuk et al. 2010; Perić and Ayari 2002). Based on a number of experimental observations (Consoli et al. 1999; Hamidi and Hooresfand 2013), adding fibre to cement treated soil reduced the initial stiffness of the improved soil composite. Hence, the proposed model assumed that elastic deformation (including  $d_v^e$  and  $d_\varepsilon^e$ , the elastic volumetric strain increment and the elastic deviatoric strain increment, respectively) depends on the combined effect of cementation and fibre reinforcement. The equations used to describe the elastic deformation of improved composite are as follows:

$$d_v^e = \left( \frac{\kappa}{1+e} \right) \left[ \frac{(1+A)dp'}{p'+p'_\Omega+p'_f} \right] \quad (3.74)$$

$$d_\varepsilon^e = \left[ \frac{2\kappa(1+\nu)}{9(1-2\nu)(1+e)} \right] \left[ \frac{(1+B)dq}{p'+p'_\Omega+p'_f} \right] \quad (3.75)$$

### 3.3.8. Extended Plastic Potential Function for FRCS

According to Boussine et al. (2001), soils generally exhibit non-associated plastic flow rule. Moreover, for clayey material, it is appropriate to describe the volumetric strains and the transition process from contractive to dilatancy by a non-associated model (Shen et al. 2012; Yuanming et al. 2010). Based on the modified plastic energy dissipation equation (Equation (3.64)) described above, a non-associated plastic flow rule to describe the directions of the plastic strain increments and also consider the combined effects of cementation degradation and fibre failure mechanisms, was developed. The plastic flow rule used to describe the relationship between  $d_v^p$  and  $d_\varepsilon^p$  (the increments of plastic volumetric strain and plastic deviatoric strain respectively) can be computed by solving and rearranging the plastic energy equation (Equation (3.64)) as shown below:

$$\frac{d_v^p}{d_\varepsilon^p} = \frac{-(1+A)[\eta^{*2}-M^2]}{2\eta^*(\alpha+1)[1-\eta^*B]+B[\eta^{*2}(1+2\alpha)+M^2]} \quad (3.76)$$

Note that when the effect of fibre reinforcement and cementation is null and the parameter ( $\alpha$ ) is set to be zero, the plastic flow rule proposed in this study will return to the MCC model associated plastic flow rule which can be found in Equation (2.13).

Moreover, the expression for the partial derivatives of the modified stress ratio ( $\eta^* = \frac{q}{p'+p'_\Omega+p'_f}$ ) with respect to  $p'$  and  $q$ , yields the following equation:

$$d\eta^* = \frac{-\eta^*(1+A)}{(p'+p'_\Omega+p'_f)} dp' + \frac{1-\eta^*B}{(p'+p'_\Omega+p'_f)} dq \quad (3.77)$$

By applying the normality rule ( $\frac{d_v^p}{d_\varepsilon^p} = -\frac{dq}{dp'}$ ) onto the proposed flow rule (Equation (3.76)), substituting it into Equation (3.76), and then integrating it with the boundary condition ( $p' = p'_0$  when  $q = 0$ ), the plastic potential function can be presented as:

$$g = q^2(1 + 2\alpha) + (p' + p'_\Omega + p'_f)^2 M^2 \left[ 1 - \left( \frac{p'^*_0}{p'+p'_\Omega+p'_f} \right)^{\frac{2\alpha+1}{\alpha+1}} \right] \quad (3.78)$$

The effect of increasing the hardening parameter ( $p'_0$ ) on the proposed plastic potential function is shown in Figure 3.17 where the value of  $p'_\Omega$  decreased as the plastic potential surface expanded to capture the effect of cementation degradation. Note that by recalling the definition of  $p'^*_0$ , the effect of fibre and its failure mechanisms on the size of the plastic potential function is null because  $q = 0$ . Figure 3.18 shows the effect of varying parameter ( $\alpha$ ) on the plastic potential function, while keeping the value of  $p'_\Omega$  constant. As  $\alpha$  decreases the peak shear strength is expected to increase and vice versa, and when  $\alpha = 0$ , the proposed plastic potential function returns to the proposed yield surface and then the proposed model becomes the associated model. Due to complex mathematical procedures, detailed derivation of the proposed plastic potential function for the improved soil composite can be found in *Appendix B*.

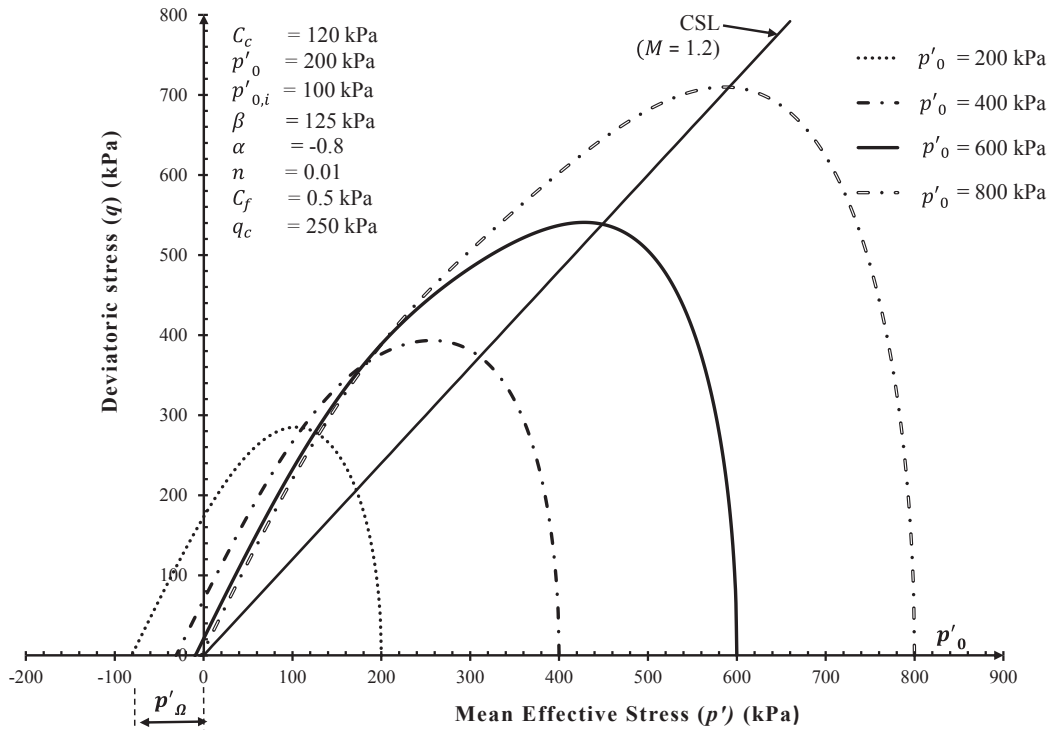


Figure 3.17: Variation of ( $p'_0$ ) on the size of the proposed yield surface

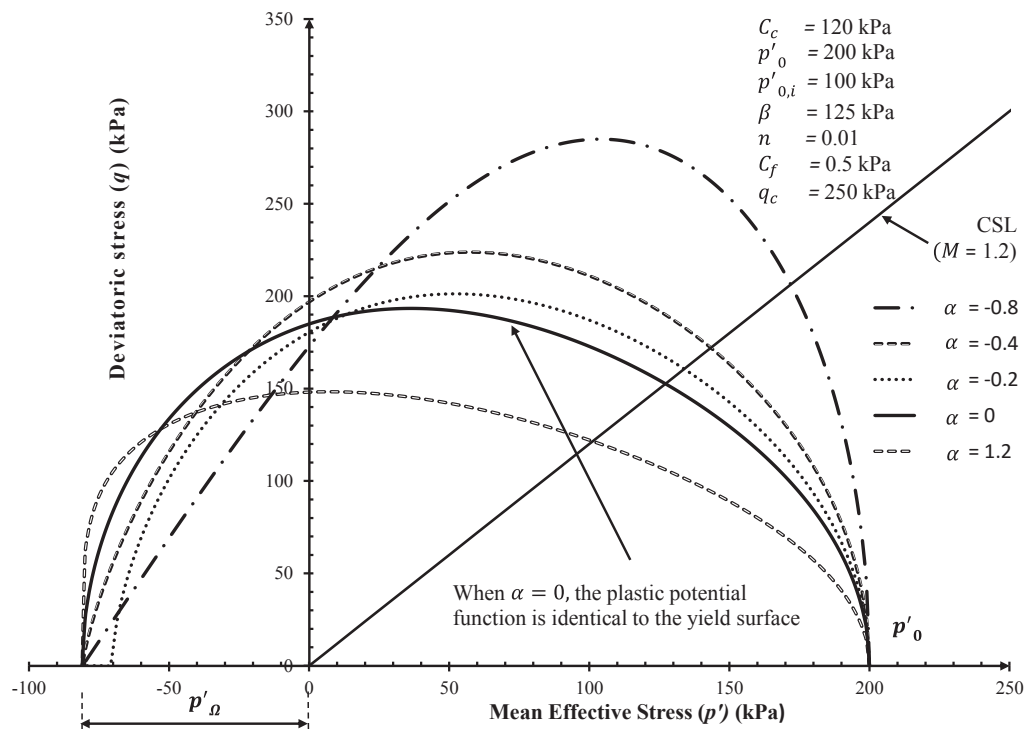


Figure 3.18: Variation of ( $\alpha$ ) on the proposed plastic potential function

### 3.3.9. Virgin Yielding Behaviour of FRCS

In this proposed model the normality rule where the plastic strain vectors were normal to the plastic potential surface was adopted such that virgin yielding occurred when the stress state of the improved composite was on the yield surface and  $dp'^*_0 > 0$ . According to Wood (1990), the yield surface expands due to the plastic volumetric strain and plastic deviatoric strain, but it was assumed that in the MCC model, expansion of the yield surface was linked directly to the incremental plastic volumetric strain (Wood, 1990). Other researchers such as Bardet (1986), Crouch et al. (1994) and Yu (2006) used the plastic volumetric strain to model the strain hardening behaviour of the material, so to follow the MCC model, the proposed model assumed that expansion of the yield surface ( $dp'^*_0$ ) would only depend on the plastic volumetric strain ( $d\epsilon^p_v$ ). By adopting the framework of plasticity, the general equations for  $d\epsilon^p_v$  and  $d\epsilon^p_\epsilon$  can be expressed in the above Equations (3.34) and (3.35), respectively.

The hardening behaviour of the improved soil composite was also assumed to be due to the plastic volumetric strain only, so the hardening equation can be computed as follows:

$$\frac{dp'^*_0}{p'^*_0} = \left( \frac{1+e}{\lambda-\kappa} \right) d\epsilon^p_v \quad (3.37 \text{ bis.})$$

Furthermore, following the above procedures in Section 3.2.8, the partial derivatives of the proposed yield surface function and the proposed plastic potential function for the FRCS were calculated to determine  $d\epsilon^p_v$ ,  $d\epsilon^p_\epsilon$ , and  $d\lambda$  as follows:

$$\frac{\partial f}{\partial p'} = \frac{-2\eta^{*2}(1+A)}{M^2(p'+p'_\Omega+p'_f)} + \frac{p'^*_0(1+A)}{(p'+p'_\Omega+p'_f)^2} \quad (3.79)$$

$$\frac{\partial f}{\partial q} = \frac{2\eta^*(1-\eta^*B)}{M^2(p'+p'_\Omega+p'_f)} + \frac{(p'^*_0)B}{(p'+p'_\Omega+p'_f)^2} \quad (3.80)$$

$$\frac{\partial f}{\partial p'^*_0} = -\frac{1}{p'+p'_\Omega+p'_f} \quad (3.81)$$

$$\frac{\partial g}{\partial p'^*} = \frac{-2\eta^{*2}(1+2\alpha)(1+A)}{M^2(p'+p'_\Omega+p'_f)} + \left(\frac{2\alpha+1}{\alpha+1}\right) \frac{(1+A)}{(p'+p'_\Omega+p'_f)} \left(\frac{p'^*_0}{p'+p'_\Omega+p'_f}\right)^{\left(\frac{2\alpha+1}{\alpha+1}\right)} \quad (3.82)$$

$$\frac{\partial g}{\partial q} = \frac{2\eta^*(1+2\alpha)(1-\eta^*B)}{M^2(p'+p'_\Omega+p'_f)} + \left(\frac{2\alpha+1}{\alpha+1}\right) \frac{B}{(p'+p'_\Omega+p'_f)} \left(\frac{p'^*_0}{p'+p'_\Omega+p'_f}\right)^{\left(\frac{2\alpha+1}{\alpha+1}\right)} \quad (3.83)$$

By combining Equations (3.79 - 3.83), the increments of plastic volumetric strain ( $d_v^p$ ) and plastic deviatoric strain ( $d_\varepsilon^p$ ) can be determined using the following equations:

$$d_v^p = \left(\frac{\lambda-\kappa}{1+e}\right) \left\{ \frac{(1+A)dp'}{(1-\eta^*B)(p'+p'_\Omega+p'_f)} + d\eta^* \left[ \frac{2\eta^*}{\left(\frac{\eta^{*2}(2\alpha+1)}{M^2}+1\right)^{\left(\frac{1+\alpha}{2\alpha+1}\right)} M^2} + \frac{B}{(1-\eta^*B)} \right] \right\} \quad (3.84)$$

$$d_\varepsilon^p = d_v^p \left\{ \frac{2\eta^*(\alpha+1)[1-\eta^*B]+B[\eta^{*2}(2\alpha+1)+M^2]}{(1+A)(M^2-\eta^{*2})} \right\} \quad (3.85)$$

### 3.3.10. Modified Mean Effective Stress while Considering the Effect of Shear Deformation

The addition of cement enables large clusters to form, which in turn increases the strength of the soil, while the beneficial effect of cementation was due to chemical interaction between the cement and particles of clay. Moreover, adding fibre to soil treated with cement improves its ductility due to the physical interaction between the clusters of soil and cement, and the fibre. However, the structural strength of this composite during shearing decreases because cementation also decreases and the fibre is pulled-out or eventually broken. In this proposed model, the reduction in strength of the improved composite during shearing was considered as two separate components, namely cementation degradation and fibre failure.

Firstly, cementation degradation reduces the shear strength as micro-cracks occur within the clusters of soil and cement that are induced mainly by the volumetric and shear deformations (Baudet and Stallebrass 2004; Kavvadas and Amorosi 2000).

Cementation degradation caused by volumetric deformation was captured by the proposed mean effective stress (Equations (3.60)), but this mean effective stress needs to be modified to include cementation degradation during shearing (or due to shear strain), so in the proposed model, Equation (3.47) can be recalled to describe the cementation degradation due to shear deformations which was linked to the plastic deviatoric strain ( $\varepsilon_q^p$ ) as follows:

$$\frac{p''_{\Omega}}{p'_{\Omega}} = \frac{1}{1 + \omega \varepsilon_q^p \exp(\omega \varepsilon_q^p - b)} \quad (3.47 \text{ bis.})$$

Secondly, according to Li (2005) in his analysis of the triaxial compression tests carried out on sand improved with fibre, the fibre was more affective at high levels of strain because the interfacial forces between the fibre and the soil matrix gradually mobilised as the strain increased. Moreover, at higher levels of strain the effect of fibre was fully utilised and consequently the loss in the strength of the soil improved with fibre was smaller. Tang et al. (2007) also observed that the peak and residual shear strengths of the FRCS occurred at higher shear strain than the soil treated with cement, which improved its ductility; this was similar to the findings by Consoli et al. (1999). Moreover, at a post peak state where the treated soil suddenly dropped to its residual value, the loss in strength of the FRCS occurred gradually due to the effect of fibre. Consoli et al. (2007) and Heineck et al. (2005) investigated the performance of sand improved with fibre at a large shear strain and concluded that fibre undergoes plastic deformation as it lengthens, and then breaks when the shear strain exceeds its elastic limit. Thus, at a large shear strain the fibre becomes ineffective as complete pull-out or possible breakage occurs. Hence, in this study, although the formulation of the effect of fibre ( $p'_f$ ) in Equation (3.56) captured the effect of fibre failures, the effect of shear strain on the loss in strength of the FRCS was not captured directly. At large shear strains, as the strength of the fibre decreases, it also stretches and degrades until it either ruptures or is completely pulled out of the cement-soil matrix, but when the mean effective stress is below the critical mean effective stress ( $p' < p'_{crit}$ ), the fibre is gradually pulled out of the soil matrix, particularly at large deviatoric strains. In the proposed model, the effect of shear strain on the degradation of fibre was linked directly to the plastic deviatoric strain ( $\varepsilon_q^p$ ), so when considering the effect of  $\varepsilon_q^p$  on the failure mechanisms, the effect of fibre contribution ( $p'_f$ ) was modified further, as follows:

$$\frac{p_f''}{p_f'} = \frac{1}{1+mq \exp \varepsilon_q^p} \quad (3.86)$$

where  $p_f''$  captures the effect of  $\varepsilon_q^p$  on the decreasing contribution made by fibre reinforcement during shearing. The parameter  $m$  affects the decreasing rate of bonding between the fibre and clusters of soil and cement due to plastic deviatoric strain.

Furthermore, combining cementation and the degradation of fibre induced by plastic shear strain ( $\varepsilon_q^p$ ) by adopting  $p_\Omega''$  and  $p_f''$  in Equations (3.47 bis.) and (3.86) with the mean effective stress in Equation (3.55), the modified mean effective stress will take the following form:

$$p'^* = p' + p_\Omega'' + p_f'' = p' + \frac{p'_{\Omega,i} \left[ 1 + \left( \frac{p'_{0,i} - p'_{\Omega,i}}{\beta} \right) \right] \exp \left( - \frac{p'_{0,i} - p'_{\Omega,i}}{\beta} \right)}{1 + \omega \varepsilon_q^p \exp(\omega \varepsilon_q^p - b)} + \frac{c_f}{M} \frac{q}{[1 + \exp^{-n(qc-q)}] (1 + mq \exp \varepsilon_q^p)} \quad (3.87)$$

Figure 3.19 shows a schematic diagram of the reduction in strength due to cementation degradation ( $p_\Omega''$ ) and fibre failure ( $p_f''$ ). At the initial stage of shearing where ( $\varepsilon_q = 0$  and  $q = 0$ ), the combined effects of fibre and cementation are represented by  $p'_{\Omega}$ , and it captures the effect of cementation degradation due to mean effective stress, while the effect of fibre reinforcement was deemed to be negligible during isotropic compression. Once shearing occurred the structural strength of the improved soil composite increased due to the fibre, as shown in Figure 3.19, but when the improved soil composite was stressed beyond the initial mean effective yield stress ( $p'_{0,i}$ ) and where  $d_\varepsilon^p > 0$ , plastic deviatoric strain occurred that caused plastic deformation. The contribution made by cementation ( $p'_\Omega$ ) and fibre ( $p'_f$ ) decreased due to the degradation induced by plastic deviatoric strain ( $p_\Omega'' < p'_\Omega$  and  $p_f'' < p'_f$ ). As  $\varepsilon_q^p$  continued to increase, the effect of cementation degradation and fibre approached zero, which indicated that the cementation bonds were completely destroyed and the fibre may have been pulled-out or ruptured. Thus, the modified mean effective stress presented in Equation (3.87) was formulated to capture the effect of cementation degradation due to mean effective stress and deviatoric strain, while considering the effect of fibre and its failure during shearing.

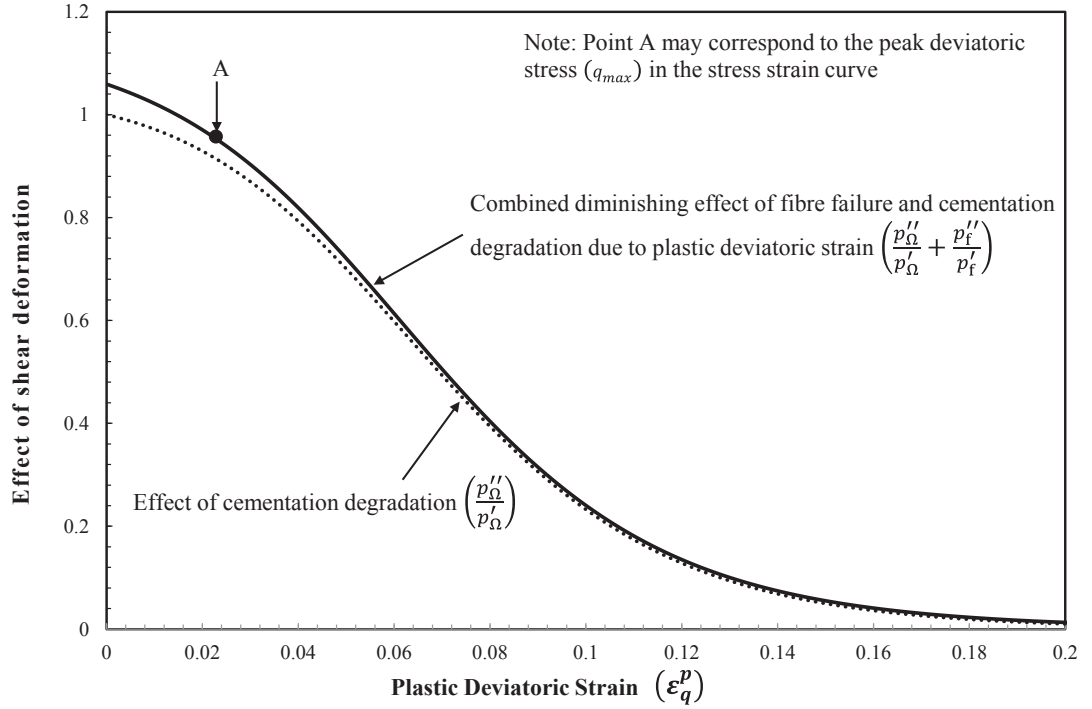


Figure 3.19: Schematic diagram of strength reduction due to cementation degradation and fibre failure

### 3.3.11. General Stress-Strain Relationship for FRCS

With regards to the modified mean effective stress proposed in Equation (3.87), during the hardening process, the elastic and plastic deformation of clay treated with cement and improved fibre can be described by the increments of total volumetric strain ( $d_v$ ) and total deviatoric strain ( $d_\varepsilon$ ), respectively. The increment of total volumetric strain can be determined by combining Equations (3.74) and (3.84) as follows:

$$d_v = \frac{1}{(1+e)} \left\{ \frac{(1+A)(\lambda-\eta^*B\kappa)dp'}{(p'+p_\Omega''+p_f'')(1-\eta^*B)} + (\lambda - \kappa)d\eta^* \left[ \frac{2\eta^*}{M^2 \left( \frac{\eta^{*2}(2\alpha+1)}{M^2} + 1 \right)^{\frac{1+\alpha}{2\alpha+1}}} + \frac{B}{(1-\eta^*B)} \right] \right\} \quad (3.88)$$

Equations (3.75) and (3.85) can be combined and then used in the following equation to calculate the increment of total deviatoric strain ( $d_\varepsilon$ ):

$$d_\varepsilon = \left[ \frac{2\kappa(1+\nu)}{9(1-2\nu)(1+e)} \right] \left[ \frac{(1+B)dq}{p' + p''_\Omega + p''_f} \right] + d_v^p \left\{ \frac{2\eta^*(\alpha+1)(1-\eta^*B) + B[\eta^{*2}(2\alpha+1) + M^2]}{(1+A)(M^2 - \eta^{*2})} \right\} \quad (3.89)$$

Furthermore, when  $\eta^* = M$  and FRCS reaches its peak deviatoric stress, softening begins while the stress state is still on the yield surface, and then cementation degradation is dramatically reduced as the cementation bonds are crushed (Horpibulsuk et al., 2010). At this stage the fibre reinforcement exceeds its plastic limit and failure may occur, depending on the level of mean effective stress, and at mean effective stresses higher than  $p_{crit}^*$  significant degradation of cementation bonds and fibre rupture may occur, so in the proposed model it was assumed that the improved soil composite gradually approaches the CSL, as shown in Figure 3.14. Moreover, the behaviour of the improved soil composite was similar to the reconstituted soil mixture.

It was also assumed in the proposed model for FRCS that when the stress state reached peak deviatoric stress it would remain on the proposed failure line [ $q = M(p' + \xi p''_\Omega + p''_f)$ ] and theoretically Equations (3.88) and (3.89) could be used to simulate the softening of the improved soil composite, as similar to the model for cement treated clay without fibre reinforcement. During the softening process, as  $\varepsilon_q^p$  increased, shear degradation abruptly reduced the combined effects of cementation and fibre reinforcement, as shown in Figure 3.19. Consequently, when  $\frac{p''_\Omega}{p'_\Omega}$  and  $\frac{p''_f}{p'_f} \approx 0$ , the stress state of the improved soil composite approached the CSL of the reconstituted soil mixture, which indicated a complete removal of the cementation and fibre effect. Therefore, by incorporating the modified mean effective stress in Equation (3.87), the failure envelope can be modified as follows to describe the softening behaviour:

$$q = M \left\{ p' + \frac{c_c \left[ 1 + \left( \frac{p'_0 - p'_{0,i}}{\beta} \right) \right] \exp \left( - \left( \frac{p'_0 - p'_{0,i}}{\beta} \right) \right)}{1 + \omega \varepsilon_q^p \exp(\omega \varepsilon_q^p - b)} + \frac{c_f q}{[1 + \exp^{-n(qc - q)}] \left( 1 + m q \exp \varepsilon_q^p \right)} \right\} \quad (3.90)$$

Note in Equation (3.90) that at a very large  $\varepsilon_q^p$ , the proposed failure envelope approached  $q = Mp'$  as the combined effects of fibre and cement completely diminished.

### 3.4. Summary

This chapter has presented a new constitutive model to simulate the behaviour of cement treated clay considering the effect of cementation and its degradation based on the framework of the Critical State Soil Mechanics and the basis of Modified Cam Clay model. Furthermore, this proposed constitutive model was extended to capture the behaviour of fibre reinforced cement treated clay, referred to as the improved soil composite. In these proposed constitutive models, the mean effective stress was modified to include the combined effect of cementation ( $C_c$ ) and fibre ( $C_f$ ), together with their degradations. While the effect of cementation was formulated depending on the mean effective yield stress or effective isotropic consolidation pressure ( $p'_0$ ), the effect of fibre depends on the level of the deviatoric stress ( $q$ ). Furthermore, increasing deviatoric strain cause crushing of cementation bonds and failure of fibre which was linked directly to the plastic deviatoric strain ( $\varepsilon_q^p$ ). Thus, the modified mean effective stress ( $p'^*$ ) was formulated in a single equation (Equation (3.87)) to consider the effect of cementation degradation ( $p''_\Omega$ ) and fibre failure ( $p''_f$ ) due to the mean effective yield stress and the deviatoric stress and strain. It can be noted that, the behaviour of the cement treated clay with or without fibre reinforcement is similar to that of the untreated clay when the mean effective yield stress or the accumulation of the plastic shear strain become sufficiently high. Moreover, the behaviour of the cement treated clay without fibre reinforcement can be simulated simply by setting the effect of fibre inclusion to zero ( $C_f = 0$ ).

The special characteristic of the proposed models includes the non-linear failure envelope, which merges with the Critical State Line (CSL) of the reconstituted soil mixture to consider the effect of cementation degradation and fibre failure to the peak shear strength of the treated soil. In addition, the non-associated plastic flow rule was proposed introducing the parameter  $\alpha$  to balance the incremental deviatoric and volumetric plastic strain parameters (i.e  $d_v^p$  and  $d_\varepsilon^p$ , respectively). Moreover, the non-associated plastic potential function ( $g$ ) was developed from the modified plastic energy dissipation equation, following the framework of plasticity. When  $\alpha = 0$ , the proposed models in this study become associated where the plastic potential function is identical to the yield surface. After the peak strength state, the softening process can be

simulated by assuming that the sample remains on the failure line with a reduction in strength caused by a diminishing effect of cementation and fibre failure (i.e.  $p_{\Omega}''$  and  $p_f'' \approx 0$ ). Hence, the general stress-strain relationship proposed in Equations (3.88) and (3.89) can be used to simulate both the hardening and softening behaviour of the improved soil composite. Furthermore, it can be noted that when the combined effect of cementation and fibre is null (i.e.  $C_c$  and  $C_f = 0$ ), and  $\alpha = 0$ , the proposed models return to the Modified Cam Clay model with associated flow rule.

In this study, laboratory experiments were carried out to investigate the effect of cementation and fibre on the behaviour of the cement treated clay with or without fibre reinforcement. The experimental program and the results are reported in Chapter 4. Moreover, the reported results are used to evaluate the performance of the proposed models and the validation exercises are presented in Chapter 5.

# Chapter 4

## Laboratory Experiments & Results

---

### 4.1. General

This chapter outlines the laboratory experiments carried out to investigate the behaviour of cement treated clay with or without fibre reinforcement. Two types of clay were selected, natural Ballina clay and artificial Kaolin clay. Sample preparation consists of Ballina clay treated with 10%, 12% and 15% cement and Kaolin clay admixed with 5% cement. The Ballina clay with 15% cement was also reinforced with 0.3% and 0.5% fibre, while 0.1% and 0.5% of fibre was added to the 5% cement treated Kaolin clay. The experimental program consisted of unconfined compression strength (UCS) tests and a Scanning Electron Microscopy (SEM) image analysis carried out on the cement treated Ballina clay with or without fibre reinforcement. Numerous undrained and drained triaxial compression tests (66 tests in total) were conducted on the natural Ballina clay and Kaolin clay treated with differing amounts of cement and fibre at confining pressures ranging from 50 kPa to 800 kPa, to determine how cementation and fibre would affect the behaviour of the improved soil composite. The structure of this chapter includes sample preparation, the experimental program, and a description of the testing equipment and test results.

## 4.2. Sample Preparation

Natural Ballina clay was obtained from a test pit located close to the bridge at Emigrant Creek North, New South Wales, Australia and commercially available Q38 clay in powder form was used for the sample of Kaolin. The location of Ballina area is shown in Figure 4.1 while the location of the natural Ballina clay is shown in Figure 4.2.



Figure 4.1: Location of Ballina in the map (courtesy of Google Maps)



Figure 4.2: Location of the natural Ballina clay (source: <http://www.rms.nsw.gov.au/images/projects/keybuildprogram/pacific-highway/ballina-bypass-4.jpg>)

Table 4.1 summarises the properties of the clay samples. In this study, General Purpose (GP) Portland cement was used as a binder, but before adding cement or fibre, the Ballina clay and Kaolin clay were mixed with water to obtain reasonable workability. The water content of Ballina Clay was raised to its liquid limit (LL=120%), whereas a water content of 75% ( $1.5 \times LL$ ) was required for Kaolin clay to produce a workable mix.

Table 4.1: Properties of adopted clay samples

	Ballina Clay	Kaolin Clay
Liquid Limit (LL)	120%	48%
Plastic Limit (PL)	52.8%	29%
Plasticity Index (PI)	67.2%	19%
Specific Gravity (Gs)	2.74	2.66
Linear Shrinkage (LS)	22%	7%
Colour	Dark grey	White
Soil Classification (USCS)	CH	CL

To prepare the sample of cement treated clay without fibre reinforcement, a cement slurry (water/cement ratio = 1 by weight) was used as a stabilising admixture; it was mixed with clay within 10 minutes so the soil-cement mixture would not begin to harden. In the experimental program, Ballina clay was treated with 10%, 12% and 15% cement while the Kaolin clay was treated with 5% cement. The amount of cement to be added was calculated based on the dry weight of the clay material, whereas the amount of cement designated in this study was as typically used in cement treated clays and as adopted by many researchers (Lorenzo and Bergado 2006; Sariosseiri and Muhunthan 2009; Suebsuk et al. 2010). The resulting mixture was then compacted in a split cylindrical mould (H =100 mm and D = 50 mm), in accordance with Australian Standards (AS 5101.4.-2008). The mixing and moulding processes were followed strictly to achieve a homogenous mixture and consistency in the samples, which were then wrapped in vinyl plastic wrap to minimise moisture loss and help the cement hydration process. After 24 hours, the samples were removed from the mould and placed in a water-lime curing bath for 28 days to achieve a maximum chemical interaction between the soil and cement.

To prepare the cement treated clay with fibre reinforcement, the clay samples were mixed with water to produce a homogenous mixture before adding fibre and cement. In this study, 18 mm long by 17  $\mu\text{m}$  diameter monofilament polypropylene fibre, supplied by Sika Australia in a dry condition, was used as shown in Figure 4.2; some of the fibre properties are summarised in Table 4.2. Since the fibre was in a

conglomerated form it was torn apart to avoid lumps and balling in the mixture. According to Kaniraj and Havanagi (2001), fibre works better in a moist mixture, so to allow for reasonable workability, fibre was distributed randomly into the mixture and then mixed with the cement slurry. The amount of fibre added was calculated based on the dry weight of the clay material. Based on a number of laboratory experiments mentioned in the literature (Consoli et al. 2010; Hamidi and Hooresfand 2013; Tang et al. 2007), the designated percentages of fibre added were 0.1%, 0.3%, and 0.5% to observe how these amounts of fibre would affect the improved soil composite. In this experimental program, 0.3% and 0.5% of fibre was added to the Ballina clay treated with 15% cement while the Kaolin clay treated with 5% cement was reinforced with 0.1% and 0.5% of fibre. It should be noted that monofilament polypropylene fibre was used rather than fibrillated fibre to prevent any clustering or tangling during the mixing process and hence allowed for a more homogenous mix. A greater fibre content (more than 0.5% polypropylene fibre) in the mixture results in low workability and prevents homogenous mixing. Thus various fibre contents were selected after considering the investigations published in the literature and the workability of mixes in the laboratory. Once the fibre had been thoroughly mixed with the clay, the General Purpose (GP) Portland cement in amounts of 15% and 5% of the dry weight of Ballina clay and Kaolin clay respectively, was mixed with water in a water/cement ratio = 1, and then the samples of clay and fibre were mixed with the cement slurry. In accordance with Australian Standard (AS 5101.4.-2008), this homogenous mixture was then compacted in a split cylindrical mould (H = 100 mm and D = 50 mm) which was covered in vinyl plastic wrap to minimise the loss of moisture and help the cement hydration process. After 24 hours the samples were removed from the mould and placed in a water-lime curing bath for 28 days, as shown in Figure 4.4. It should be noted that, the curing bath was prepared by saturating water with lime in accordance with the Australian Standard (AS 1012.8.1.-2014). These processes were strictly adhered to, to ensure that the samples were consistent and homogenous. Note that samples of clay treated with cement followed this procedure but no fibre was added.



Figure 4.3: Polypropylene fibre adopted in this study (the illustrated scale is in cm)

Table 4.2: Average properties of the adopted fibre

Type	Polypropylene
Diameter ( $d_f$ ) (mm)	0.017
Length ( $l_f$ ) (mm)	18
Plastic limit stress ( $\sigma_f^p$ ) (MPa)	300*
Unit weight ( $kN/m^3$ )	8.93*
$E$ ( $N/mm^2$ )	3500*

Note: (\*) obtained from Sika product data sheet



(a)



(b)



(c)



(d)

Figure 4.4: Sample preparation stages: (a) sample moulded in slipt cylindrical mould, (b) wrapped in vinyl plastic wrap, (c) demoulded sample after 24 hours, (d) placed in curing bath

### 4.3. Experimental Program

The experimental program in this study includes unconfined compressive strength (UCS) tests and a series of undrained and drained triaxial compression tests using the advanced triaxial apparatus while the microstructure of the treated clay was studied using the Scanning Electron Microscopy (SEM). Table 4.3 summarises the experimental program used in this study.

Table 4.3: Experimental program in this study

Clay type	Cement content (%)	Fibre content (%)	Curing time (days)	Confining pressure (kPa)	Test program
Ballina clay	0	0	28	200 – 800	SEM, UCS, CU
	10	0	28	50 – 800	SEM, UCS, CU & CD
	12	0	28	50 – 800	UCS, CU & CD
	15	0	28	50 – 800	UCS, CU & CD
	15	0.3	28	100 – 800	SEM, UCS, CU
	15	0.5	28	100 – 800	UCS, CU
Kaolin clay	0	0	28	100 – 800	CU
	5	0	28	50 – 800	
	5	0.1	28	50 – 800	
	5	0.5	28	50 – 800	

Note: SEM: Scanning Electron Microscopy; UCS: Unconfined Compression Strength test; CU: Consolidated-Undrained triaxial compression test; CD: Consolidated-Drained triaxial compression test.

### **4.3.1. Unconfined Compression Strength (UCS) Tests**

Since confining pressure is not applied in a UCS test, the actual field conditions and real behaviour of the treated soil are not simulated. However, unconfined compression strength (UCS) test is one of the tests widely performed in a geotechnical laboratory due to its economical and practical advantages. According to Sariosseiri (2008), a UCS test is often used to measure the effectiveness of treated soil because the strength of a cement treated soil with or without fibre is governed by the cementation bonds which can be destroyed by confining pressures in triaxial test conditions. Maher and Ho (1993) suggested that the treatment of soil with cement or fibre is less effective in a triaxial test than under UCS test because the sample is quite stiff in triaxial conditions. Hence, in this study a series of UCS tests were carried out on Ballina clay treated with differing amounts of cement (i.e 10%, 12% and 15%) to quantify the effectiveness of cement treatment. The experimental program also includes UCS tests on the Ballina clay treated with 15% cement and reinforced with 0.3% and 0.5% fibre to study the effectiveness of fibre reinforcement in unconfined conditions. The result of the UCS on un-treated Ballina clay was used as a benchmark for comparison. It can be noted that all the treated samples were tested at 28 day curing time. The experimental program for UCS tests is summarised in Table 4.3.

The UCS apparatus consists of a load frame, a linear variable displacement transformer (LVDT), a load cell and a data logging box. The sample and the top cap are placed in the middle of the load cell so that the applied load can be distributed uniformly onto the sample area. During loading, the sample is pushed upwards against the rigid beam, and then the load cell measures the applied load (in kN) while the LVDT measures displacement (in mm). The data logging box records and transfers the applied load and the displacement readings to the computer. The chosen compression rate for all the samples was 1 mm/minute. Figure 4.5 shows the UCS test setup used in this study.

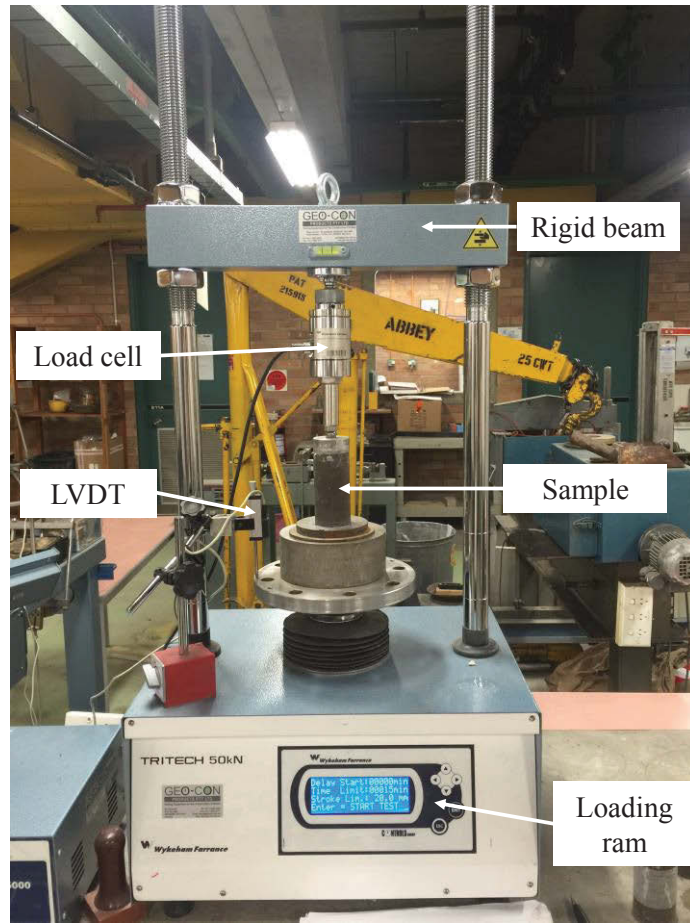


Figure 4.5: Unconfined compression strength (UCS) test setup

### 4.3.2. Scanning Electron Microscopy (SEM)

The effect of cementation on the behaviour of cement treated clay was examined at microstructural level to identify any differences in the clay structure caused by the cement and the loading conditions. The structure of the cement treated clay with fibre reinforcement was also studied to further examine the interaction between the fibre and clusters of soil and cement at the pre-and-post shearing stages. A visual characterisation of the particle structure and cementation bonding between the cement, the fibre, and the clay particles can be observed closely using a Zeiss Evo LS15 with extended pressure for the Scanning Electron Microscopy (SEM). In the SEM analysis, the surface of the sample is scanned by an electron beam in an extended pressure mode and the image is displayed in the computer.

In this experimental program SEM analyses were carried out on untreated Ballina clay, and Ballina clay treated with 10% cement, before and after undrained triaxial testing. The sample of Ballina clay treated with 15% cement and 0.3% fibre was used for SEM analysis to observe the effect of fibre reinforcement.

### **4.3.3. Triaxial Compression Apparatus**

The main part of this study is to examine the combined effects of cement and fibre on the behaviour of soft clay under different loading conditions. In this study, a series of undrained (CU) and drained (CD) triaxial compression tests were carried out on Ballina and Kaolin clays treated with differing amounts of cement and with or without fibre reinforcement at different confining pressures. Undrained triaxial tests were also carried out on un-treated Ballina and Kaolin clays to provide a benchmark for measuring the effectiveness of cement and fibre inclusion. The triaxial compression test program is summarised in Table 4.3.

The triaxial apparatus used in this experimental program consists of a triaxial cell, a 250 kN automated loading frame, and a base. The triaxial cell has an external diameter of 250 mm and a height of 500 mm and can hold a 200 mm high by 100 mm diameter sample. The triaxial cell has a two way drainage system at the top and bottom of the sample. A pressure transducer is used to measure the pore water pressure at the bottom of the sample when drainage from the base is prevented. Two GDS Enterprise Level Pressure/Volume Controllers (ELDPC) were used to apply and control the cell and back pressures, and to record the changes in volume; this ELDPC can apply up to 1MPa of pressure with a 200cc volume. Axial displacement is measured using an LVDT (Linear Variable Differential Transformer) attached to the load cell shaft. The pore water pressure transducer (PWPT) and the LVDT are connected to the data acquisition box which can transfer the data reading to the computer. In this system the reservoir is used to supply de-aerated water to the controllers and the triaxial cell. The automated loading frame applies an axial load by pushing the triaxial cell upwards against a rigid beam at a defined rate of deformation. The triaxial system and a schematic diagram of the triaxial cell setup are shown in Figure 4.6. The testing

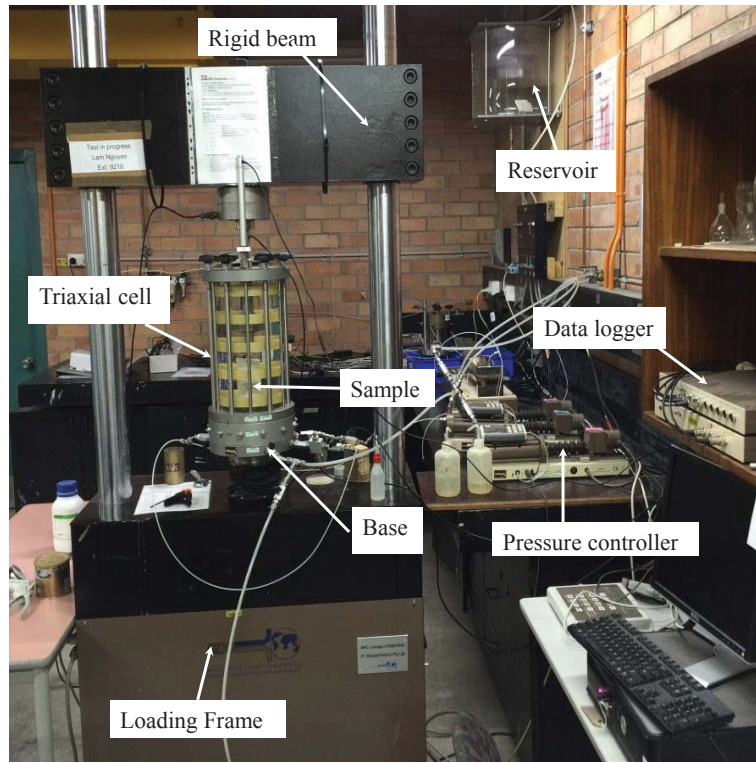
conditions are fully computer controlled and the results are recorded via GDSLAB software.

Before commencing triaxial testing, all the pipes connecting the cell and back pressures to the triaxial cell, particularly the pore water pressure transducer, are flushed with water to de-air the system. The sample that was cured for 28 days was placed on top of the base and wrapped in a 0.2 mm thick rubber membrane. Note that double membranes were used for triaxial testing at 600 and 800 kPa confining pressures to prevent possible rupture of membrane at high pressures. Moreover, two O-rings were placed around the membrane at the top cap and the base to seal the sample. The triaxial cell was then held securely to the base by tightening rods.

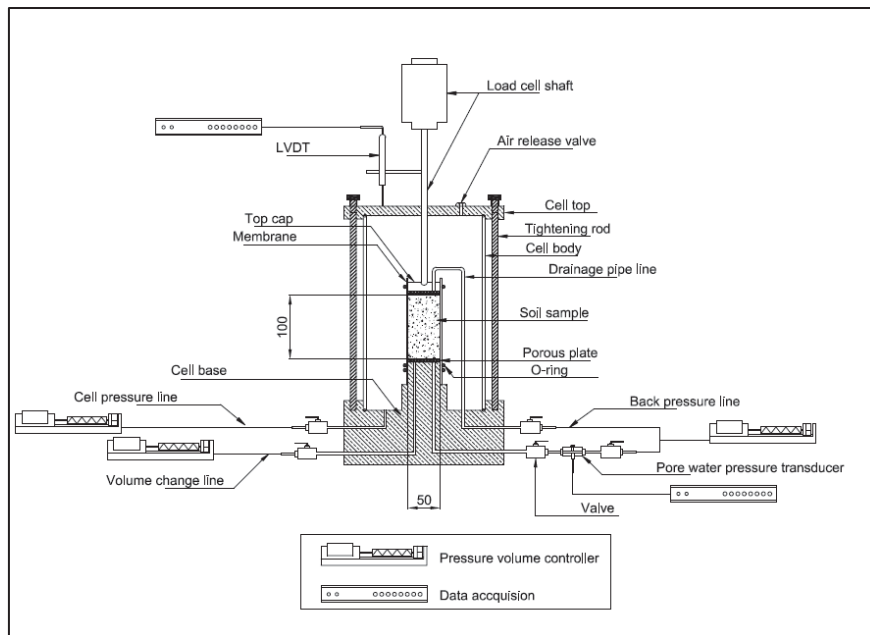
The sample was tested in the triaxial apparatus and the pore water pressure was measured in accordance with Australian Standard (AS1289.6.4.2-1998). At the saturation stage, a back pressure and cell pressure were applied incrementally up to 180 kPa and 200 kPa, respectively, to allow the sample to be fully saturated. B-value checks were carried out after the saturation stage, and in general, a B-value greater than 0.95 is deemed acceptable for 95% saturation. For stiff clay, a B-value of 0.913 is satisfactory in accordance with the Australian Standard (AS1289.6.4.2-1998). When the sample is deemed to be fully saturated, consolidation can begin. In this study the effective consolidation pressure varied from 50 to 800 kPa. When consolidation was completed, the samples were subjected to shearing at an axial straining rate ( $\dot{\epsilon}$ ) that was determined from the strain level at failure ( $\epsilon_f$ ) (assumed to be 5% for firm clay based on Australian Standard (AS1289.6.4.2-1998)) and the time to failure ( $t_f$ ). The strain rate ( $\dot{\epsilon}$ ) was calculated using the following equation:

$$\dot{\epsilon} < \frac{\epsilon_f}{t_f} \quad (4.1)$$

According to Australian Standard (AS1289.6.4.2-1998),  $t_f$  was calculated and a strain rate ( $\dot{\epsilon}$ ) of 0.0185 mm/min was used for drained and undrained triaxial testing. This adopted strain rate facilitates to achieve a more uniform distribution of pore water pressure within the sample, particularly at the time of failure.



(a)



(b)

Figure 4.6: (a) Triaxial test setup used in this study; (b) Schematic diagram of the triaxial cell

## **4.4. Experimental Results**

### **4.4.1. Scanning Electron Microscopy (SEM)**

#### **4.4.1.1. SEM Image Analysis for the Cement Treated Clay**

The SEM analysis reveals how the untreated clay has been transformed from holding a compacted and dispersed fabric, unlike the flocculated structure in the Ballina clay treated with cement, as shown in Figures 4.7 and 4.8. Moreover, the cement treated clay has a more open and reticular structure than the untreated clay due to the addition of cement. As a result of the hydration and subsequent pozzolanic reactions, the cementation bonds are evident and an aggregation of clay particles (clay clusters) has formed within the structure of the cement treated Ballina clay, while precipitated crystals have formed individually or as clusters due to the cementitious bridges connecting the clay particles, both of which create an open type structure in the clay, as shown in Figure 4.8. It should be noted that this degree of reticulation increases as the amount of cement increases, as suggested by Kamruzzaman et al. (2009). Furthermore, Sasanian (2011) observed that crystals form as curing commences and they could damage the surrounding soils due to high volumetric expansion. As a result of the cementation bonds between the clay particles, cement treated soil can sustain a higher yield stress than untreated soil at the same level of void ratio.

The effect of cementation and broken cementation bonds can be studied in SEM analysis as the sample was subjected to shearing with a high mean effective stress of 800 kPa, as shown in Figure 4.9. The SEM sample was taken from the shear band after an undrained triaxial test. The morphology of treated clay at this ultimate stage shows broken clay particles and crushed clusters of clay-cement, that were similar to the observations made by Kamruzzaman et al. (2009) of cement treated Singapore clay. Moreover, after shearing under high confining pressure, there is no evidence of precipitated crystals in the structure of cement treated Ballina clay as the cementation bonds were completely removed due to the mean effective stress and the deviatoric strain. Since these cementation bonds were removed, the behaviour of cement treated Ballina clay at the ultimate state could be similar to the reconstituted soil-cement mixture, and therefore this SEM analysis can further explain the effect of cementation and its degradation on the behaviour of cement treated clay.

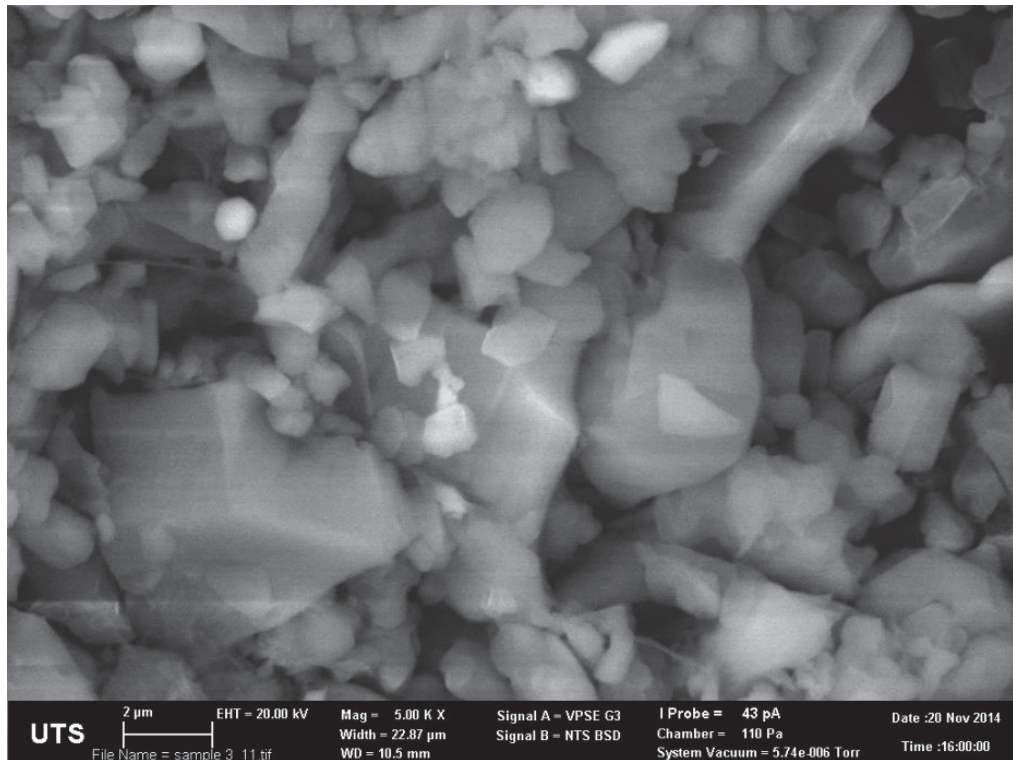


Figure 4.7: SEM images of the un-treated Ballina clay at  $2 \mu\text{m}$  with the magnification of 5000

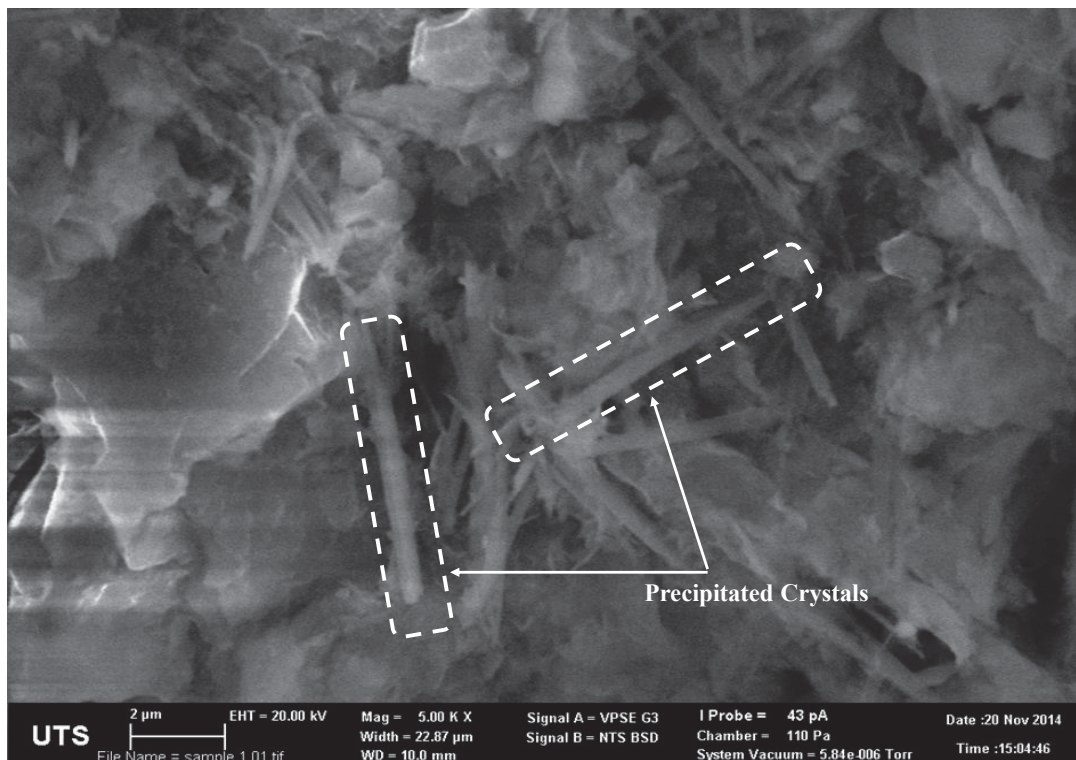


Figure 4.8: SEM images of the 10% cement treated Ballina clay at  $2 \mu\text{m}$  with the magnification of 5000

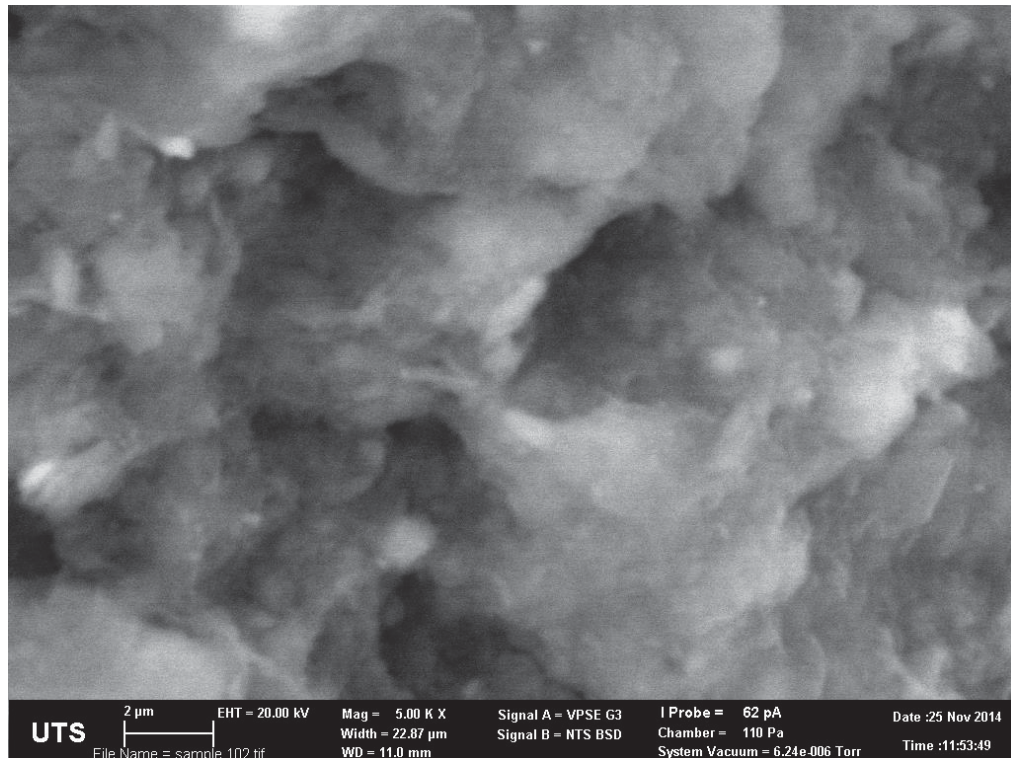


Figure 4.9: SEM images of the 10% cement treated Ballina after shearing at 800 kPa at  $2\ \mu\text{m}$  with a magnification of 5000

#### 4.4.1.2. SEM Image Analysis for the Improved Clay Composite

SEM image analyses of Ballina clay treated with 15% cement and 0.3% fibre after undrained shearing at 800 kPa confining pressure were carried out, and Figure 4.10 shows the morphology of the improved Ballina matrix before triaxial testing. As a result of cement hydration and pozzolanic reactions, large clusters of clay and cement were formed within the material matrix. Figure 4.10 shows that the surface of the fibre was smooth and the fibre was surrounded by clusters of clay and cement with relatively large openings. Figure 4.11 shows the SEM image taken from the shear band of the improved Ballina clay composite, while Figure 4.12 shows that the cementation bonds consisted of precipitated needle shaped crystal products.

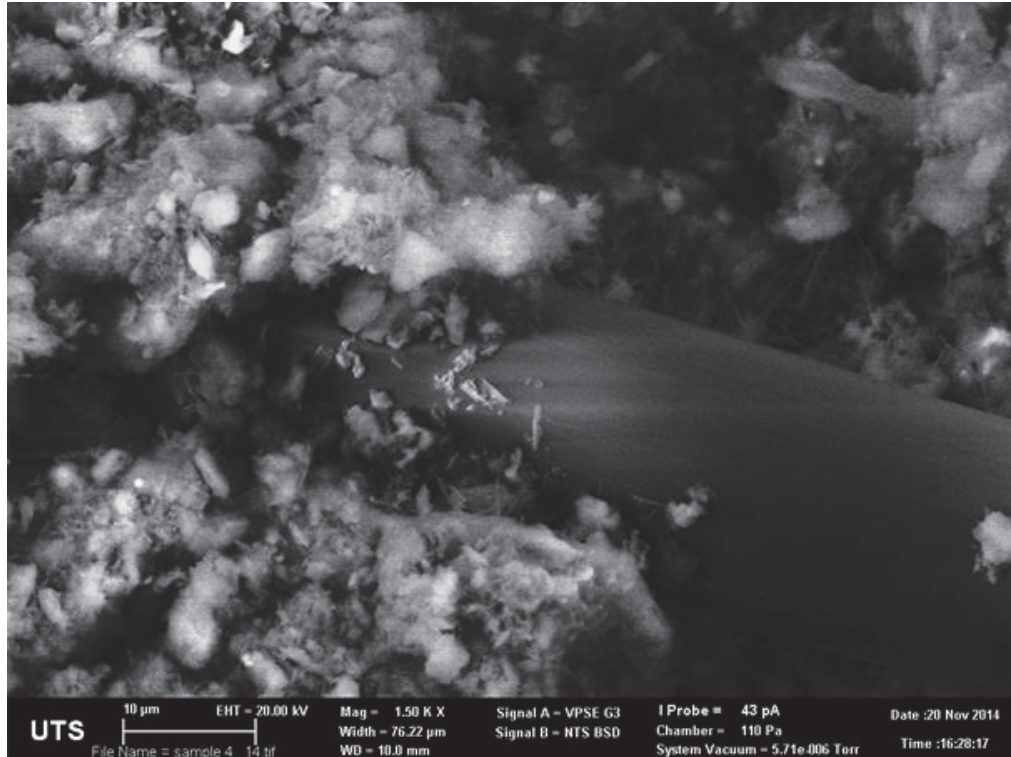


Figure 4.10: SEM image of the improved Ballina clay (15% cement content and 0.3% fibre content) before triaxial test at 1500 magnification

After isotropic consolidation and shearing, the improved Ballina clay composite displayed a compacted matrix with small openings where the fibre was closely surrounded by the soil-cement matrix. As Tang et al. (2007) explained, the fibre is restricted from moving under loading by the surrounding clusters of soil and cement, which induces tension in the body of the fibre. A closer observation of the surface of the fibre shows some grooves caused as the cementation bonds were crushed after shearing. Moreover, as evident in Figure 4.12, the needle shaped hydrated products formed by the cementation process are attached tightly and cause damage to the body of the fibre due to plastic deviatoric strain. This result indicates that fibre reinforcement connects the adjacent clusters of soil and cement together such that the load applied to the clusters of soil and cement are transferred to the body of the fibre. Thus, the load transfer mechanism prevents any further development of micro-cracks within the sample, which leads to an increase in the strength and ductility of the composite material.

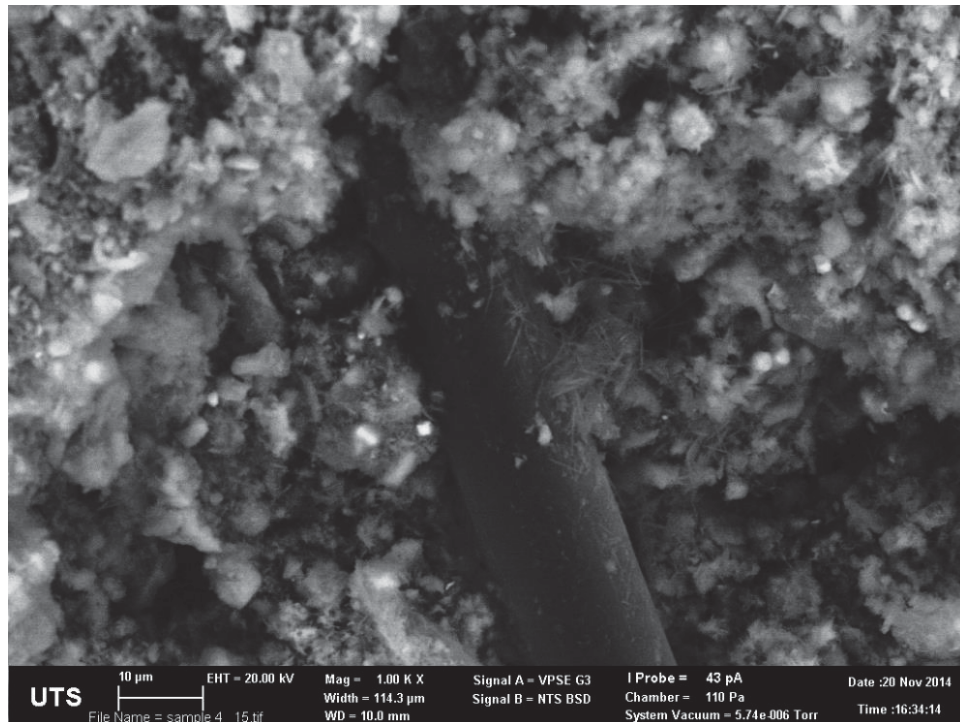


Figure 4.11: SEM image of the improved Ballina clay (15% cement and 0.3% fibre) after shearing at 800 kPa (taken at the shear band) at 1000 magnification

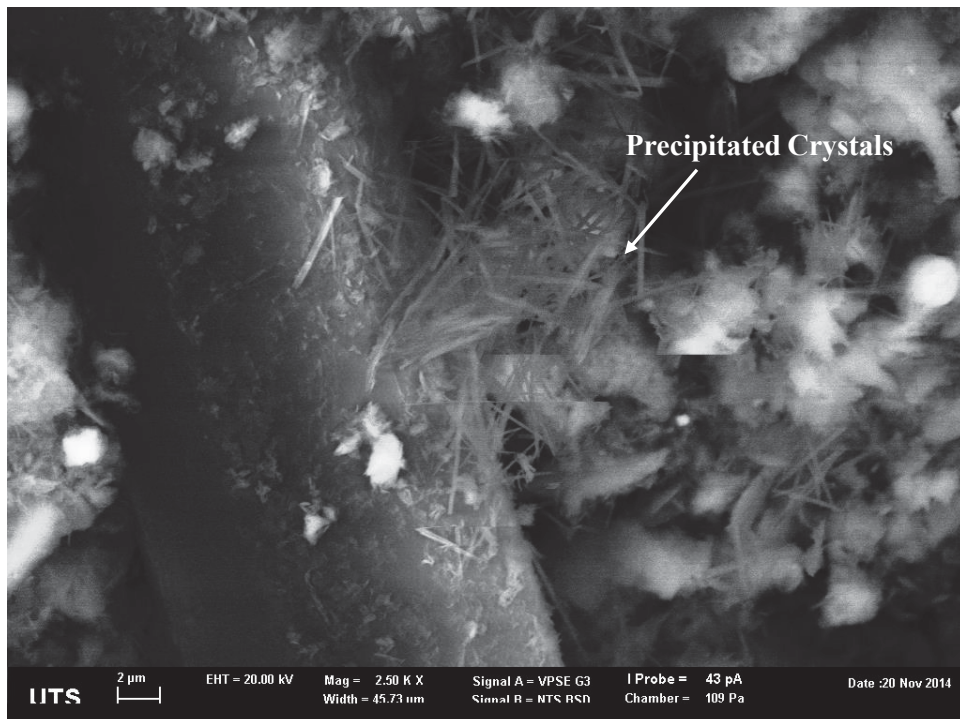


Figure 4.12: SEM image of the improved Ballina clay (15% cement content and 0.3% fibre content) after shearing at 800 kPa (taken at shear band) at 2500 magnification

#### 4.4.2. Unconfined Compression Strength (UCS) Test Results

The effect of cementation on the behaviour of Ballina clay treated with differing cement contents (i.e. 10%, 12% and 15%) using the unconfined compression strength (UCS) results are presented in Figure 4.13. The cement treated samples were prepared by thoroughly mixing soil at 120% water content with cement slurry with different amounts of cement. The samples were then placed into a water-lime curing bath for 28 days prior to testing.

The stress mobilised in the untreated Ballina clay increased to a peak ( $q_{peak} = 56.2$  kPa) and then decreased slightly as the strain increased. The addition of 10% cement increased the peak shear strength by 35% ( $q_{peak} = 75.9$  kPa) while a significant (i.e. 200%) increase in  $q_{peak}$  was observed when 15% cement was used as compared to the un-treated clay. This means that increasing the cement content led to an increase in the peak shear strength of the cement treated clay in unconfined compression. Researchers such as Lorenzo and Bergado (2006), Uddin et al. (1997), and Tan et al. (2002) also reported an increase in UCS depending on the amount of cement. However, as shown in Figure 4.13, increasing the amount of cement reduces the axial strain at its peak state ( $\varepsilon_{peak}$ ). While  $q_{peak}$  of the clay treated with 10% cement occurred at  $\varepsilon_{peak} = 1.28\%$ , the addition of 12% cement resulted in  $\varepsilon_{peak}$  occurring at 0.92%. Moreover, higher cement content also led to lower strain at the residual state. The residual strain ( $\varepsilon_{res}$ ) of the 15% cement treated Ballina clay occurred at  $\varepsilon_{res} = 2.67\%$ , compared to  $\varepsilon_{res} = 4.91\%$  with 10% cement, so this reduction in strength occurred at a higher rate and with increasing cement content. As observed in Figure 4.13, the strength of the treated sample with 15% cement suddenly dropped to its residual strength, compared to rather gradual reduction in the sample with 10% cement. Furthermore, a significant reduction at the post-peak state in UCS was observed when higher cement content was used.

The brittleness index ( $I_B$ ) can be used to measure material ductility as adopted by Consoli et al. (1998) and Maher and Ho (1993). The expression for  $I_B$  can be defined as follows:

$$I_B = \frac{q_f}{q_u} - 1 \quad (4.2)$$

where  $q_f$  and  $q_u$  are the shear strength at the peak and residual states, respectively (Consoli et al. 1998).

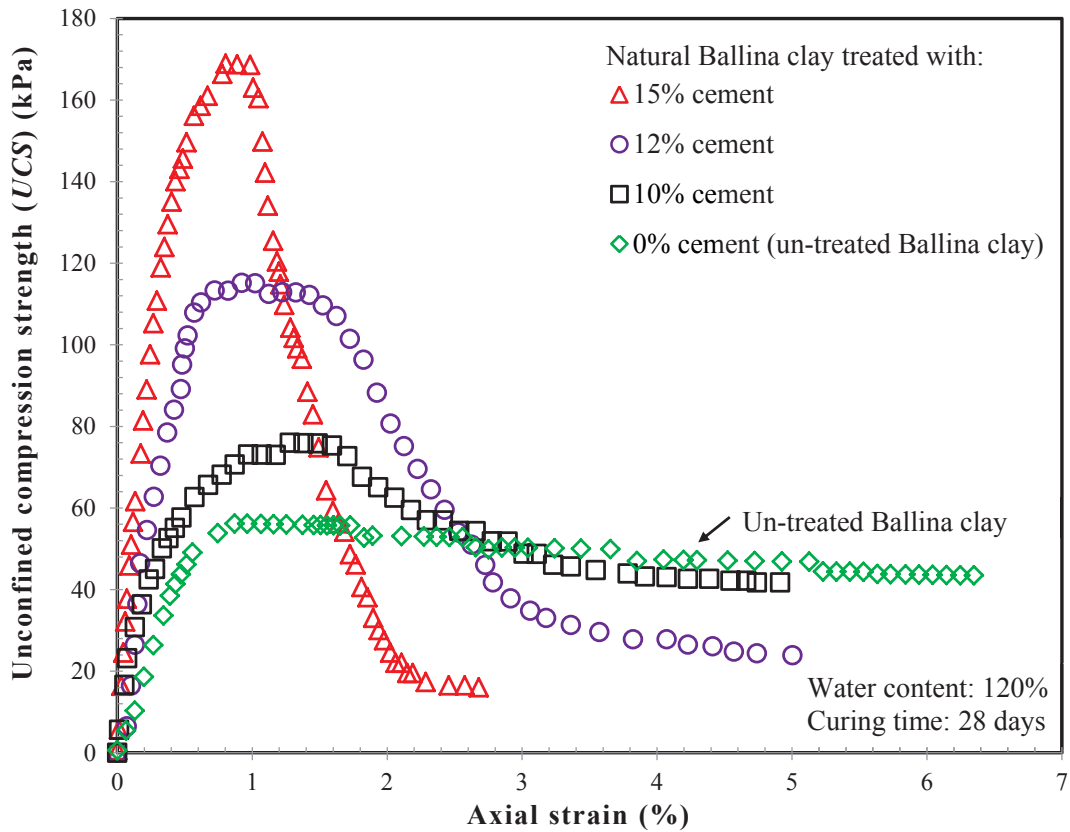


Figure 4.13: UCS results of the Ballina clay treated with differing cement contents (10%, 12% and 15%)

For example, after the peak strength state, the clay treated with 15% cement experienced a 90.5% loss in strength, corresponding to  $I_B = 9.51$ , compared to  $I_B = 0.82$  for the clay treated with 10% cement. The peak UCS increases with cement content while the treated clay becomes more brittle when more cement is used. The addition of cement allows the treated clay to carry a higher load than the un-treated clay due to the effect of the cementation bonds, but the reduction in strength during the post-peak state due to the cementation bonds breaking would impose a significant risk to structures such as road pavements or embankments. Moreover, since the failure of cement treated clay is much more sudden and catastrophic when higher amounts of cement are used, as

explained above, reducing the brittleness of cement treated clay is important from a practical perspective. In recent years natural and synthetic fibres have been used to improve material ductility, particularly at the post-peak stress states, which is why the effect of fibre reinforcement on the behaviour of cement treated clay was examined in this study via an unconfined compression strength (UCS) test on Ballina clay treated with 15% cement and differing amounts of fibre contents (i.e. 0.3% and 0.5%). The experimental results in an unconfined condition are reported in Figure 4.14. Due to cementation, the peak shear strength of the improved clay composite increased significantly compared to the un-treated clay, although the contribution made by the fibre content to the peak shear strength of the improved clay composite is marginal because there was only a 4% increase in the peak strength when 0.5% fibre was added to the cement treated soil. Moreover, the peak strength of the clay treated with cement and fibre occurred at higher strains as the amount of fibre increased. For example,  $\varepsilon_{peak} = 2.27\%$  and  $2.58\%$  when 0.3% and 0.5% of fibre were used in the cement treated soil, respectively, compared to  $\varepsilon_{peak} = 0.8\%$  in treated sample without fibre. Furthermore, the key goal for adding fibre into sample treated with cement is to improve material ductility. As shown in Figure 4.14, the residual shear strength ( $q_{res}$ ) increased with the fibre content, e.g.  $q_{res} = 102.4$  kPa and  $134.3$  kPa for 0.3% and 0.5% fibre contents respectively, compared to  $q_{res} = 16.08$  kPa for 0% of fibre.

Furthermore, the brittleness index ( $I_B$ ) also decreased when fibre was added to the cement treated soil. Figure 4.15 displays the effect of fibre and cement reinforcement on the brittleness index of natural Ballina clay. Here,  $I_B$  increased with cement content and decreased with fibre content; in fact, the  $I_B$  for 15% cement treated clay dropped from 9.51 to 0.72 when 0.3% of fibre was added. A further reduction in  $I_B$  occurred when 0.5% of fibre ( $I_B = 0.39$ ) was added, which was similar to the un-treated Ballina clay ( $I_B = 0.29$ ). Tang et al. (2007) described how the applied load is transferred from the clusters of soil-cement to the fibre body, so the fibre provides a bridging effect, particularly at a post peak state when fibre is fully mobilised. Indeed, fibre reinforcement steadily reduced the strength of the improved soil composite, compared to sudden collapse (brittle) experienced by the cement treated clay, as shown in Figure 4.14. Hence, in unconfined conditions, the ductility of cement treated clay was improved mainly by the inclusion of fibre while the peak strength is governed by the amount of cement added.

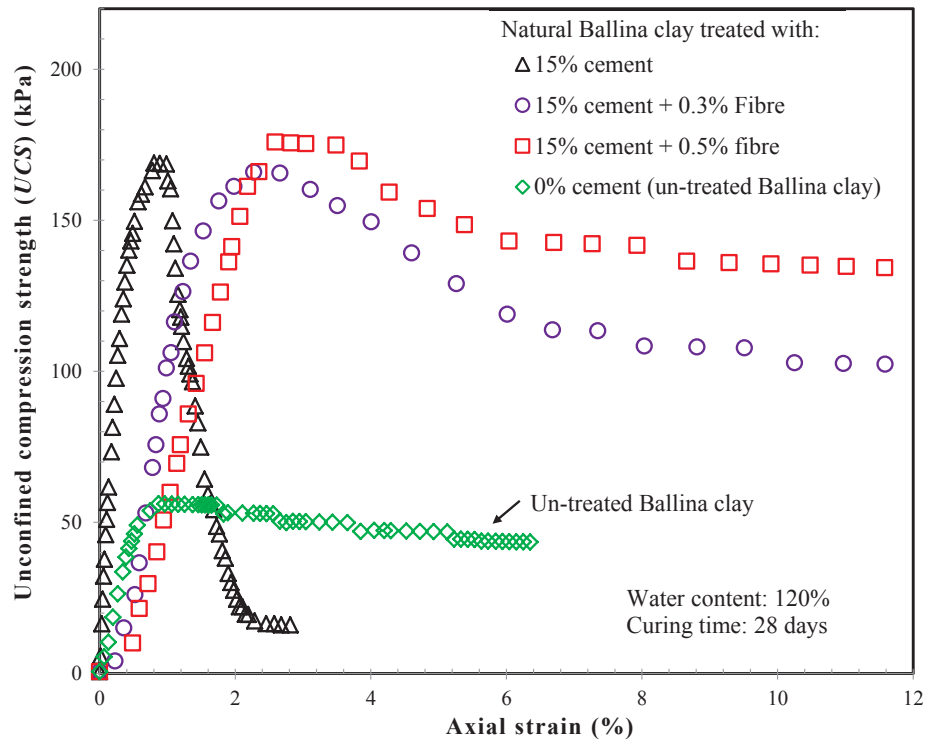


Figure 4.14: UCS results of 15% cement treated Ballina clay reinforced with increasing fibre contents (0.3% and 0.5%)

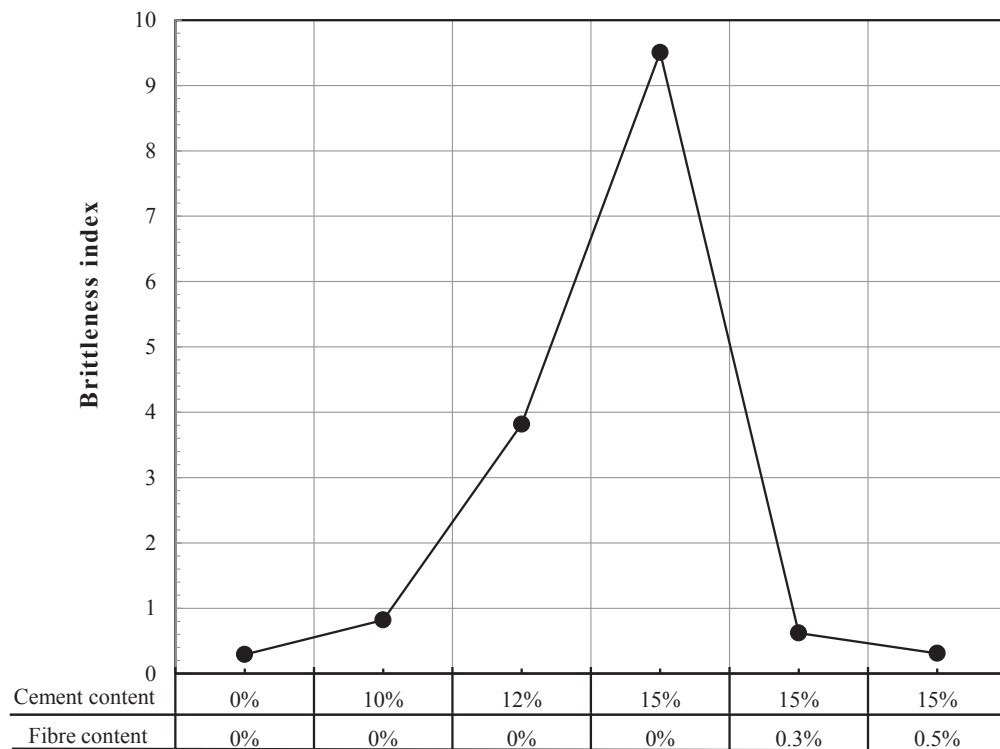


Figure 4.15: Effect of fibre and cement inclusion on the brittleness index of natural Ballina clay in an unconfined compression condition

### 4.4.3. Results of Triaxial Compression Tests

#### 4.4.3.1. Triaxial Test Results of Cement Treated Ballina Clay

Consolidated Undrained (CU) and drained (CD) triaxial compression tests were carried out on samples of Ballina clay treated with 0%, 10%, 12% and 15% cement. The clay samples were prepared with 120% water content and mixed with different amounts of cement into slurry. The confining pressures ranged from 50 to 800 kPa with a back pressure of 180 kPa. The experimental results are shown in Figures 4.15 to 4.36 in terms of isotropic consolidation ( $e - \ln p'$  plane), stress path ( $p' - q$  plane), stress-strain relationship ( $\varepsilon_q - q$  plane) and an excess pore water pressure response ( $\varepsilon_q - \Delta u$  plane). Table 4.4 summarises the results of undrained triaxial compression tests of treated Ballina clay with or without fibre reinforcement.

##### 4.4.3.1.1. Isotropic Compressibility of Cement Treated Ballina Clay

Figure 4.16 describes the isotropic compression of Ballina clay with differing amounts of cement and confining pressures ranging from 20 to 800 kPa. The initial void ratio ( $e_0$ ) was measured at 2.99 with 10% cement while the  $e_0$  values of Ballina clay treated with 12% and 15% cement were recorded at 3.1 and 3.17, respectively. The Isotropic Compression Line (ICL) of the treated Ballina clay is positioned above the reconstituted soil-cement mixture, while the initial mean effective yield stress ( $p'_{o,i}$ ) increased with the amount of cement due to the formation of cementation bonds, unlike the reconstituted mixture of soil-cement at the same void ratio. For example,  $p'_{o,i}$  was estimated as 115.6 kPa and 149.92 kPa (i.e. a 30% increase) when the amount of cement increased from 10% to 15%, respectively. As the mean effective yield stress ( $p'_o$ ) increased the void ratio of the treated Ballina clay gradually approached the ICL of the reconstituted mixture of soil-cement, thus showing the effect of cementation degradation. At high mean effective yield stress where  $p'_o = 800$  kPa, means that the ICL of clay treated with 10% cement approached a meta-stable state with a significant

breaking of cementation bonds while the ICLs of clay treated with 12% and 15% cement indicated that the effect of cementation is still present after the consolidation stages. Moreover, the post-yield response of the treated clay with 12% and 15% (Figure 4.16) cement was approximately linear, indicating a gradual cementation degradation than the steeper curve in the clay treated with 10% cement. As Sasanian (2011) explained, the steady post-yield response of the cement treated clay, particularly clay treated with higher cement content was due to the highly uniform matrix of interconnected cementation bonds within the sample, a result that was also reported by many other researchers (Kamruzzaman et al. 2009; Miura et al. 2001; Rotta et al. 2003). Hence, the compressibility of cement treated clay depends on the amount of cement added because as this amount increases, so too does the initial mean effective yield stress. Moreover, the change in fabric is more significant when higher cement content is added.

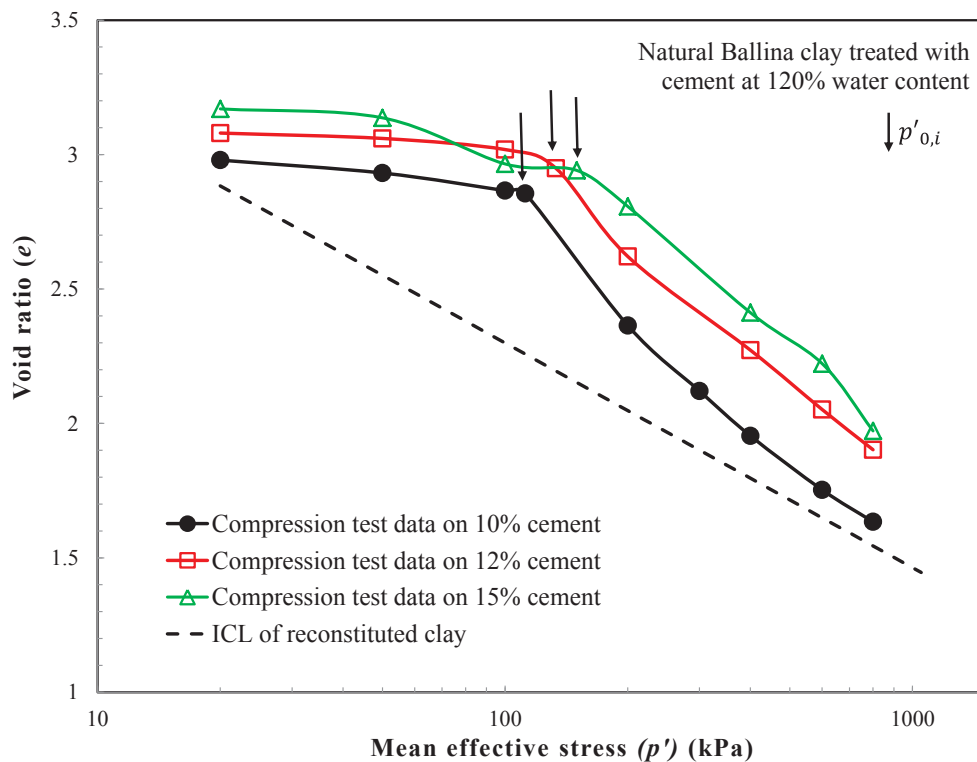


Figure 4.16: Results of isotropic compression tests of Ballina clay treated with different cement contents

Table 4.4: Summary of results of undrained triaxial tests of the treated Ballina clay

<b>Cement content</b>	<b>Fibre content</b>	<b>Confining pressure</b>	<b>Peak strength</b>	<b>Strain at peak stress</b>	<b>Residual strength</b>	<b>Brittleness index</b>	<b>Maximum excess pore water pressure</b>
<b>%</b>	<b>%</b>	<b><math>p'_0</math> (kPa)</b>	<b><math>q_{peak}</math> (kPa)</b>	<b><math>\epsilon_{peak}</math> (%)</b>	<b><math>q_{res}</math> (kPa)</b>	<b><math>I_B</math></b>	<b><math>\Delta u_{max}</math> (kPa)</b>
0	0	200	157.14	10.53	150.10	0.05	130.31
		400	270.40	8.13	250.50	0.08	262.04
		800	486.64	12.68	460.52	0.06	540.79
10	0	50	74.35	3.32	57.64	0.29	43.3
		100	119.98	3.68	95.73	0.25	68.17
		200	175.22	2.78	99.41	0.76	176.72
		300	254.76	3.57	146.37	0.74	254.28
		400	314.48	2.41	177.01	0.78	321.41
		600	447.81	2.34	249.87	0.79	447.03
12	0	800	604.34	1.89	350.55	0.72	604.78
		100	92.52	6.24	84.91	0.09	86.53
		200	162.44	5.19	130.78	0.24	166.1
		400	333.45	2.76	224.88	0.48	336.96
		600	480.85	4.61	296.94	0.62	425.59
		800	618.68	3.07	298.10	1.08	606.21

Table 4.4 (cont.): Summary of results of undrained triaxial tests of treated Ballina clay

<b>Cement content</b> %	<b>Fibre content</b> %	<b>Confining pressure</b> $p'_0$ (kPa)	<b>Peak strength</b> $q_{peak}$ (kPa)	<b>Strain at peak stress</b> $\epsilon_{peak}$ (%)	<b>Residual strength</b> $q_{res}$ (kPa)	<b>Brittleness index</b> $I_B$	<b>Maximum excess pore water pressure</b> $\Delta u_{max}$ (kPa)
15	0	100	173.70	2.17	156.71	0.11	98.8
		200	259.45	1.44	115.03	1.26	159.44
		400	420.46	2.14	228.14	0.84	340.9
		600	631.13	2.69	317.21	0.99	476.37
		800	727.85	2.68	441.10	0.65	610.29
15	0.3	100	121.82	2.38	104.20	0.17	88.24
		200	266.34	2.49	198.81	0.34	198.29
		400	417.63	2.16	304.06	0.37	364.6
		600	572.41	2.07	356.68	0.60	535.18
		800	725.83	2.78	500.91	0.45	671.52
15	0.5	100	127.92	3.82	123.68	0.03	89.89
		200	267.41	2.96	203.77	0.31	241.78
		400	413.70	2.57	306.82	0.35	380.82
		600	540.44	3.12	429.83	0.26	525.1
		800	726.17	2.54	552.68	0.31	686.81

#### 4.4.3.1.2. Undrained Stress Path

Figure 4.17 shows the undrained stress path of natural Ballina clay with 0% cement at 200, 400, and 800 kPa mean effective yield stress (or effective confining pressure) in the  $p' - q$  plane. The stress path of this un-treated clay bends to the left, seeking a failure state in the  $p' - q$  plane. The samples at different mean effective stresses approached a unique line known as the Critical State Line (CSL), where the slope ( $M$ ) was measured at 1.21. However, compared to the peak shear strength of natural Ballina clay in an unconfined condition ( $q_{peak} = 56.2$  kPa), the confining pressure increased  $q_{peak}$  significantly (e.g.  $q_{peak} = 157.14$  kPa when sample was tested at  $p'_o = 200$  kPa).

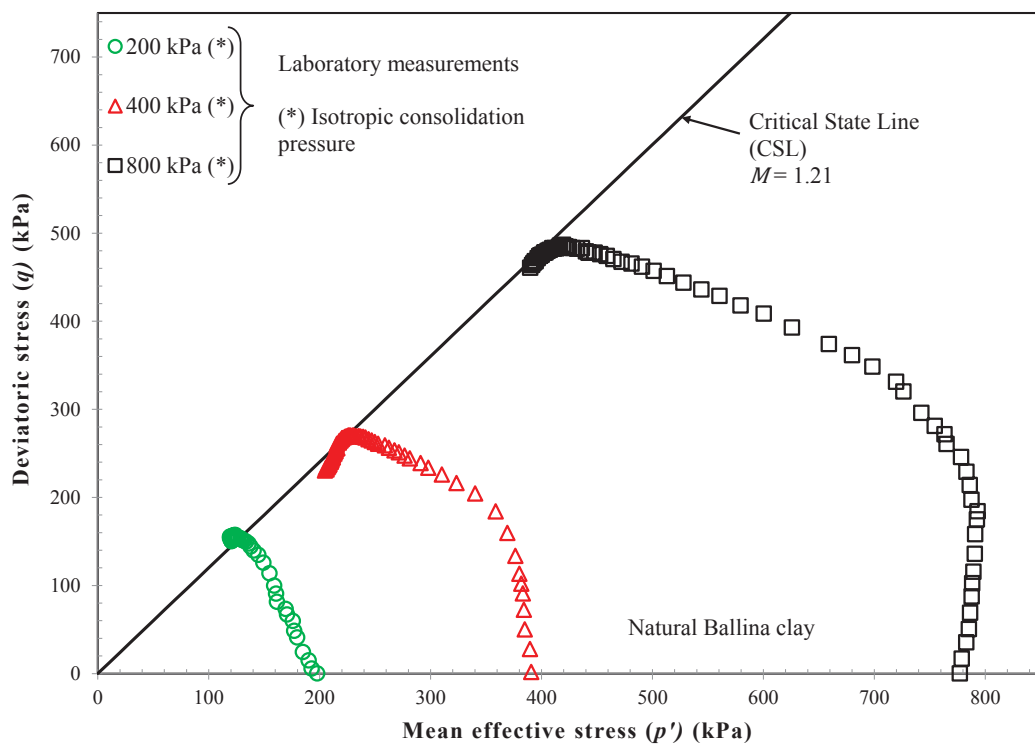


Figure 4.17: Undrained stress paths of natural Ballina clay

Compared to the un-treated clay, the clay treated with cement generally showed a higher peak shear strength ( $q_{peak}$ ) due to the effect of cementation as all the samples treated at differing mean effective yield stresses ( $p'_o$ ) attained  $q_{peak}$  above the Critical State Line (CSL) of the reconstituted mixture of soil-cement. For example, at  $p'_o = 400$  kPa, a 16% increase in the peak strength occurred when 10% cement was added to the

soil, but at  $q_{peak}$  of 10%, the clay treated with cement increased by 35% compared to the un-treated clay in an unconfined condition (i.e. UCS), so the mean effective yield stress contributes to the reduction in the effectiveness of cement inclusion.

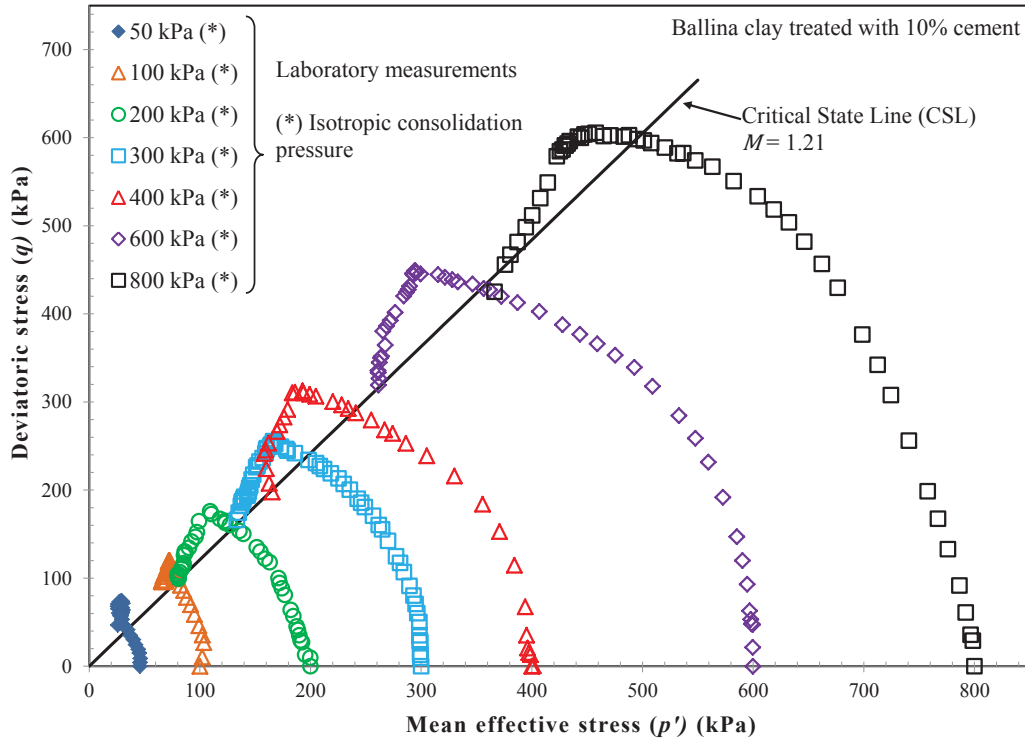


Figure 4.18: Undrained stress paths of Ballina clay treated with 10% cement

Since the initial mean effective yield stress ( $p'_{o,i}$ ) of Ballina clay treated with 10% cement was measured at 115.6 kPa, the stress states of the samples tested under a mean effective yield stress of 50 and 100 kPa were located inside the initial yield surface, hence only elastic deformation occurred. Moreover, the stress paths of these samples rose vertically upwards as they were undergoing hardening until they reached the initial yield surface, as shown in Figure 4.18. When the samples were tested beyond the initial mean effective yield stress (i.e.  $p'_o > p'_{o,i}$ ), plastic deformation occurred as the samples were on the current yield surface. Moreover, there was significant positive excess pore water pressure generated within the sample in which reduced the mean effective stress, which is why the stress paths of these samples bend to the left and reach their peak strength state above the Critical State Line (CSL) due to the effect of cementation. After reaching the peak strength state, the stress paths changed direction toward the CSL with a further reduction in the mean effective stress. The deviatoric

stress ( $q$ ) decreased as the sample began to soften, along with significant breaking of the cementation bonds or cementation degradation. Zhu et al. (2010) explained that the physical mechanism at the post peak state of the cement based material was due to an accumulation of plastic shear strain which causes damage and cracking within soil-cement matrix, so when the cementation bonds had been completely destroyed, the sample reached the ultimate state at the CSL, as shown in Figure 4.18.

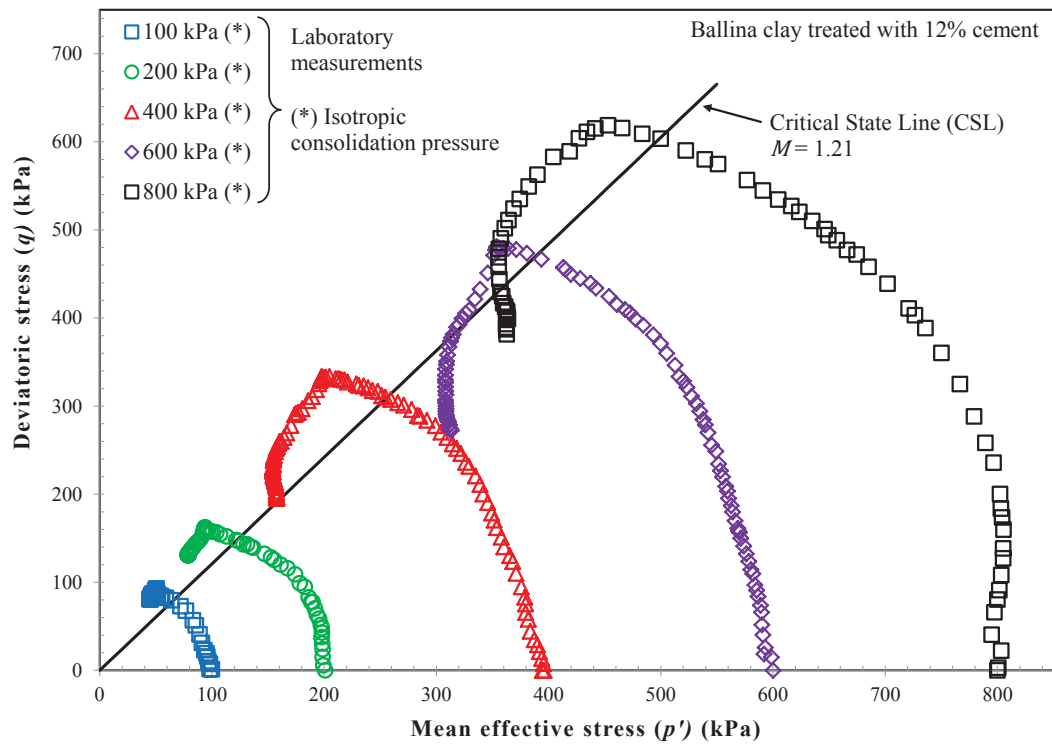


Figure 4.19: Stress paths of Ballina clay treated with 12% cement

The undrained stress paths of Ballina clay treated with 12% cement are shown in Figure 4.19, and indicate that the peak shear strength increased with cement content and the mean effective yield stress. Compared to the clay treated with 10% cement, the peak shear strength increased when 12% cement was added to the soil, but this amount is marginal as an average 6% increase in strength occurred in samples under  $p'_0 = 100$  kPa to 800 kPa. Moreover, the UCS results showed a significant 52% increase in strength in unconfined conditions when the cement content increased from 10% to 12%; this confirmed that the mean effective yield stress reduced the effectiveness of cement

contribution to the shear strength. The undrained stress paths in Figure 4.19 showed that the behaviour of clay treated with cement was similar to typical over-consolidated soil in  $p' - q$  plane.

Due to the increasing cement content, the peak shear strength ( $q_{peak}$ ) of the Ballina clay treated with 15% cement increased compared to the clay treated with 10% and 12% cement, as shown in Figure 4.20. For example, a 60% increase in  $q_{peak}$  occurred when the cement content increased from 12% to 15% at  $p'_0 = 200$  kPa. However, compared to the sample treated with 12% cement, the beneficial contribution made by cementation to the shear strength of the samples with higher cement content (i.e. 15%) decreased as the percentage of improvement in  $q_{peak}$  decreased from 60% to 17% as  $p'_0$  increased from 200 kPa to 800 kPa, respectively. Compared to the 10% cement treated clay, there was a similar trend, i.e., the percentage of improvement in  $q_{peak}$  decreased from 48% to 20% when  $p'_0$  increased to 800 kPa. This shows that increasing the mean effective yield stress results in significant cementation bonds breaking before reaching the peak strength state, particularly for higher cement content.

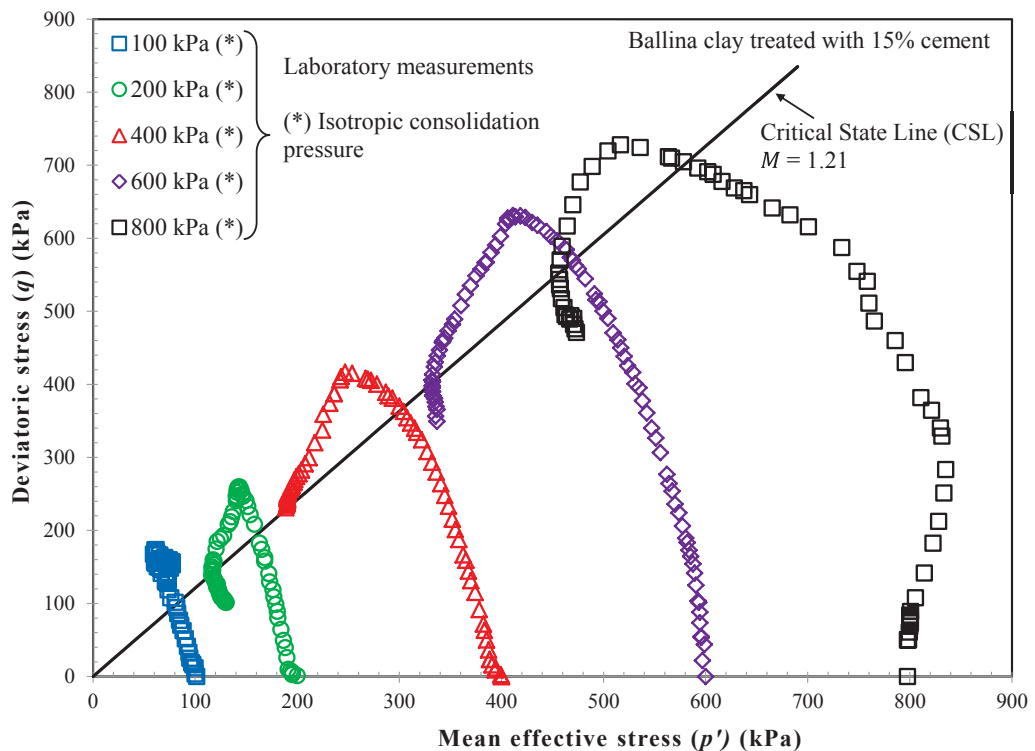


Figure 4.20: Stress paths of Ballina clay treated with 15% cement

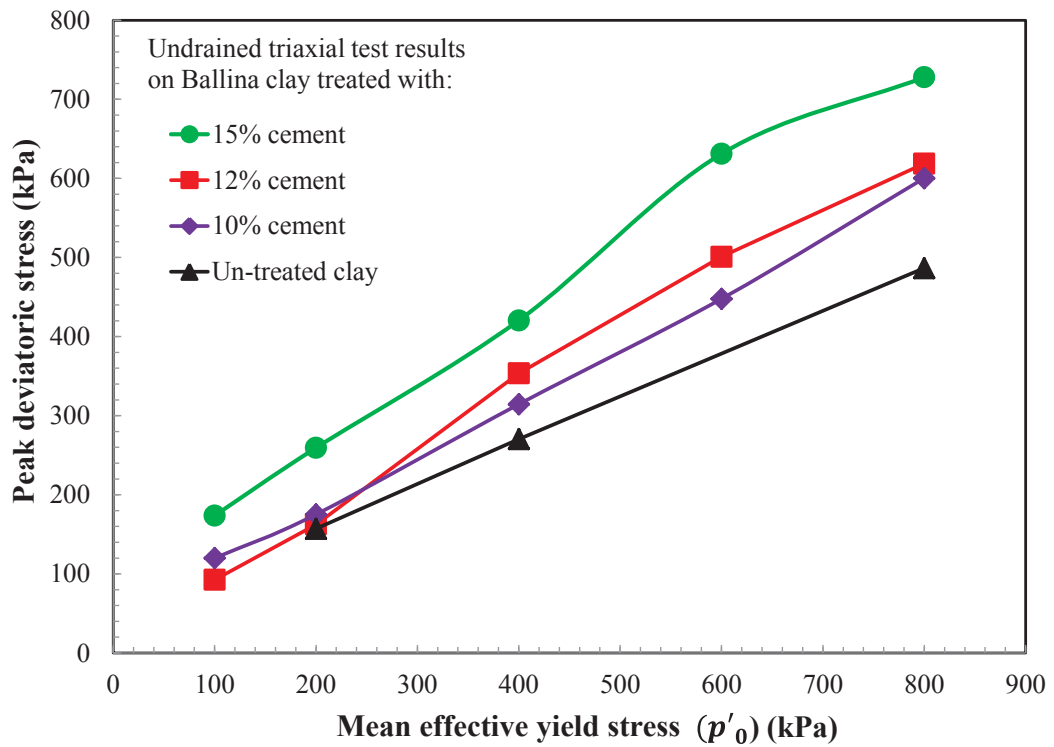


Figure 4.21: Effect of increasing cement content on the peak shear strength of the Ballina clay treated with cement in undrained triaxial conditions.

In summary, the effect of increasing the cement content on the peak shear strength of treated Ballina clay in an undrained condition is shown in Figure 4.21. Here the peak shear strength of treated clay increased with the mean effective yield stress ( $p'_0$ ) and differing cement contents (i.e. 10%, 12% and 15%). Unlike un-treated clay, the cement treated clay can sustain a higher shear stress due to the formation of cementation bonds. For example, at the same  $p'_0 = 400$  kPa, the peak shear strength increased by 16% and 55% when 10% and 15% cement was added to the un-treated clay, respectively. However, the peak shear strength of clay treated with 10% and 12% cement increased slightly compared to the un-treated clay at  $p'_0 = 200$  kPa. On the other hand, at a high mean effective yield stress ( $p'_0 = 800$  kPa), the peak shear strength increased with the amount of cement, which indicated that cementation was still present at the peak strength state. As Figure 4.21 shows, the contribution made by cementation to the shear strength was more pronounced with higher amounts of cement (i.e. 15%) at different mean effective yield stresses, whereas cementation was more effective at higher mean effective yield stress when lower cement contents were used (e.g. 10% and

12%). However, as discussed above, the enhanced shear strength when more cement is used, decreased with increasing mean effective yield stress inducing cementation degradation.

#### 4.4.3.1.3. Stress-Strain Relationship and Excess Pore Water Pressure Response

The un-treated clay showed typical strain hardening ductile behaviour as the stress in the sample increased with increasing strain after yielding, as shown in the stress-strain curves (Figure 4.22) and the excess pore water pressure response (Figure 4.23). Figure 4.22 shows that the strength increased with the mean effective yield stress, but there was a slight reduction in the strength of the samples at high mean effective yield stress (i.e. 400 and 800 kPa), so the strain level at failure for soft un-treated Ballina clay was adopted at 10%, as suggested by Australian Standards (AS1289.6.4.2-1998).

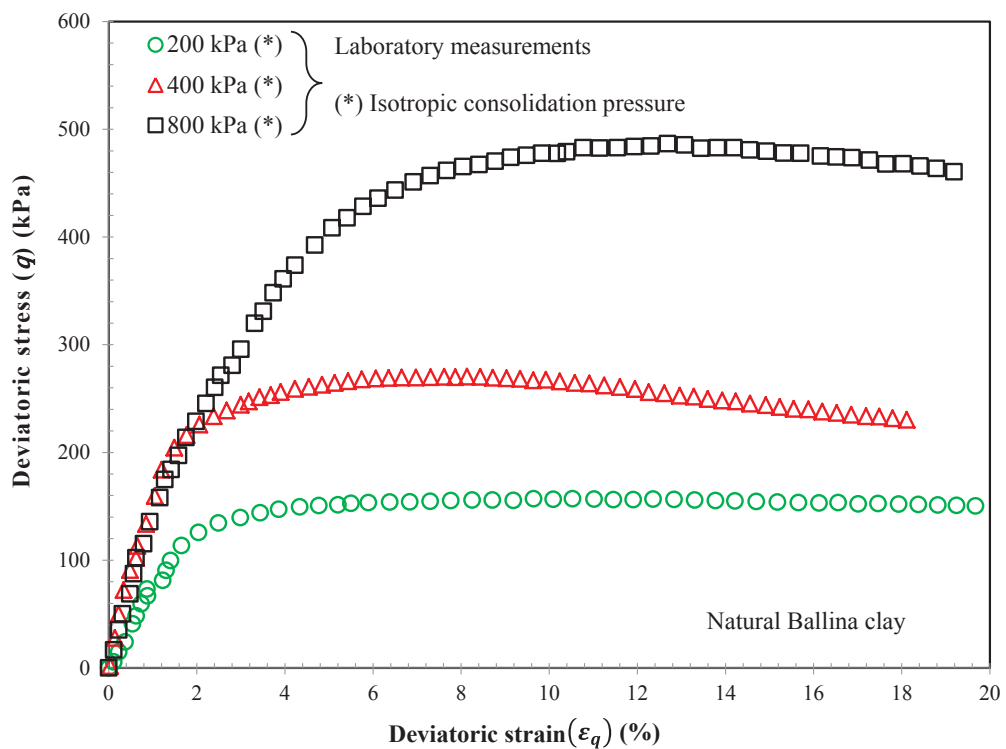


Figure 4.22: Stress-strain relationships of natural Ballina clay

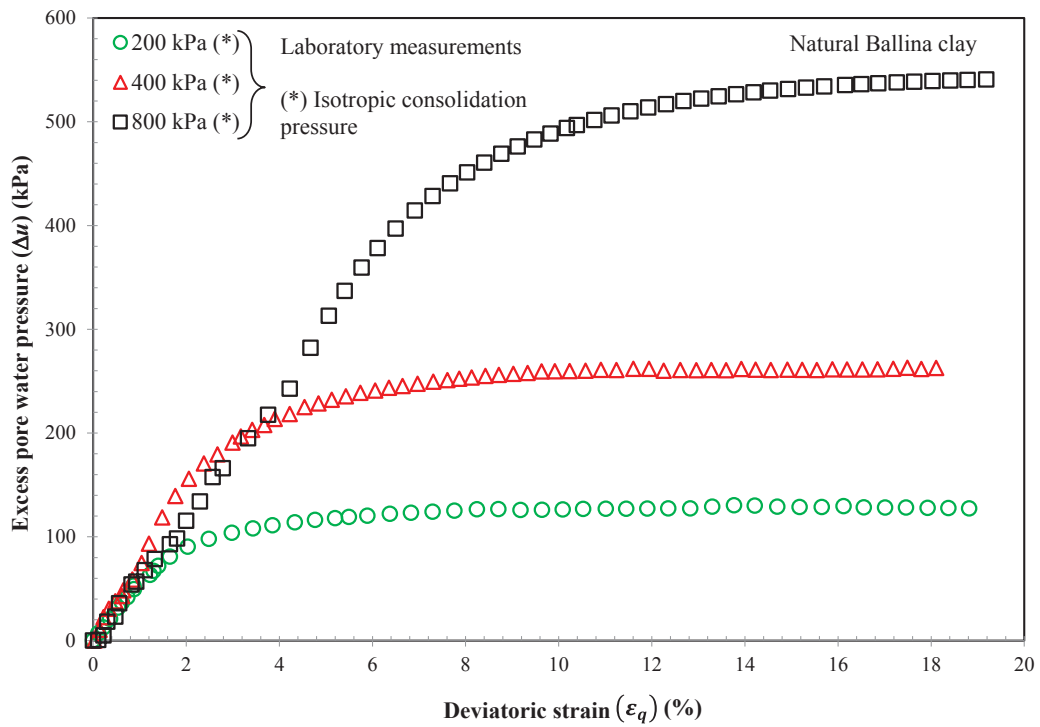


Figure 4.23: Excess pore water pressure response of natural Ballina clay

Unlike the un-treated clay, the addition of cement into clay changed its behaviour from ductile to brittle, which means the brittleness index (Equation 4.2) can be used to measure how brittle the material becomes when cement is added. While  $I_B$  of un-treated Ballina clay ranged from 0.05 - 0.08,  $I_B$  of for the clay treated with 10% cement at different  $p'_o$  was calculated to be between 0.25 – 0.79, which corresponds to a brittle material. Moreover, the axial strain ( $\epsilon_q$ ) at peak stress for the 10% cement treated clay occurred at a much lower  $\epsilon_q$  than the un-treated clay. For example, at  $p'_o = 400$  kPa,  $\epsilon_q = 2.41\%$  and  $8.13\%$  at peak strength for treated and un-treated clay were achieved, respectively. Moreover, at the same deviatoric strain, the peak deviatoric strength ( $q_{peak}$ ) increased with mean effective yield stress, as shown in Figure 4.24.

Furthermore, the clay treated with 10% cement became more brittle with an increasing mean effective yield stress. The samples under low mean effective yield stress (i.e.  $p'_o = 50$  and  $100$  kPa) showed ductile behaviour whereas the samples tested under mean effective yield stress beyond  $p'_{o,i}$  exhibited clear brittle failure. Specifically,  $I_B$  changed from 0.25 to 0.72 when  $p'_o$  increased from  $100$  kPa to  $800$  kPa, respectively, which indicated there was significant cementation degradation (breaking

of cementation bonds) at high mean effective yield stresses and higher reduction in strength at the post-peak state than the sample under lower  $p'_o$ . Moreover, the effect of cementation degradation due to deviatoric strain can attribute to the unfavourable brittle behaviour of clay treated with cement. For example, at  $p'_o = 800$  kPa, the peak deviatoric strain occurred at  $\varepsilon_q = 1.89\%$ , followed by a significant reduction in stress with increasing  $\varepsilon_q$ , while the peak deviatoric strain of the treated sample at  $p'_o = 100$  kPa occurred at  $\varepsilon_q = 3.68\%$ , followed by a steady reduction in stress as  $\varepsilon_q$  increased. Hence, cementation degradation is due to a combination of mean effective yield stress (related to the plastic volumetric strain) and the increasing plastic shear strain when plastic shear deformation occurs.

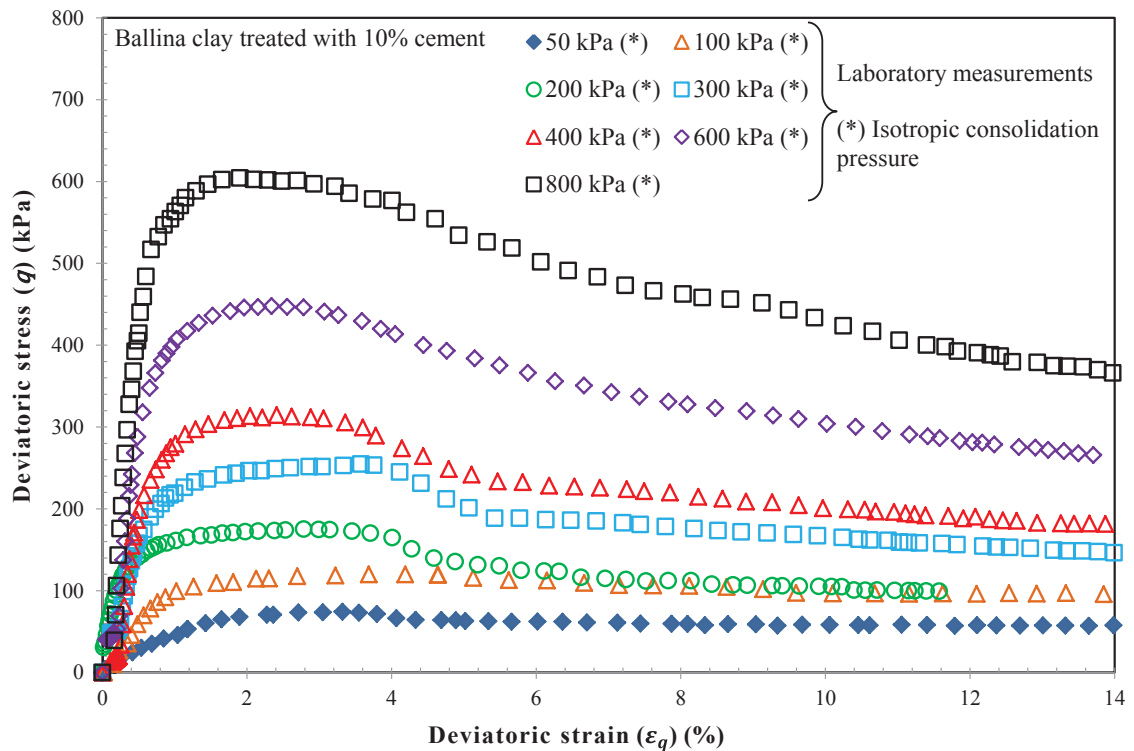


Figure 4.24: Stress-strain relationship of Ballina clay treated with 10% cement

At the same shear strain, the excess pore water response ( $\Delta u$ ) of Ballina clay treated with 10% cement increased with the mean effective yield stress, as shown in Figure 4.25. When the treated sample was subjected to shearing, the load applied onto the soil-cement clusters increased, which resulted in a rise in the excess pore water pressure; in fact it increased up to the peak value and then decreased slightly with increasing deviatoric strain as the sample underwent softening process. The maximum

excess pore water pressure ( $\Delta u_{max}$ ) of treated clay occurred at a lower deviatoric strain than the un-treated clay, as shown in Figures 4.23 and 4.25. Compared to the maximum excess pore water pressure ( $\Delta u_{max}$ ) of the un-treated clay,  $\Delta u_{max}$  of treated clay attained a higher value due to the inclusion of cement. For example, at  $p'_o = 800$  kPa,  $\Delta u_{max}$  was measured at 604.78 kPa and 540.79 kPa for clay treated with 10% cement and un-treated clay, respectively. This may be explained that the formation of cementation bonds and soil-cement clusters would result in a more contractive response rather than the dilative tendency observed in un-treated soil.

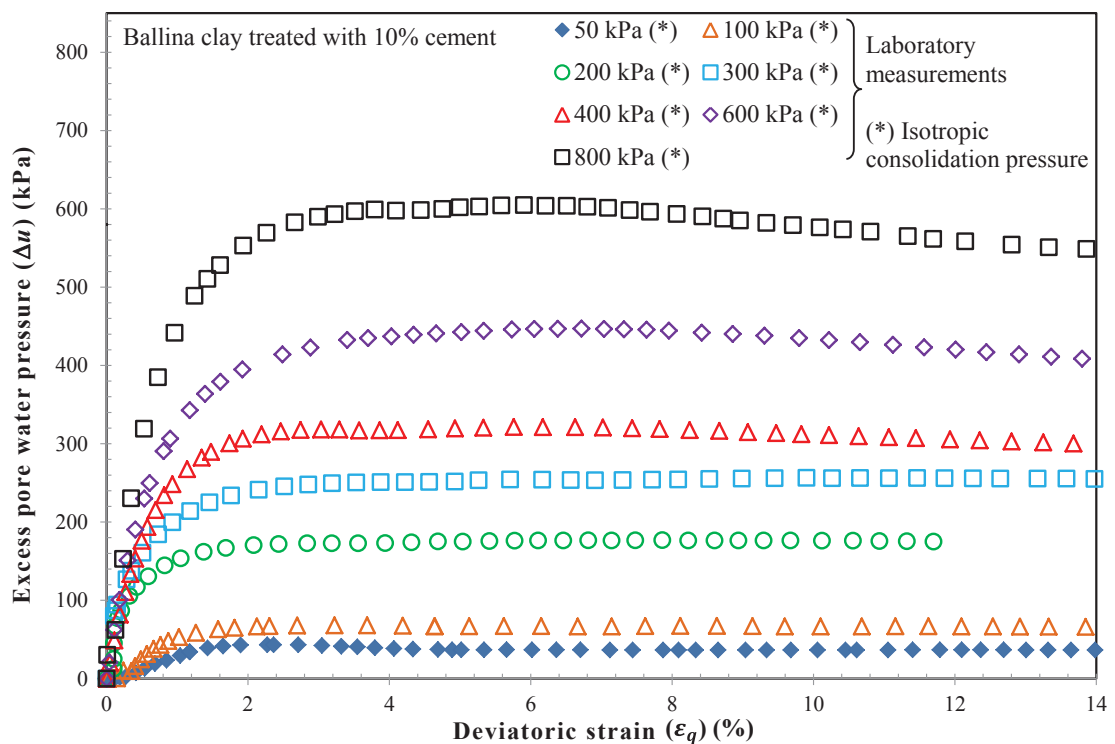


Figure 4.25: Excess pore water pressure response of Ballina clay treated with 10% cement

Like the Ballina clay treated with the 10% cement, the stress-strain curve for the sample treated with 12% cement at  $p'_o = 100$  kPa, which is below  $p'_{o,i}$  of 133.26 kPa, showed strain hardening behaviour rather than the straining softening behaviour exhibited by samples under higher  $p'_o$ , as shown in Figure 4.26. Furthermore, the brittleness of the clay treated with 12% cement increased with the mean effective yield stress as  $I_B$  increased from 0.09 to 1.08 when  $p'_o$  increased from 100 kPa to 800 kPa, respectively. This suggested that the cementation bonds break at a higher rate as the

mean effective yield stress increases. As explained by Kamruzzaman et al. (2009), the change in volume of the cement treated clay is minimal at low confining pressure, however it is significant at higher confining pressure due to the breaking of cementation bonds. Furthermore, the effect of increasing mean effective yield stress also causes higher excess pore water pressure (shown in Figure 4.27), a phenomenon seen by many researchers (Kamruzzaman et al. 2009; Porbaha et al. 2000; Uddin et al. 1997).

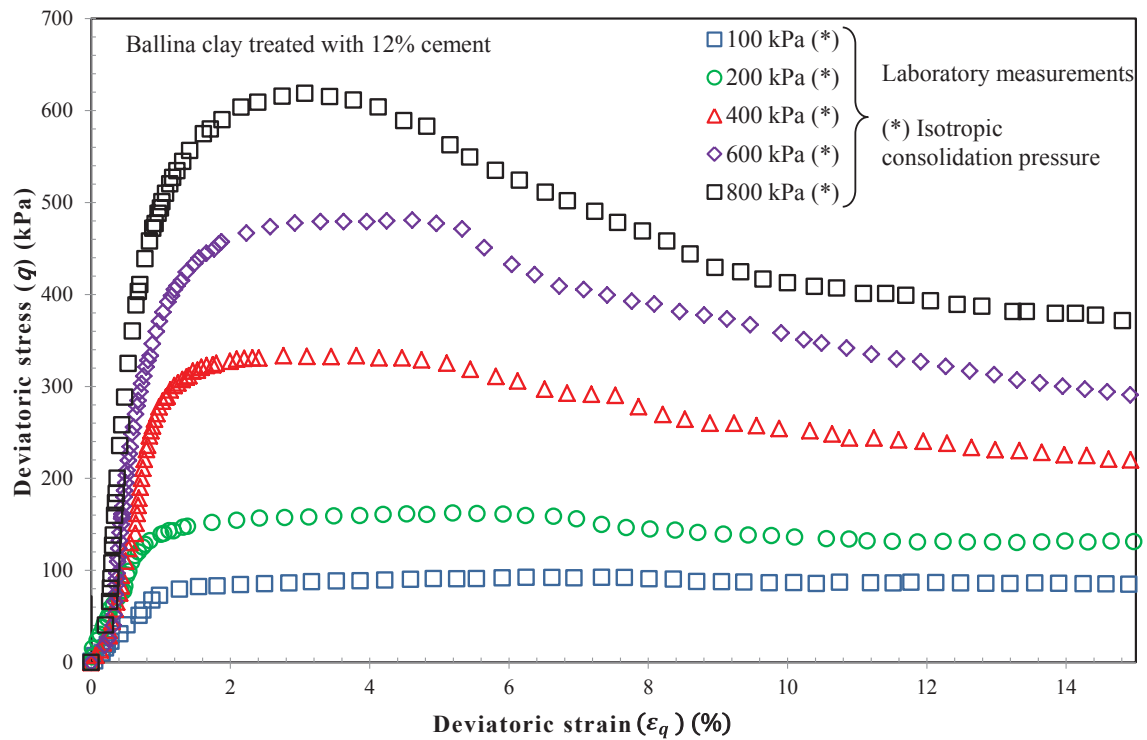


Figure 4.26: Stress strain relationship of Ballina clay treated with 12% cement

Figures 4.28 and 4.29 show the results of undrained triaxial compression test of Ballina clay treated with 15% cement in  $\epsilon_q - q$ , and  $\epsilon_q - \Delta u$  planes, respectively. Similar to the clay treated with 10% and 12% cement, the stress-strain relationships and excess pore water pressure response of Ballina clay treated with 15% cement at  $p'_0 > p'_{0,i}$  showed strain softening and brittle behaviour as the shear stress increased to the peak state, and then it dropped to the residual strength state. As summarised in Table 4.4, the clay treated with 15% cement showed higher maximum excess pore water pressure ( $\Delta u_{max}$ ) than the clay treated with 10% and 12% cement contents. This increase in  $\Delta u_{max}$  may have occurred because the clay with higher cement content

tended to contract more since stronger cementation bonds were formed within the soil matrix.

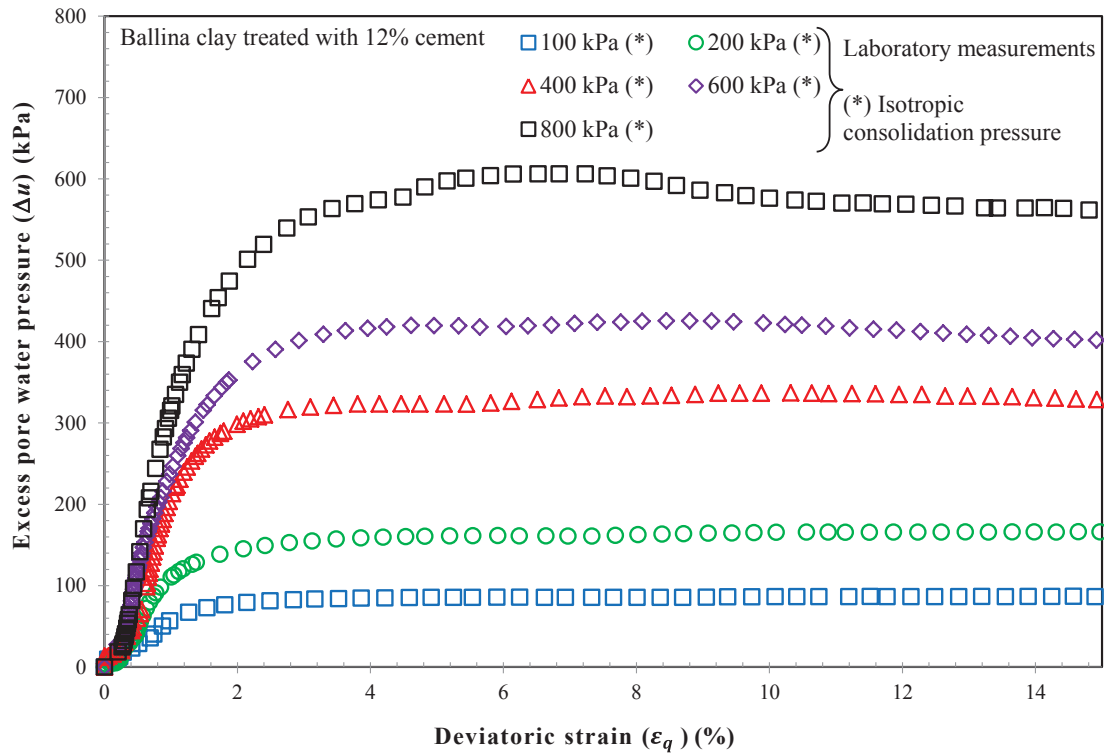


Figure 4.27: Excess pore water pressure responses of Ballina clay treated with 12% cement

Moreover, the reduction in stress for the 15% cement treated clay at the post peak state was more significantly when  $p'_0$  ranged from 200 kPa to 600 kPa, unlike the clay treated with 10% and 12% cement. For example, at  $p'_0 = 600$  kPa,  $I_B$  increased from 0.62 to 0.99 as the cement content increased from 12% to 15%, respectively. Furthermore, as Figure 4.29 shows, the excess pore water pressure decreased at the post peak state with an increasing deviatoric strain; this was more evident at high confining pressures (e.g.  $p'_0 = 800$  kPa). It can be explained that higher cement content would result in higher amount of soil-cement clusters and stronger cementation bonds. During shearing, at the post-peak state the cementation bonds are crushed, leading to significant change in the volume of soil treated with higher cement content, so increasing the amount of cement leads to an increase in the brittleness index, meaning the material becomes more brittle.

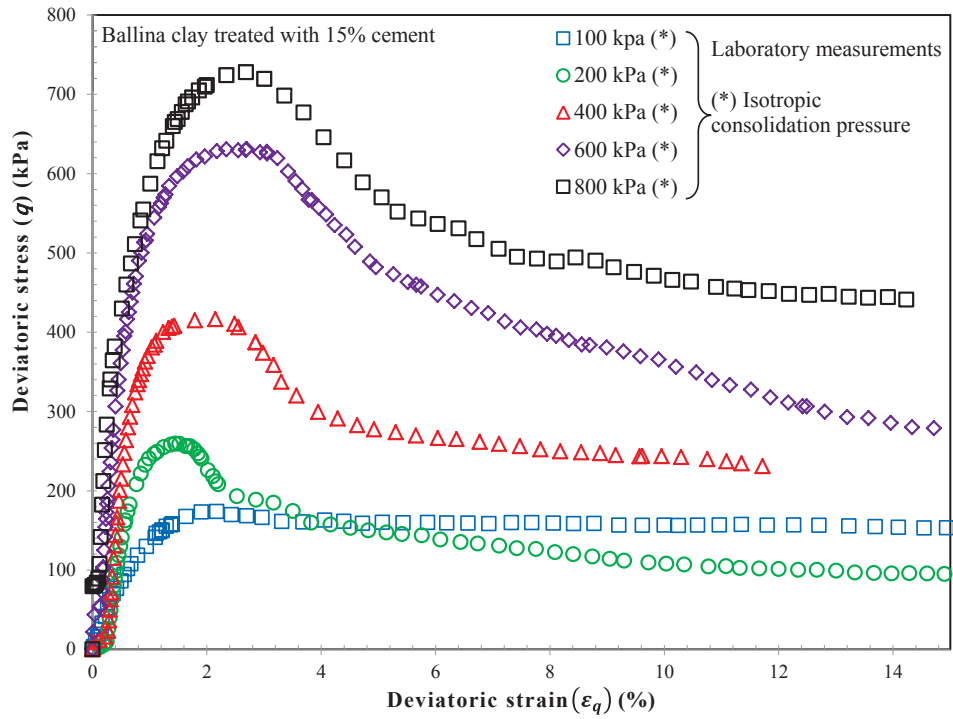


Figure 4.28: Stress strain relationship of Ballina clay treated with 15% cement

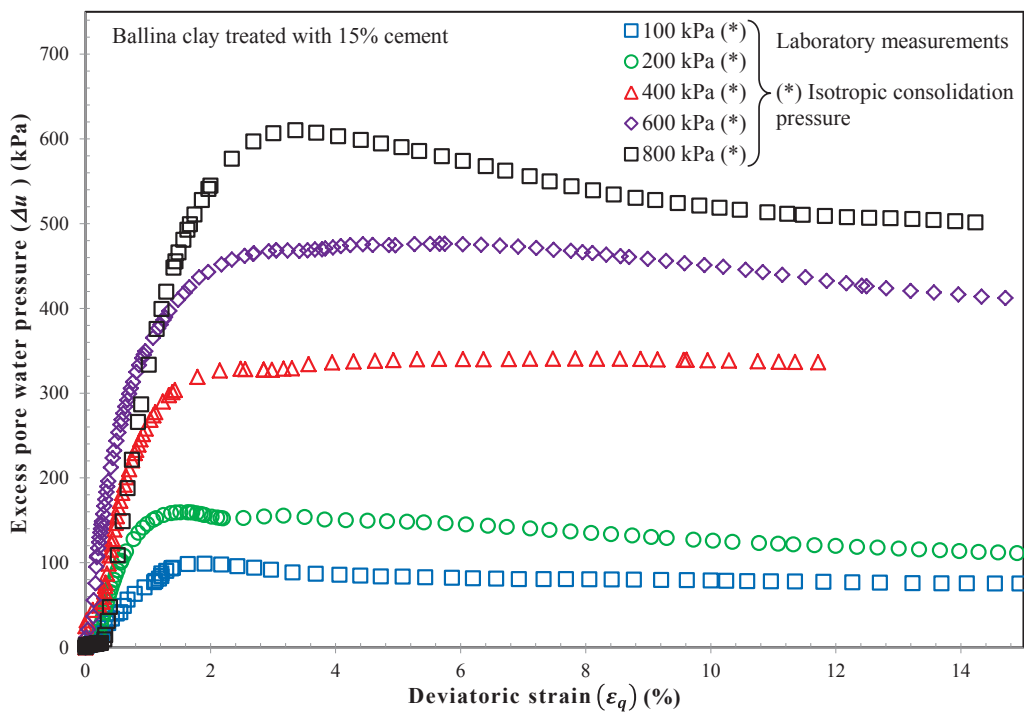


Figure 4.29: Excess pore water pressure responses of Ballina clay treated with 15% cement

#### 4.4.3.1.4. Behaviour of Cement Treated Clay in Drained Triaxial Conditions

The results of the experiment carried out on Ballina clay treated with 10% cement in drained conditions are shown in Figures 4.30 and 4.31 for stress path and stress-strain relationship, respectively. Similar to undrained conditions, an increasing mean effective yield stress ( $p'_0$ ) in a drained condition also causes an increase in the peak deviatoric stress ( $q_{peak}$ ). At low mean effective yield stress (i.e. 50 to 200 kPa), the beneficial effect of cementation contributed significantly to an increase in the shear strength of treated clay as the sample reached a peak strength state that was well above the CSL, as shown in Figure 4.30. However, as  $p'_0$  increased to a sufficiently high pressure, the peak shear strength was slightly above the CSL, indicating there was a significant removal of cementation bonds due to the mean effective yield stress and plastic deviatoric strain in the process leading to peak strength.

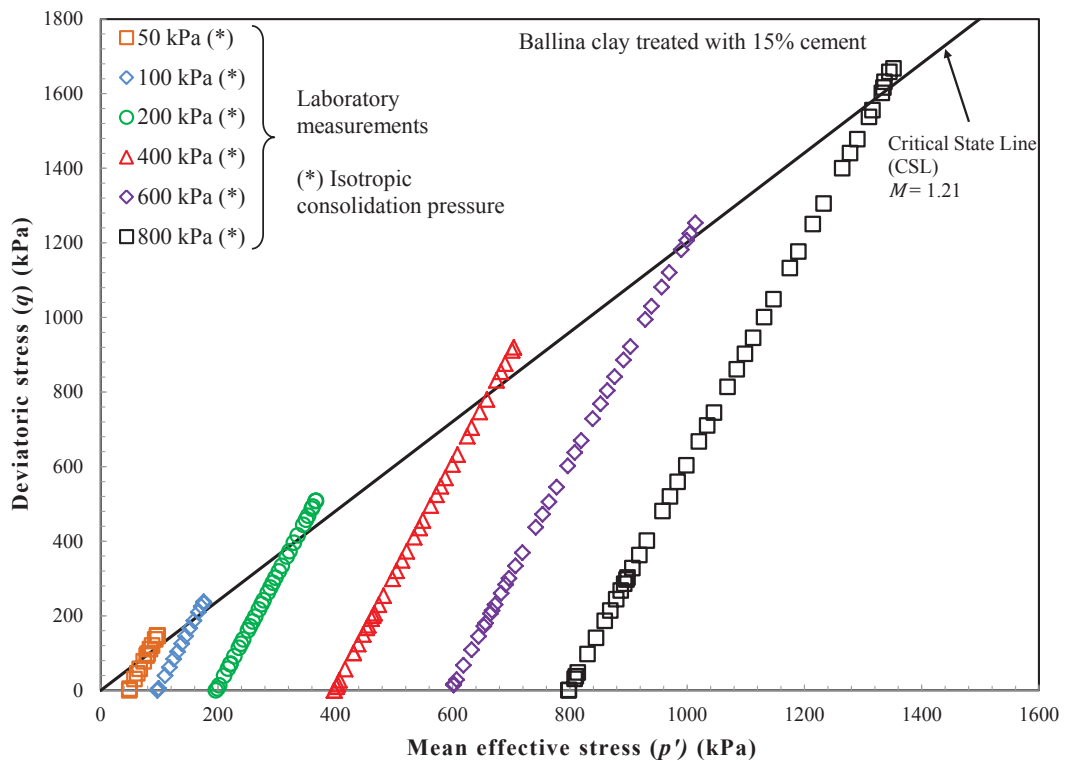


Figure 4.30: Drained stress paths of the Ballina clay treated with 10% cement

Furthermore, Figure 4.31 shows there was a slight softening behaviour in the samples of treated soil, which indicated a slight reduction in  $q$  as  $\varepsilon_q$  continued to increase beyond the peak point. As the mean effective yield stress increased, a corresponding deviatoric stress at a particular deviatoric strain also increased, as shown in Figure 4.31 (e.g. an increase of up to 140% in  $q$  when  $p'$  increased from 200 kPa to 400 kPa at  $\varepsilon_q = 10\%$ ). The samples with higher mean effective yield stresses (e.g.  $p'_0 \geq 100$  kPa) experienced failure at approximately  $\varepsilon_q = 15\% - 20\%$ . The shear strength of treated clay at higher mean effective yield stress decreased slightly after the peak strength state and then reached its residual strength state. In a drained triaxial condition, the peak shear strength occurs at very large deviatoric strains (typically  $\varepsilon_q \geq 10\%$ ), thus the effect of cementation degradation at this stage is significant while  $\varepsilon_q$  continues to increase. The stress-strain curve of the treated Ballina clay in a drained triaxial condition behaves like a typical normally consolidated soil as the deviatoric stress continues to increase with an increasing deviatoric strain.

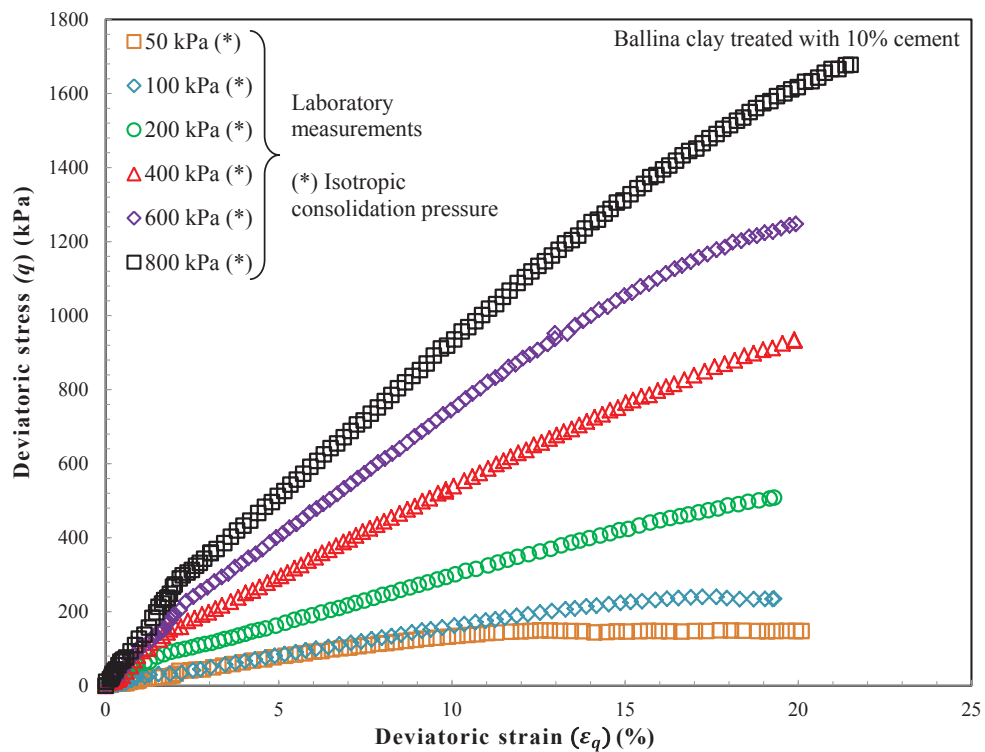


Figure 4.31: Stress-strain relationship of the Ballina clay treated with 10% cement in drained condition

Figure 4.32 also displays a comparison of the typical failure of Ballina clay treated with 10% cement in drained and undrained triaxial conditions at  $p'_0 = 800$  kPa. The treated Ballina clay in an undrained condition showed brittle failure behavior with a distinct shear band (Figure 4.32 (b)) while strain hardening ductile behaviour occurred in a drained condition as the sample was barrelling (Figure 4.32 (a)). This was due to the generation of excess pore water pressure within the sample in undrained conditions, particularly close to the failure plane.

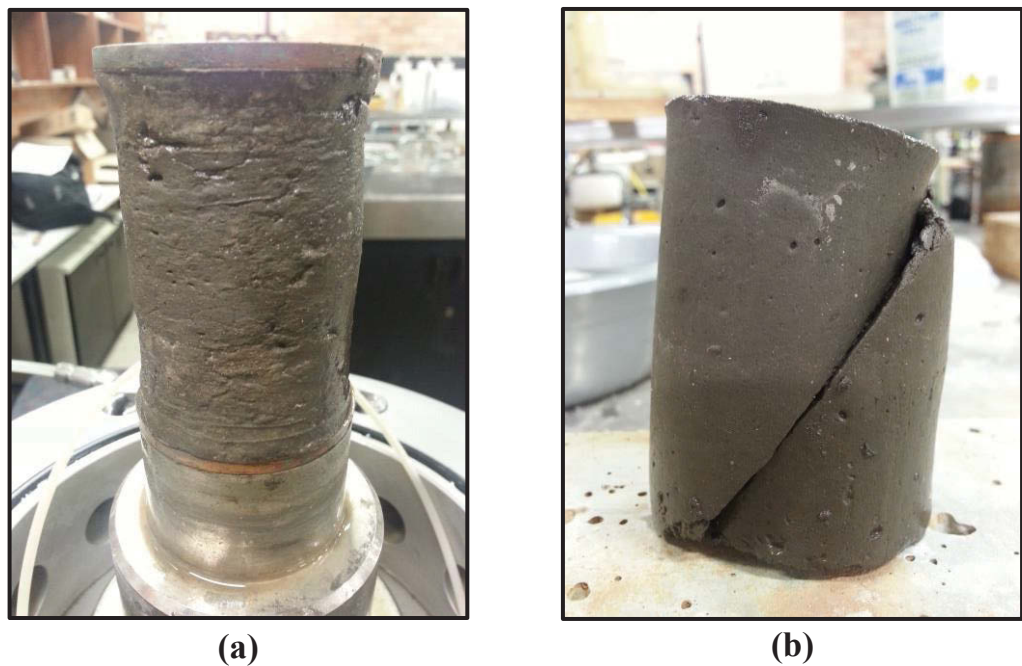


Figure 4.32: Failure behaviour of the 10% cement treated Ballina clay at  $p'_0 = 800$  kPa in: (a) drained and (b) undrained triaxial condition

Similar to the Ballina clay treated with 10% cement, the drained stress paths of clay treated with 12% cement rose linearly with the increasing mean effective stress (slope of  $q = 3p'$ ), which is typical for soil in a drained triaxial condition, as shown in Figure 4.33. At a low mean effective yield stress (i.e. at  $p'_0 = 50$  and  $100$  kPa), an increase in shear strength up to 8% occurred when the cement content increased from 10% to 12%. However, as  $p'_0$  increased, there was a loss in strength, unlike the clay treated with 10% cement. In fact at  $p'_0 = 800$  kPa, the peak shear strength ( $q_{peak}$ ) of clay treated with 12% cement was below the CSL and the value was recorded at 1505 kPa (a loss of 10.2% compared to  $q_{peak} = 1677$  kPa in 10% cement content). This

showed the effect of cementation degradation due to a combination of increasing mean effective yield stress and shear deviatoric strain. As the pore water within the sample was allowed to drain, Figure 4.34 shows the strain hardening ductile behaviour of 12% cement treated clay, and with slight softening occurring at low mean effective yield stress (i.e.  $p'_0 = 50$  kPa).

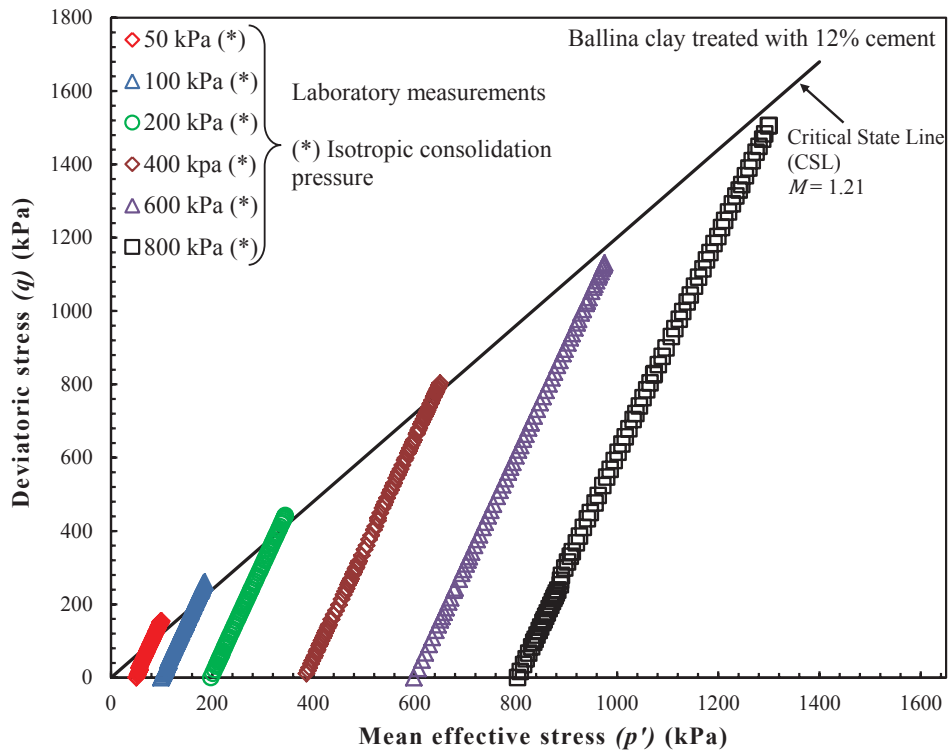


Figure 4.33: Drained stress paths of Ballina clay treated with 12% cement

The triaxial test results in drained condition of 15% cement treated clay are shown in Figures 4.35 and 4.36. Similar to the 12% cement treated clay, at a high mean effective yield stress (i.e.  $p'_0 = 800$  kPa), the peak shear strength occurred below the Critical State Line (CSL) indicating a significant breaking of cementation bonds prior to achieving the peak shear strength. In addition, at a low mean effective yield stress (i.e.  $p'_0 = 50$  kPa), the 15% cement treated Ballina clay showed strain softening behaviour while strain hardening ductile behaviour was observed for samples at higher mean effective yield stress in drained triaxial condition. Kamruzzaman et al. (2009) explained that when higher cement content is used, the strength of cementation bonds is higher, hence the behaviour of cement treated clay at low mean effective yield stress is similar to the heavily over-consolidated clay.

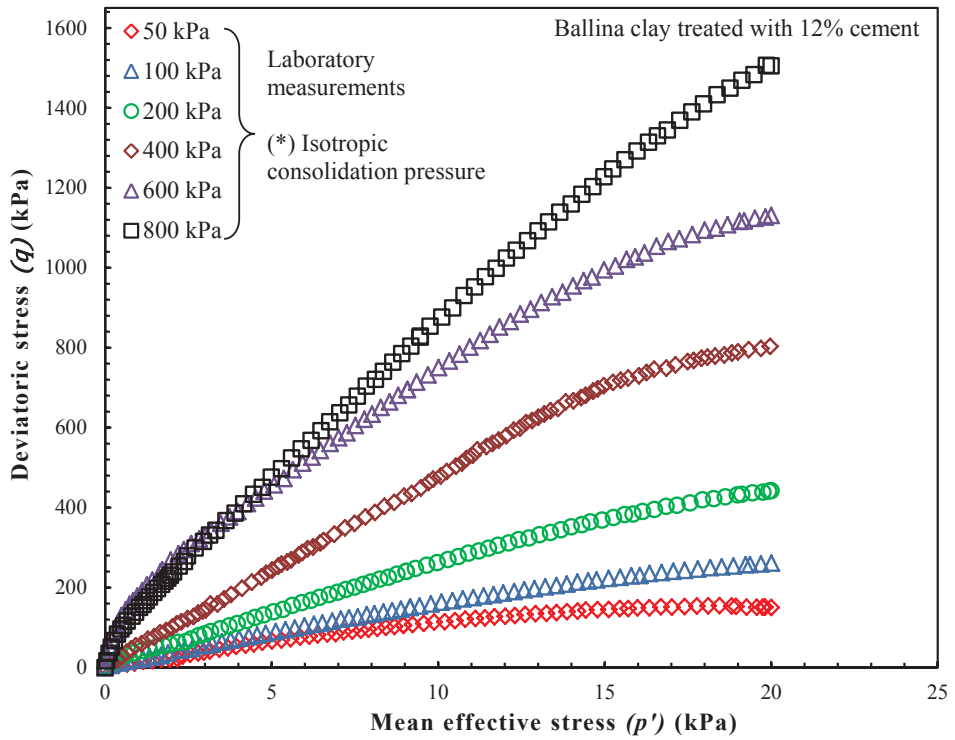


Figure 4.34: Stress-strain relationship of the Ballina clay treated with 12% in drained condition

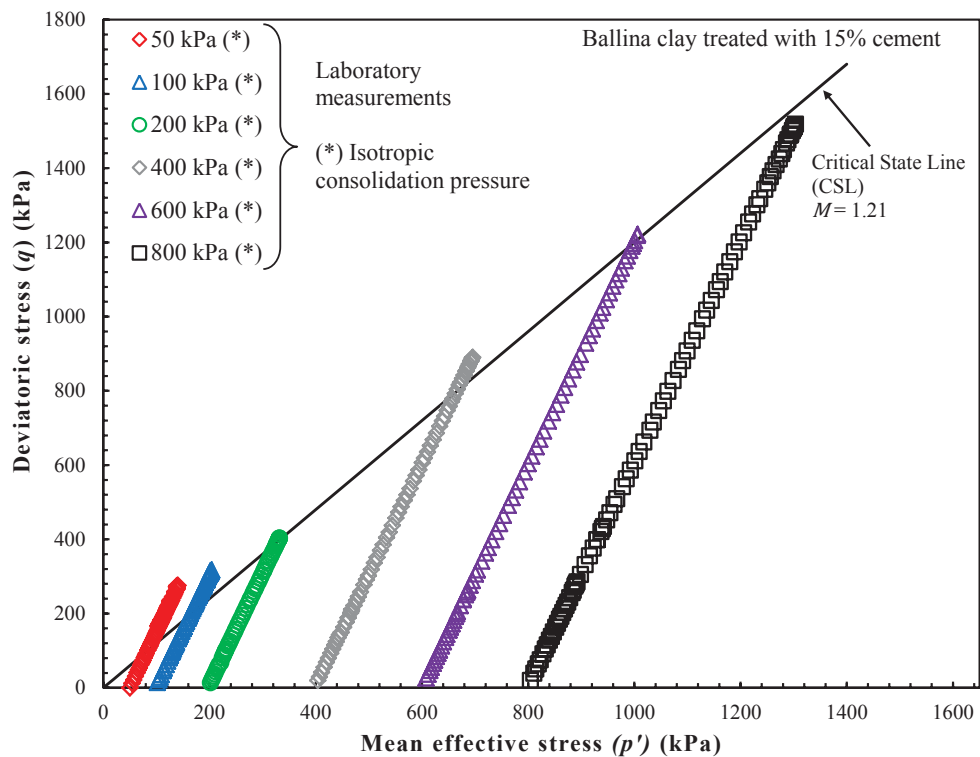


Figure 4.35: Drained stress paths of the Ballina clay treated with 15% cement

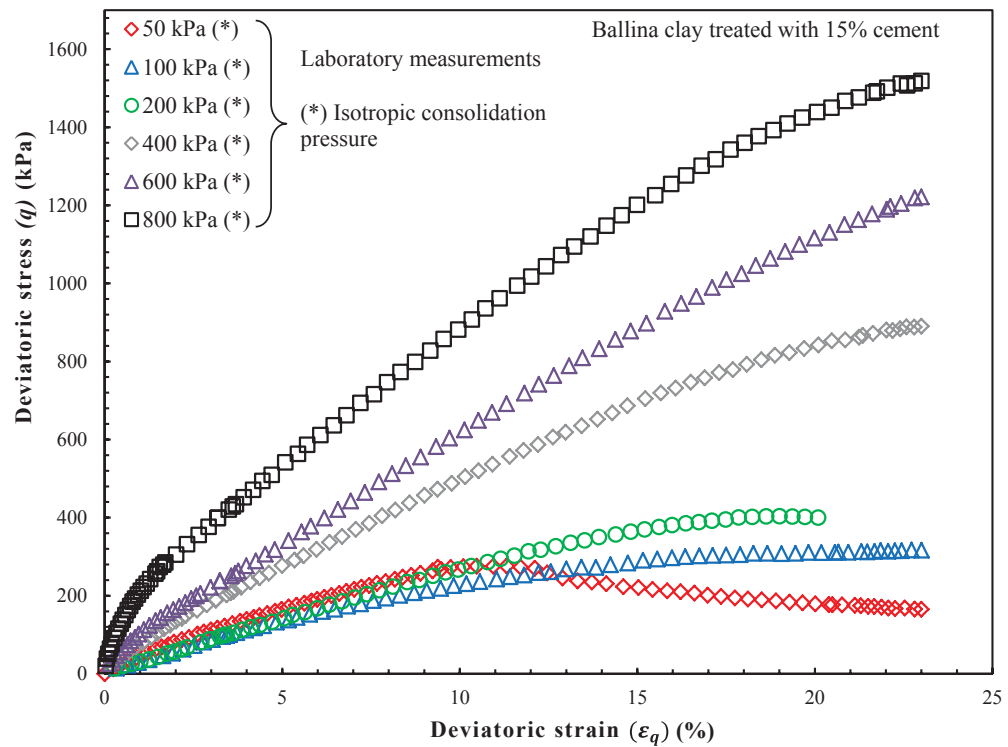


Figure 4.36: Stress-strain relationship of the Ballina clay treated with 15% cement in drained condition

In summary, the peak shear strength of the cement treated clay in a drained condition increased with cement content which was more effective at low mean effective yield stress (i.e.  $p'_0 < 100$  kPa) as the peak shear strength was located above the CSL. However, as  $p'_0$  increased, the effect of increasing amount of cement reduced the contribution of cementation to the peak shear strength due to cementation degradation, particularly with higher amount of cement (i.e. 15% cement). In fact, the degradation of cementation for 12% and 15% of cement was very significant at sufficiently high mean effective yield stress ( $p'_0 = 800$  kPa) as the peak shear strength of the cement treated clay was below the CSL (see Figures 4.33 and 4.35). It should be noted that, the peak shear strength of treated samples occurred at very large deviatoric strains (typically  $\epsilon_q \geq 10\%$ ) or even as high as  $\epsilon_q = 20\%$  at high  $p'_0$ . Hence, in drained conditions, the accumulation of plastic deviatoric strains and the effect of mean effective yield stress caused significant breaking of cementation bonds which lead to a reduction in the peak shear strength, particularly with higher amounts of cement.

#### 4.4.3.2. Triaxial Test Results of Improved Ballina Clay Composite

The results of undrained triaxial tests on Ballina Clay treated with 15% cement and then improved with 0.3%, and 0.5% fibre in  $e - \ln p'$ ,  $p' - q$ ,  $\varepsilon_q - q$ ,  $\varepsilon_q - \Delta u$  are reported in Figures 4.37 to 4.49 for mean effective yield stresses ranging from 50 kPa to 800 kPa. The experimental results for different fibre contents, including the peak shear strength ( $q_{peak}$ ), residual shear strength ( $q_{res}$ ), brittleness index ( $I_B$ ), peak deviatoric strain ( $\varepsilon_{peak}$ ) and maximum excess pore water pressure ( $\Delta u_{max}$ ) are summarised in Table 4.4 (cont.)

##### 4.4.3.2.1. Isotropic Compressibility of Improved Ballina Clay Composite

The compressibility of Ballina clay in  $e - \ln p'$  plane for different amounts of fibre is shown in Figure 4.37, where the Isotropic Compression Line (ICL) of the improved soil composite generally follows the ICL of treated clay without fibre reinforcement. The results confirmed that fibre had a negligible effect on compressibility because the fibre is compressed in all directions. The initial mean effective yield stress ( $p'_{0,i} = 149.92$  kPa) of the soil composite increased mainly due to cementation where large clusters of clay and cement had formed within the soil matrix (Kamruzzaman et al. 2006). However, at a high mean effective yield stress (i.e.  $p'_0 = 800$  kPa) beyond the initial mean effective yield stress ( $p'_0 > p'_{0,i}$ ), the void ratio decreased significantly as the cementation bonds broke. As Figure 4.37 shows, the effect of fibre on isotropic compression was insignificant since only minor variations were observed in the measurements for differing amounts of fibre. Thus, it can be concluded that the compressibility of the improved soil composite is mainly governed by cementation and its degradation while the fibre has an insignificant effect.

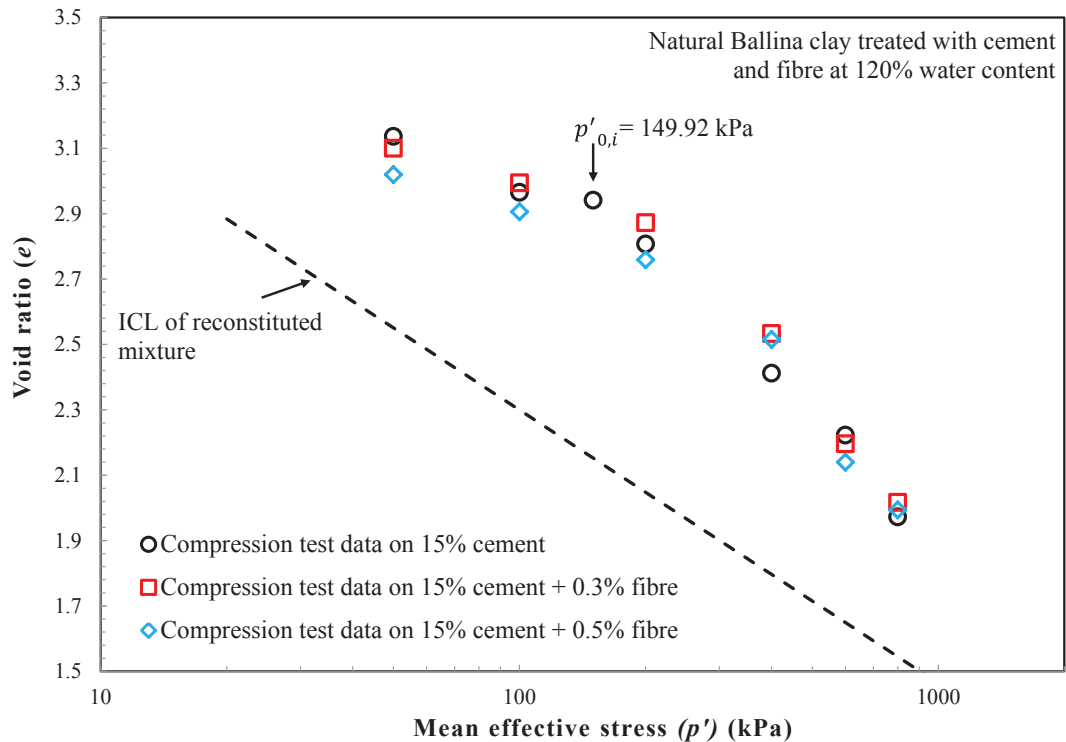


Figure 4.37: Results of isotropic compression tests on Ballina clay treated with 15% cement and different fibre contents (0%, 0.3% and 0.5%)

#### 4.4.3.2.2. Undrained Stress Path

Figure 4.38 summarises the stress paths in  $p' - q$  plane for soil improved with different amounts of fibre at different mean effective yield stresses (i.e.  $p'_0 = 200, 400$  and  $800 \text{ kPa}$ ). The initial mean effective yield stress was  $149.92 \text{ kPa}$  ( $p'_{0,i} = 149.92 \text{ kPa}$ ), so all the tested samples were outside the initial yield surface. The undrained stress paths of the improved soil composite generally bent to the left before reaching their peak state, just like clay treated with cement. All the samples reached a peak strength ( $q_{peak}$ ) that was above the Critical State Line (CSL) of the reconstituted composite mixture due to the combined effects of cement and fibre. Furthermore, when comparing the effect of fibre reinforcement to the shear strength of the cement treated Ballina clay at different mean effective yield stress, Figure 4.39 shows that the peak shear strength of the improved soil composite was mainly governed by cementation, because the increasing amount of fibre did not contribute notably to the shear strength.

For example, the increase in shear strength was 3% when 0.3% fibre was added to Ballina clay with 15% cement at 200 kPa of mean effective yield stress, and there was almost no increase in the shear strength when the fibre was increased to 0.5%. Moreover, at  $p'_0 = 600$  kPa, the peak shear strength of the improved soil composite reduced by 10% and 16% when fibre content increased from 0.3% to 0.5%, respectively, compared to the cement treated clay without fibre reinforcement. Hence, in the case of the improved Ballina clay composite, the contribution of fibre to the peak shear strength decreases with an increase in the fibre content; this result agreed with the experimental findings by Jiang et al. (2010). Moreover, increasing the mean effective yield stress reduces the effectiveness that fibre made to the peak shear strength as the fibre might rupture prior to reaching the peak strength state. Furthermore, the contribution of fibre to the peak shear strength was insignificant in the case of Ballina clay, particularly at high mean effective yield stress.

The peak shear strength of soil with 0.3% and 0.5% fibre occurred at a lower mean effective stress than for cement treated clay with no fibre; this indicated that the fibre contributed to the generation of higher excess pore water pressure. Furthermore, increasing the amount of fibre in cement treated Ballina clay led to a slight increase in the peak shear strength and a decrease in the mean effective stress, as shown in Figure 4.38. After the peak strength was reached, the shear stress decreased as the stress path changed its direction toward the CSL as the sample was experiencing strain softening. The stress paths in the samples of Ballina clay with 15% cement and 0% fibre reached the CSL, while increasing the amount of fibre resulted in a higher residual shear strength ( $q_{res}$ ), located above the CSL. The improved soil composite reached its residual shear strength at a lower mean effective stress since the fibre reinforcement contributed to higher excess pore water pressure.

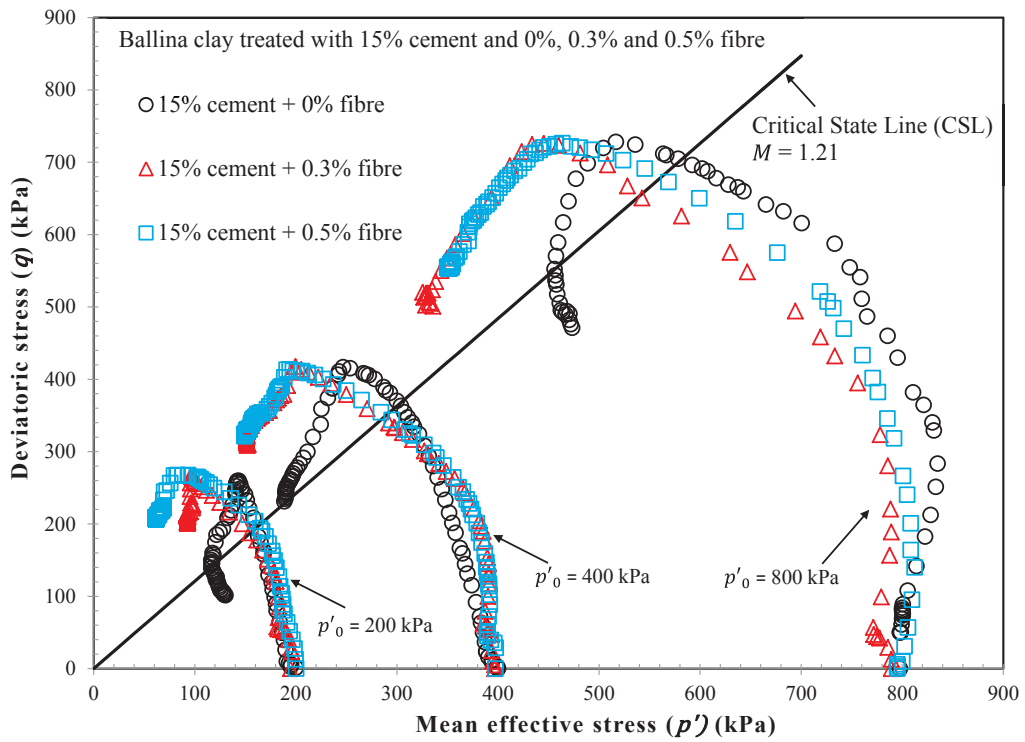


Figure 4.38: Undrained stress paths of the 15% cement treated Ballina clay and improved with fibre (fibre contents: 0%, 0.3% and 0.5%) in  $p' - q$  plane

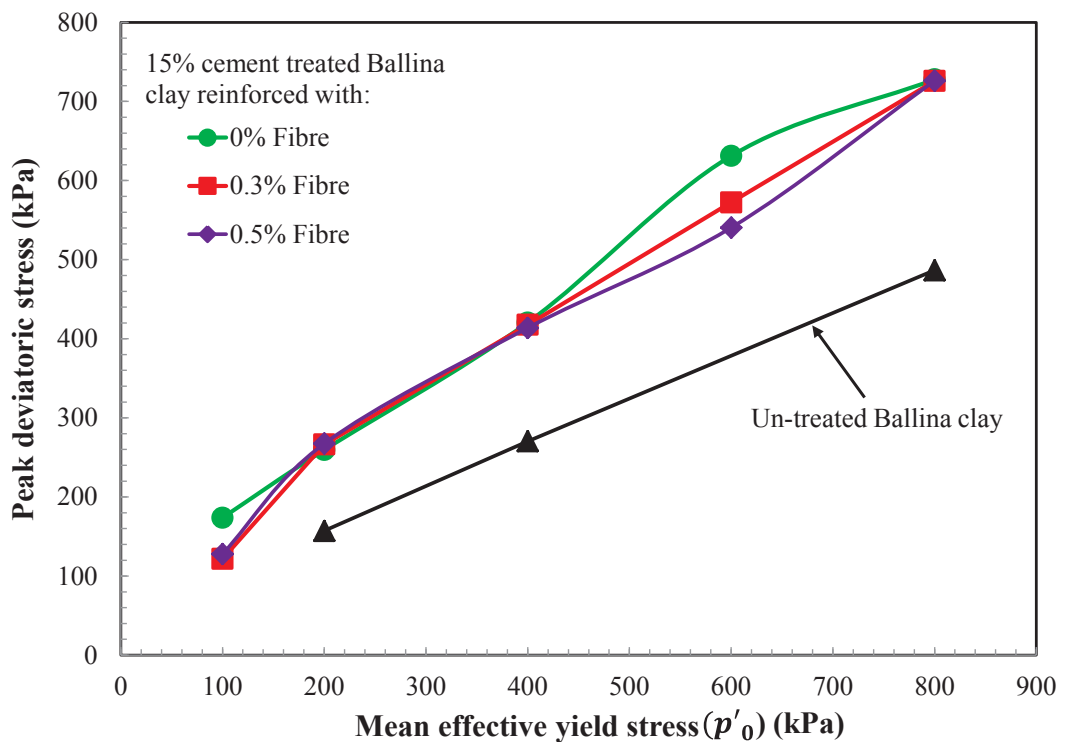


Figure 4.39: Effect of increasing fibre content on the peak shear strength of the improved Ballina composite

#### 4.4.3.2.3. Stress-Strain Relationship

Figure 4.40 shows the plots of the stress-strain relationship in the  $\varepsilon_q - q$  plane showing that adding fibre to clay treated with cement improved its ductility. This figure also shows that the peak shear strength of the soil composite with differing amounts of fibre increased as the mean effective yield stress increased. Furthermore, the peak shear strength of the improved soil composite occurred at higher deviatoric strain ( $\varepsilon_q$ ) than the corresponding values for the cement treated clay without fibre reinforcement. For example, at  $p'_0 = 200$  kPa, the peak deviatoric strain of clay treated with 15% cement occurred at  $\varepsilon_q = 1.44\%$  while the cement treated clay with 0.3% and 0.5% fibre reached a peak strength state at  $\varepsilon_q = 2.49\%$  and  $\varepsilon_q = 2.96\%$ , respectively. Furthermore, as the deviatoric strain continued to increase, the shear stress of the cement treated clay dropped at a faster rate as compared to gradual reduction in stress that occurred when fibre was added to the material, as shown in Figure 4.40. Many researchers (e.g. Consoli et al. 1999; Kamruzzaman et al. 2009; Uddin et al. 1997) reported that this reduction in the shear strength of the cement treated clay is dramatic, indicating its brittleness, so adding fibre as well as cement, gradually reduces the shear stress as the deviatoric strain ( $\varepsilon_q$ ) increases. The brittleness of the cement treated clay can be attributed to the effect of cementation degradation due to shear deformation. When the fibre is added to the cement treated soil, soil-cement clusters are connected and the applied load is distributed along the fibre body, as explained by Tang et al. (2007). Hence, the cement treated soil reinforced with fibre shows a strain softening ductile behaviour.

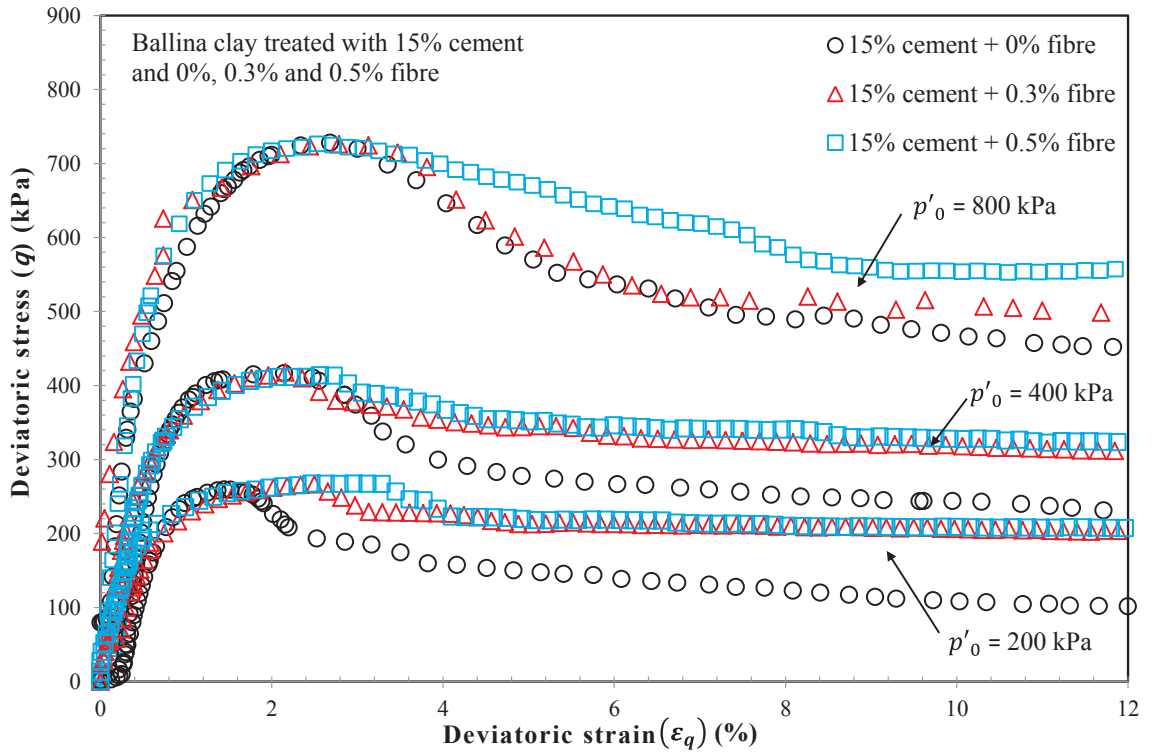


Figure 4.40: Stress-strain relationship of the 15% cement treated Ballina clay and improved with fibre (fibre contents: 0%, 0.3% and 0.5%) in  $\epsilon_q - q$  plane.

Furthermore, Figure 4.41 summarises how increasing the amount of fibre affected on the brittleness index (calculated using Equation 4.2) of the improved soil composite at differing mean effective yield stresses while Table 4.4 reports the calculated  $I_B$  values for different fibre contents and mean effective yield stresses. As  $I_B$  decreases ( $I_B \rightarrow 0$ ) the material would become more ductile, but increasing the amount of fibre at a lower mean effective yield stress (i.e.  $p'_0 = 200$  and 400 kPa), contributes to increase the residual shear strength and improve ductility. For example, at  $p'_0 = 200$  kPa,  $I_B$  decreased from 0.34 to 0.31 as the amount of fibre increased from 0.3% to 0.5%, respectively, compared to the corresponding  $I_B = 1.26$  for clay improved with cement only. Moreover, the values reported for brittleness index indicated a 75% increase in ductility when 0.5% fibre was added to the cement treated soil at  $p'_0 = 200$  kPa, but at 800 kPa of mean effective yield stress, the soil composite with 0.3% fibre was brittle, just like the treated clay with no fibre, while there was 30% increase in  $I_B$ . However,  $I_B$  increased by 52% as 0.5% of fibre was added to the treated soil at  $p'_0 = 800$  kPa, which meant the fibre had a notable effect on sample ductility. This observation is due to the

fact that at high mean effective stresses, the fibre degrades and its effect decreases because the applied load transferred from the soil-cement matrix over a large area increases localised stress in the fibre. Moreover, the precipitated crystals caused some damage to the fibre body, as shown in the SEM image (Figure 4.12) but for treated clay with a higher amount of fibre, the transferred load was distributed to adjacent fibres as the contact area increased. Furthermore, the effect of increasing fibre content results in the higher probability of fibre crossing the weak plane during shearing, so while increasing the amount of fibre generally increased the ductility of the soil composite, increasing the mean effective yield stress reduced the effectiveness of the fibre.

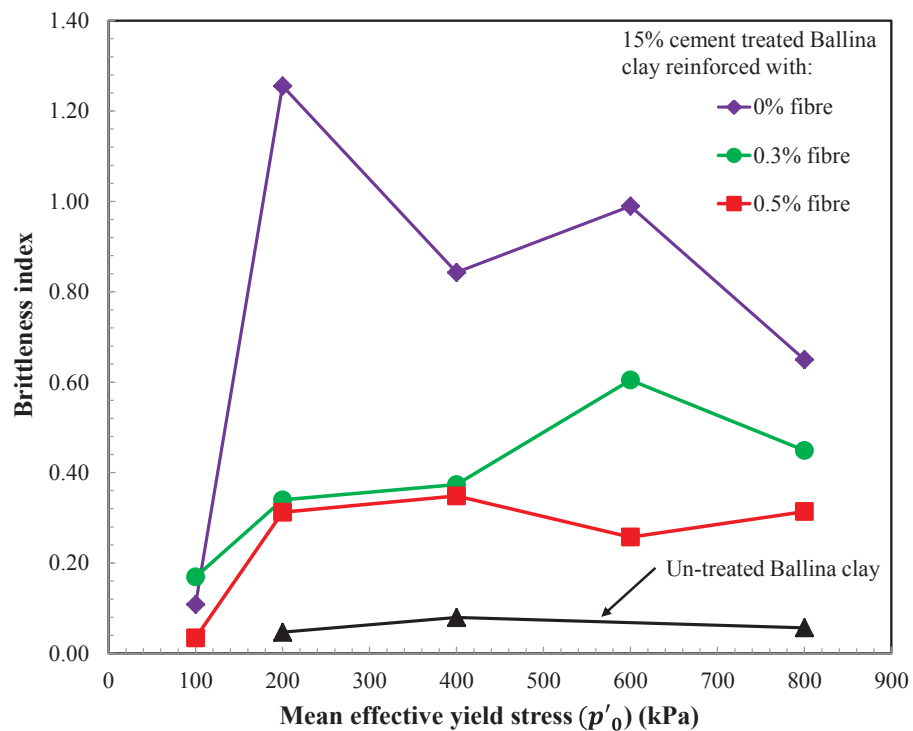


Figure 4.41: Effect of increasing fibre content on the brittleness index of the cement treated Ballina clay

The effect of increasing fibre content on the failure of improved Ballina clay composite is reported in Figure 4.42. At  $p'_0 = 800$  kPa, the 15% cement treated clay without fibre reinforcement showed a distinct shear plane (see Figure 4.42 (a)), but when fibre was added to the treated soil, the gap between the shear band became less

visible as the sample was bridged by the fibre. In fact, the cement treated clay with 0.5% fibre, as illustrated in Figure 4.42 (c), showed almost indistinct multiple shear bands as the applied load was transferred to the adjacent fibre within the compacted matrix, which as a consequence, preventing further cracking. Overall, despite some variations on the effect of fibre inclusion due to increasing mean effective yield stress, adding fibre into the cement treated soil can change its brittle behaviour towards more ductile behaviour, as shown in Figure 4.41.

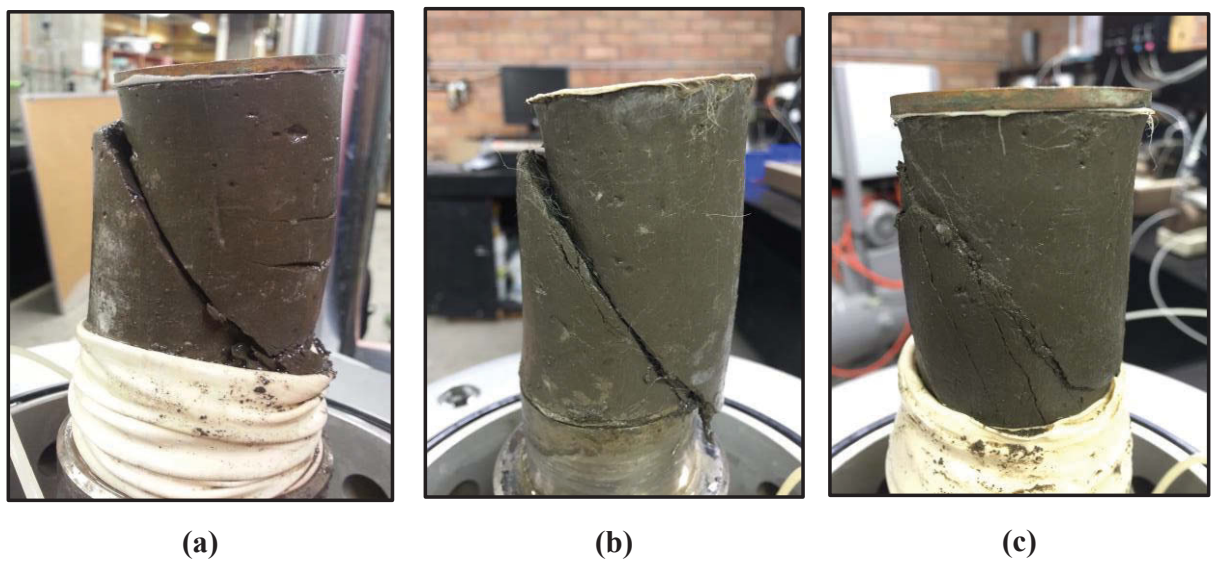


Figure 4.42: Failure of the 15% cement treated Ballina clay and reinforced with: (a) 0% fibre, (b) 0.3% fibre, (c) 0.5% fibre, in undrained shearing at  $p'_0 = 800$  kPa

#### 4.4.3.2.4. Excess Pore Water Pressure Response

Figure 4.43 shows the excess pore water pressure responses at selected mean effective yield stresses (i.e.  $p'_0 = 200, 400$  and  $800$  kPa) for Ballina clay treated with 15% cement and 0%, 0.3%, and 0.5% of fibre. In the triaxial apparatus, a pressure transducer was used to measure the pore water pressure at the bottom of the sample. The excess pore water pressure increased until it reached its peak strength which corresponded to the peak deviatoric strain (i.e.  $\epsilon_q = 1.5\%$  to  $2.7\%$  depending on the fibre content). Basically, increasing the amount of fibre resulted in an increase in excess

pore water pressure, which agrees well with the results reported in the existing literature (e.g. Li 2005), so the tendency of soil composite for a change in volume affects the generation of excess pore water pressure along the interface between the soil and the fibre. Obviously, when the fibre reinforced soil contracts during shearing, positive excess pore water pressure is generated along the body of the fibre (Li 2005). Moreover, the excess pore water pressure in soil with 0.3% and 0.5% fibre continued to increase at a steady rate with an increasing  $\epsilon_q$ , but it decreased in the treated soil with no fibre at high mean effective yield stress ( $p'_0 = 800$  kPa) after reaching the peak value, as shown in Figure 4.43.

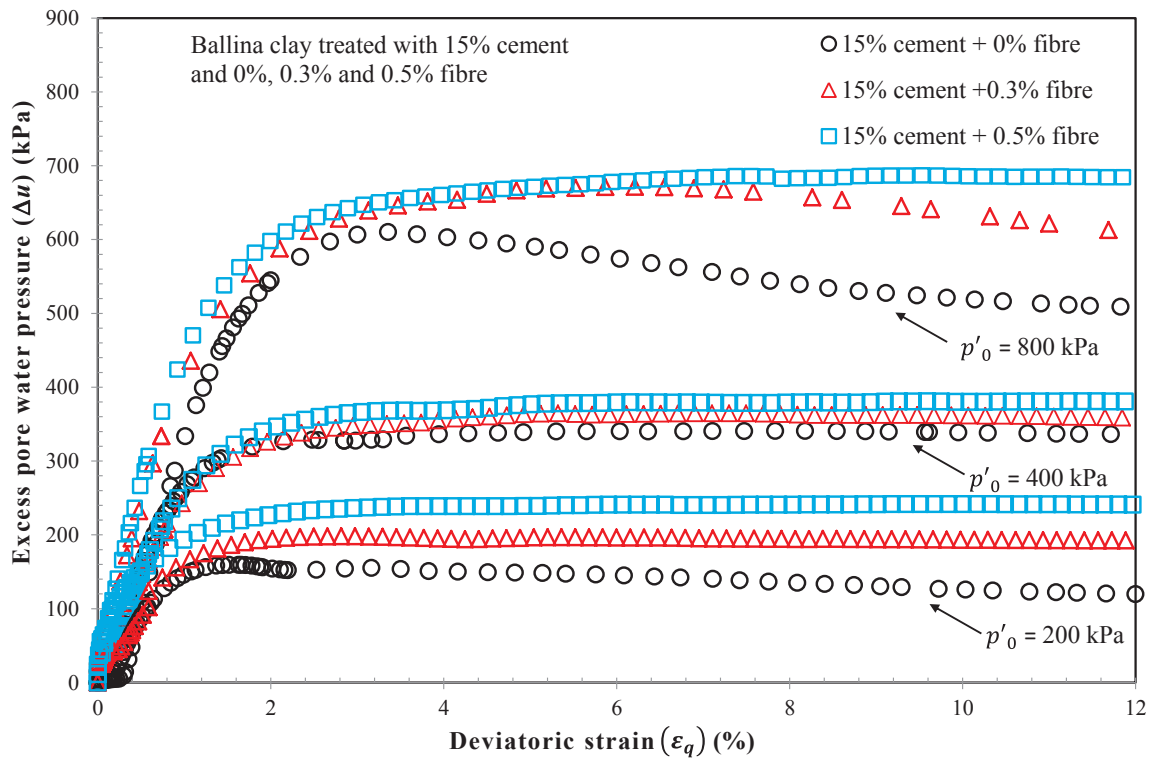


Figure 4.43: Excess pore water pressure response of Ballina clay treated with 15% cement and improved with fibre (fibre contents: 0%, 0.3% and 0.5%).

For the sake of completeness, Figures 4.44 to 4.49 report the triaxial test results of Ballina clay treated with 15% cement and reinforced with 0.3% and 0.5% fibre at different mean effective yield stresses ranging from 100 kPa to 800 kPa.

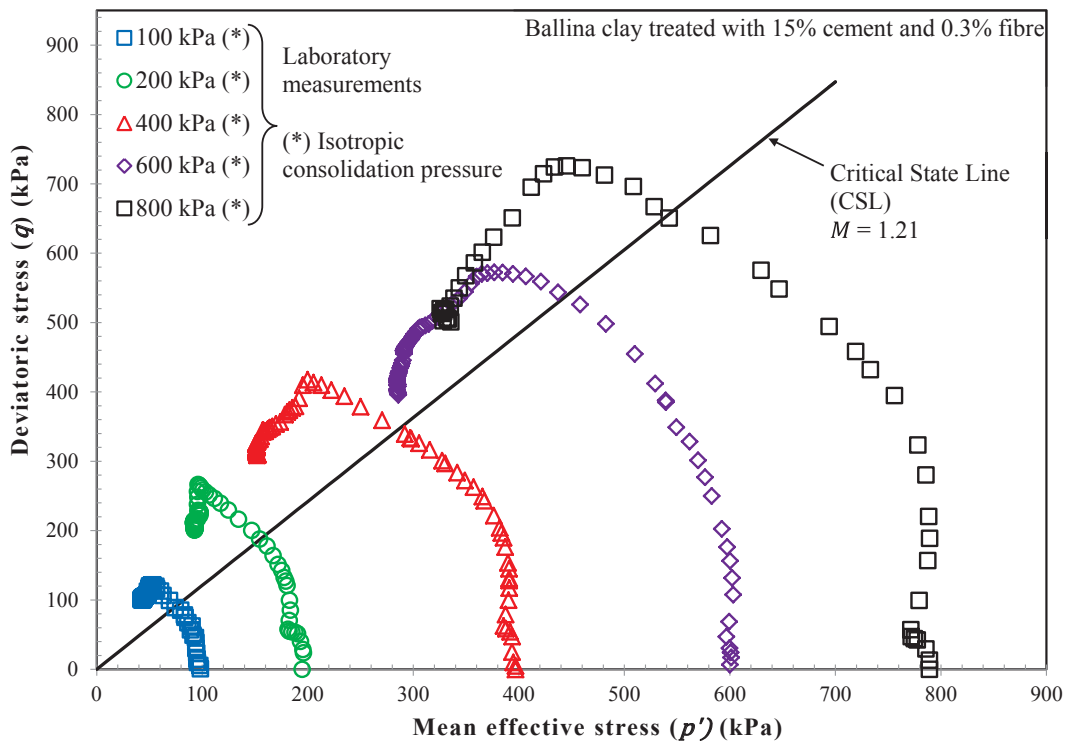


Figure 4.44: Stress paths of Ballina clay treated with 15% cement and 0.3% fibre

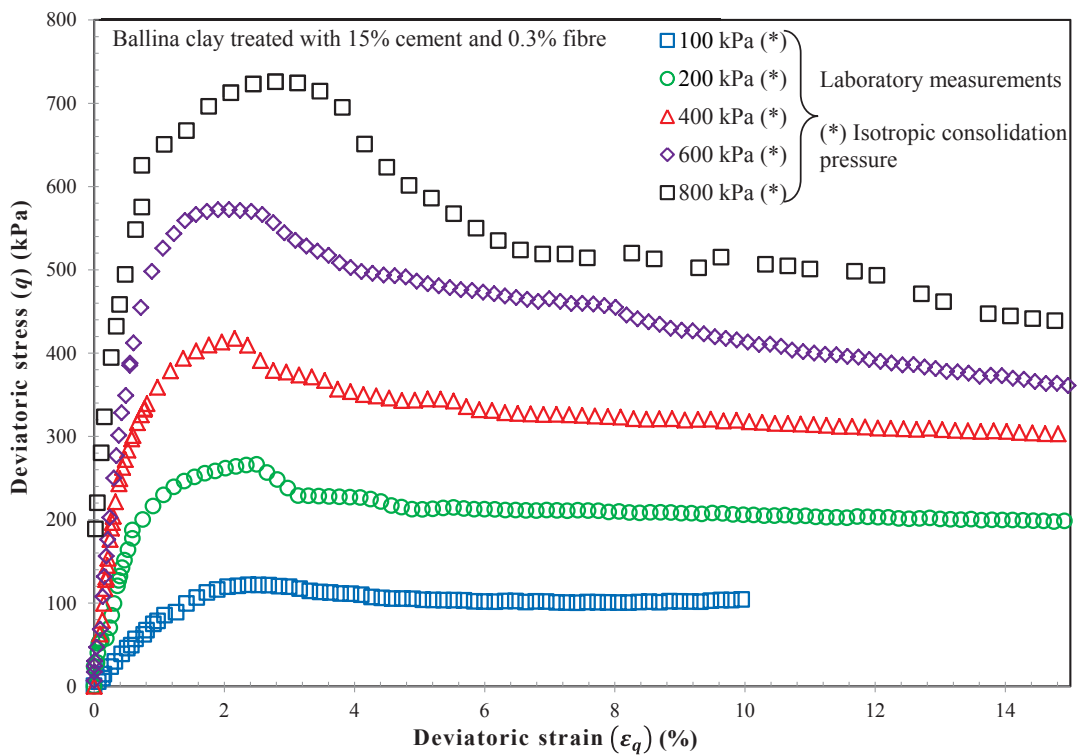


Figure 4.45: Stress-strain relationship of Ballina clay treated with 15% cement and 0.3% fibre

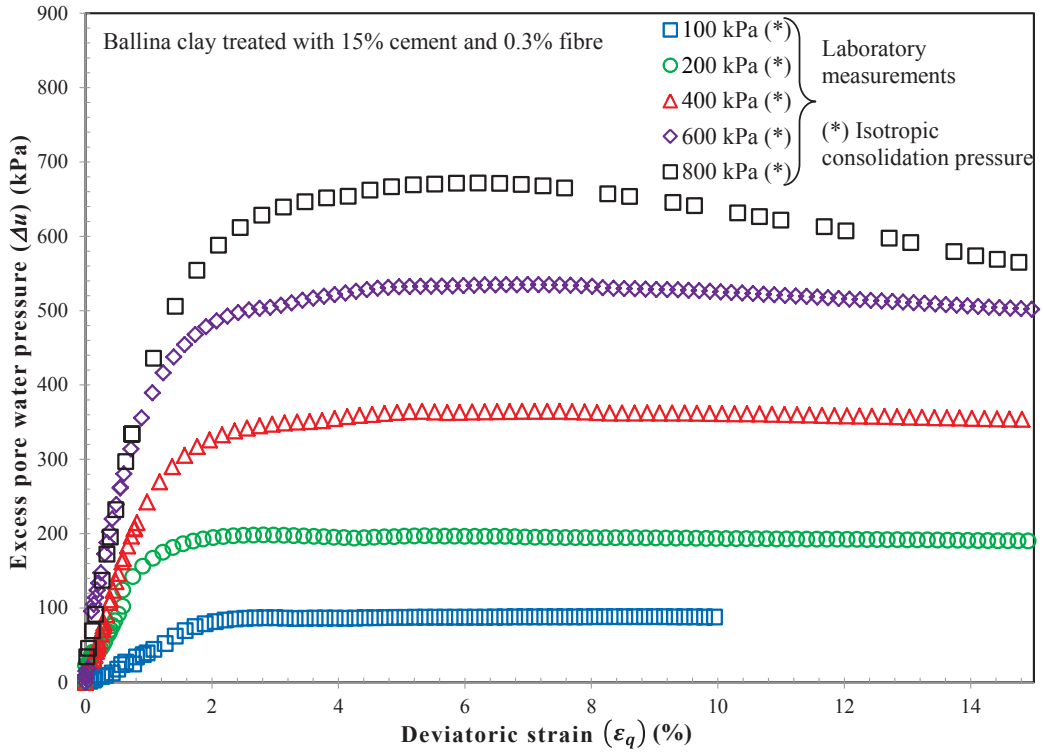


Figure 4.46: Excess pore water pressure response of Ballina clay treated with 15% cement and 0.3% fibre

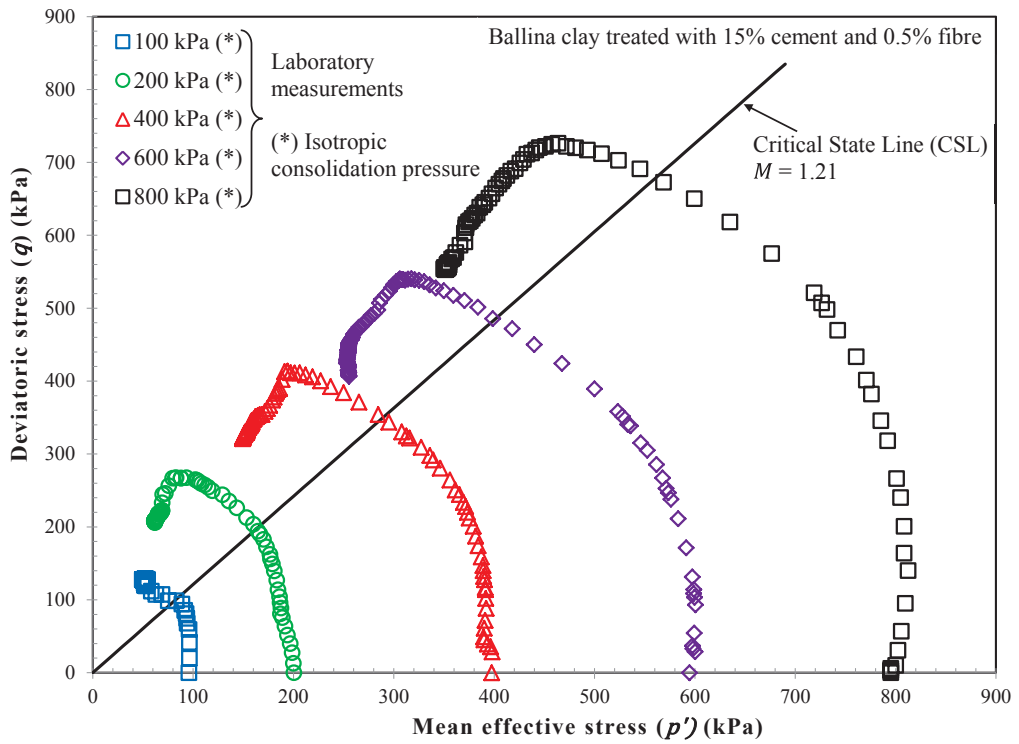


Figure 4.47: Stress paths of Ballina clay treated with 15% cement and 0.5% fibre

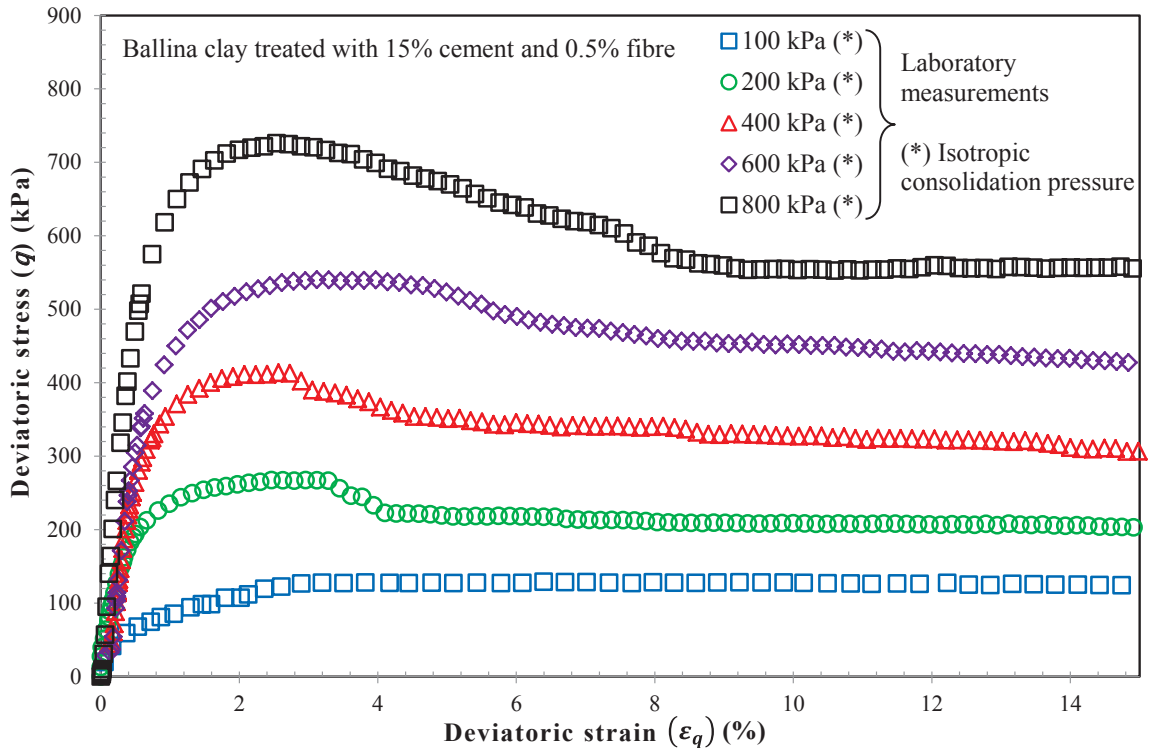


Figure 4.48: Stress-strain relationship of Ballina clay treated with 15% cement and 0.5% fibre

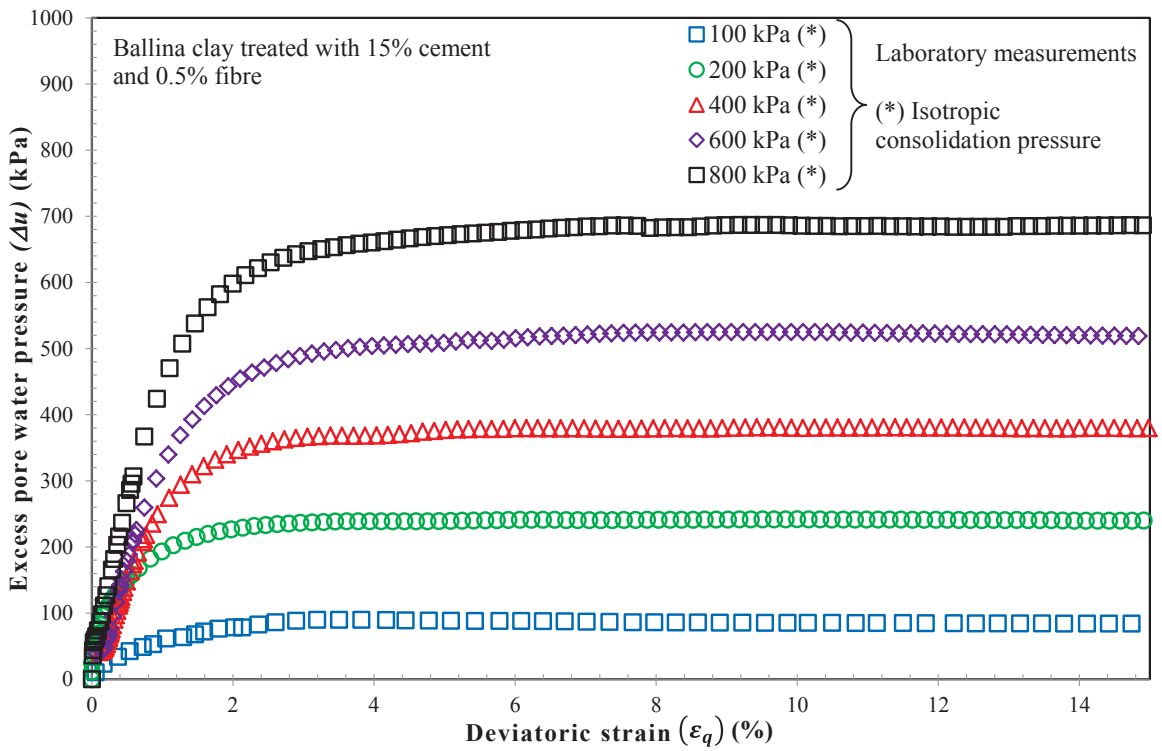


Figure 4.49: Excess pore water pressure response of Ballina clay treated with 15% cement and 0.5% fibre

### 4.4.3.3. Triaxial Test Results of Treated Kaolin clay

A set of Kaolin clay samples treated with 5% General Purpose (GP) Portland cement and polypropylene fibre with differing fibre contents (i.e. 0%, 0.1% and 0.5%) were tested with the triaxial testing apparatus under undrained conditions to further evaluate how the inclusion of fibre affected of the improved Kaolin composite; the results are displayed in Figures 4.50 to 4.64. The undrained triaxial test was conducted on un-treated Kaolin clay to measure any improvements provided by the cement and fibre. Table 4.5 provides a summary of the undrained triaxial test results of the Kaolin clay treated with cement and different amounts of fibre.

#### 4.4.3.3.1. Isotropic Compressibility of Improved Kaolin Clay Composite

Figure 4.50 summarises the results of the isotropic compression test of Kaolin clay treated with 5% cement and various fibre contents (i.e. 0.1% and 0.5%) in  $e - \ln p'$  plane. The initial void ratio and initial yield stress of the 5% cement treated Kaolin clay were 2.15 and 185 kPa, respectively. The inclusion of cement increased the initial yield stress ( $p'_{0,i} = 185$  kPa) compared to the corresponding value for the reconstituted soil mixture ( $p'_{0,i} = 95$  kPa) at the same void ratio, due to the formation of large clusters of soil and cement. The inclusion of fibre had a minor influence on the initial void ratio such that the initial void ratio of Kaolin clay with 5% cement was less than 1%. When the samples were subjected to isotropic compression loading up to the initial mean effective yield stress (i.e.  $p'_{0,i} = 185$  kPa), they all followed the same swelling line with slope  $\kappa$ , with insignificant changes in the void ratio. Beyond the initial yield stress, the void ratio of cement treated Kaolin clay gradually decreased, which indicates the effect of cementation degradation. Note that fibre has no effect on isotropic compression because it can bend easily in all directions. At high mean effective yield stresses (e.g.  $p'_0 = 800$  kPa), the soil composite approached the stable state defined by the fabric of the soil composite structure that cannot be destroyed under isotropic compression. Similar to the improved Ballina clay discussed in Section 4.4.3.2.1, Figure 4.50

confirms that fibre reinforcement played an insignificant role in isotropic compressibility because the test data on the Kaolin clay treated with 5% cement and 0.1% and 0.5% of fibre followed the ICL of the sample of clay treated with cement only. Thus, the reduction in the void ratio was mainly induced by cementation degradation.

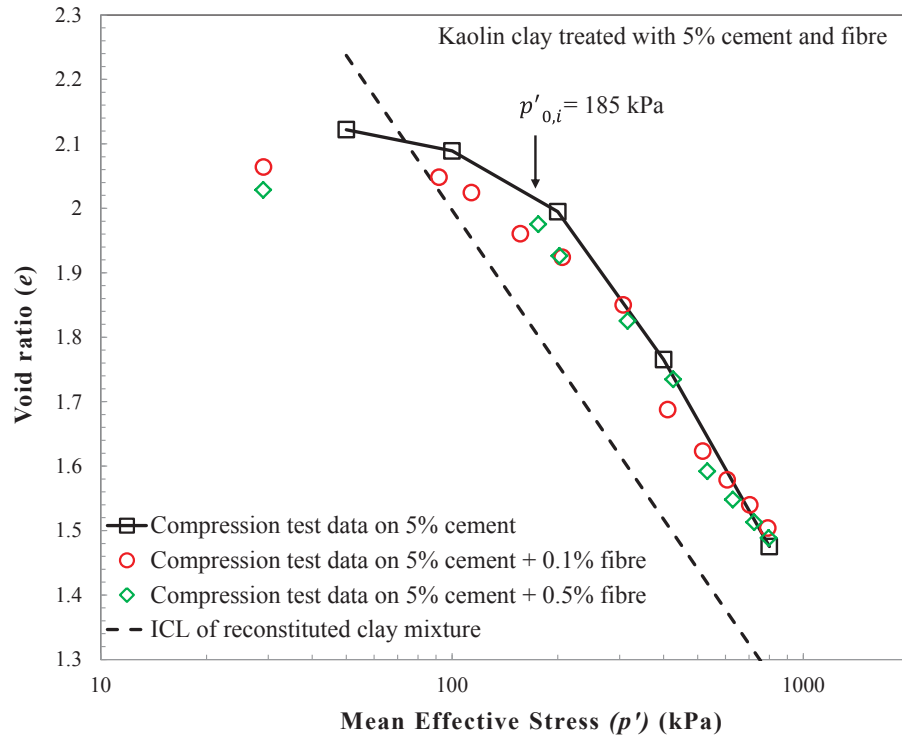


Figure 4.50: Results of isotropic compression test on Kaolin clay treated with 15% cement and different fibre content (0%, 0.3% and 0.5%)

Table 4.5: Summary of results of undrained triaxial tests of the treated Kaolin clay

Cement content	Fibre content	Confining pressure	Peak strength	Strain at peak stress	Residual strength	Brittleness index	Maximum excess pore water pressure
%	%	$p'_0$ (kPa)	$q_{peak}$ (kPa)	$\epsilon_{peak}$ (%)	$q_{res}$ (kPa)	$I_B$	$\Delta u_{max}$ (kPa)
0	0	100	70.40	7.05	67.82	0.04	69.82
		200	103.31	9.42	100.20	0.03	102.20
		400	238.56	8.52	226.75	0.05	232.15
		800	482.16	11.45	472.71	0.02	496.87
5	0	50	109.06	2.03	89.85	0.21	36.53
		100	130.82	2.15	85.99	0.52	78.19
		200	179.87	1.74	103.97	0.73	158.44
		400	325.18	1.91	208.85	0.56	294.88
		800	520.27	1.89	334.77	0.55	595.19
5	0.1	100	113.73	0.55	84.97	0.34	85.01
		200	223.86	0.49	178.22	0.26	178.24
		400	363.86	1.59	246.86	0.47	338.67
		800	533.95	1.40	379.65	0.41	627.41
5	0.5	50	128.11	3.88	123.79	0.03	44.33
		100	172.22	2.55	165.73	0.04	91.23
		200	220.08	1.29	191.94	0.15	181.47
		400	331.67	1.49	277.36	0.20	321.39
		800	523.21	1.59	440.04	0.19	584.39

#### 4.4.3.3.2. Undrained Stress Path

The undrained triaxial tests were carried out adopting the effective confining pressures ranging from 50 kPa to 800 kPa to study the pre-and-post yield behaviours of un-treated and cement treated clay with or without fibre reinforcement. The undrained stress paths of un-treated Kaolin clay was used to estimate the slope of the Critical State Line (CSL) ( $M = 1.09$ ) as shown in Figure 4.51. Since the virgin yielding of the 5% cement treated Kaolin clay occurred at  $p'_{o,i} = 185$  kPa, the stress path of samples at low mean effective yield stresses (e.g. 50 kPa and 100 kPa) was almost vertical with minor variations in the mean effective stress, indicating the elastic deformation shown in Figure 4.52. In contrast to the un-treated clay where its peak shear strength state lay on the CSL, the cement treated sample exhibited peak strength well above the CSL. At the post peak state, the stress path changed direction towards the CSL, showing the cementation bonds breaking, similar to the cement treated Ballina clay. At this stage, the residual shear strength depended on friction rather than the cementation bonds, as suggested by Sasanian (2011).

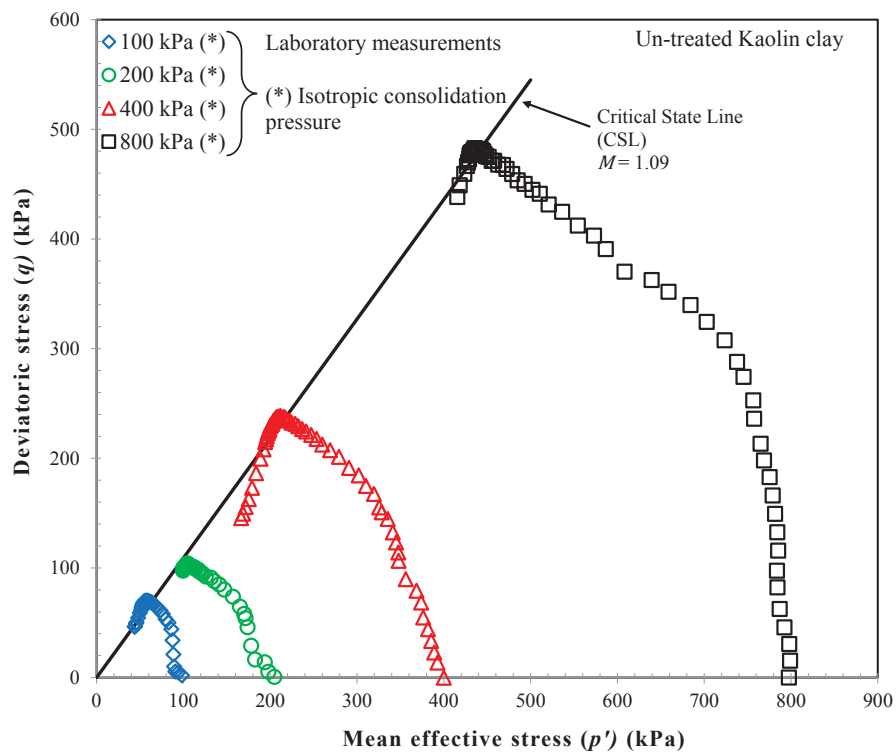


Figure 4.51: Undrained stress paths of the un-treated Kaolin clay

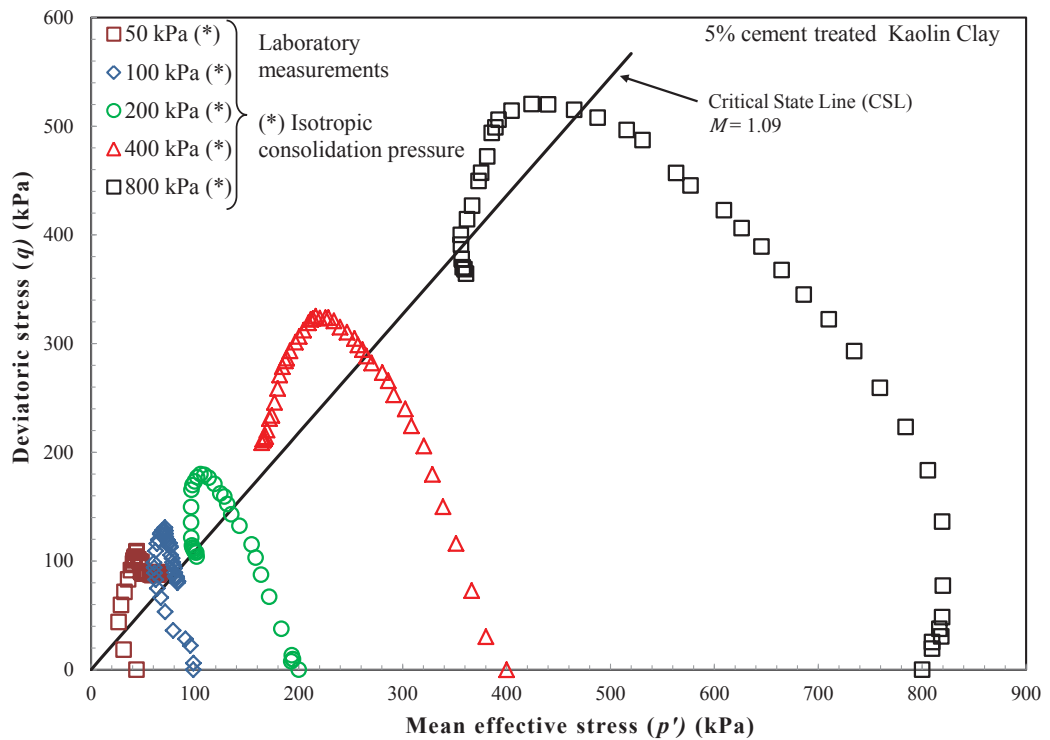


Figure 4.52: Undrained stress paths of the Kaolin clay treated with 5% cement

Furthermore, when the samples were tested under mean effective yield stresses higher than the initial yield stress, the stress paths of the un-treated and cement treated Kaolin clay bent to the left, approaching the CSL in  $p' - q$  plane with a decreasing mean effective stress and generation of positive excess pore water pressure. Due to the effect of cementation, the shear strength of the cement treated clay continued to increase above the CSL while the untreated clay obtained a peak shear strength located on the CSL. Once the cement treated clay reached its peak strength, softening occurred resulting in a decrease in the shear strength as the cementation bonds were crushed. The stress path finally reached its ultimate state at the CSL indicating a complete removal of cementation bonds at the ultimate state.

Similar to the cement treated clay, the improved Kaolin clay composite reached its peak shear strength above the CSL and then a loss in strength occurred as the sample approached the residual strength state. While the samples of cement treated clay eventually reached the CSL of the reconstituted mixture of soil and cement, the samples of soil composites with 0.1% fibre (for tests with  $p'_0 = 200$  kPa and 400 kPa) reached a

higher residual strength above the CSL as the fibre was gradually pulled-out from the composite matrix during the softening process. However, for the test with 800 kPa of mean effective yield stress, as the fibre was ruptured before obtaining the peak strength, the post-peak behaviour of the soil composite behaved the same as the cement treated clay shown in Figure 4.53. Moreover, Figure 4.54 showed that the cement treated Kaolin clay reinforced with 0.5% fibre for the adopted shear strain limit, reached its residual strength state above the CSL. So when the amount of fibre was increased (e.g. 0.5%), the fibre reinforcement was more effective as the contact area between the clusters of soil-cement and the fibre increased. Furthermore, higher fibre content increases the probability of the fibre crossing the weak shear plane during shearing. It can therefore be concluded that the increase in the residual strength of the improved soil composite is mainly due to inclusion of fibre, and this strength increases with the amount of fibre.

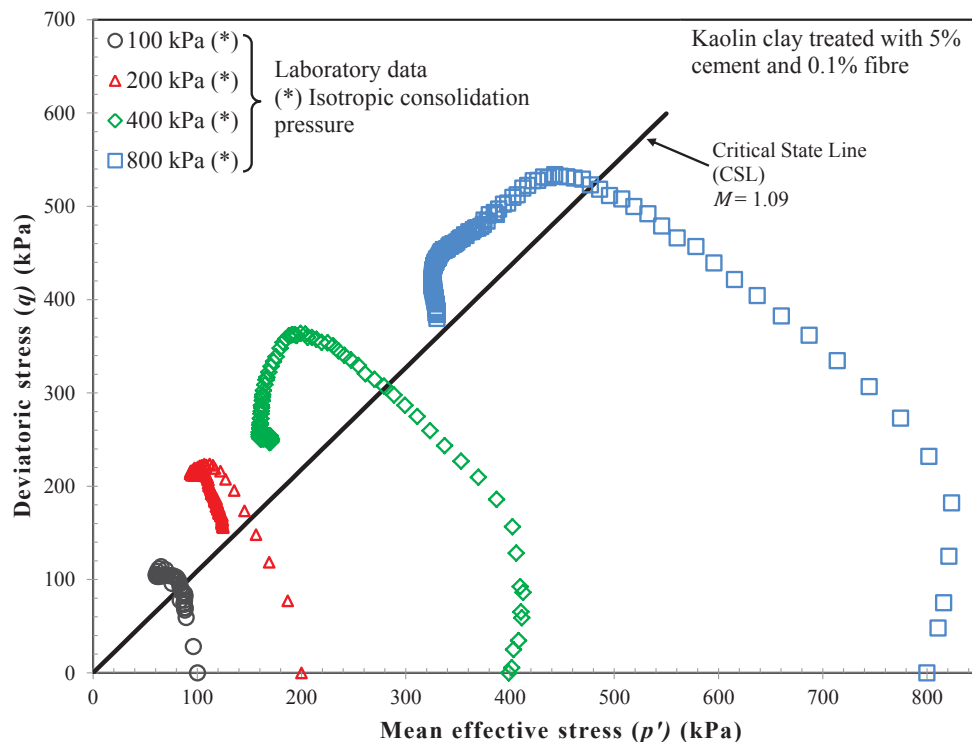


Figure 4.53: Undrained stress paths of the Kaolin clay treated with 5% cement and 0.1% fibre

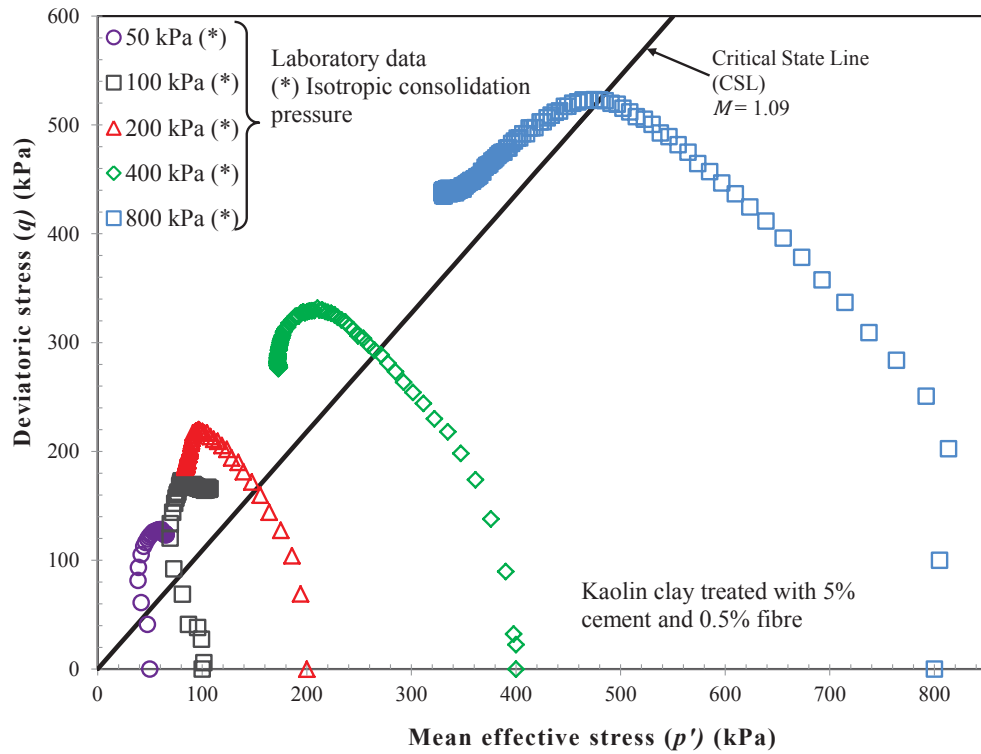


Figure 4.54: Undrained stress paths of the Kaolin clay treated with 5% cement and 0.5% fibre

Figure 4.55 summarises the effect of cement and fibre reinforcement on the peak shear strength of Kaolin clay at different mean effective yield stresses. Due to the combined effect of cement and fibre inclusion, the peak shear strength increased significantly compared to un-treated clay, whereas the peak shear strength of improved Kaolin composite was generally higher than cement treated Kaolin clay due to fibre reinforcement. For example, at  $p'_0 = 200$  kPa, the peak shear strength increased by 27% when 0.1% fibre was added to the cement treated clay, but this increase in strength decreased as the mean effective yield stress increased. When  $p'_0$  increased to 400 and 800 kPa, the shear strength decreased by 12.5% and 2.1%, respectively, possibly due to fibre failure because localised stress on the fibre body increased when the mean effective yield stress increased. At  $p'_0 = 800$  kPa, the peak shear strength of the improved soil composite with 0.1% fibre was almost identical to the treated clay without fibre reinforcement, probably because the fibre might have ruptured before it reached its peak state. Hence, the contribution of fibre reinforcement decreased at high  $p'_0$ , particularly near the shear plane. Moreover, the additional strength of the improved

soil composite with 0.5% fibre induced by the fibre reinforcement was negligible at  $p'_0 = 400$  and  $800$  kPa, as shown in Figure 4.55. Thus, increasing the fibre content from 0.1% to 0.5% may not necessarily improve the peak shear strength in the triaxial tests. It can also be concluded that the peak shear strength of the improved soil composite is mainly governed by the effect of cementation.

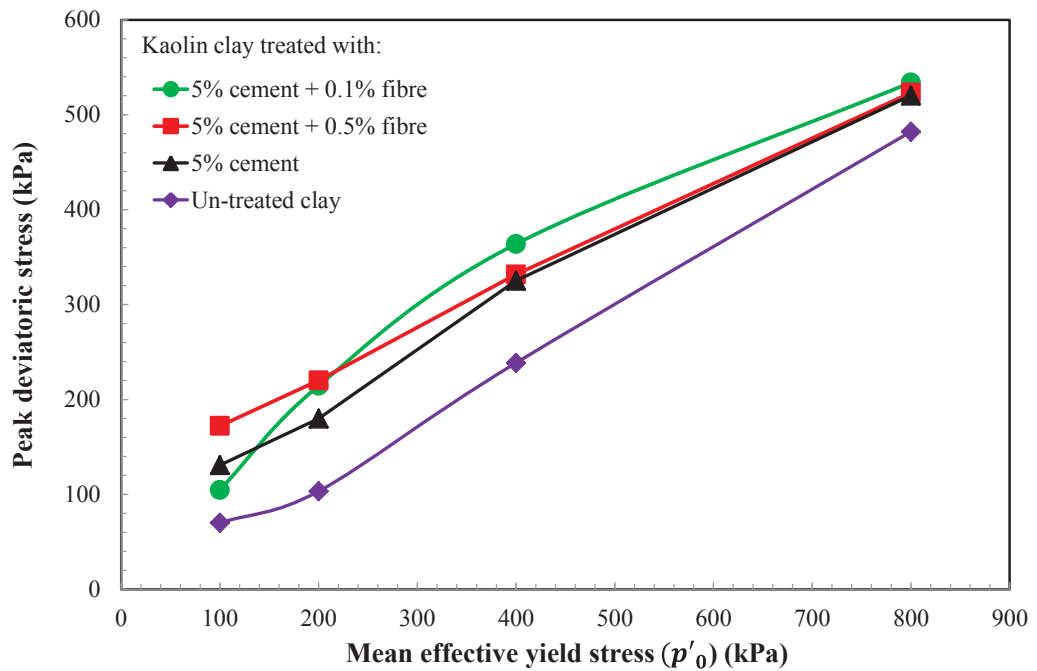


Figure 4.55: Effect of cement and fibre reinforcement on the peak shear strength of the improved Kaolin clay.

Compared to the improved Ballina clay composite (refer to Figure 4.39), the contribution of the fibre to the peak shear strength of the Kaolin clay was more pronounced, probably due to the difference in soil mineralogy as Ballina is natural soft clay with high plasticity while artificial Kaolin clay is classified as low plasticity clay. The type of soil can affect the cementation process, particularly the formation of soil-cement clusters and the strength of cementation bonds, and as a consequence, may influence the load transfer mechanism which relies on the frictional and interlocking forces between the fibre and clusters of soil-cement. Based on an experimental study of sand treated with polypropylene fibre and various cement contents, Consoli et al.

(2009b) suggested that the fibre is not as stiff as the surrounding soil-cement clusters when higher amount of cement (e.g. 10% cement) is used, so the tensile strength of the fibre has not mobilised effectively before reaching the peak strength state. With the same fibre content (i.e. 0.5% fibre) and considering the cement content of the treated Ballina clay (i.e. 15% cement) and the treated Kaolin clay (i.e. 5% cement), the contribution of fibre to the peak shear strength would be more in the Kaolin clay because the soil-cement matrix is not as stiff. Thus, the improvement in the peak shear strength due to the effect of fibre depends on the type of soil and the cement content.

#### **4.4.3.3.3. Stress Strain Relationship and Excess Pore Water Pressure Response**

In this study the ultimate strength of the un-treated clay was determined at failure strain of 10%, as suggested by Australian Standards (AS1289.6.4.2-1998). The un-treated Kaolin clay exhibited ductile behaviour as the shear stress continued to increase at a large deviatoric strain ( $\varepsilon_q > 10\%$ ), as shown in Figure 4.56, behaviour that was similar to the un-treated Ballina clay. However, cement inclusion reduced the deviatoric strain at failure as all the samples of treated Kaolin clay reached their peak shear strength at  $\varepsilon_q = 1.7\% - 2.2\%$  (Figure 4.57), which means the shear stress decreased with an increasing  $\varepsilon_q$  at the post-peak state. The amount of loss in strength depends on the accumulation of plastic shear strain and the level of mean effective yield stress, both of which are significant at high effective pressures, as shown in Figure 4.57. Moreover, the excess pore water pressure response ( $\Delta u$ ) of the Kaolin clay treated with 5% cement (shown in Figure 4.59) was higher than the un-treated clay (Figure 4.58). Moreover,  $\Delta u$  reduced steadily at the post-peak state as the treated sample was undergoing the softening process, while  $\Delta u$  of the un-treated clay continued to increase with deviatoric strain. This shows that the generation of excess pore water pressure depends on the effect of cementation since the cementation bonds increased the contractive tendency of the sample treated with cement.

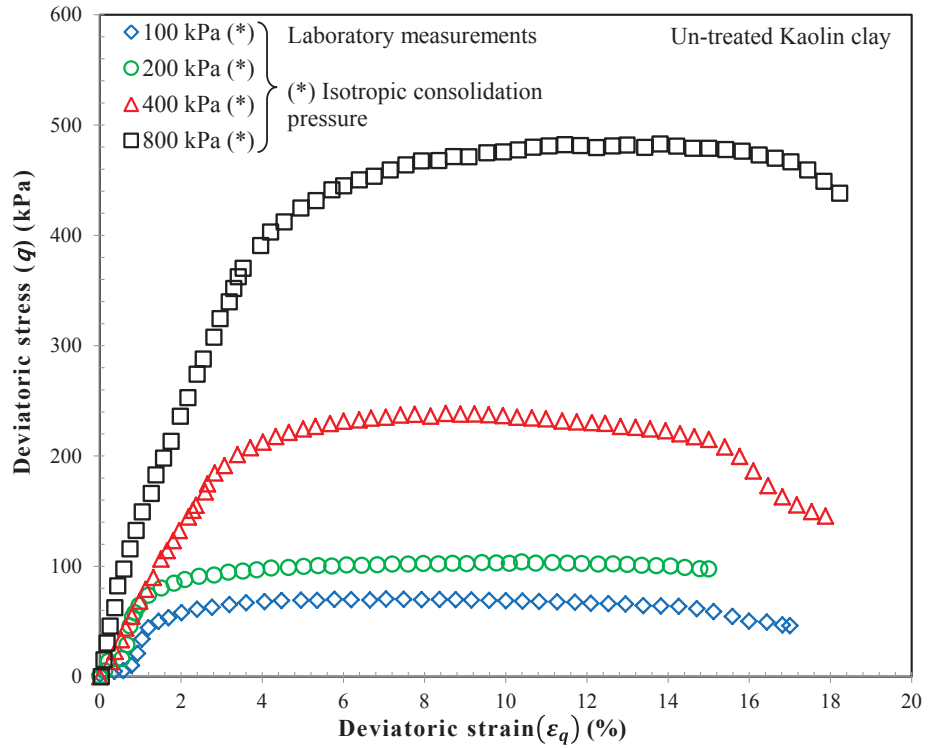


Figure 4.56: Stress-strain relationship of the un-treated Kaolin clay

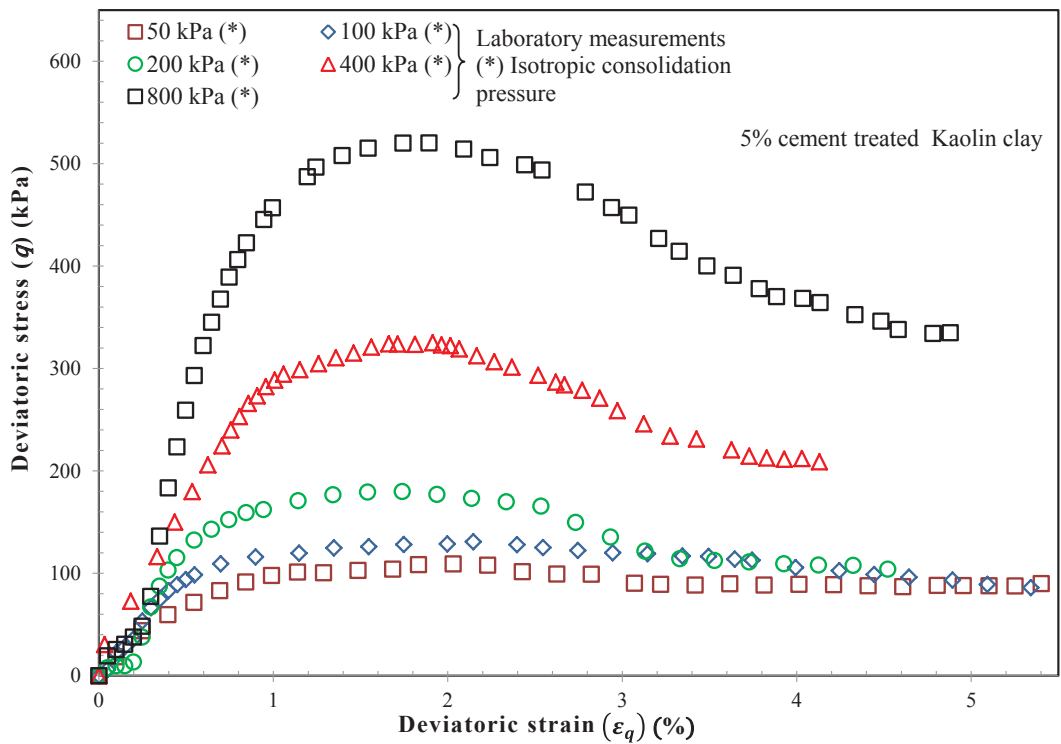


Figure 4.57: Stress-strain relationship of the Kaolin clay treated with 5% cement

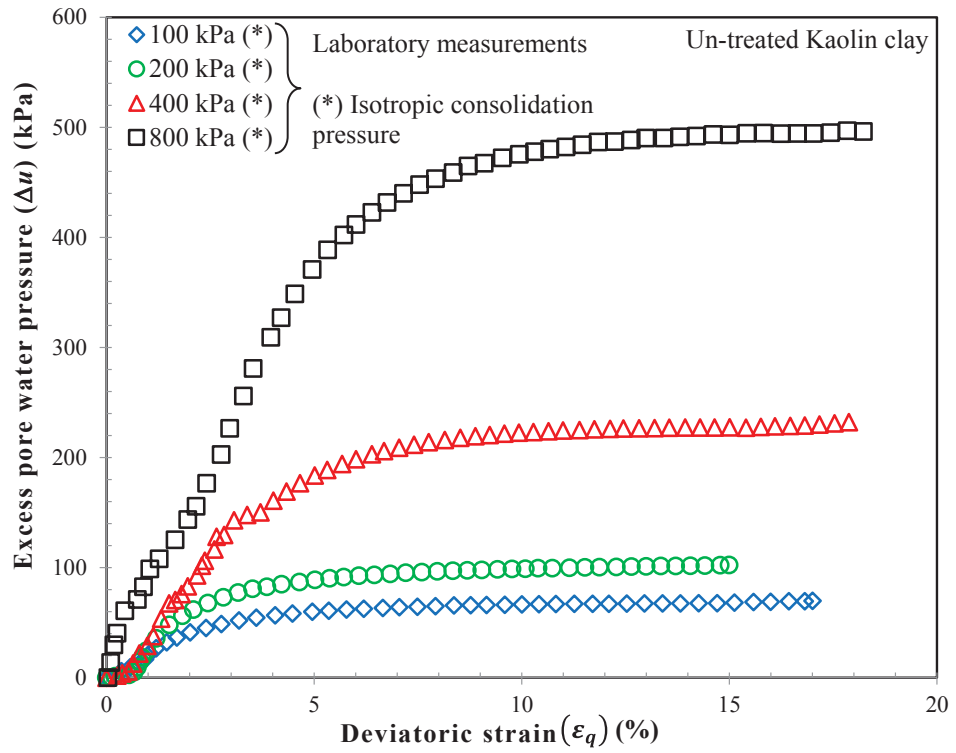


Figure 4.58: Excess pore water pressure response of the un-treated Kaolin clay

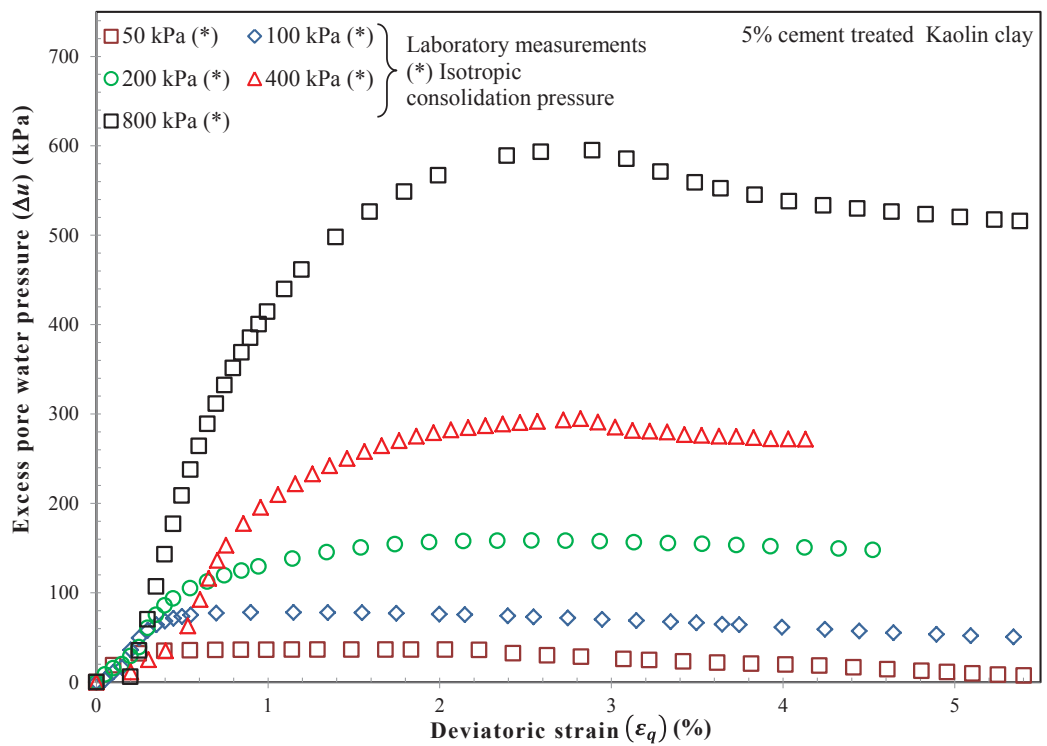


Figure 4.59: Excess pore water pressure response of the Kaolin clay treated with 5% cement

The effect of fibre reinforcement on the stress-strain relationship and the excess pore water pressure response of the improved Kaolin composite was examined using the results obtained from the undrained triaxial tests on the 5% cement treated Kaolin reinforced with 0.1% and 0.5% polypropylene fibre, as shown in Figures 4.60 to 4.63. Table 4.5 summarises the experimental values of the Kaolin clay improved with differing amounts of fibre. While the cement treated clay reached its peak shear strength at  $\varepsilon_q = 1.8\%$ , the peak deviatoric strain of the soil composite improved with 0.1% fibre occurred at  $\varepsilon_q < 1\%$  for  $p'_0 = 100$  and 200 kPa and  $\varepsilon_q = 1.6\%$  for higher  $p'_0$  values (i.e. 400 and 800 kPa) as shown in Figure 4.60. Figure 4.61 also shows that increasing the fibre content to 0.5% increased in the peak deviatoric strain for  $p'_0 = 50$  and 100 kPa. However, the loss in strength at the post peak state in low  $p'_0$  was not as significant as in higher  $p'_0$  for all fibre contents added. Thus, it can be concluded that the improved soil composite is more ductile in low mean effective yield stress, and the fibre reinforcement is more effective in this stress range. Overall, despite some variations in the contribution of fibre reinforcement to the shear strength, the improved soil composite becomes more ductile compared to the brittle behaviour of the cement treated clay.

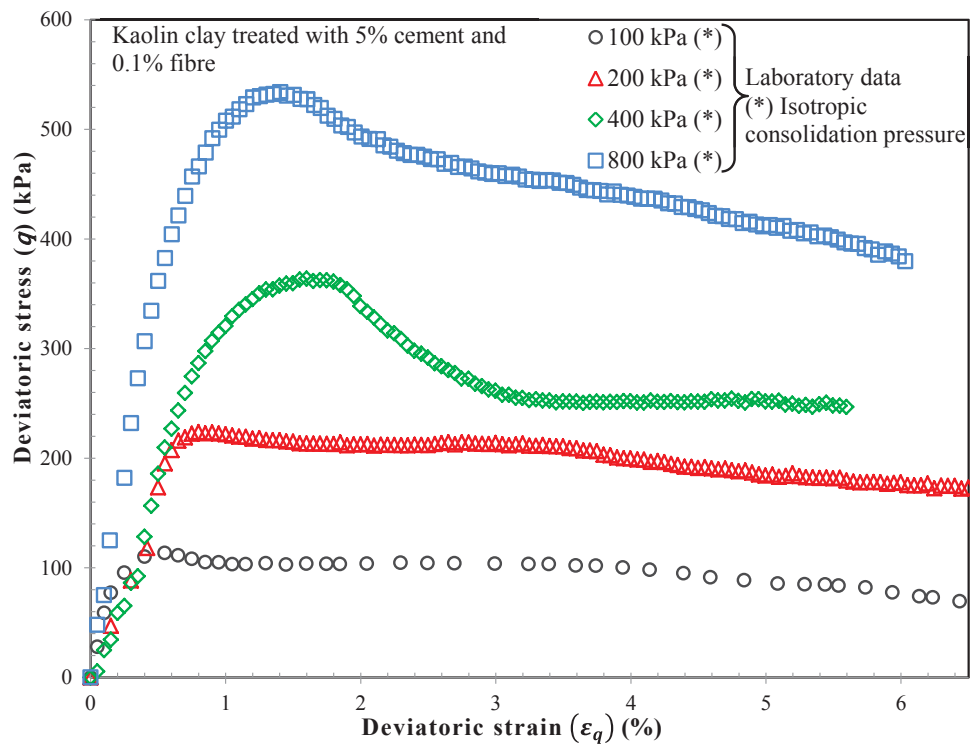


Figure 4.60: Stress-strain relationship of the Kaolin clay treated with 5% cement and 0.1% fibre

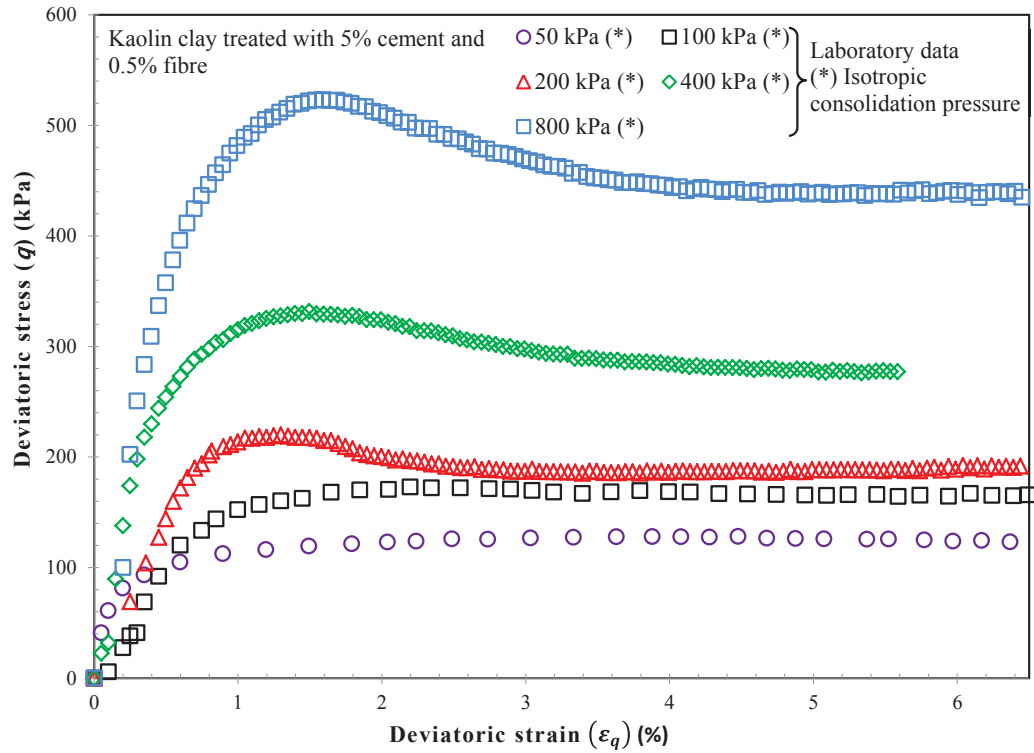


Figure 4.61: Stress-strain relationship of the Kaolin clay treated with 5% cement and 0.5% fibre

Figures 4.62 and 4.63 show the excess pore water pressure for the Kaolin clay treated with 5% cement and reinforced with 0.1% and 0.5% fibre, respectively. Compared to the excess pore water pressures reported for treated soil with 0.1% fibre in Figure 4.63, the addition of 0.5% of fibre into treated clay influenced the post peak behaviour with a steady increase of excess pore water pressure ( $\Delta u$ ) as shown in Figure 4.62. The excess pore water pressure of the 5% cement treated Kaolin clay with 0.5% fibre increased to a peak state and remained steady as  $\epsilon_q$  continued to increase, while the maximum excess pore water pressure ( $\Delta u_{max}$ ) for the improved soil composite was higher than  $\Delta u_{max}$  of the cement treated clay at different mean effective yield stresses. For example, at  $p'_0 = 400$  kPa,  $\Delta u_{max}$  of soil improved with 0.1% fibre was 319 kPa ( $\epsilon_q = 2.05\%$ ), while  $\Delta u_{max}$  of cement treated clay was 286 kPa ( $\epsilon_q = 2.8\%$ ). Furthermore, the maximum excess pore water pressure ( $\Delta u_{max}$ ) of the improved Kaolin clay with 0.5% fibre occurred at deviatoric strains higher than the shear strains corresponding to the peak shear strength ( $q_{peak}$ ) (e.g. during shearing at 800 kPa the mean effective yield stress,  $\Delta u_{max}$  occurred at  $\epsilon_q = 3.8\%$ , while  $q_{peak}$  occurred at  $\epsilon_q = 2\%$ ). Li (2005) explained that due to fibre reinforcement, the applied loads are distributed between the

fibres within the soil matrix, and hence the dilatancy of the composite soil is restricted during shearing.

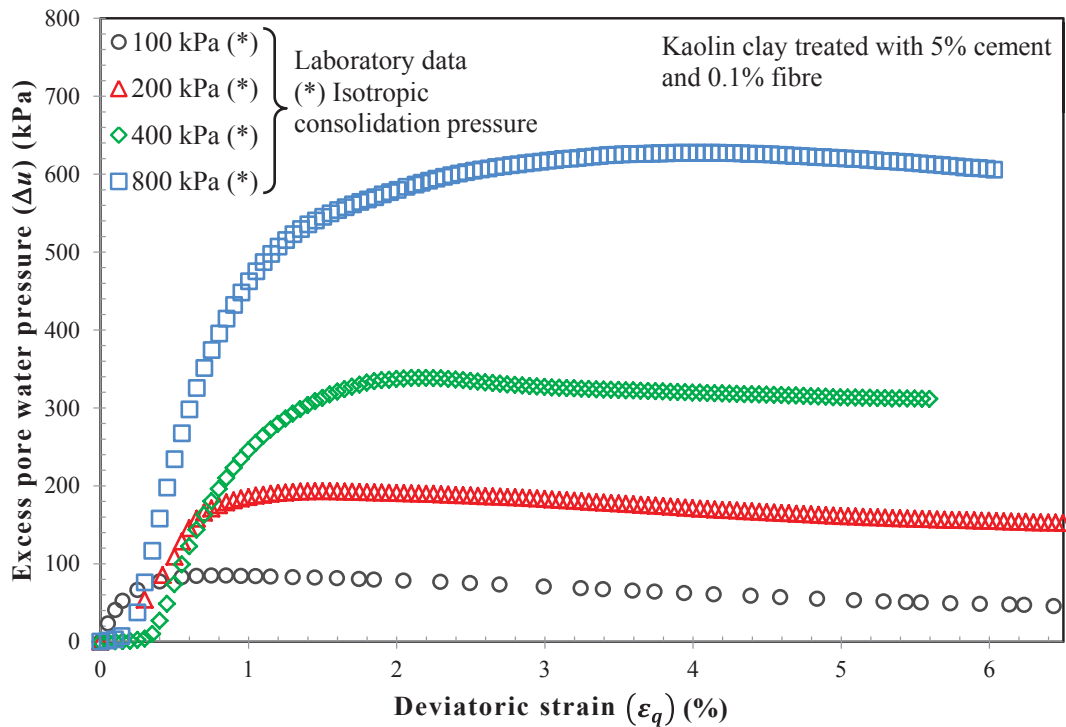


Figure 4.62: Excess pore water pressure response of the Kaolin clay treated with 5% cement and 0.1% fibre

The brittleness index ( $I_B$ ) (see Equation 4.2) can also be used to measure the effect of fibre reinforcement on the ductility of improved Kaolin clay. Figure 4.64 shows that the cement treated clay exhibited highly brittle behaviour as  $I_B$  on average was 0.55 across different mean effective yield stresses compared to the un-treated clay ( $I_B = 0.03$ ). When fibre was added to the cement treated clay,  $I_B$  dropped significantly as the improved soil composite became more ductile. The main reason for fibre inclusion is to provide the bridging effect between soil-cement clusters within the soil matrix under a shearing load. Hence, beyond the peak strength state, where significant breaking of cementation bonds occurs, the fibre is mobilised and the applied load is transferred from the clusters of soil-cement to the fibre. Thus, the residual shear strength

increases due to the load transfer mechanism and the load being redirected from the soil to the fibre.

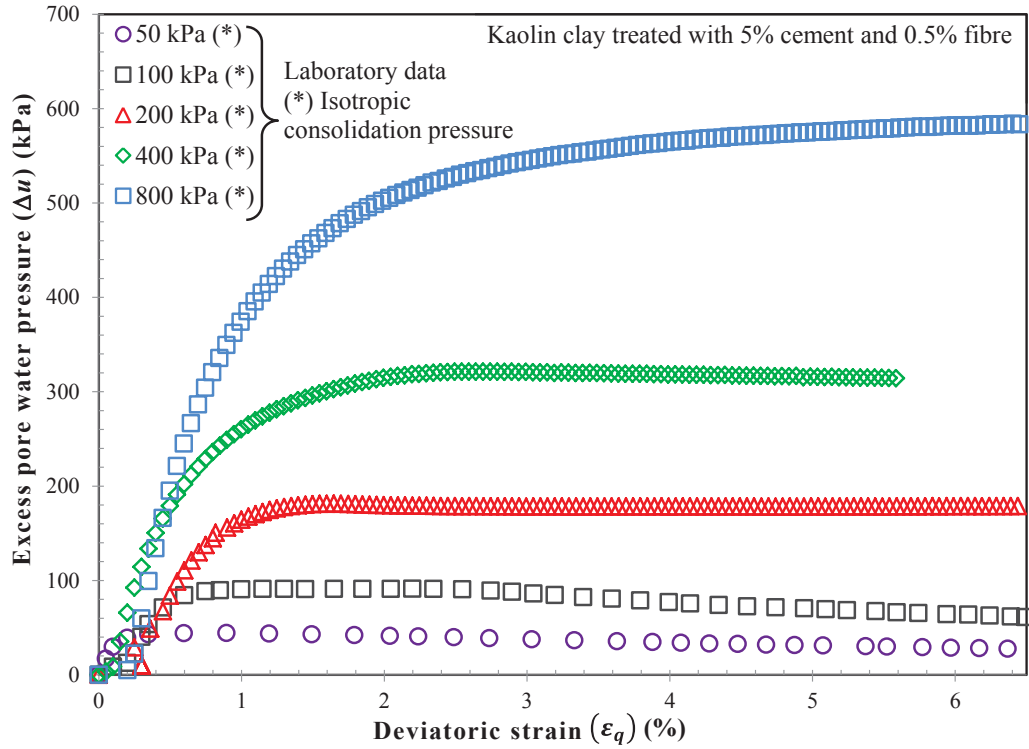


Figure 4.63: Excess pore water pressure response of the Kaolin clay treated with 5% cement and 0.5% fibre

As Figure 4.64 shows, increasing the amount of fibre reduced the brittleness of the cement treated clay as the residual shear strength increased. It can be noted that,  $I_B \approx 0$  indicates ductile behaviour. At 200 kPa of mean effective yield stress, the  $I_B$  of the improved soil composite was 0.26 for treated soil with 0.1% fibre, compared to  $I_B = 0.73$  for cement treated clay. There was a significant improvement in ductility due to fibre reinforcement, but at  $p'_0 = 800$  kPa, the improvement in ductility was moderate (e.g.  $I_B$  values were 0.41 and 0.55 for treated soil with 0.1% and 0% fibre, respectively), which was attributed to the fibre rupturing. Similarly, fibre reinforcement was more effective at  $p'_0 = 200$  kPa as  $I_B$  increased by 80% ( $I_B = 0.15$ ) when 0.5% fibre was added to the cement treated soil. The material became much more ductile at  $p'_0 = 100$  kPa which was almost identical to the un-treated Kaolin clay. However, as  $p'_0$  increased,

$I_B$  of the composite soil was 0.20 and 0.19, (65% and 66% improvement in  $I_B$ ) at  $p'_0 = 400$  kPa and 800 kPa, respectively. Therefore, the fibre was more effective in low mean effective stresses. Increasing the mean effective yield stress may reduce the effectiveness of the fibre as the fibre may rupture prior to reaching the failure state, although material ductility increases with the amount of fibre added. Furthermore, fibre reinforcement affected the brittleness of the cement treated Kaolin clay in a similar way to treated Ballina clay (see Figure 4.41), as  $I_B$  of cement treated clay as the amount of fibre increased. It can therefore be concluded that the addition of fibre can improve the ductility of the cement treated clay for different types of soil tested.

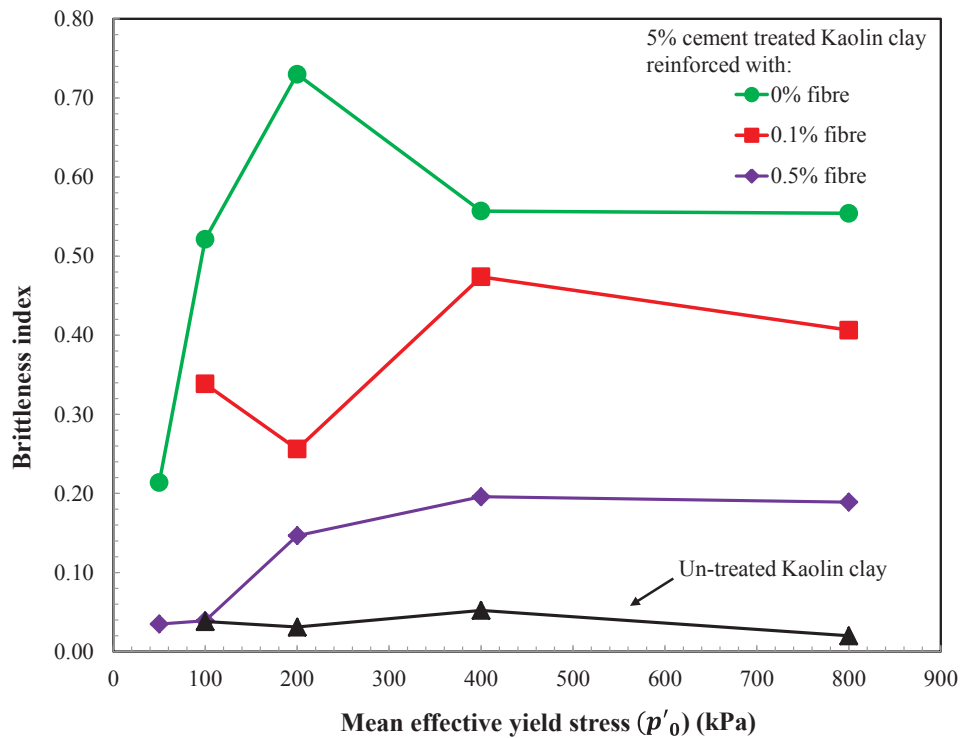


Figure 4.64: Effect of fibre reinforcement on the brittleness index of the improved Kaolin clay

## 4.5. Summary

This chapter outlined an experimental program used to investigate the effect of cement and fibre reinforcement on the behaviour of natural Ballina clay and artificial Kaolin clay. This program included Scanning Electron Microscopy (SEM), Unconfined Compression Strength (UCS) tests, and an extensive series of triaxial compression tests in drained and undrained conditions. To study the effect of cementation, natural Ballina clay was treated with different amounts of cement (i.e. 10%, 12% and 15%), while the Kaolin clay was treated with 5% cement. Furthermore, to investigate the effect of fibre reinforcement on the behaviour of cement treated clay, the Ballina clay treated with 15% cement was reinforced with differing fibre contents (i.e. 0.3% and 0.5%), while the 5% cement treated Kaolin clay was improved with 0.1% and 0.5% fibre. A description of sample preparation and the testing apparatus is provided in Sections 4.2 and 4.3, respectively while the experimental results are reported in Section 4.4. Furthermore, the results of the triaxial tests were used to verify the model proposed in Chapter 5. The experimental findings can be summarised as follows:

- The SEM image analysis revealed a flocculated structure with cementation bonding and an aggregation of clay particles (clay clusters) in clay treated with cement as a result of cement hydration and pozzolanic reactions. The SEM results revealed the effect of cementation where the precipitated crystals connecting the clay particles within the structure of the cement treated clay disappeared after shearing at high mean effective stresses. The SEM image of the cement treated clay reinforced with fibre showed that the fibre was surrounded by clusters of clay and cement with relatively small opening after shearing. There were some grooves on the fibre body caused by the cementation bonds being crushed at large deviatoric strains. This indicated that the soil-cement clusters were connected by the fibre and the applied load could be transferred to the fibre body, consequently the improved soil composite exhibited increased shear strength and ductility.
- The peak unconfined compression strength of cement treated clay increased with cement content, while the treated clay became more brittle when higher amounts of cement were used. Increasing the cement content also led to a significant reduction in the post peak stress state in unconfined compression. Moreover, the peak unconfined

compression strength of cement treated clay with fibre was mainly due to the contribution of cementation while the residual shear strength increased with fibre content.

- The compressibility of the cement treated clay depended on the amount of cement in isotropic consolidation. The initial mean effective yield stress increased ( $p'_{o,i}$ ) with cement content due to cementation. As the mean effective yield stress ( $p'_o$ ) increased beyond  $p'_{o,i}$ , the void ratio decreased significantly approaching the ICL of the reconstituted soil-cement mixture due to the breaking of cementation bonds. At high  $p'_o$ , the cement treated clay relied mainly on the fabric which could not be destroyed during isotropic compression. Moreover, the compressibility of the improved soil composite was mainly governed by cementation and its degradation, while the fibre made an insignificant contribution.
- In undrained triaxial conditions, the peak shear strength of the cement treated clay increased with cement content and the mean effective yield stress ( $p'_o$ ). However, an increasing  $p'_o$  caused a significant breaking of the cementation bonds, particularly with higher amounts of cement. As the deviatoric strain increased, the cement treated clay became more brittle with an increasing mean effective yield stress and the cement content. In drained triaxial conditions, the cement treated clay showed strain hardening ductile behaviour with significant cementation degradation prior to reaching its peak strength state at  $p'_o \gg p'_{o,i}$ . Thus, when plastic deformation occurs, cementation degradation is caused by a combination of mean effective yield stress (or plastic volumetric strain) and the plastic shear strain.
- The inclusion of fibre improved the brittleness of the cement treated clay as the fibre provided a bridging effect among the soil-cement clusters, and the applied load could be transferred onto the fibre body. The peak shear strength of the improved soil composite depended on the type of treated soil and was mainly governed by the effect of cementation. Moreover, the ductility of the soil composite increased with fibre content for both types of soil adopted. Increasing the mean effective yield stress and deviatoric strain reduced the effectiveness of the fibres as they were ruptured prior to reaching the failure state.

# Chapter 5

## Model Verification and Discussion

---

### 5.1. General

In this chapter, the proposed models for the cement treated clay with or without fibre reinforcement (described in Chapter 3) are validated by comparing the model predictions with the experimental triaxial test results conducted on the treated clay (presented in Chapter 4) and available test results from the literature. The model parameters are estimated following the procedures described in Section 5.2. The predictions are presented in terms of isotropic consolidation in  $e - \ln p'$  plane, the stress path in  $p' - q$  plane, the stress-strain relationship in  $\varepsilon_q - q$  plane and the excess pore water pressure response in  $\varepsilon_q - \Delta u$  plane. The proposed model developed for the cement treated clay in Section 3.2 is verified against the triaxial test results on the Ballina clay treated with different cement contents (i.e. 10%, 12% and 15%) and the 5% cement treated Kaolin clay. Furthermore, the performance of the proposed model is further evaluated with the available case studies in the literature. In addition, the validation of the proposed model extended for the improved clay composite or FRCS (developed in Section 3.3) involves the simulation of the triaxial test results on the 15% cement treated Ballina clay reinforced with 0.3% and 0.5% polypropylene fibre; and the Kaolin clay treated with 5% cement and different fibre contents (i.e. 0.1% and 0.5%).

## 5.2. Estimation of Model Parameters

To simulate the behaviour of cement treated clay without fibre reinforcement, the proposed model includes twelve parameters that can be estimated via the following steps:

- The first four parameters, including  $M, \lambda, \kappa$  and  $\nu$  are reasonably assumed to be independent of the soil structure and consequently can be determined using a set of conventional isotropic compression tests similar to the parameter determination used in the MCC model. However, as Horpibulsuk et al. (2010) and Liu and Carter (2002) reported, these parameters can be reasonably estimated by reconstituted soil properties (excluding cement), particularly when small amounts of chemical additives are used.
- Parameter  $\beta$  can be estimated using curve fitting to data obtained from the isotropic consolidation tests on cement treated clays in  $e - \ln p'$  space. In other words, Equations (3.6) and (3.7) should be fitted to isotropic consolidation data (e.g. Figure 3.2) to obtain  $\beta$ .
- The mean effective stress when initial virgin yielding occurs ( $p'_{0,i}$ ) is estimated from the isotropic consolidation tests using Equation (3.9) or by finding the point corresponding to conventional pre-consolidation pressure (e.g. point  $p'_{0,i}$  in Figure 3.1). The parameter  $p'_{\Omega,i}$  can be determined by the difference between  $p'_{0,i}$  and  $p'_d$  (the intersection point between the ICL of the cement treated clay and the A-line in Figure 3.1)
- Furthermore, parameter  $C_c$  can be estimated from fitting the data in  $p' - q$  plane, particularly fitting the peak deviatoric stresses ( $q_{peak}$ ).
- The correlation factor ( $\xi$ ) can be calculated from Equation (3.12) after finding  $p'_{\Omega,i}$  from isotropic consolidation curve and parameter  $C_c$ .
- The most appropriate  $\alpha$  value results in the best fitted stress-strain curves in  $\varepsilon_q - q$  plane.
- Parameters  $\omega$  and  $b$ , affecting the degradation process during shearing, can be estimated by plotting the stress-strain curve in the  $\varepsilon_q - q$  plane of cement treated

clay, particularly during post peak stages or when significant deviatoric strains occur.

To simulate the behaviour of cement treated clay with fibre reinforcement, with the parameters associated with the effect of cementation ( $C_c$ ,  $\xi$ ,  $\omega$  and  $b$ ), it is better to conduct a series of triaxial tests on the cement treated clay only (i.e. fibre content = 0%) to determine the parameters as described above for cement treated clay. Moreover, as discussed in Section 3.3, the effect of fibre was assumed to be insignificant in isotropic compression conditions, so the ICL of the improved soil composite follows the ICL of the cement treated clay without fibre reinforcement.

For the parameters associated with the effect of fibre reinforcement ( $C_f$ ,  $q_c$ ,  $m$  and  $n$ ), it is suggested that a series of triaxial tests be carried out on the cement treated clay improved with fibre. After using the above procedure to determine the model parameters related to soil cementation, the parameters associated with the fibre can be determined as follows:

- The value of  $C_f$  that refers to the contribution the fibre makes to the shear strength, can be estimated by fitting the stress path data of the improved soil composite into the  $p' - q$  plane.
- The parameter  $q_c$  can be determined by finding the point on the failure envelope (Equation (3.90)) that corresponds to the critical mean effective stress ( $p_{crit}^*$ ), or  $q_c$  can also be approximated by trial and error. Note that the parameters required to solve  $p_{crit}^*$  in Equation (3.57) can be obtained using the properties of a single fibre.
- The model parameters  $m$  and  $n$  that affect the diminishing rate of fibre failure mechanisms should be fitted to the stress strain curve in the  $\varepsilon_q - q$  plane, with special attention given to the post peak behaviour

### 5.3. Proposed Model Verification

In this section, the performance of the proposed model is evaluated by comparing the model predictions with the triaxial test results presented in Section 4.4.3 on cement treated Ballina clay with or without fibre reinforcement. In addition, the behaviour of the improved Kaolin clay composite with different fibre content under triaxial compression is simulated to further verify the proposed model. The simulation results are presented in stress path ( $p' - q$  plane), stress-strain curve ( $\varepsilon_q - q$  plane) and the excess pore water pressure response in  $\varepsilon_q - \Delta u$  plane.

#### 5.3.1. Cement Treated Ballina Clay

Undrained and drained triaxial compression tests were carried out on samples of Ballina clay treated with different cement content (i.e. 10%, 12% and 15%) and mean effective stresses ranging from 200 to 800 kPa. The experimental results can be found in Section 4.4.3.1. Moreover, following the above mentioned procedure described in Section 5.2, the model parameters for the cement treated clay were calculated and summarised in Table 5.1 for different cement contents.

##### 5.3.1.1. Isotropic compressibility

Figure 5.1 describes the isotropic compression of 10% cement treated Ballina clay at different mean effective stresses, ranging from 20 to 800 kPa. The initial void ratio ( $e_0$ ) was measured at 2.99 while the initial mean effective yield stress ( $p'_{o,i}$ ) was estimated as 115.6 kPa. The results from isotropic compression tests were then used to estimate the properties of the soil and the fitting of the model parameters. When the cement treated clay is subjected to a low mean effective yield stress (i.e.  $p'_o < p'_{o,i}$ ), the samples behave as an elastic material, following the slope of  $\kappa$ . As the mean effective yield stress increases beyond  $p'_{o,i}$  (i.e.  $p'_o > p'_{o,i}$ ), the yield surface expands in size resulting in plastic deformation and the void ratio of the cement treated Ballina clay

gradually approaches the ICL of reconstituted soil, showing the effect of cementation degradation. This behaviour of the cement treated clay is captured in the proposed model by the formulation of  $p'_{\Omega}$  in Equation (3.7).

Table 5.1: Model values for cement treated Ballina clay

<b>Cement content</b>	<b>10%</b>	<b>12%</b>	<b>15%</b>
$M$	1.21	1.21	1.21
$\lambda$	0.363	0.363	0.363
$\kappa$	0.0355	0.0355	0.0355
$p'_{o,i}$ (kPa)	115.6	133.26	149.92
$\xi$	0.49	0.54	0.66
$\alpha$	-0.299	-0.35	-0.11
$C_c$ (kPa)	68	87	120
$\beta$ (kPa)	1250	1780	3125
$\nu$	0.25	0.25	0.25
$e_0$	2.99	3.1	3.12
$\omega$	64	38	65
$b$	5.3	4.4	3.2
$\Delta s$	0.065	0.38	0.47

Moreover, the reduction of  $p'_{\Omega}$  as  $p'$  increases is controlled by an estimation of the model parameter  $\beta$ . In the proposed model, it was assumed that the ICL of the cement treated clay would merge with the A-line to consider the effect of fabric which cannot be destroyed during isotropic compression. The value  $\Delta s = 0.065$  indicates that fabric has a minimal effect on the structure of cement treated Ballina clay. In this case the mineralogy (high plasticity clay) and the amount of cement may constitute to the effect of fabric change. As Figure 5.1 shows, the proposed model simulated the isotropic compression of cement treated Ballina clay very well.

Furthermore, the simulation results of the Ballina clay treated with different cement contents (i.e. 10%, 12% and 15%) are shown in Figure 5.2. The initial mean effective yield stress ( $p'_{o,i}$ ) increased with the effect of cement content which was captured effectively by adopting the procedure in Section 5.2. Furthermore, the reduction in void ratio at the post-yield stage occurred at a lower rate when higher cement content was used. It was indicated in higher value of the parameter  $\beta$  which influenced the degradation rate of cementation (i.e  $\beta = 1250$  and  $3125$  when cement content increases from 10% to 15%, respectively). It can be noted that, increasing  $\beta$  value simulates lower degradation rate in isotropic compression. Moreover, it was observed that, the fabric component of cement treated clay depends on the effect of cement. Even at high stress level (e.g.  $p'_o = 800$  kPa), increasing the effect of cement content results in higher void ratio. As cement content increases from 10% to 15%, the values of  $\Delta s$  change significantly from 0.065 to 0.47, respectively. Hence the compressibility behaviour of cement treated clay depends mainly on the effect of cement and relies on the effect of fabric at high stress level. Overall, the compressibility behaviour of the cement treated clay can be simulated well by adopting the proposed model.

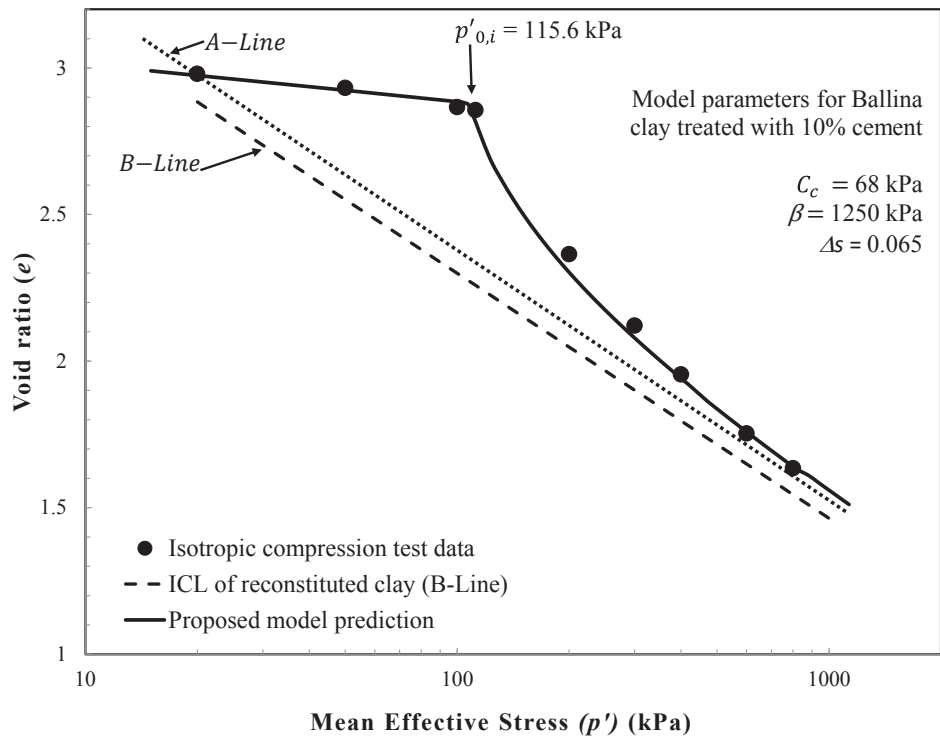


Figure 5.1: Simulation of isotropic compression of 10% cement treated Ballina clay

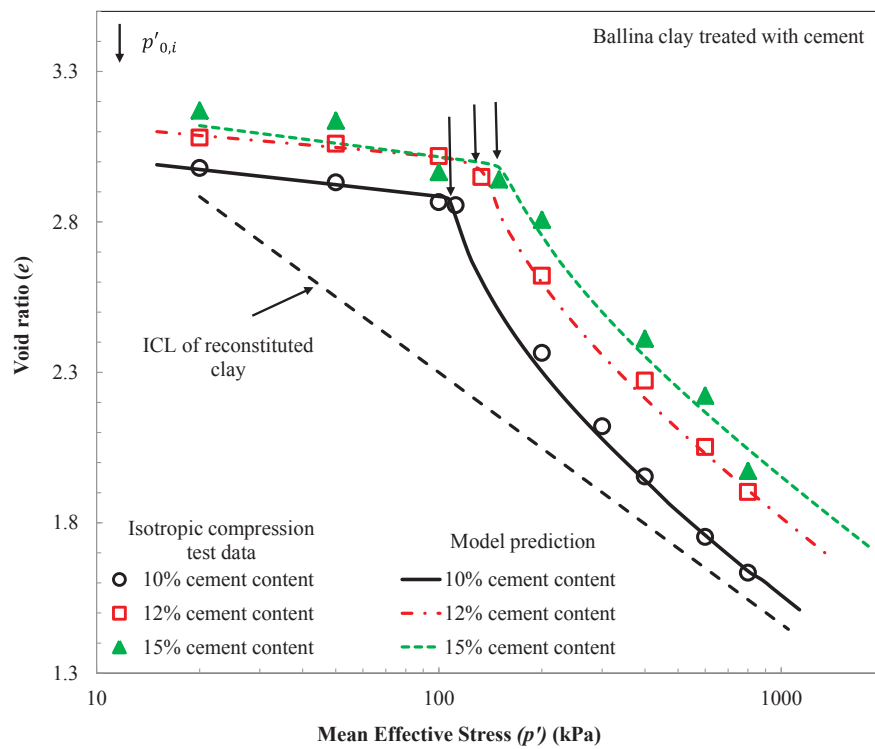


Figure 5.2: Simulation of isotropic compression of Ballina clay treated with different cement content (i.e. 10%, 12% and 15%)

### 5.3.1.2. Undrained Triaxial Compression

The reliability of the proposed model was verified by comparing its predictions with the results of the undrained and drained shearing test of treated Ballina clay obtained from the triaxial test. The model predictions of the undrained stress paths in  $p' - q$  plane for the Ballina clay treated with different cement contents are shown in Figures 5.3 – 5.5 while the simulation results of the stress-strain curves in  $\varepsilon_q - q$  plane are displayed in Figures 5.6 – 5.8. The values of model parameters adopted in the simulation are summarised in Table 5.1.

The undrained stress paths and stress-strain curves showed that the test data was simulated quite well for all cement contents in this study. All the undrained triaxial tests were simulated under effective confining pressures (i.e.  $p'_o = 200 - 800$  kPa) beyond the initial mean effective yield stress  $p'_{o,i} = 115.6$  kPa and showed that the behaviour of cement treated clay is similar compared with normally consolidated clay samples. The peak shear strength of 10% cement treated Ballina clay reported in Figure 5.3 was captured quite well by Equation (3.53). As Figure 5.3 shows, the failure envelope progressively merges with the CSL of reconstituted soil-cement mixture; this indicates that the effect of cementation degradation is influenced by the mean effective yield stress and deviatoric strain. The contribution of cementation to the shear strength of the cement treated clay is represented by the parameter  $C_c$ . Hence increasing  $C_c$  can simulate the increase in shear strength when higher cement content is used. The value of  $C_c$  increases from 68 kPa to 120 kPa as the cement content changes from 10% to 15%, respectively. Thus, by accurate estimation of the parameter  $C_c$ , in particular, the peak shear strength of the cement treated clay can be captured very well for different cement contents as observed in Figures 5.3 – 5.5. Furthermore, at the post-peak state, softening process occurred as the cementation bonds were significantly crushed. The stress path changed its direction toward the CSL which were predicted by adopting Equation (3.53). The proposed model assumed that the stress state of the cement treated soil remains on the failure line with a reduction in the effect of cementation ( $p''_{\Omega}$ ) due to increasing plastic deviatoric strain ( $\varepsilon_q^p$ ). The predicted stress paths reached the residual strength state on the CSL, indicating complete removal of cementation bonds.

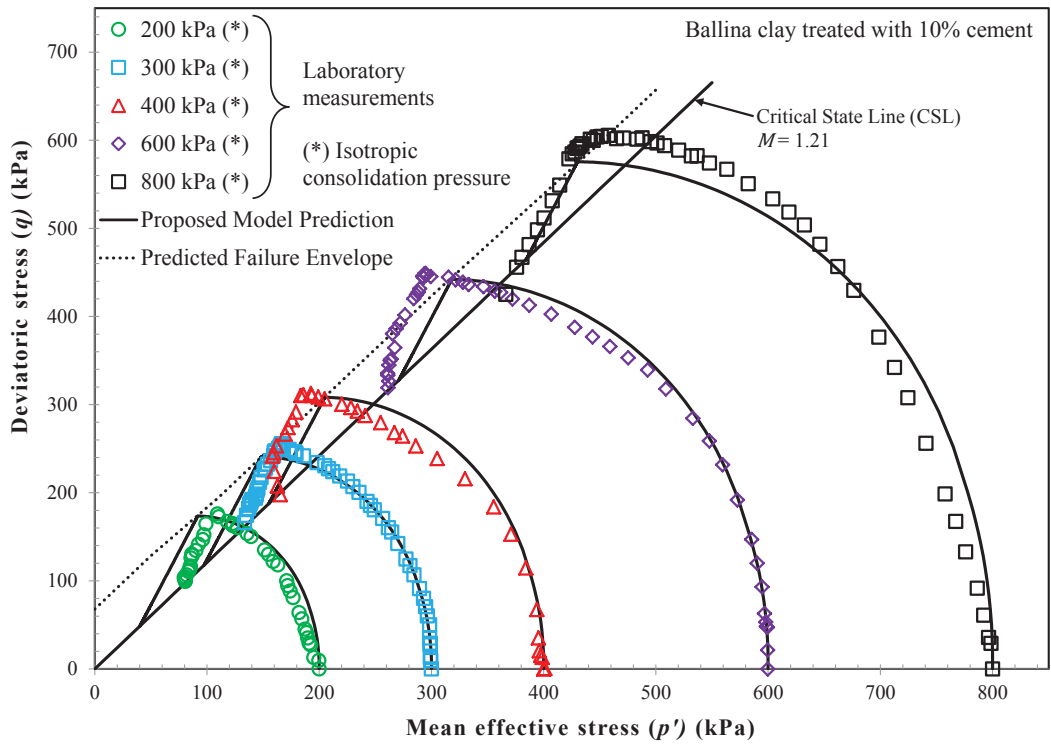


Figure 5.3: Predicted stress paths of undrained triaxial tests of 10% cement treated Ballina clay

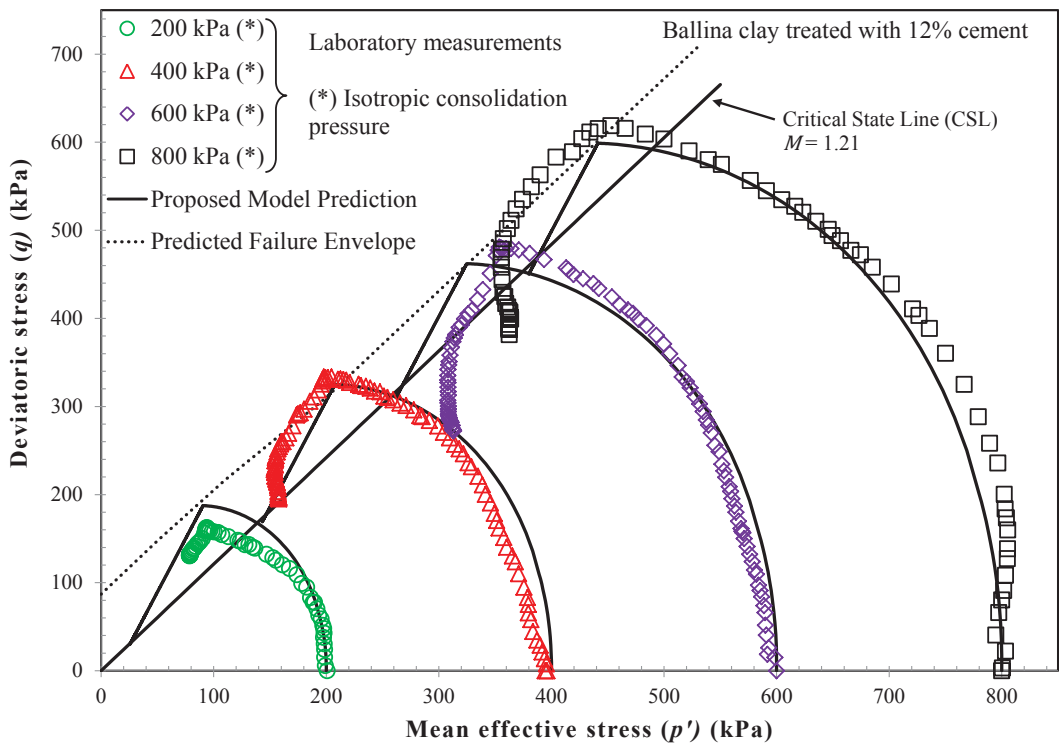


Figure 5.4 Predicted stress paths of undrained triaxial tests of 12% cement treated Ballina clay

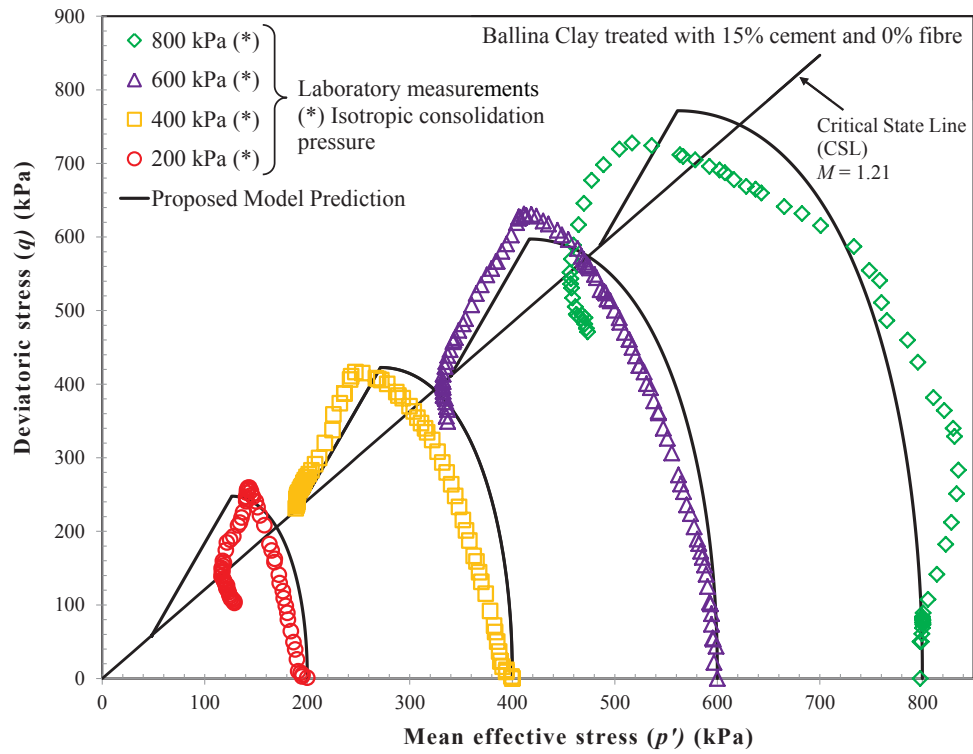


Figure 5.5: Predicted stress paths of undrained triaxial tests of 15% cement treated Ballina clay

In addition, the development of the deviatoric stress ( $q$ ) up to the peak strength was predicted very well by the proposed model, as shown in the stress strain curves in Figures 5.6 – 5.8 for different cement content (i.e. 10%, 12% and 15%). Deviatoric (shear) straining plays an important role on the behaviour of cement treated clays, particularly when the plastic deviatoric strain becomes very large. It can be noted that the effect of cementation degradation due to deviatoric strain after reaching a peak strength state shows a significant crushing of cementation bonds, which results in a sudden reduction in the effect of cementation ( $p''_{\Omega}$ ) as the plastic deviatoric strain continues to increase. The formulation of  $p''_{\Omega}$  in Equation (3.47) was proposed in such a way that  $p''_{\Omega}$  approaches zero as the accumulation of  $\varepsilon_q^p$  becomes very large. For instance, the proposed model simulated the diminishing effect of cementation degradation of 10% cement treated Ballina clay due to deviatoric strain as the contribution of cementation towards the shear strength approaches a minimal value ( $p''_{\Omega} \approx 0$ ) when  $\varepsilon_q \rightarrow \infty$  as shown in Figure 5.9.

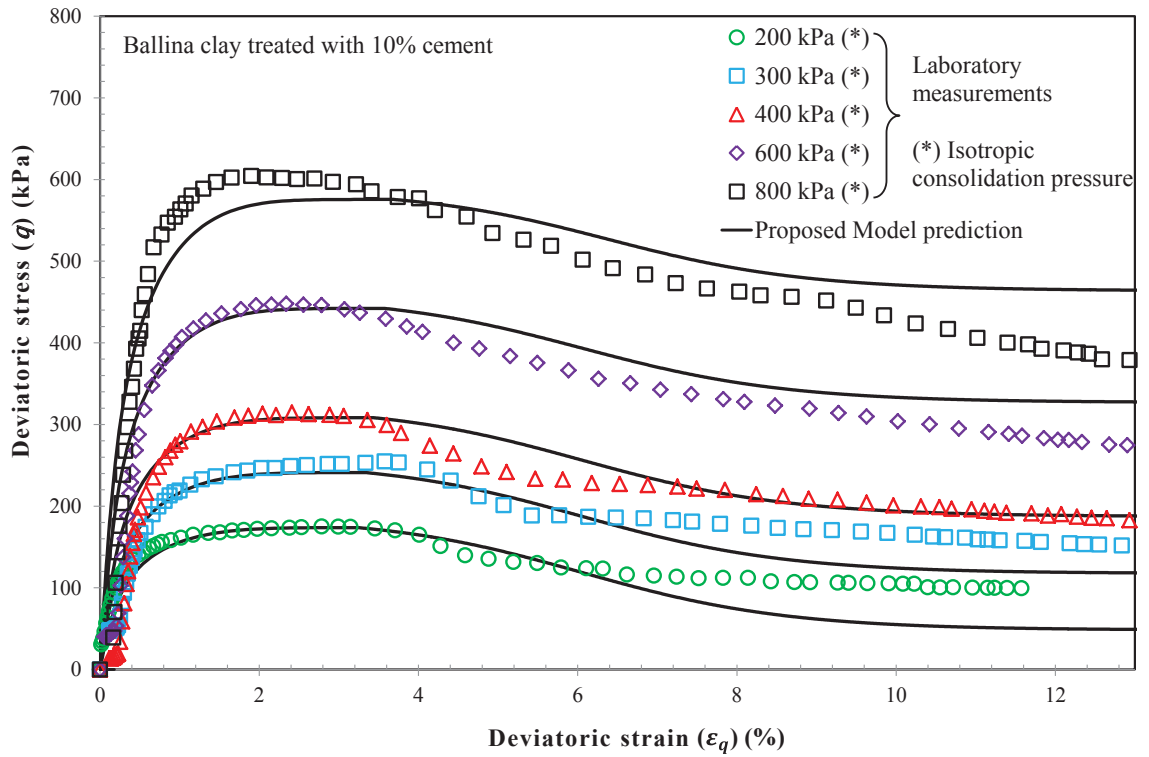


Figure 5.6: Predicted stress-strain curves of undrained triaxial tests of 10% cement treated Ballina clay

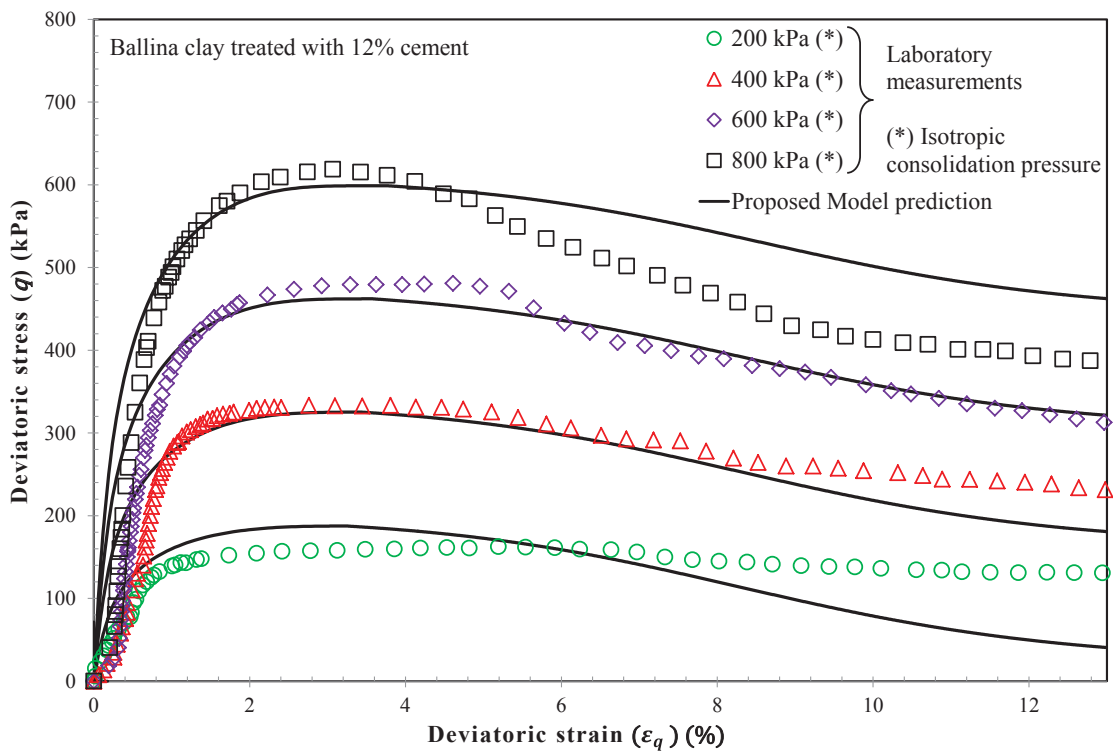


Figure 5.7: Predicted stress-strain curves of undrained triaxial tests of 12% cement treated Ballina clay

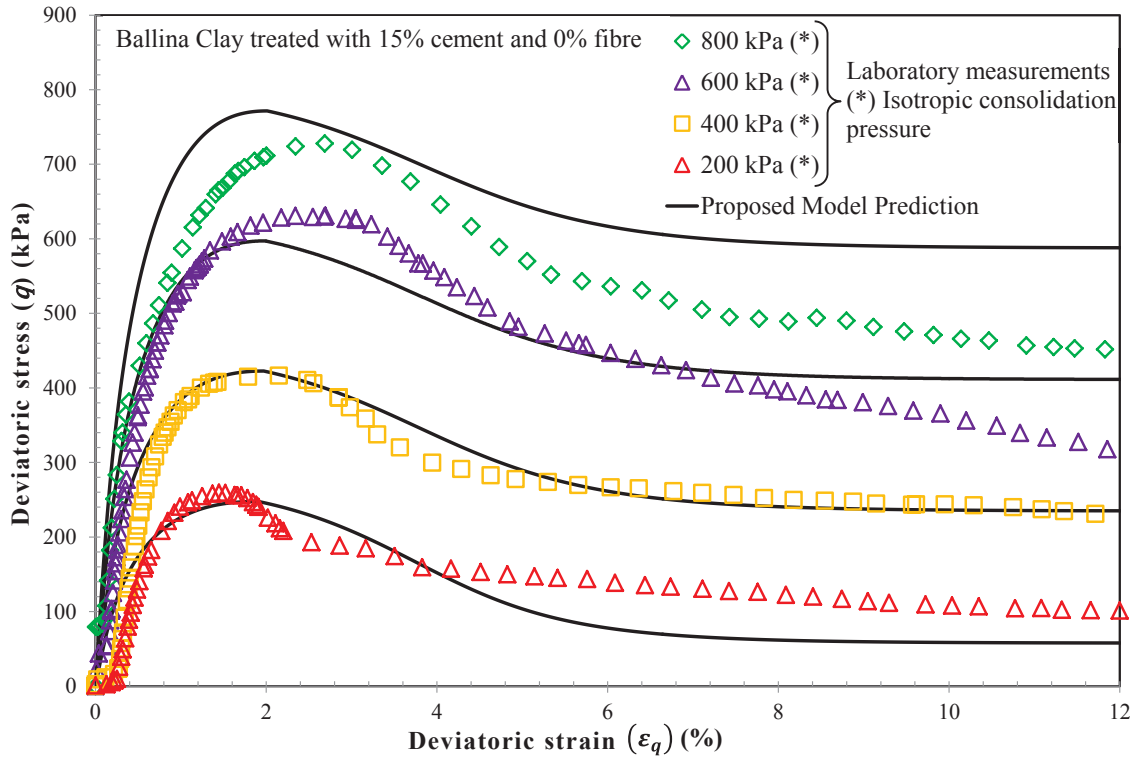


Figure 5.8: Predicted stress-strain curves of undrained triaxial tests of 15% cement treated Ballina clay

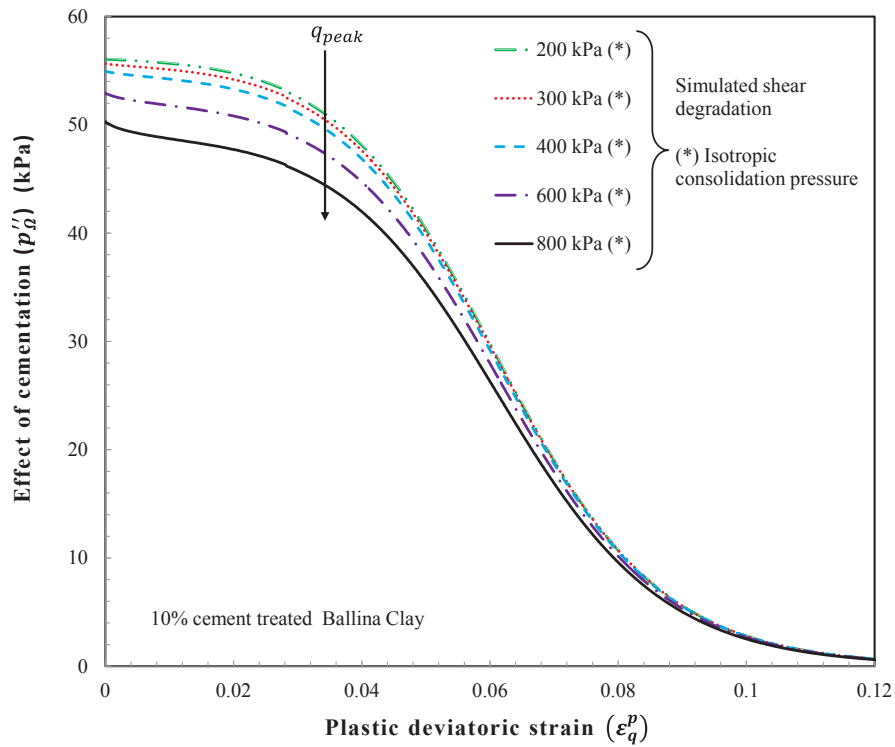


Figure 5.9: Simulated reduction in structure strength due to cementation degradation of 10% cement treated Ballina clay

Moreover, the initial values of  $p''_{\Omega}$  in Figure 5.9 decreased as the mean effective yield stress increased, and thus captures the effect of cementation degradation due to the mean effective yield stress. In addition, the proposed model has simulated the reduction in strength during the softening process reasonably well by accurate estimation of the parameters  $\omega$  and  $b$  which influence the degradation rate due to shear deformation. Although there were some disparities in simulating the softening of cement treated clay, particularly at its residual strength, the transitioning process from the peak to the residual strength state was simulated smoothly by using Equation (3.53). Moreover, the incorporation of  $p''_{\Omega}$  (Equation (3.47)) into  $p'^*$  (Equation (3.48)) to capture the reduced effect of cementation due to cementation degradation in a single equation conveniently simulates the behaviour of cement treated clay in both the pre and post peak states.

Additionally, the development of pore-water pressure in an undrained condition was also predicted well for treated Ballina clay with different cement contents, as shown in Figures 5.10 - 5.12. A pressure transducer was used to measure the pore-water pressure at the bottom of the sample in the triaxial apparatus, and in the proposed model, the pore-water pressure is calculated using the following equations:

$$u = p - p' \quad (5.1)$$

$$p = \frac{\sigma_1 + 2\sigma_3}{3} \quad (5.2)$$

where  $u$  is the actual pore water pressure,  $p$  is the total mean stress, and  $\sigma_1$  and  $\sigma_3$  are the total axial stress and total radial stress, respectively. The value of  $p'$  was calculated using Equations (3.51) and (3.52) for pre and post peak states, respectively. The predictions of excess pore water pressure ( $\Delta u$ ) stem from the difference between the actual and the initial values of pore water pressure.

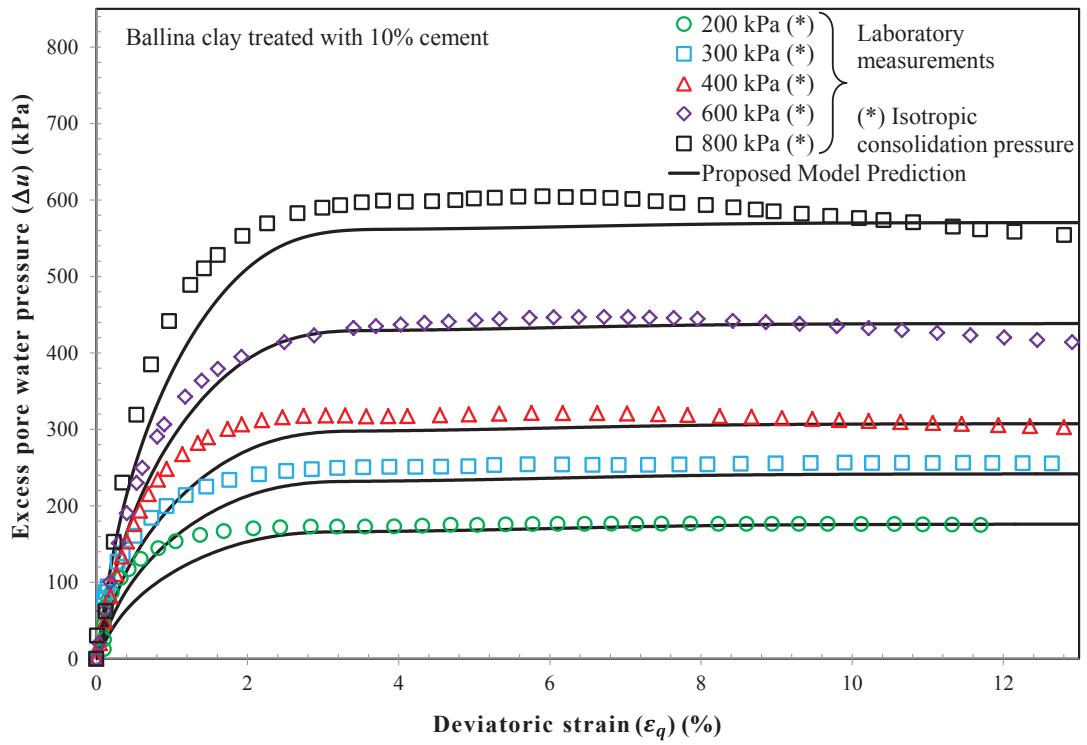


Figure 5.10 Predictions on the excess pore water pressure response of the Ballina clay treated with 10% cement

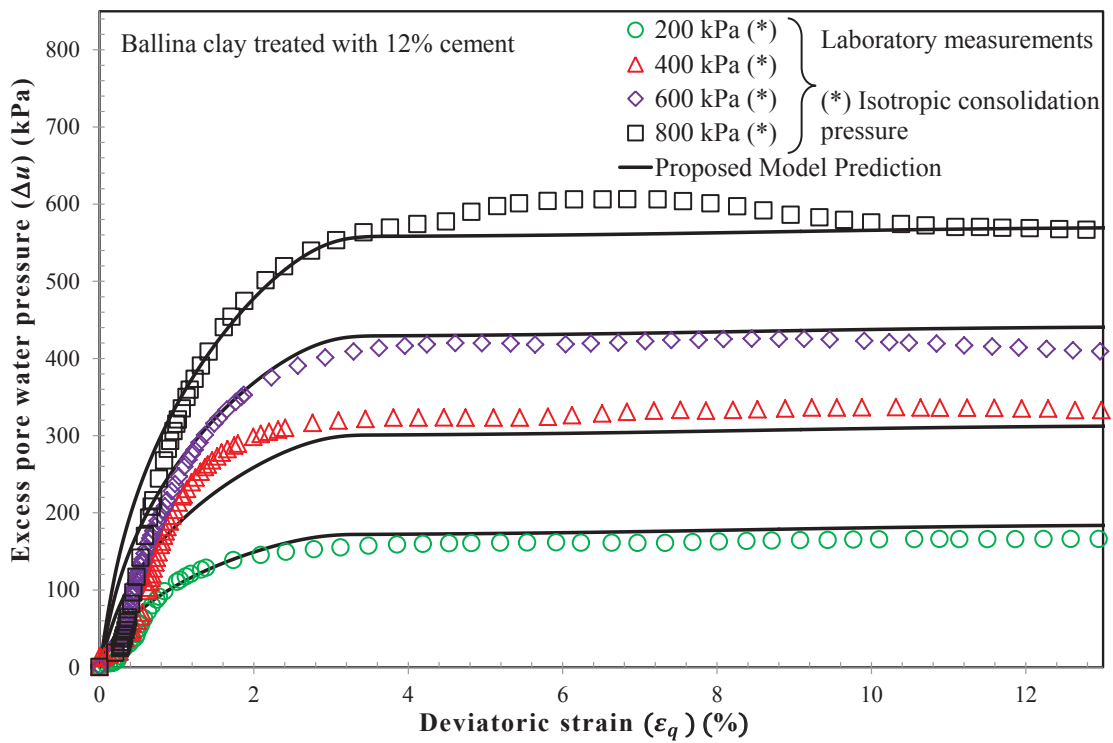


Figure 5.11: Predictions on the excess pore water pressure response of the Ballina clay treated with 12% cement

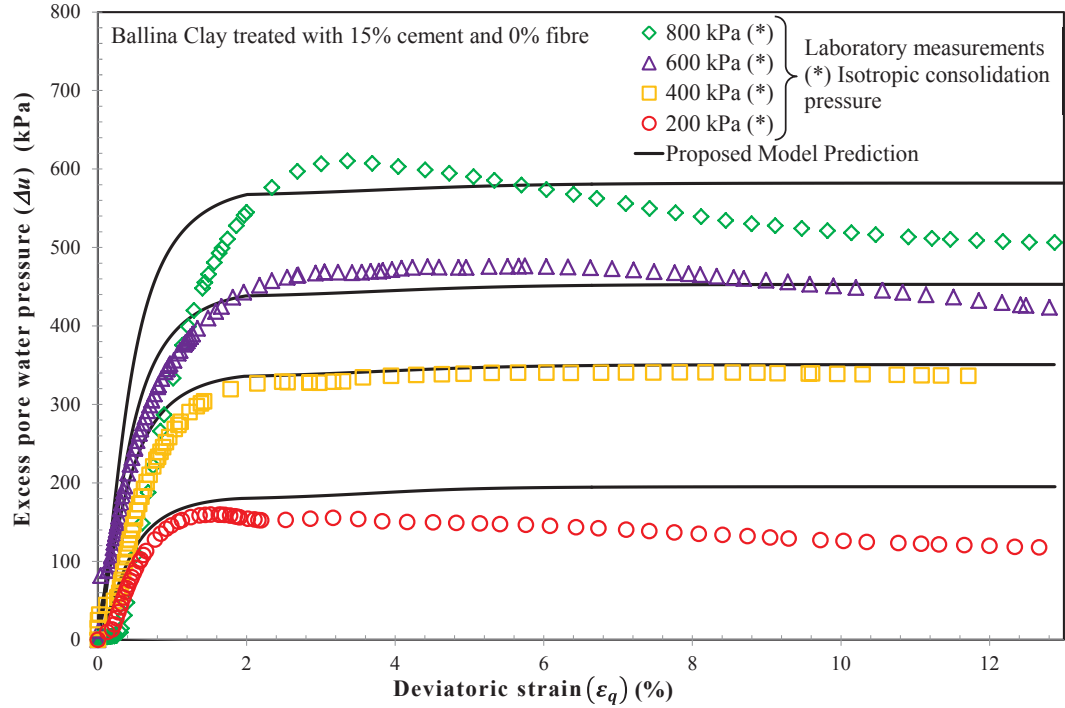


Figure 5.12: Predictions on the excess pore water pressure response of the Ballina clay treated with 15% cement

### 5.3.1.3. Drained Triaxial Compression

The proposed model was further verified by comparing its predictions with the laboratory measurements for drained triaxial tests for Ballina clay treated with differing cement contents (i.e. 10%, 12% and 15%). Figures 5.13 - 5.18 show the model predictions against the test data in terms of the stress path and the stress-strain curves. Moreover, Equations (3.51) and (3.52) were adopted in the model predictions to calculate the total volumetric and deviatoric strain increments, respectively. The same set of model parameters reported in Table 5.1 was used to simulate the drained behaviour. For different cement contents, an increasing  $p'_0$  causes an increase in the peak deviatoric stress ( $q_{peak}$ ). As shown in Figures 5.13 – 5.15, the predicted stress paths rise linearly upward with increasing in mean effective yield stress (slope of  $q = 3p'$ ) as the pore water is allowed to drain. The predicted peak shear strength of cement treated Ballina clay is slightly above the CSL of the reconstituted soil-cement mixture; capturing significant breaking of cementation bonds prior to the peak strength state.

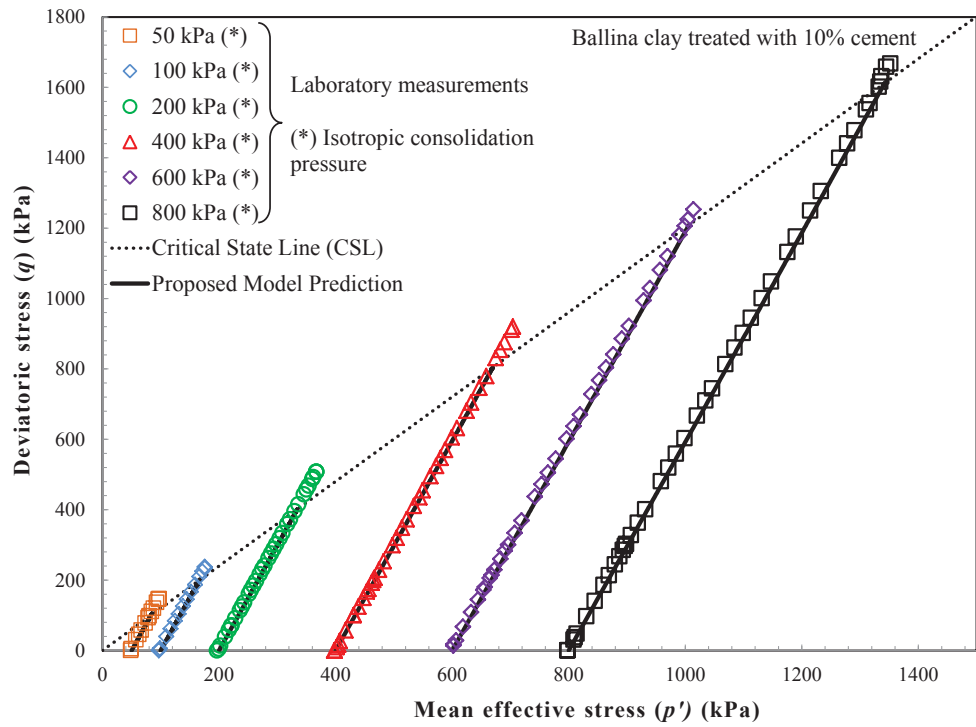


Figure 5.13: Predicted stress path of drained triaxial tests of 10% cement treated Ballina clay

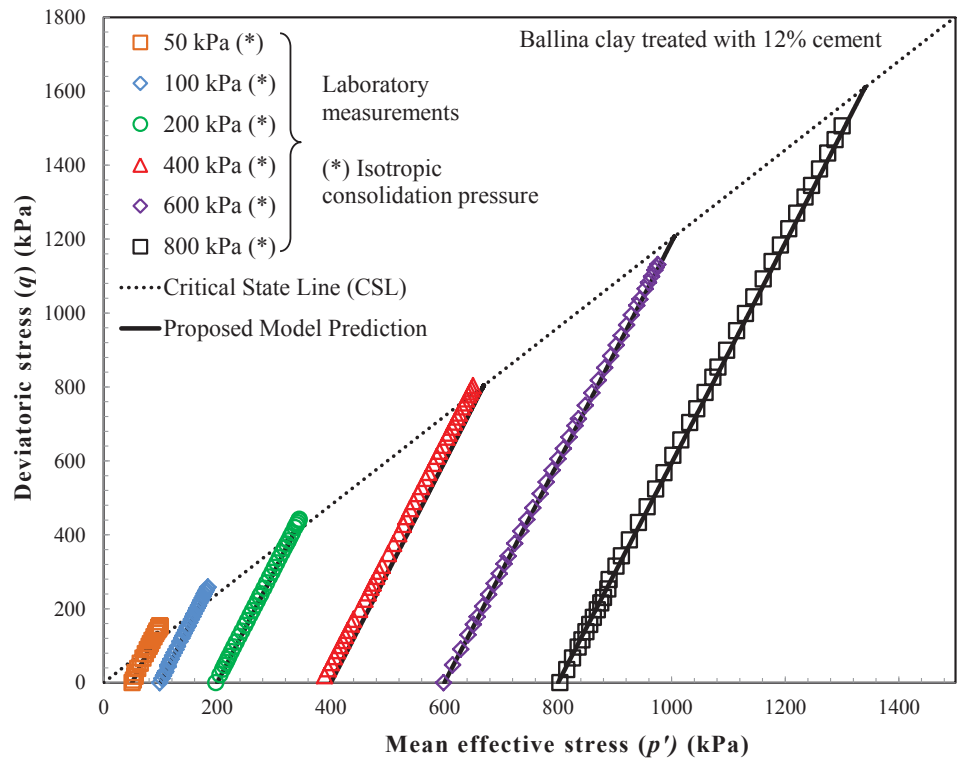


Figure 5.14: Predicted stress path of drained triaxial tests of 12% cement treated Ballina clay

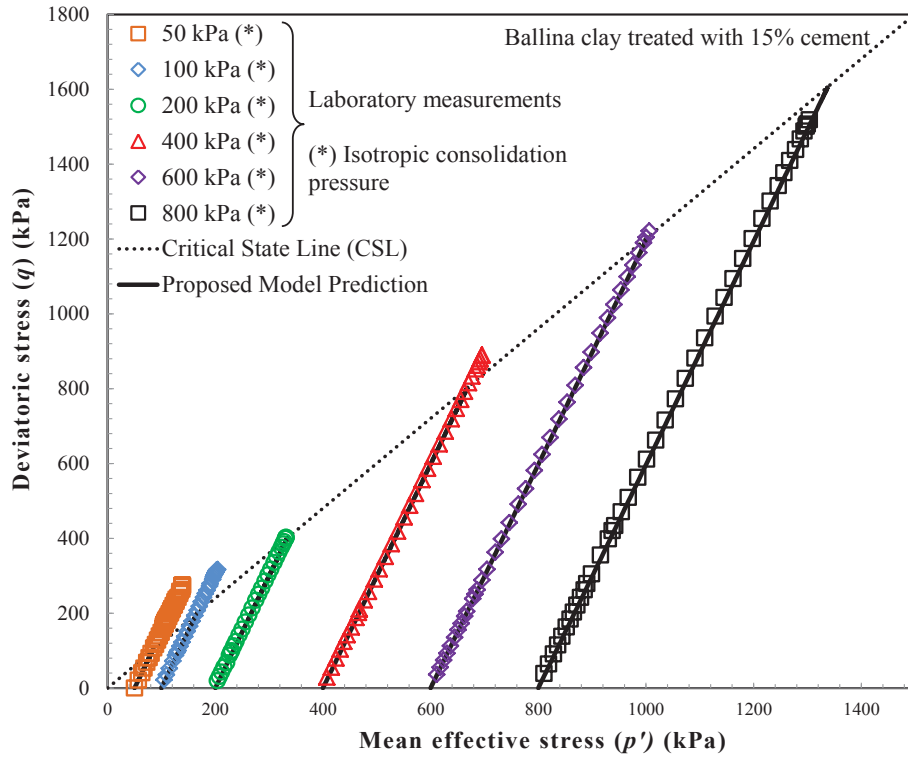


Figure 5.15: Predicted stress path of drained triaxial tests of 15% cement treated Ballina clay

Furthermore, as Figures 5.16 – 5.18 show, the proposed model simulated the behaviour of cement treated Ballina clay very well. It can be noted that, the effect of cement content in drained condition is considered by adopting the accurate estimation of the parameter  $C_c$  in undrained condition. Moreover, as water drainage is allowed,  $p'_0$  keeps increasing resulting to significant reduction in the effect of cementation ( $p''_{\Omega}$ ) formulated in Equation (3.47). Thus, this leads to better prediction on the behaviour of cement treated clay capturing significant cementation degradation in drained condition as described in Section 4.4.3.1.4. However, there are some disparities between the model predictions and the test data, particularly at low stress range (i.e.  $p'_0 = 50$  kPa and 100 kPa) for different cement content. In fact, for 15% cement content, Figure 5.18 showed that the proposed model under-estimated the shear strength of the cement treated clay quite considerably. It may be due to high degree of over-consolidation in low stress range when higher cement content is used. Moreover, Kamruzzaman et al. (2009) observed the heavily over-consolidated behaviour of cement treated clay in low pressure range. However, for 10% and 12% cement content, the proposed model can

simulate the slight softening behaviour exhibited beyond  $\varepsilon_q = 10\%$ , as shown in Figures 5.16 and 5.17. Overall, despite the limitation of the proposed model in low stress range, the proposed model can capture the important features of the behaviour of cement treated clay in drained condition by using the same set of model parameters adopted in undrained condition. It should be noted that, the main objective of the proposed model is to simulate the behaviour of cement treated clay capturing the effect of cementation degradation, particularly at high mean effective yield stress.

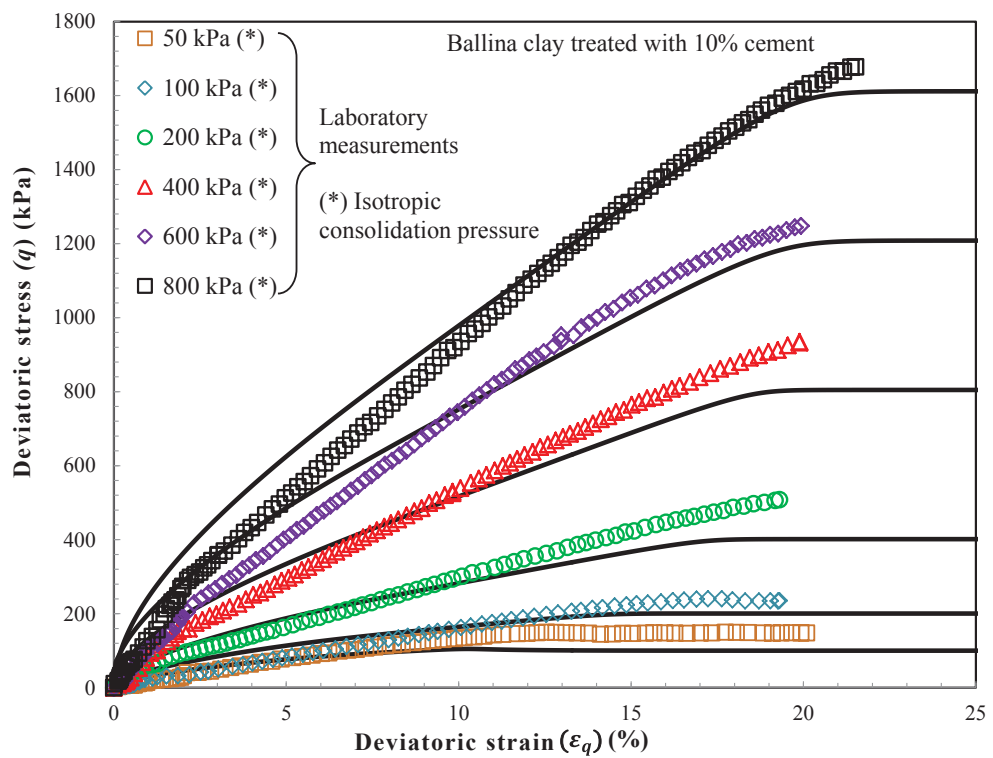


Figure 5.16: Predicted stress-strain curves of drained triaxial tests of 10% cement treated Ballina clay

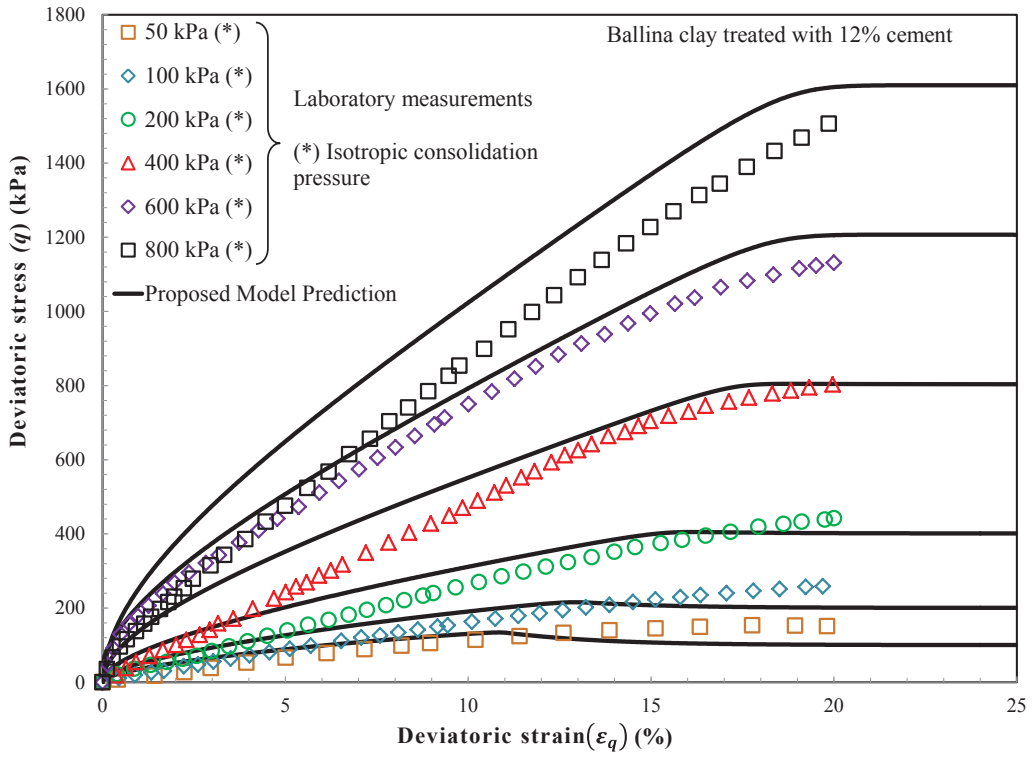


Figure 5.17: Predicted stress-strain curves of drained triaxial tests of 12% cement treated Ballina clay

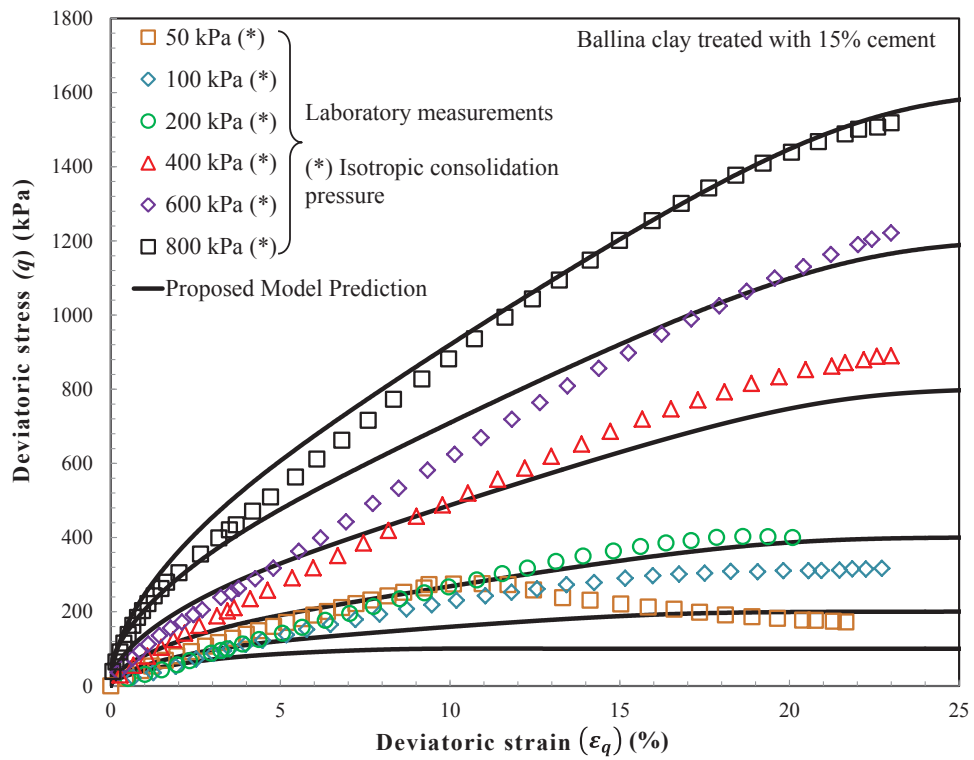


Figure 5.18: Predicted stress-strain curves of drained triaxial tests of 15% cement treated Ballina clay

### 5.3.2. Improved Ballina Clay Composite

In this section, the performance of the proposed model (described in Section 3.3) is evaluated by comparing the model predictions with the experimental results of the 15% cement treated Ballina clay reinforced with different fibre contents (i.e. 0.3% and 0.5%) reported in Section 4.4.3.2. The model parameters are estimated following the procedure described in Section 5.2 and summarised in Table 5.2. The simulation results are displayed in Figures 5.19 – 5.25 in terms of  $e - \ln p'$ ,  $p' - q$ ,  $\varepsilon_q - q$ , and  $\varepsilon_q - \Delta u$  plane. It can be noted that, the model parameters associated with the effect of cementation and its degradation (i.e.  $C_c$ ,  $\beta$ ,  $\omega$ ,  $b$ ) are estimated using the set of undrained triaxial test results conducted on 15% cement treated Ballina clay without fibre reinforcement as summarised in Table 5.1.

#### 5.3.2.1. Isotropic compressibility for FRCS (Ballina clay composite)

In implementing the proposed model and the procedures described in Section 5.2, the prediction of compressibility of Ballina clay with 15% cement and differing amounts of fibre agreed with the results of experimental isotropic compression. The contribution of cementation to the initial yield stress was presented by the parameter  $p'_{\Omega,i}$  which can be calculated adopting Equation (3.9). The prediction assumed that the void ratio of the soil composite would approach the *A*-line (in Figure 5.19) after a significant amount of cementation bonds broke at high mean effective stress. Furthermore, the fabric change parameter ( $\Delta_s = 0.47$ ) was estimated using Equation (3.10) which also defined the position of the *A*-line, located above the ICL of the reconstituted composite mixture (*B*-line). Since the effect of fibre reinforcement in isotropic compression is insignificant, the ICL of the improved clay composite is assumed to follow that of the cement treated clay. The simulation result showed that the compressibility of the FRCS can be captured successfully adopting the proposed model.

Table 5.2: Model values for the improved Ballina clay composite

	15% cement only	15% cement + 0.3% fibre	15% cement + 0.5% fibre
$M$		1.21	
$\lambda$		0.363	
$\kappa$		0.0355	
$p'_{o,i}$ (kPa)		149.92	
$\xi$		0.66	
$C_c$ (kPa)		120	
$\beta$ (kPa)		3125	
$\nu$		0.25	
$\omega$		65	
$b$		3.2	
$\Delta s$		0.19	
$e_0$	3.12	3.10	3.05
$\alpha$	-0.11	0.65	0.98
$C_f$ (kPa)		57	80
$a_{sf}$		0	0
$\delta_{sf}$	N/A	27°	27°
$q_c$ (kPa)		480	497
$m$		0.21	0.26
$n$		0.0081	0.0074

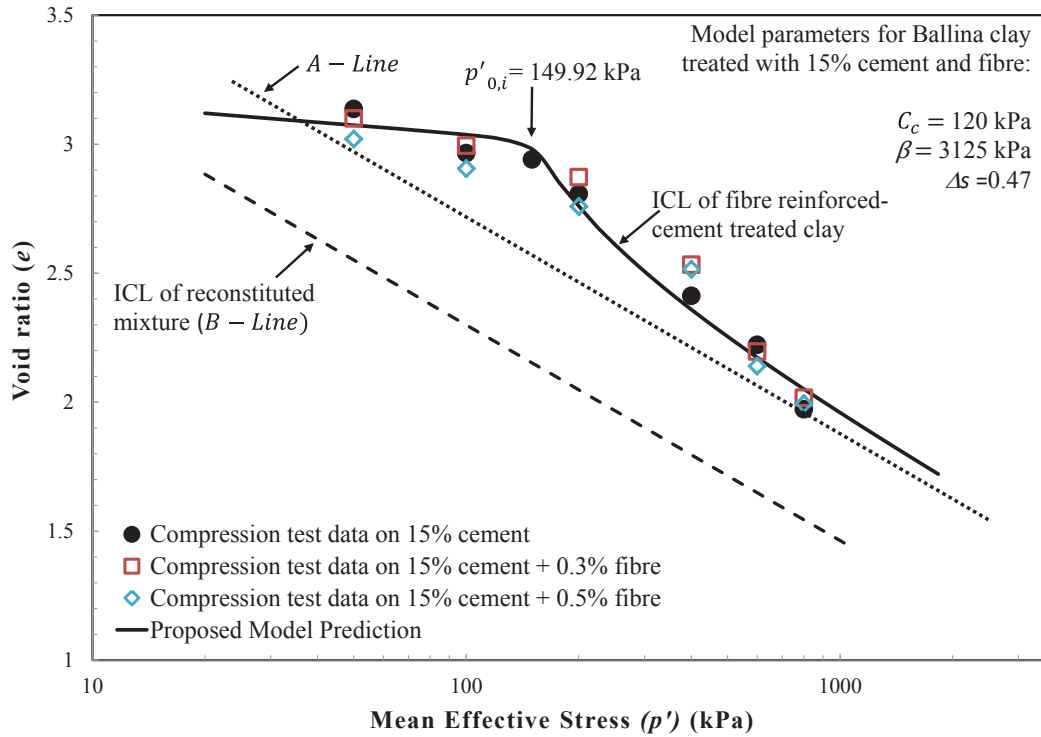


Figure 5.19: Predictions on the isotropic consolidation test result of the Ballina clay treated with 15% cement and fibre contents of 0%, 0.3% and 0.5%.

### 5.3.2.2. Undrained Triaxial Compression for FRCS ( Ballina clay composite)

The proposed model was validated by comparing its predictions with the undrained triaxial tests on improved Ballina clay at different mean effective yield stress (i.e.  $p'_0 = 200, 400, 600$  and  $800$  kPa) in  $p' - q, \varepsilon_q - q$  planes and with excess pore water pressure. The parameters of this model were determined by following the procedures set out in Section 5.2, and the values are summarised in Table 5.2. In the model predictions, the stress-strain relationship of the improved Ballina clay composite were simulated adopting Equations (3.88) and (3.89) for the total volumetric ( $d_v$ ) and deviatoric ( $d_\varepsilon$ ) strain increments, respectively. Moreover, the modified mean effective stress ( $p'^*$ ) to include the combined effect of cementation and fibre, together with their degradations can be found in Equation (3.87).

The model predictions of the undrained stress paths are shown in Figures 5.20 and 5.21 for 0.3% and 0.5% of fibre, respectively, and the stress-strain relationships are simulated in Figures 5.23 and 5.24. It can be noted that, the simulation results for 15% cement treated Ballina clay with 0% fibre can be found in Section 5.3.1. Since all the samples were sheared with an isotropic consolidation pressure greater than the initial mean effective yield stress ( $p'_{0,i} = 149.92$  kPa), the stress state is on the current yield surface. The effect of increasing mean effective yield stress ( $p'_0$ ) on the yield surface of the 15% cement treated Ballina clay reinforced with 0.5% fibre is shown in Figure 5.22. It can be noted that the initial yield surface of the FRCS can be derived using Equation (3.62) with  $p'_0$  corresponding to the initial mean effective yield stress ( $p'_{0,i} = 149.92$  kPa). The size of the initial yield surface ( $p'^*_{0,i}$ ) can be determined using the following equation:

$$p'^*_{0,i} = p'_{0,i} + p'_{\Omega,i} \quad (5.3)$$

where  $p'_{\Omega,i} = \frac{c_c}{\xi_M}$ , presenting the beneficial contribution of cementation. The effect of fibre reinforcement on the initial size of the yield surface is null due to the absence of the deviatoric stress ( $q = 0$ ). Furthermore, increasing the mean effective yield stress  $p'_0$  results in an expansion of the yield surface. It should be noted that, when the sample is subjected to  $p'_0 > p'_{0,i}$ , plastic deformation occurs resulting in the breaking of cementation bonds. As shown in Figure 5.22,  $p'_{\Omega}$  decreases with increasing  $p'_0$  considering the effect of cementation degradation due to mean effective yield stress.

The proposed model predicted the peak shear strength by considering the combined effects of cementation and fibre and their degradations in the modified mean effective stress (Equation (3.87)) very well. Moreover, when the FRCS reached its peak shear strength all the samples became softer as the shear strength decreased with increasing deviatoric strain. The model predictions captured this softening behaviour reasonably well, particularly with 0.3% and 0.5% of fibre (Figures 5.23 and 5.24). By considering the contribution of fibre ( $C_f$ ) to the shear strength, the residual strength of the improved soil was simulated effectively, so when softening began the sample changed its direction and approached the CSL in the  $p' - q$  plane. For cement treated clay with 0% fibre, the proposed model simulated the reduction in shear strength until it

reached the CSL by assuming that the stress state remains on the proposed failure line (Equation (3.53)) as shown in Figure 5.5. However, for soil improved with 0.3% and 0.5% fibre reached its critical state above the CSL due to the inclusion of fibre (Figures 5.20 and 5.21) adopting the proposed failure line for the improved soil composite (Equation (3.90)).

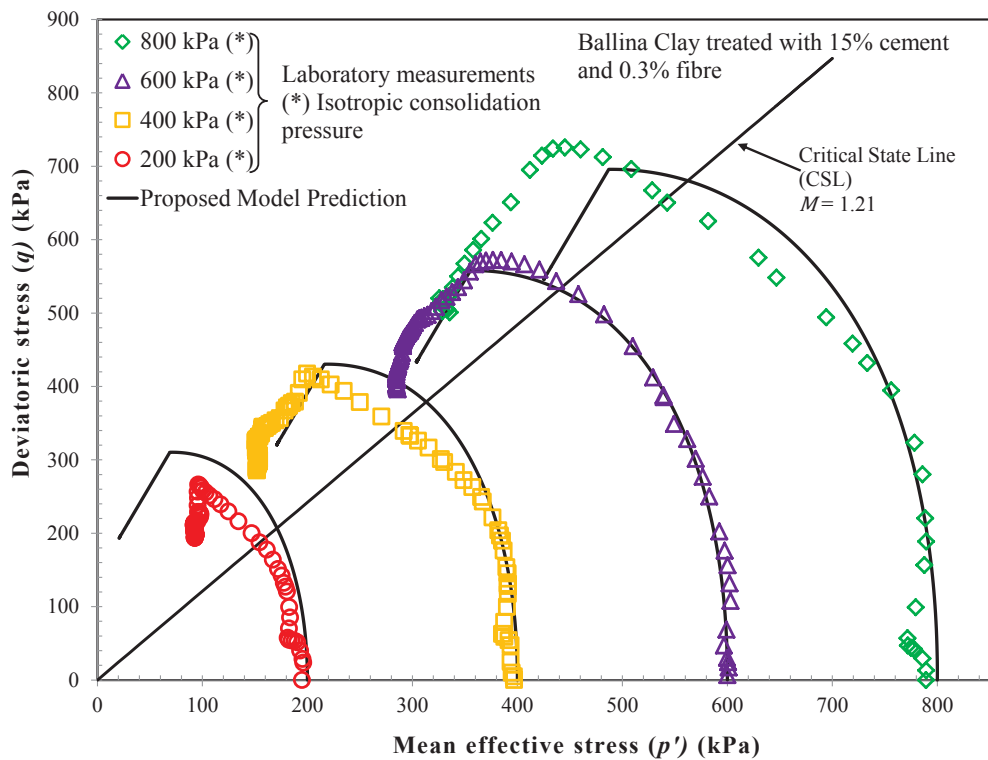


Figure 5.20: Predictions on the stress path curves of the Ballina clay treated with 15% cement and 0.3% fibre

Some disparities were observed in the simulation results, e.g. the peak shear strength values for soil improved with 0.3% and 0.5% fibre were over-predicted at  $p'_0 = 200$  kPa while it was un-predicted at  $p'_0 = 800$  kPa. It can be explained that the peak shear strength of the FRCS depends on the effect of cementation which is represented by the parameter  $C_c$  in the proposed model, while the effect of fibre reinforcement ( $C_f$ ) is more pronounced at the post-peak state where the fibre is fully mobilised. The peak shear strength for sample tested at  $p'_0 = 200$  kPa was predicted adopting the same parameter  $C_c$  determined from the triaxial test results of the cement treated clay without

fibre while the effect of balling or large lumps of fibre during the preparation stage may reduce the formation of cementation bonds which leads to a reduction in the peak shear strength. Besides, at high mean effective yield stress (i.e.  $p'_0 = 800$  kPa), the peak shear strength is influenced by significant breaking of cementation bonds and fibre rupture, resulting in a considerate reduction in the effect of cement and fibre ( $p''_{\Omega}$  and  $p''_f$ ) in the pre-peak stage. Despite this limitation, the transitioning process from the peak to the residual shear strength of the improved soil composite is smoothly simulated for different mean effective yield stress adopting the proposed model, as shown in Figures 5.23 and 5.24.

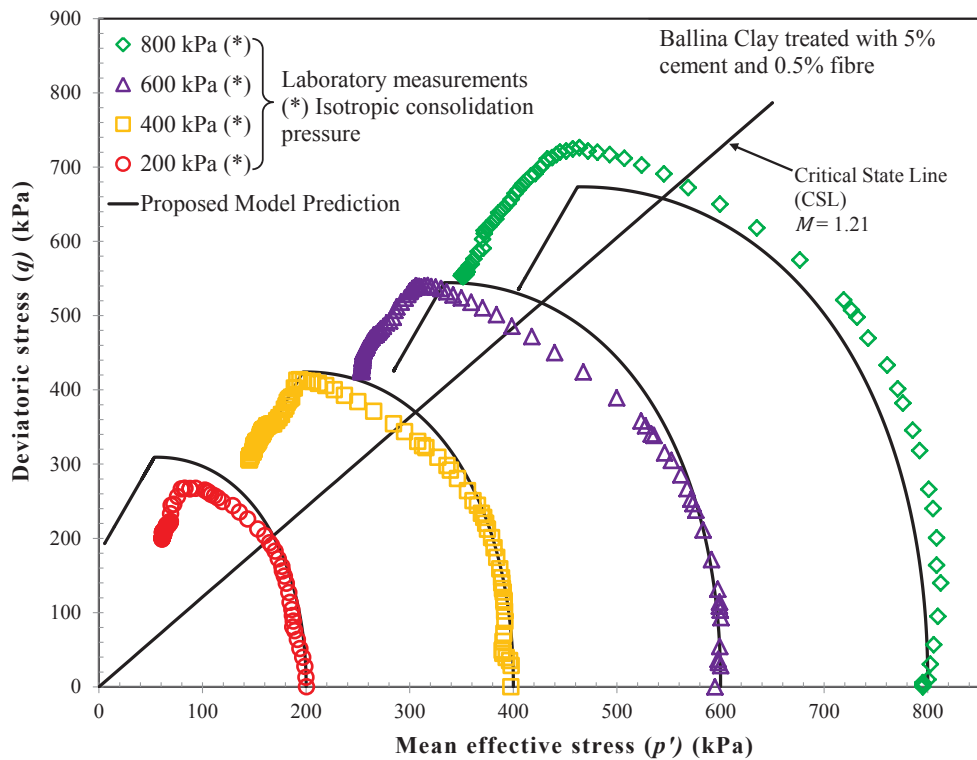


Figure 5.21: Predictions on the stress path curves of the Ballina clay treated with 15% cement and 0.5% fibre

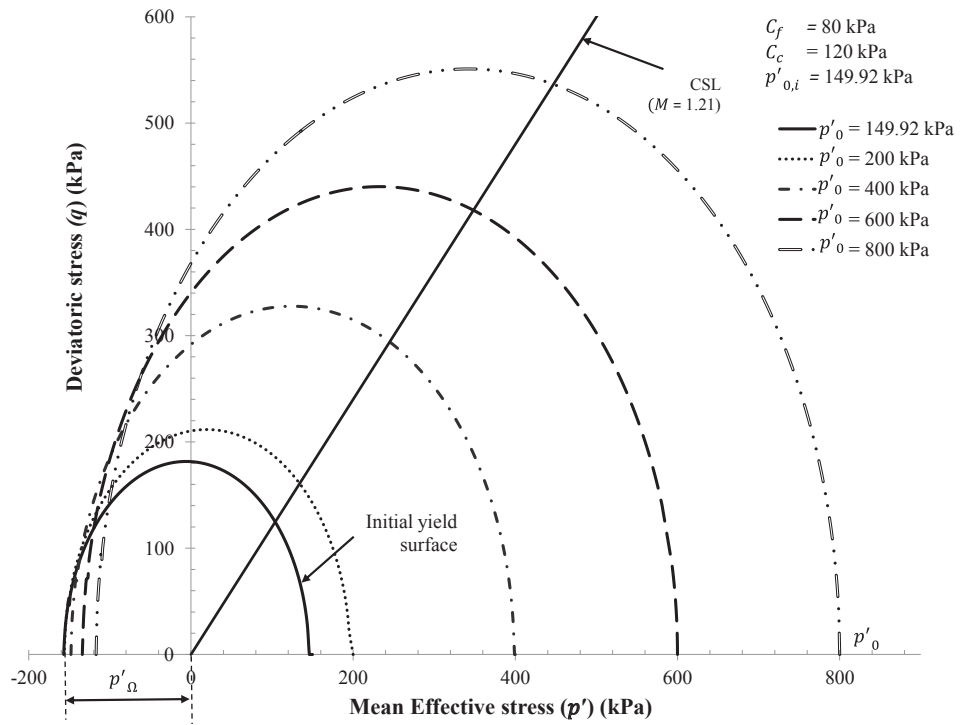


Figure 5.22: Effect of increasing isotropic consolidation pressure ( $p'_0$ ) on the yield surface of the Ballina clay treated with 15% cement and 0.5% fibre.

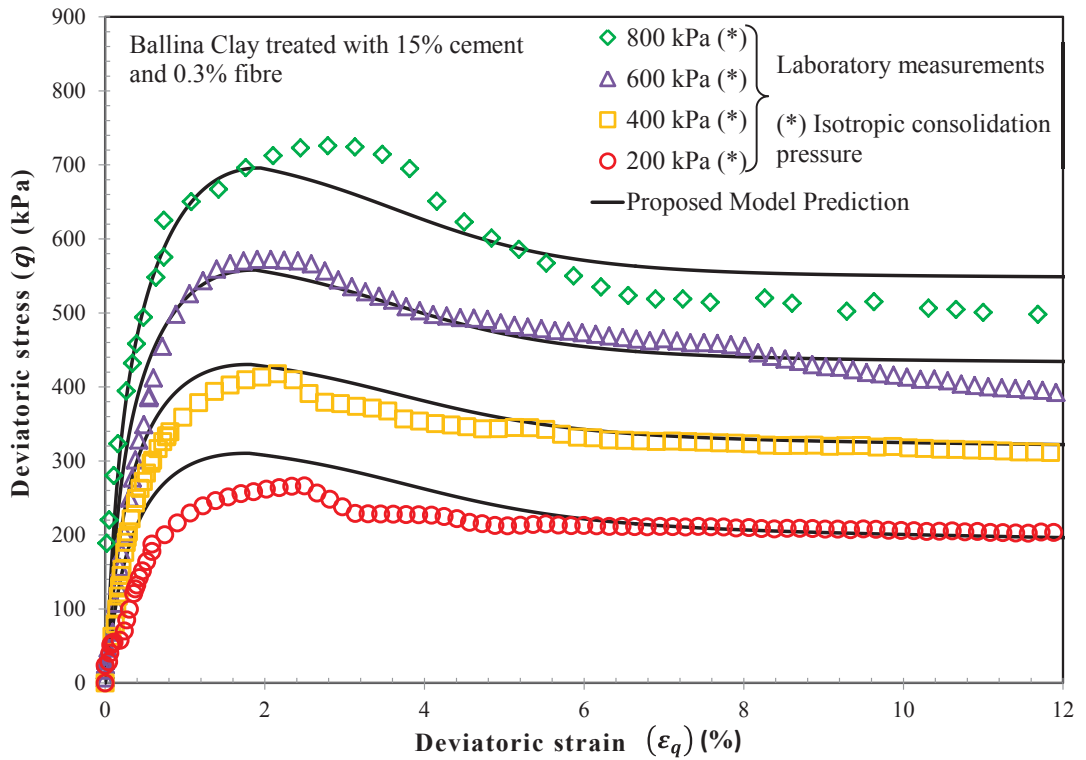


Figure 5.23: Predictions on the stress strain relationship of the Ballina clay treated with 15% cement and 0.3% fibre

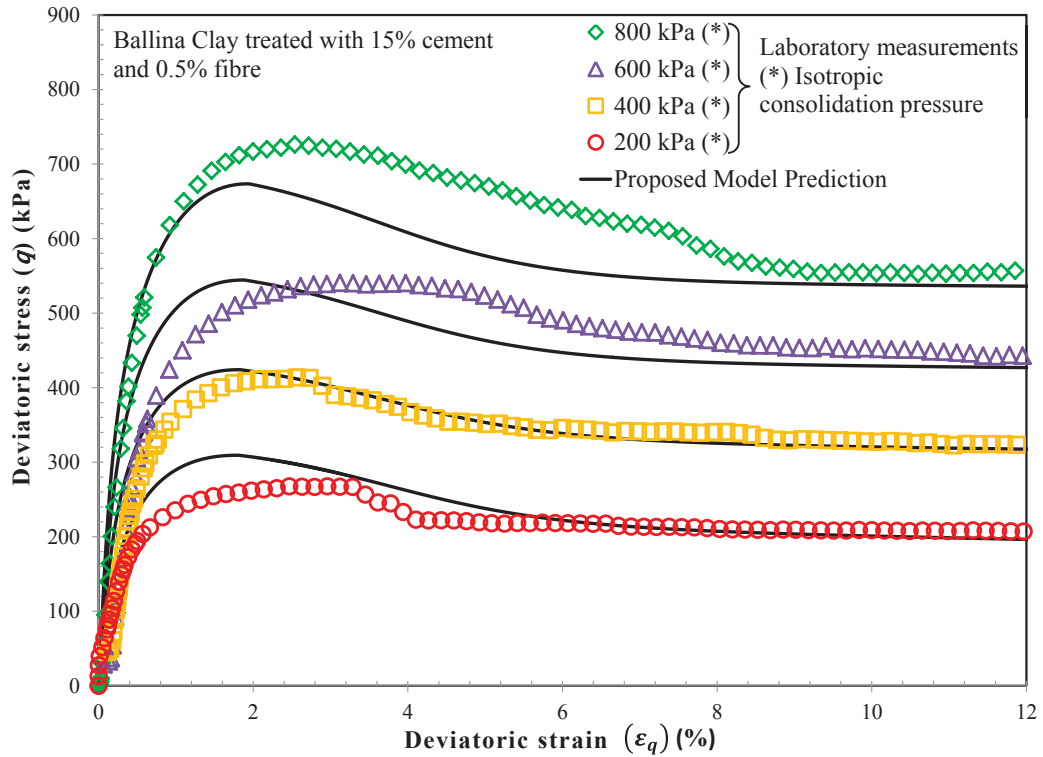


Figure 5.24: Predictions on the stress strain relationship of the Ballina clay treated with 15% cement and 0.5% fibre

Moreover, the predicted excess pore water pressures are shown Figures 5.25 and 5.26 for samples with 0.3%, and 0.5% of fibre, respectively. Equations (5.1) and (5.2) were used to predict the excess pore water pressure response. The proposed model captured the excess pore water pressure response reasonably well by adopting the formulation proposed for the modified mean effective stress ( $p'^*$ ) in Equation (3.87), which led to an accurate prediction of the mean effective stress ( $p'$ ). Overall, the treated Ballina clay became less brittle and more ductile after fibre was added, and its residual strength increased significantly as increasing amounts of fibre were added. Furthermore, the important features of this Ballina clay with differing amounts of fibre such as the peak and residual shear strengths were captured very well using the proposed model.

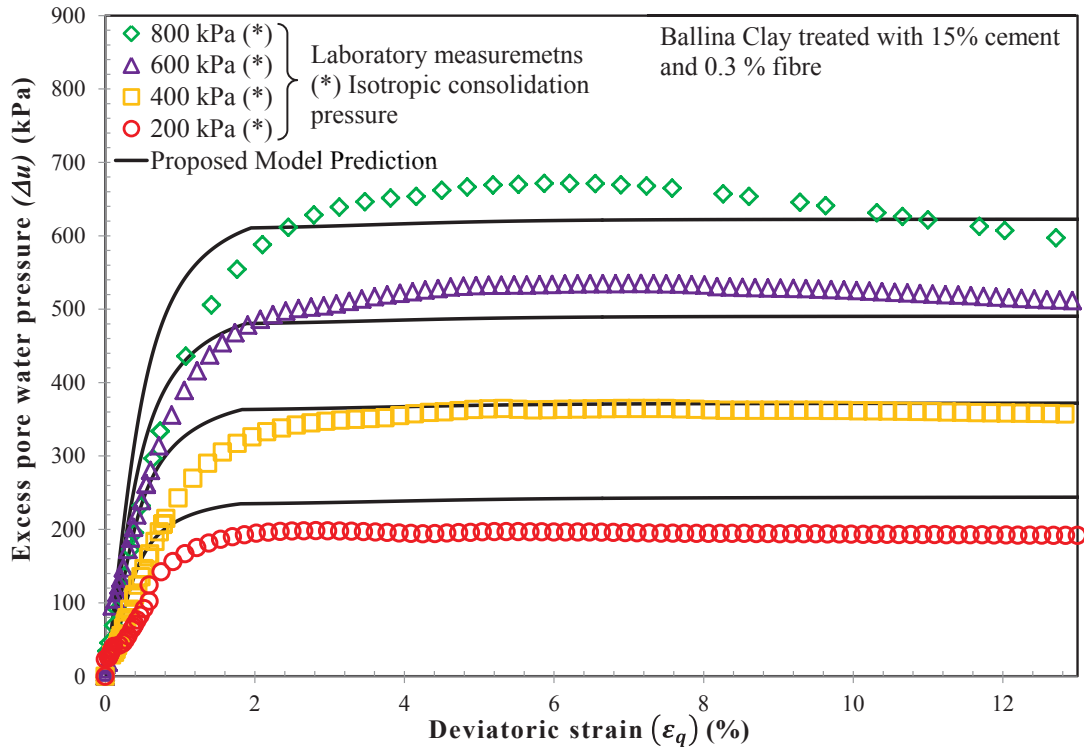


Figure 5.25: Predictions on the excess pore water pressure response of the Ballina clay treated with 15% cement and 0.3% fibre

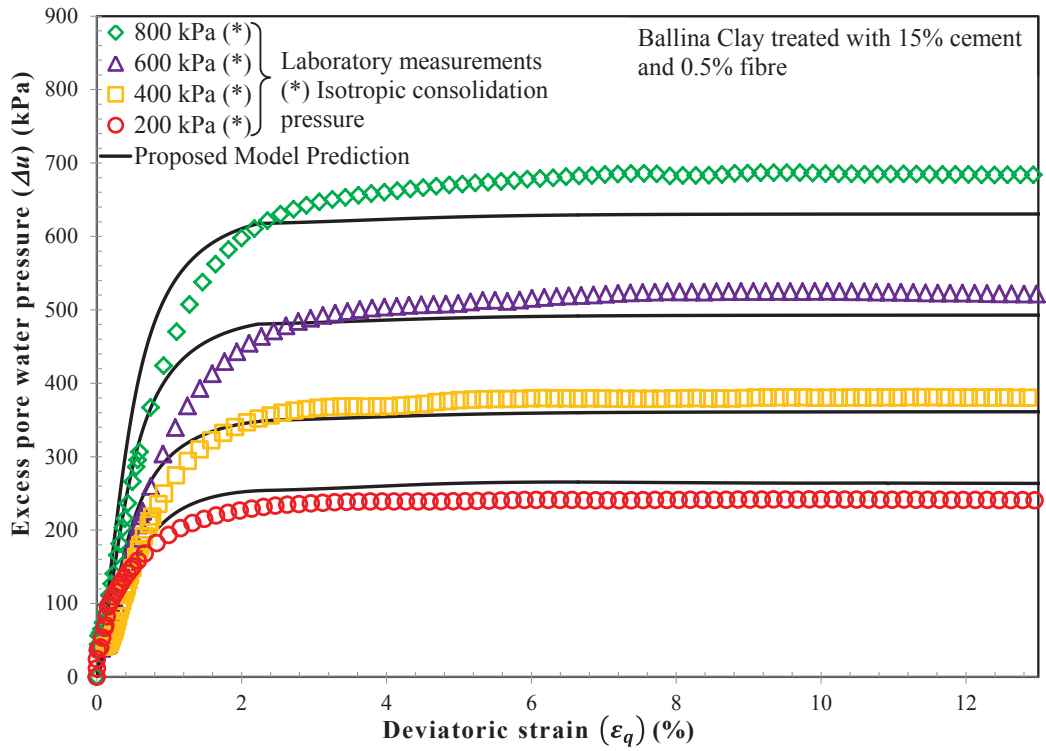


Figure 5.26: Predictions on the excess pore water pressure response of the Ballina clay treated with 15% cement and 0.5% fibre

### 5.3.3. Improved Kaolin Clay Composite

In order to further verify the proposed model and examine the effect of increasing the amount of fibre, a series of undrained triaxial tests were conducted on Kaolin clay treated with 5% cement and differing fibre contents of 0%, 0.3% and 0.5%. In this section, the proposed model is further evaluated by comparing the model predictions with the experimental results (presented in Section 4.4.3.3) in  $e - \ln p'$ ,  $p' - q$ ,  $\varepsilon_q - q$ , and  $\varepsilon_q - \Delta u$  plane. Note that the model parameters in Table 5.3 were obtained in accordance with the procedures described in Section 5.2. Moreover, the parameters associated with cementation are kept the same across cement treated samples with different fibre contents. The simulation results are shown in Figures 5.27 – 5.37.

#### 5.3.3.1. Isotropic Compressibility for FRCS (Kaolin clay composite)

Figure 5.27 shows the results of the isotropic compression tests of the Kaolin clay composite, and indicate that the inclusion of cement increased the initial mean effective yield stress ( $p'_{0,i} = 185$  kPa) compared to the reconstituted soil mixture (B-line) at the same void ratio. The results from the isotropic compression tests (Figure 4.50) were used to determine some of the model parameters described in Section 5.2. In elastic region ( $p' < p'_{0,i}$ ), the proposed model assumes that the improved clay composite sample follows the swelling line with slope  $\kappa$  which can be determined by conducting a conventional isotropic consolidation test. Moreover, within this elastic region, only elastic deformation occurs, so the effect of cementation degradation is negligible. Hence the parameter  $p'_{\Omega,i}$  (Equation (3.9)) representing the effect of cementation is assumed constant with insignificant change in void ratio. Beyond the  $p'_{0,i}$ , the void ratio of improved Kaolin clay composite gradually decreases, which indicates the effect of cementation degradation. At high mean effective yield stress (e.g.  $p'_{0,i} = 800$  kPa), the ICL of the improved soil is assumed to merge with the A-line

defined by the effect of fabric change ( $\Delta s$ ). The value of  $\Delta s = 0.13$  captures the effect of fabric change that cannot be completely destroyed even at high mean effective yield stresses. As explained in Section 4.4.3.3.1, the role of fibre is insignificant in isotropic compression and the reduction in void ratio at the post-yield stage is mainly influenced by the effect of cementation degradation. Hence the compressibility of the improved soil composite can be simulated in a similar way as the cement treated clay. Moreover, as shown in Figure 5.27, the predictions from the proposed model agreed with the test data in the elastic and plastic regions during isotropic consolidation. The model formulation in Equation (3.7) simulated the decreasing void ratio due to an increasing mean effective stress very well, so by using a set of model parameters such as  $\Delta s$ ,  $\beta$ ,  $C_c$ , the change in volume of the improved soil composite can be predicted accurately.

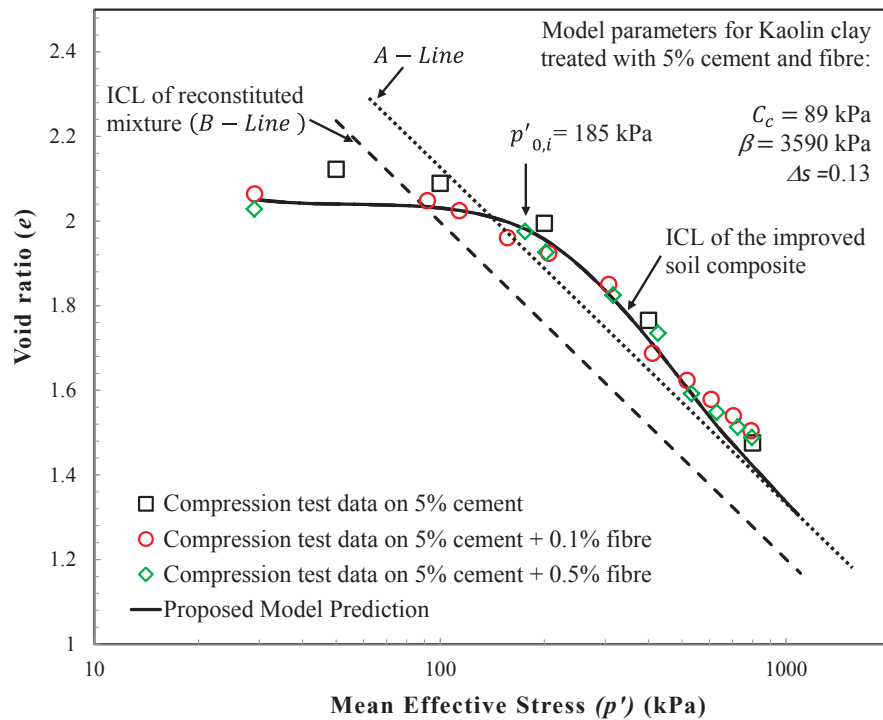


Figure 5.27: Predictions on the isotropic consolidation test result of the improved soil composite

Table 5.3: Model values for the improved Kaolin clay composite

	5% cement only	5% cement + 0.1% fibre	5% cement + 0.5% fibre
$M$		1.09	
$\lambda$		0.346	
$\kappa$		0.048	
$p'_{o,i}$ (kPa)		185	
$\xi$		0.44	
$C_c$ (kPa)		89	
$\beta$ (kPa)		3590	
$\nu$		0.25	
$\omega$		121	
$b$		5.2	
$\Delta s$		0.13	
$e_0$	2.12	2.09	2.07
$\alpha$	-0.22	-0.21	-0.22
$C_f$ (kPa)		120	135
$a_{sf}$		0	0
$\delta_{sf}$	N/A	27°	27°
$q_c$ (kPa)		375	387
$m$		0.64	0.5
$n$		0.01	0.0081

### 5.3.3.2. Undrained Triaxial Compression for FRCS (Kaolin clay composite)

The comparisons between the model predictions and the test results on the 5% cement treated Kaolin clay reinforced with different fibre contents ( i.e. 0%, 0.1% and 0.5%) at different mean effective yield stresses (200, 400 and 800 kPa) in terms of  $p' - q$ ,  $\varepsilon_q - q$  and the excess pore water pressure response are shown in Figures 5.28 – 5.37. Since virgin yielding occurred at 185 kPa ( $p'_{o,i} = 185$  kPa), the stress states of all the samples in an undrained triaxial condition are outside the initial yield surface. Figure 5.28 shows that the proposed failure envelope (Equation (3.53)) captures the peak shear strength of cement treated Kaolin clay sensibly well, considering the effect of cementation degradation due to the mean effective stress and deviatoric strain. Moreover, the general stress-strain relationship for the cement treated clay in Equations (3.51) and (3.52) was used to calculate the relationship between  $p'$  and  $q$  with increasing  $\varepsilon_q$ . The undrained stress paths of the cement treated clay were captured in both hardening and softening processes by accurate estimation of the model parameters following the procedures in Section 5.2. After reaching the peak strength, the predicted stress path changed its direction and travelled on the CSL, indicating the complete removal of cementation bonds.

Futhermore, the stress paths for 5% cement treated Kaolin clay with 0.1% and 0.5% fibre in undrained condition (in  $p' - q$  plane) are shown in Figures 5.29 and 5.30, respectively. Similar to the cement treated clay, the predicted stress paths of the FRCS bends to the left, seeking the peak strength state above the CSL. As concluded in Chapter 4, the peak shear strength of the FRCS depends mainly on the effect of cementation ( $C_c$ ) and the improvement in the residual shear strength is due to the contribution of fibre ( $C_f$ ). When the amount of fibre increased from 0.1% to 0.5%,  $C_f$  of the improved Kaolin clay increased from 120 kPa to 135 kPa, respectively, while the values of  $C_f$  for the cement treated Ballina clay improved with 0.3% and 0.5% were estimated at 57 kPa and 80 kPa, respectively. Hence, the contribution of fibre to the peak and the residual shear strength of Kaolin clay is more pronounced than that in Ballina clay. As shown in Figures 5.29 and 5.30, appropriate estimation of the

parameter  $C_f$  could result in accurate prediction of the shear strength of the improved Kaolin composite.

In addition, the effectiveness of the fibre inclusion reduces with mean effective yield stress due to fibre failure including pull-out and breakage. It can be noted that, the effect of fibre failure mechanisms is considered in modified mean effective stress ( $p'^*$  in Equation (3.87)). When the FRCS is under the mean effective yield stress ( $p'_0$ ) less than the critical mean effective stress ( $p_{crit}^* = 278$  kPa), e.g. for the test where  $p'_0 = 200$  kPa, the sample was assumed to be pulled-out from the clusters of soil and cement as the frictional resistance of the fibre was not fully mobilised. Moreover, where  $p'_0 = 800$  kPa  $\gg p_{crit}^*$ , fibre breakage may occur prior to reaching the peak state, so the effect of fibre reinforcement decreases as shown in improved sample with 0.1% and 0.5% fibre content in Figures 5.29 and 5.30, respectively. Consequently, due to fibre rupture, the effect of fibre reinforcement was diminished, hence the predicted stress path of improved Kaolin clay composite under  $p'_0 = 800$  kPa approached the CSL at the residual state while the predicted stress path of the improved Ballina clay composite was above the CSL. During the softening process, it was observed that the behaviour of the improved Kaolin clay composite was mainly governed by the effect of cementation degradation.

However, it was noticed that the peak shear strength of the improved clay with 0.5% fibre at  $p'_0 = 200$  kPa was over-predicted. It may be due to excessive amounts of fibre that may form large lumps and balling at the preparation stage which may restrict further chemical interaction between the particles of clay and cement. Overall, by considering the effect of cement and fibre reinforcement in  $p'^*$  (Equation (3.87)), the model predictions have simulated the stress path and the peak shear strength of the FRCS and cement treated clay reasonably well while capturing the important combined effect of cement and fibre. The peak shear strength of composite soil was mainly governed by the cementation bonds, while the addition of fibre into the treated clay filled the pore space between clusters of soil and cement and helped to bridge them under shearing, thus increasing its strength.

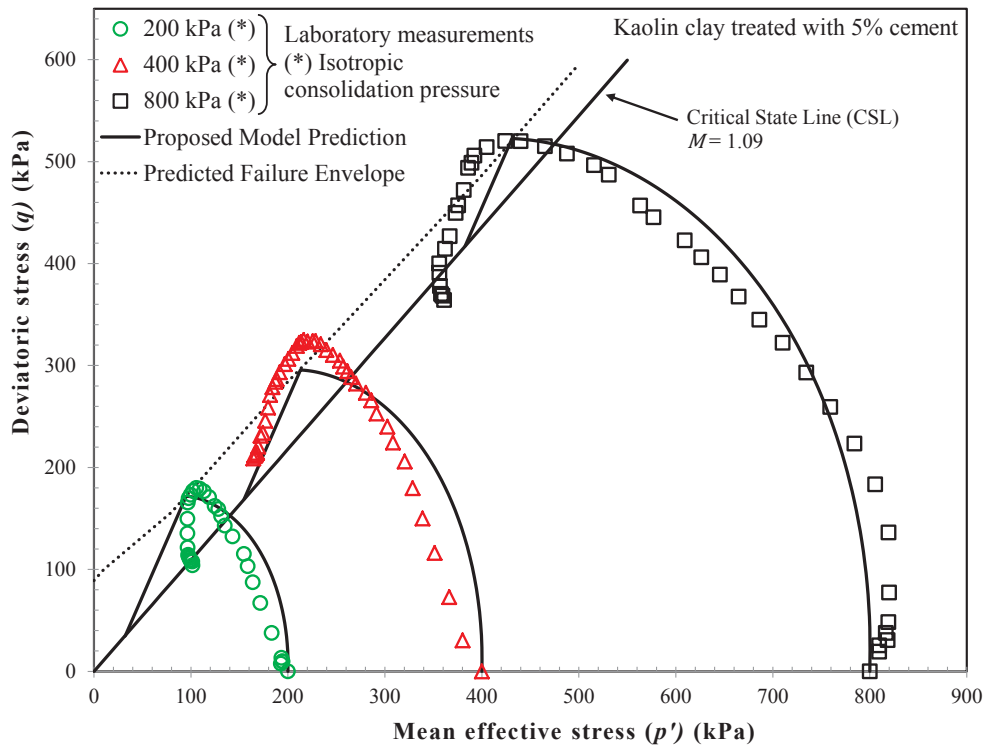


Figure 5.28: Predictions on the stress path of the Kaolin clay treated with 5% cement

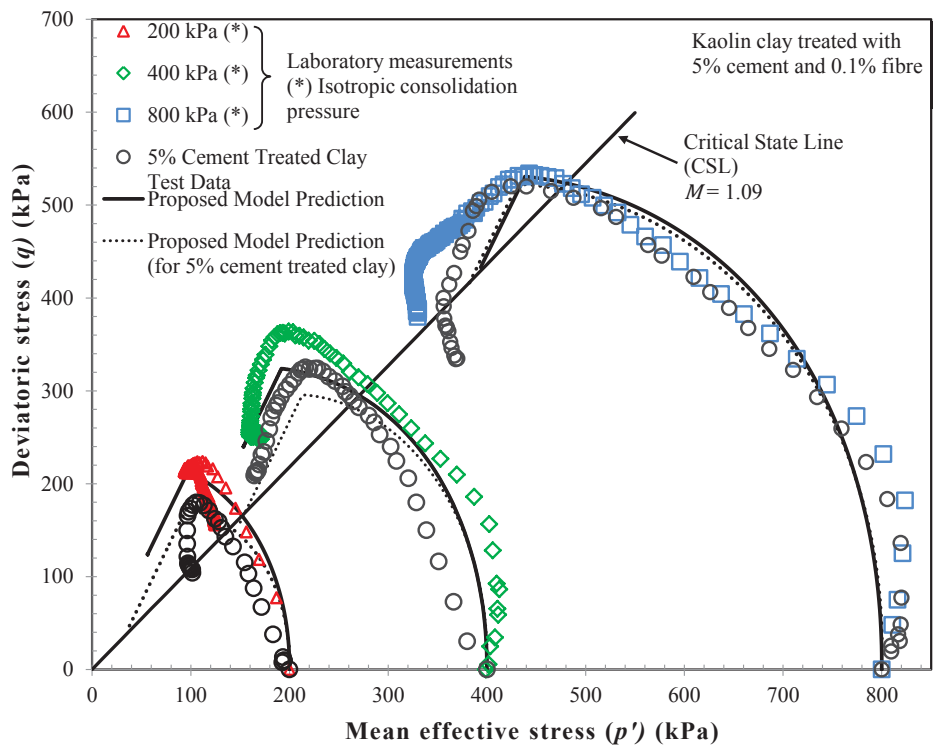


Figure 5.29: Predictions on the stress path of the improved Kaolin composite with 5% cement and 0.1% fibre

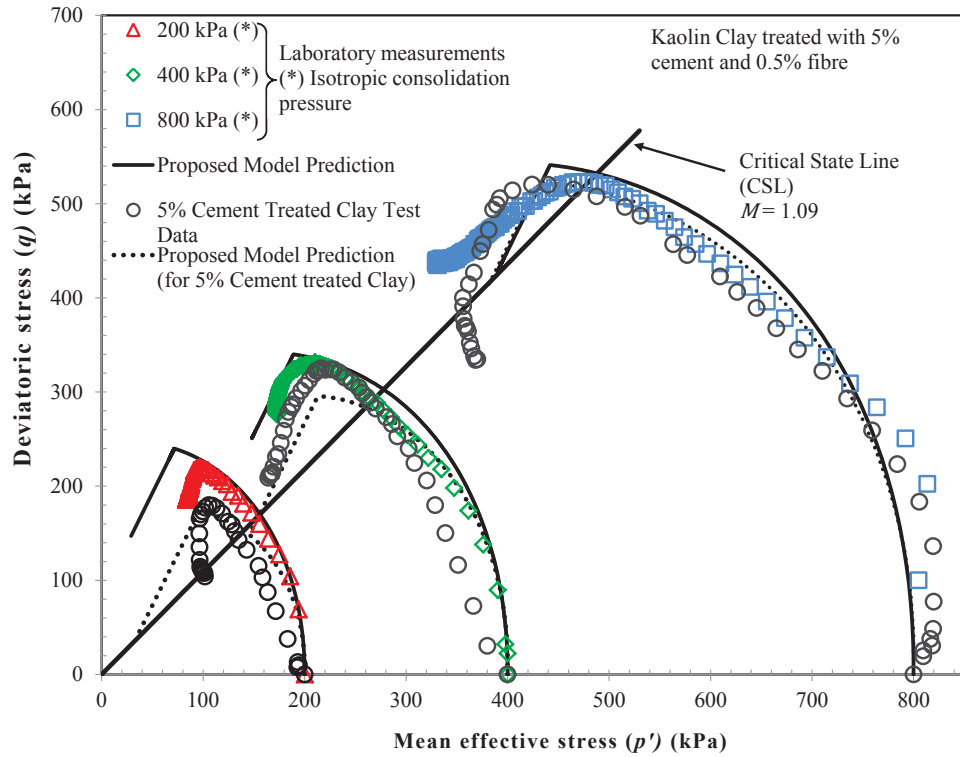


Figure 5.30: Predictions on the stress path of the improved Kaolin composite with 5% cement and 0.5% fibre

The performance of the proposed model can be further evaluated by analysing the predicted stress-strain relationship of the improved Kaolin clay composite with 0%, 0.1% and 0.5% fibre content in  $\epsilon_q - q$  plane which can be found in Figures 5.31 – 5.33. During the softening process the deviatoric stress ( $q$ ) gradually drops as the deviatoric strain ( $\epsilon_q$ ) increases, while the residual shear strength is reached in large deviatoric strains. The model predictions for the stress strain relationship of the improved Kaolin clay composite for all fibre contents show that increasing the mean effective yield stress leads to an increase in the peak and residual shear strength. Moreover, the addition of fibre improved the ductility of cement treated clay because the FRCS achieved a higher residual strength, as also predicted by the proposed model.

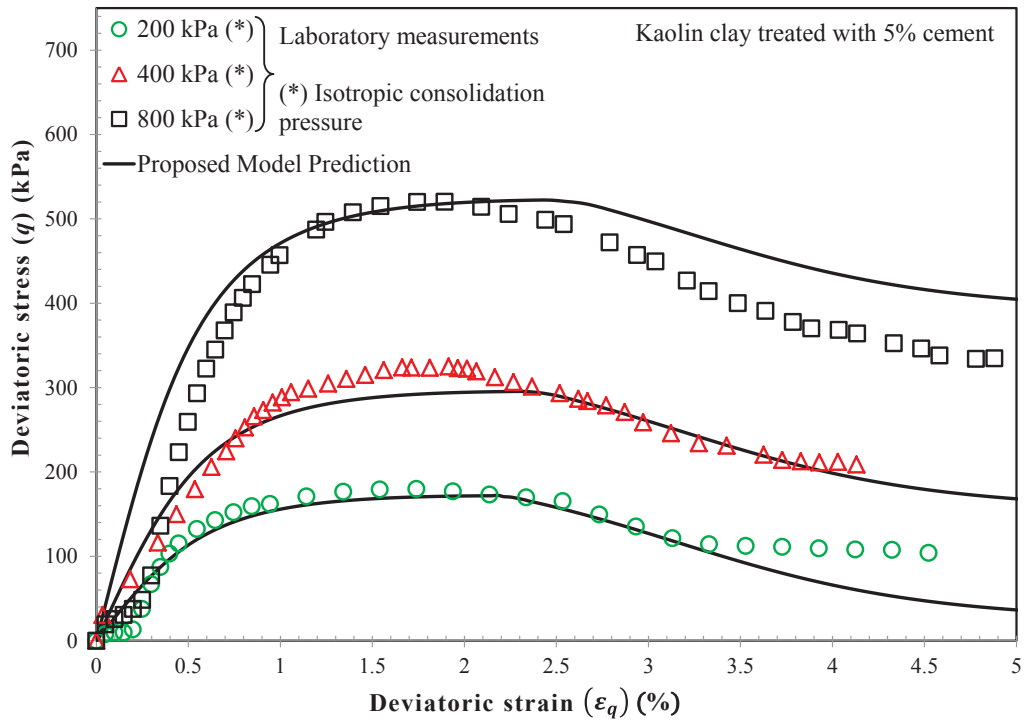


Figure 5.31: Predictions on the stress-strain relationship of the Kaolin clay treated with 5% cement

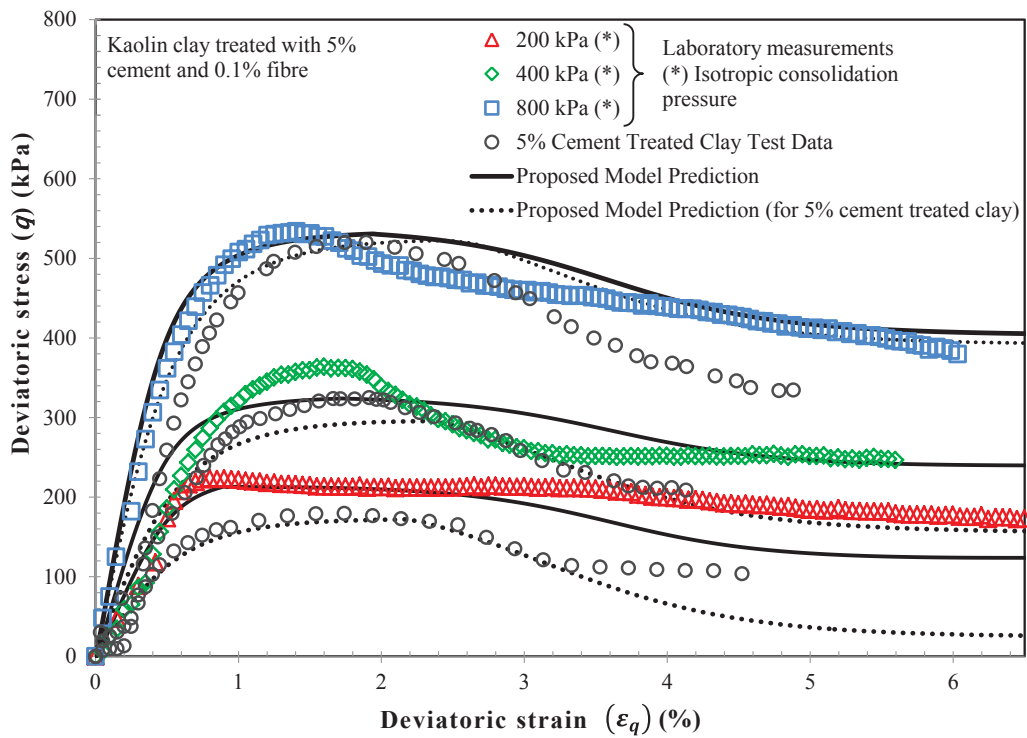


Figure 5.32: Predictions on the stress strain relationship of the improved Kaolin composite with 5% cement and 0.1% fibre.

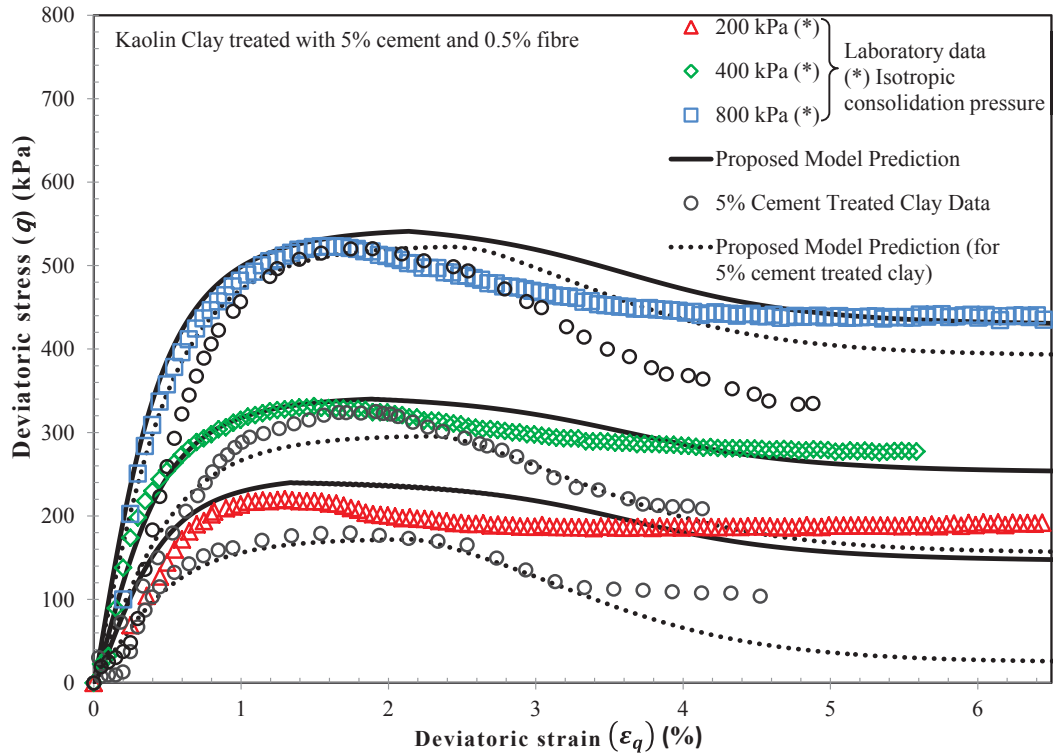


Figure 5.33: Predictions on the stress strain relationship of the improved Kaolin composite with 5% cement and 0.5% fibre

Furthermore, deviatoric straining played a significant role in the behaviour of cement treated clay with or without fibre reinforcement, particularly at large strain. As the plastic deviatoric strain ( $\epsilon_q^p$ ) increased the effect of cementation and fibre contribution ( $p''_{\Omega}$  and  $p''_f$ ) gradually decreased, indicating that the cementation bonds were being crushed and the fibre was failing. Figure 5.34 shows that for Kaolin clay with 0.5% fibre shearing at  $p'_0 = 800$  kPa, the effect of reinforcement approached zero as the sample reached constant residual values at a large deviatoric strain. The proposed model captures the effect of shear deformation due to plastic deviatoric strain in the formulation of  $p'^*$  in Equation (3.87). Note that the transition from peak strength to the residual state was simulated smoothly by an accurate estimation of the model parameters, particularly the parameters  $\omega$  and  $b$  for cementation degradation and the parameters  $m$  and  $n$  for the failure of fibre. Hence, by considering the effect of cementation degradation and fibre failure in Equation (3.87), the proposed model has captured the peak and residual shear strength of Kaolin clay with cement and fibre very well.

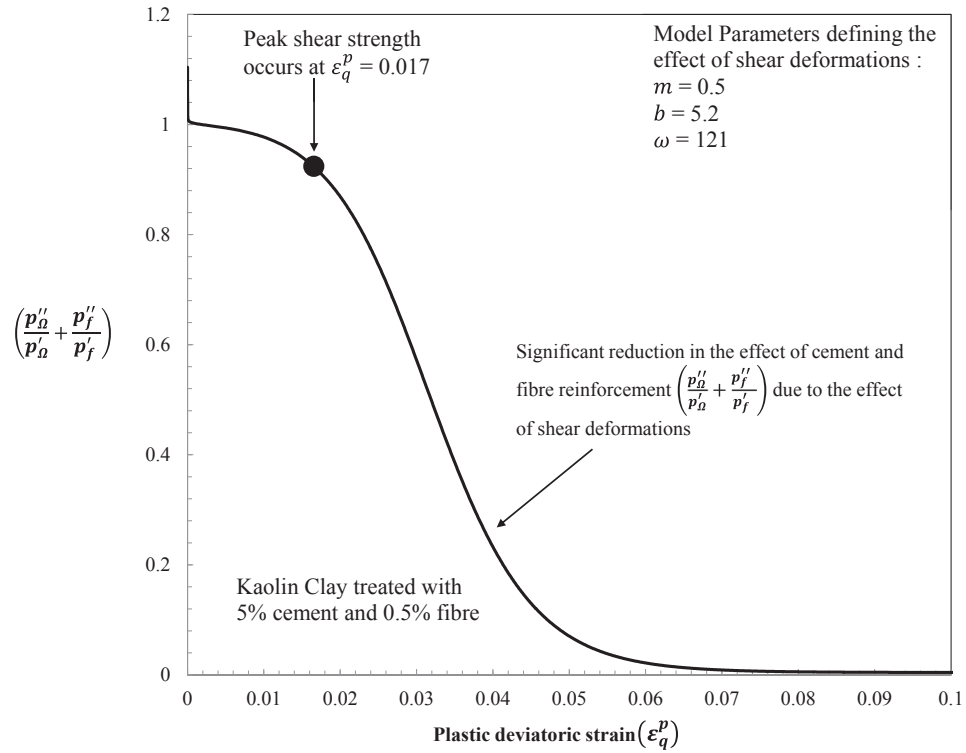


Figure 5.34: The effect of shear deformations on the contribution of cement and fibre reinforcement to the improved Kaolin composite

Figures 5.35 – 5.37 also show reasonable predictions of excess pore water pressure for the composite soil and the Kaolin clay with cement. Note that Equations (5.1) and (5.2) were used to predict the excess pore water pressure. The excess pore water pressure of the improved soil composite increased to a peak state and remained steady as  $\epsilon_q$  continued to increase. As  $\epsilon_q$  increased the peak excess pore water pressure ( $u_{peak}$ ) for the improved soil composite was predicted higher than the cement treated clay for all mean effective yield stresses. Li (2005) explained that due to fibre reinforcement, the applied loads are distributed between the fibres within the soil matrix, and hence the dilatancy of the composite soil is restricted during shearing. Overall, despite some limitations as described above, the behaviour of improved soil composite in an undrained triaxial test was simulated very well using the proposed model.

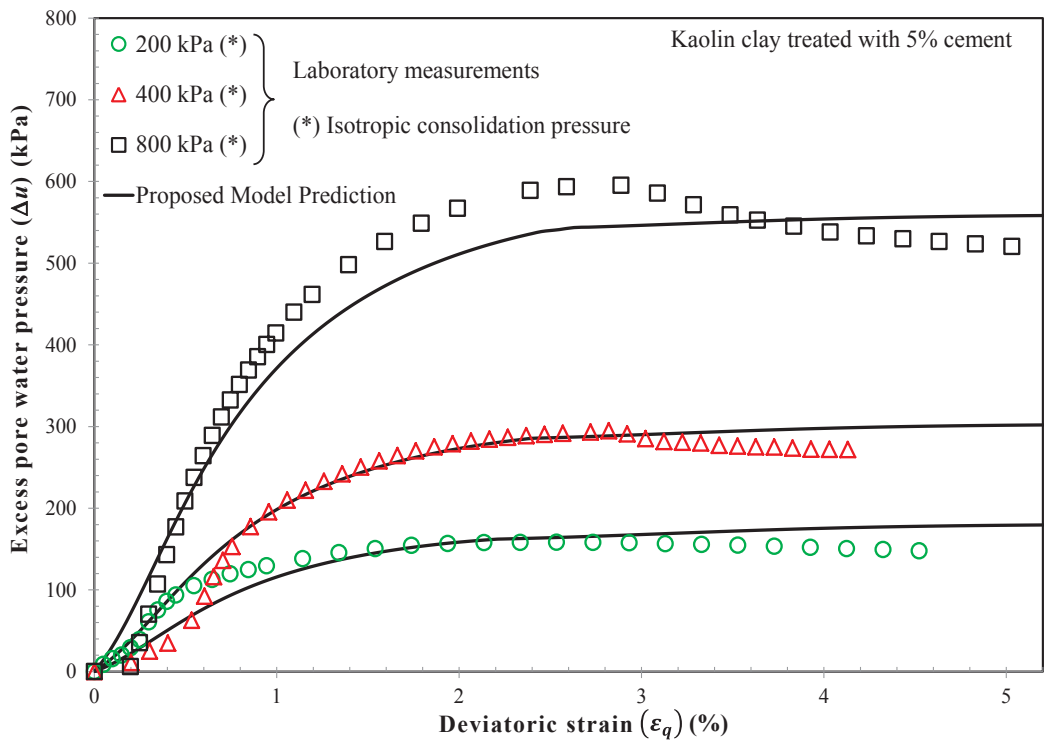


Figure 5.35: Predictions on the excess pore water pressure response of the Kaolin clay treated with 5% cement

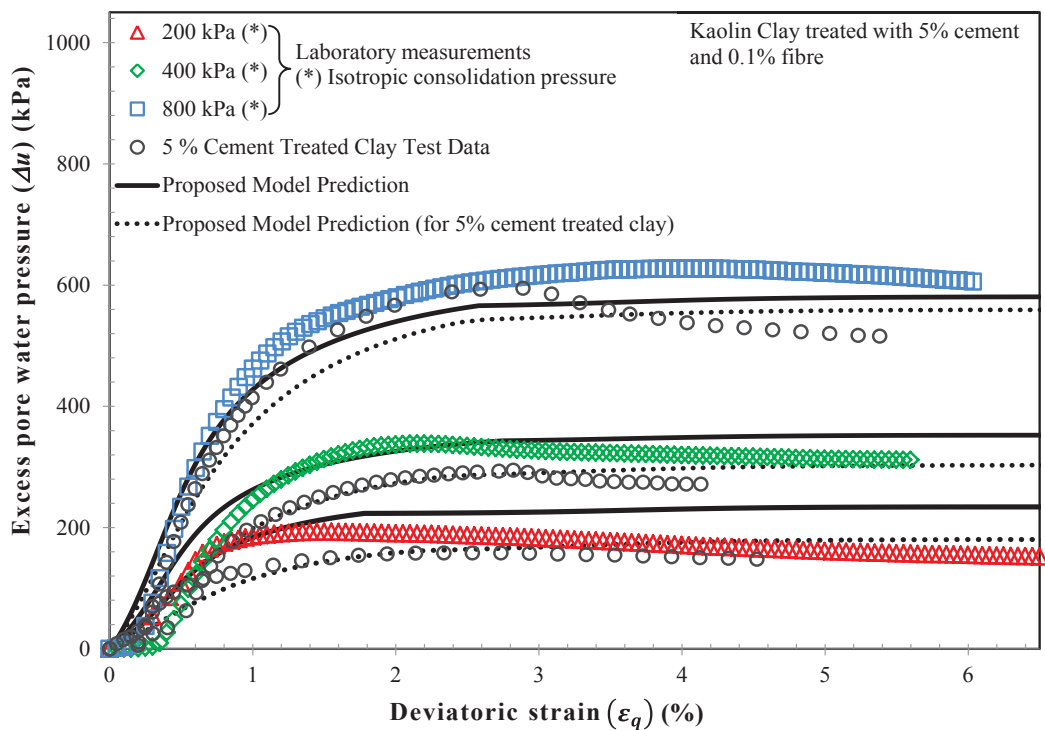


Figure 5.36: Predictions on the excess pore water pressure response of the improved Kaolin composite with 5% cement and 0.1% fibre

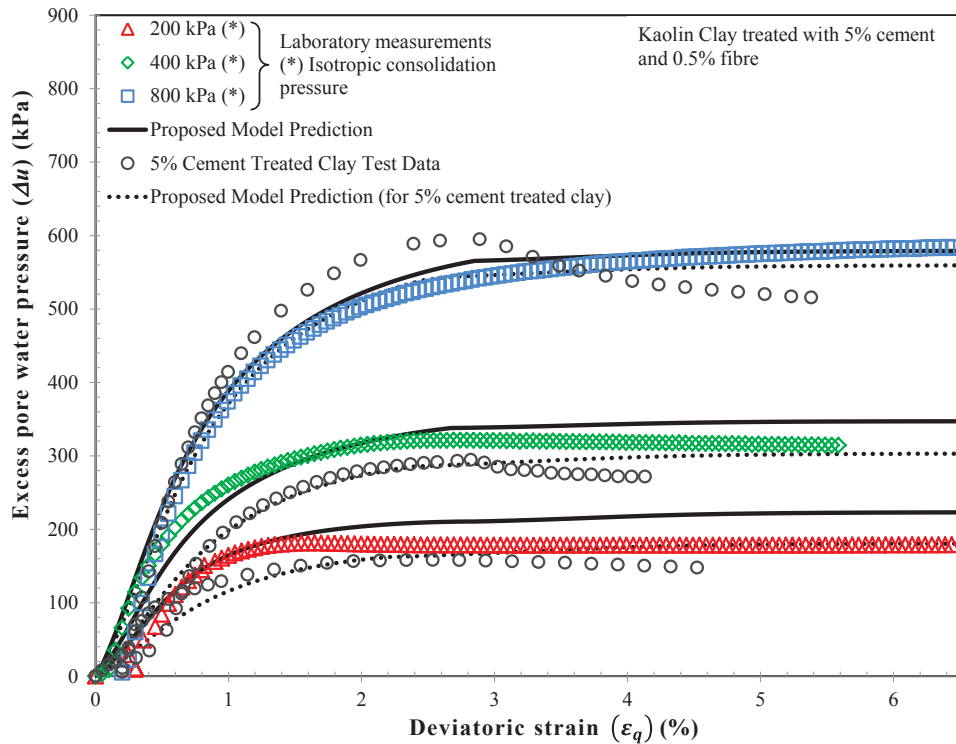


Figure 5.37: Predictions on the excess pore water pressure response of the improved Kaolin composite with 5% cement and 0.5% fibre

#### 5.3.4. Further Verification for the Cement Treated Clay

In this section, the performance of the proposed model for the cement treated clay is further evaluated by comparing the model prediction with available experimental data in literature. The three groups of test data including consolidated-undrained triaxial test results on cement treated Aberdeen soil (reported by Sariosseiri 2008), Singapore marine clay (reported by Kamruzzaman et al. 2009) and Ariake clay (reported by Horpibulsuk et al. 2004) are adopted in this study for further verification exercise. The amount of cement content is calculated in percentage by a ratio of dry weight of cement and dry weight of clays (Horpibulsuk et al. 2004; Kamruzzaman et al. 2009; Sariosseiri 2008). The model parameters have been obtained based on the procedure explained in Section 5.2. The adopted model parameters for the three selected cemented clays are summarised in Table 5.4. Figures 5.38 – 5.47 display a comparison amongst the proposed model predictions and available experimental data in terms of  $p' - q$ ,  $\varepsilon_q - q$  and  $\varepsilon_q - \Delta u$  planes. It can be noted that the excess pore water pressure is simulated

using Equations (5.1) and (5.2). It is observed that the model predictions are in a good agreement with the experimental results, particularly in higher confining pressure ranges. Detailed discussions are presented below.

Predicted and measured stress paths for treated Aberdeen soil at 400 and 600 kPa mean effective yield stress are displayed in Figure 5.38. Since the initial mean effective yield stress ( $p'_{o,i}$ ) was measured at 286.4 kPa, so all the samples were on the current yield surface with plastic deformation. At  $p'_o = 600$  kPa, it can be seen that the peak shear strength lied almost on the critical state line (CSL) of the reconstituted soil-cement mixture as the cementation bonds were completely destroyed. It should be noted that the existing constitutive model is unable to capture this behaviour as the failure envelope was assumed to be linear and parallel to the CSL. Moreover, the proposed failure envelope (Equation (3.53)) has captured the strength reduction considering the cementation degradation due to mean effective yield stress during isotropic consolidation and plastic deviatoric strain during shearing. Figure 5.38 showed the proposed failure envelope gradually merging with the CSL of the reconstituted soil-cement mixture as the mean effective yield stress continues to increase. Additionally, as shown in Figures 5.39 and 5.40, the stress-strain relationship and the excess pore water pressure response of the cement treated Aberdeen soil have been simulated successfully.

Table 5.4: Model values for the cement treated clays

	Aberdeen soil treated with 5% cement <sup>(a)</sup>	Ariake clay treated with 6% cement <sup>(b)</sup>	Singapore clay treated with 10% cement <sup>(c)</sup>
$M$	1.4	1.85	0.9
$\lambda$	0.162	0.446	0.73
$\kappa$	0.048	0.044	0.067
$p'_{o,i}$ (kPa)	286.4	60	300
$\xi$	0.68	0.38	0.87
$\alpha$	-0.82	-0.02	-0.83
$C_c$ (kPa)	143	28	180
$\beta$ (kPa)	164	250	980
$\nu$	0.25	0.25	0.25
$e_0$	1.97	4.37	2.85
$\omega$	21	32	55
$b$	2.5	4.3	0.4
$\Delta s$	N/A	1.02	N/A

Note: laboratory data obtained from (a) Sariosseiri (2008); (b) Horpibulsuk et al. (2004); (c) Kamruzzaman et al. (2009)

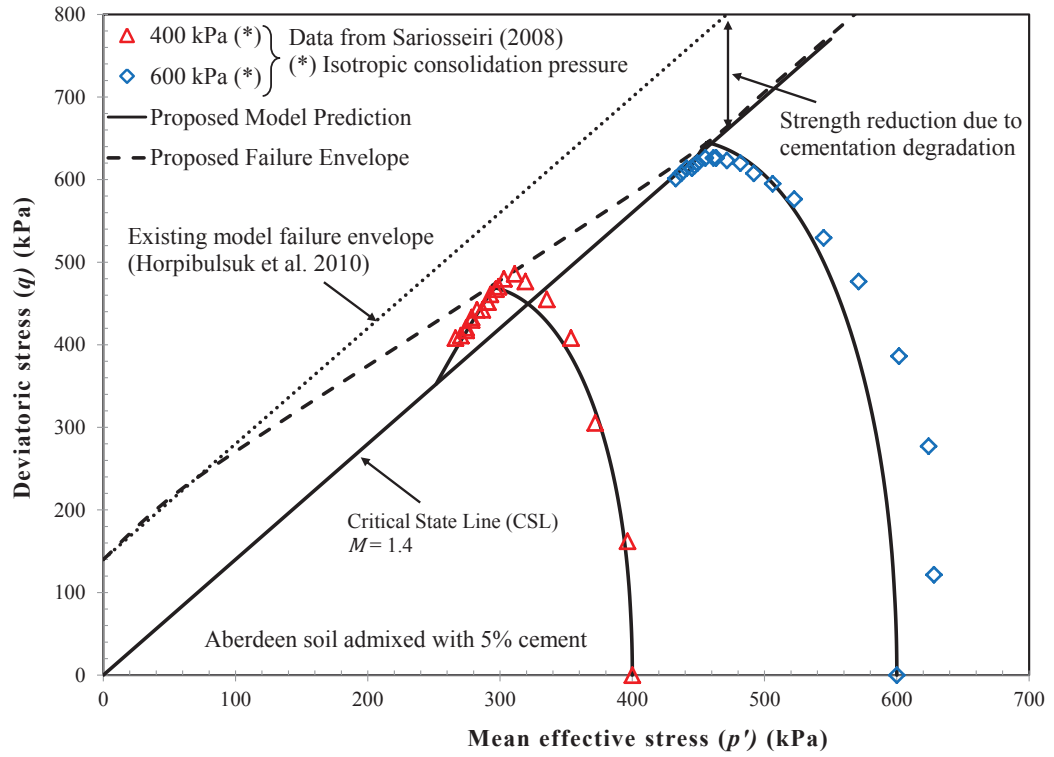


Figure 5.38: Predictions on the stress path curves of the Aberdeen soil admixed with 5% cement.

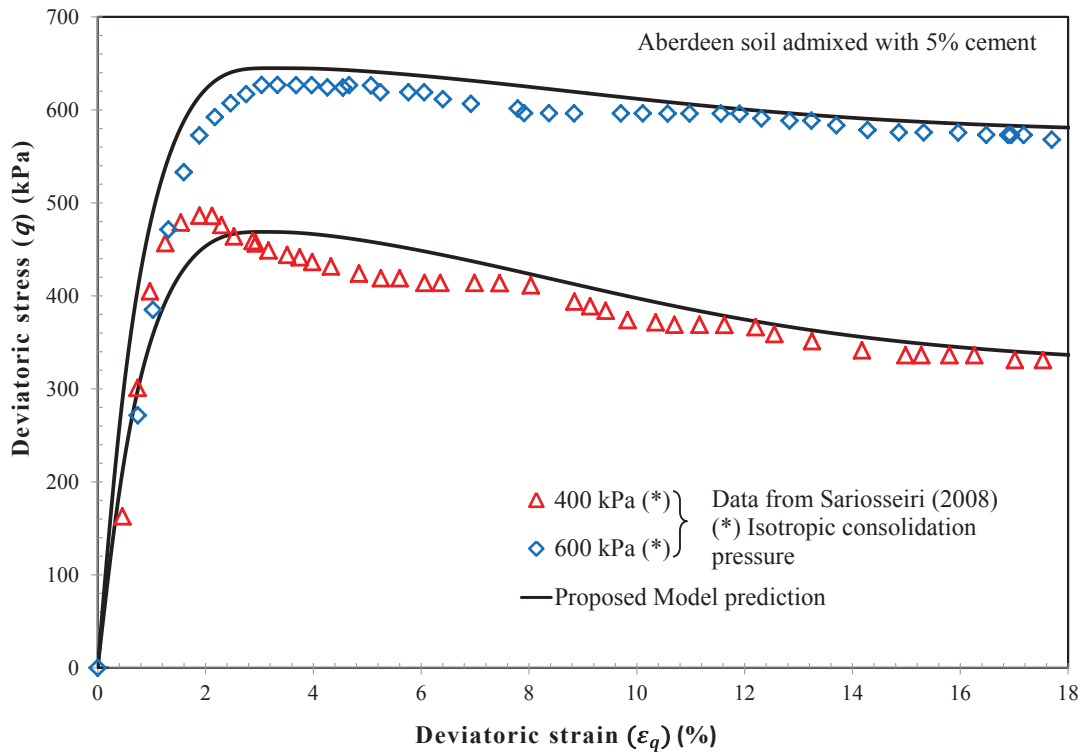


Figure 5.39: Predictions on the stress strain of the Aberdeen soil admixed with 5% cement.

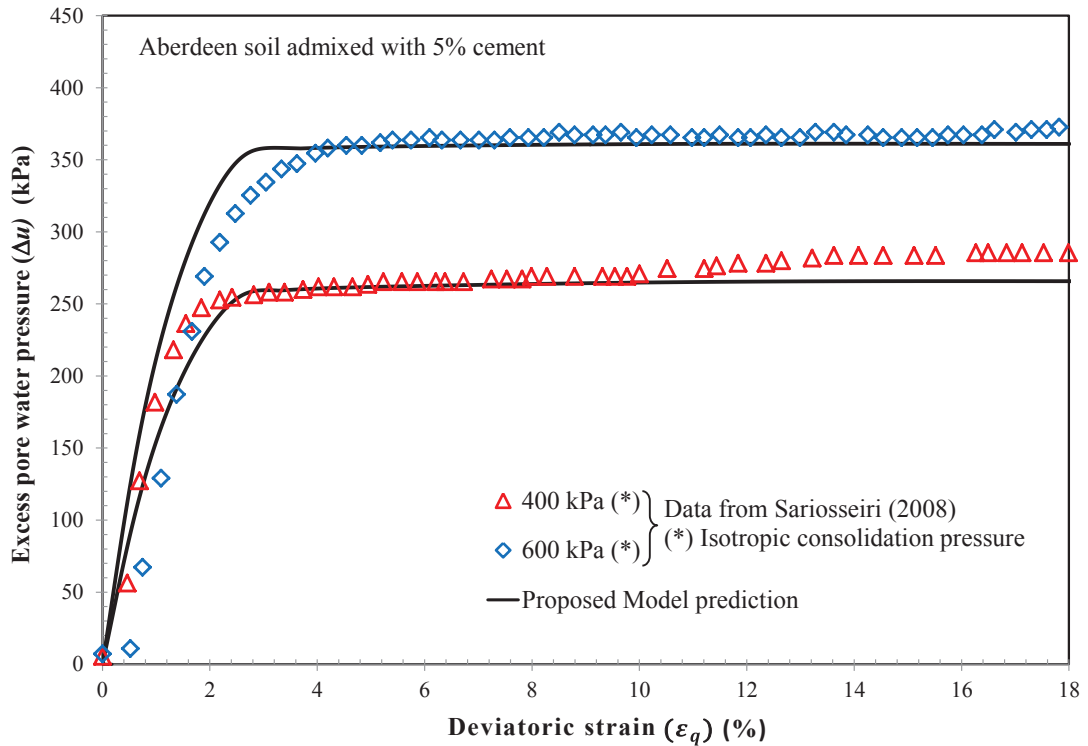


Figure 5.40: Predictions on the excess pore water pressure response of the Aberdeen soil admixed with 5% cement

Figures 5.41 – 5.44 display the comparison between the proposed model and the experimental data for the consolidated-undrained triaxial tests data performed on Ariake clay admixed with 6% cement content reported by Horpibulsuk et al. (2004). The compressibility behaviour of the cement treated clay was simulated by considering the effect of fabric change ( $\Delta s = 1.02$ ) very well. Moreover, Figure 5.41 showed that the volume change (void ratio change) at the post yield stage was captured accurately by correct estimation of the parameter  $\beta$  influencing the degradation rate. In addition, the initial confining pressures of 100, 200, and 400 kPa in undrained condition were adopted for the simulation. The virgin yielding occurred at  $p'_{o,i} = 60$  kPa, so the stress state of all samples was outside the initial yield surface. The peak shear strength of the cement treated clay was captured quite well by adopting the non-linear failure envelope proposed in Equation (3.53), as shown in Figure 5.42. However, as observed in Figure 5.43, the model predictions deviated from the experimental data, particularly during the post-peak state for sample under high mean effective yield stress ( $p'_o = 400$  kPa  $\gg p'_{o,i} = 60$  kPa). It can be explained that, the breakage of cementation bonds occurs at a

higher rate at  $p'_o \gg p'_{o,i}$  due to high mean effective yield stress (large plastic volumetric strain) and the accumulation of the plastic deviatoric strain, resulting in a large reduction in the post-peak strength, similar to the reported experimental data conducted on cement treated Ballina and Kaolin clays. Moreover, Kamruzzaman et al. (2009) further explained that the sample experiences high volume change during consolidation under high confining pressure leading to more evident softening effect in the post-peak state. Thus, to better simulate the behaviour of the cement treated clay during shearing, particularly for samples tested under high mean effective yield stress, the effect of plastic volumetric strain ( $\epsilon_p^p$ ) should be considered in the modified mean effective stress. Overall, the proposed model provide a good prediction for the behaviour of treated Ariake clay in isotropic compression, the stress path, stress-strain curve and the excess pore water pressures as shown in Figures 5.41 – 5.44, respectively.

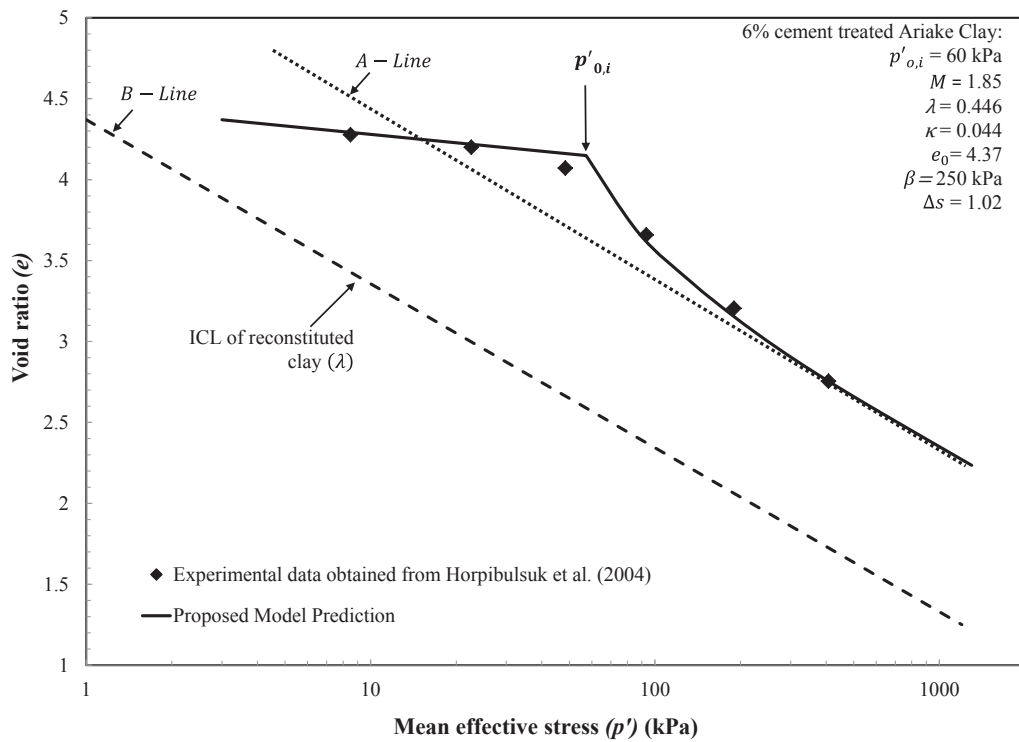


Figure 5.41: Predictions on the isotropic consolidation test result of the Ariake clay treated with 6% cement

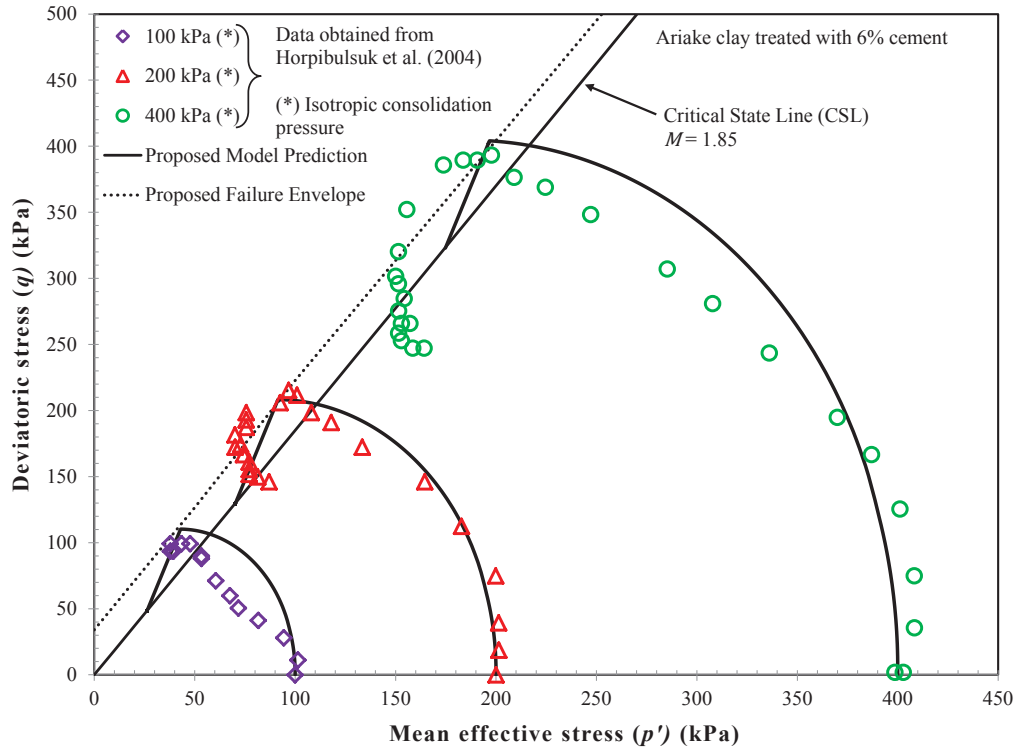


Figure 5.42: Predictions on the stress path curves of the Ariake clay treated with 6% cement.

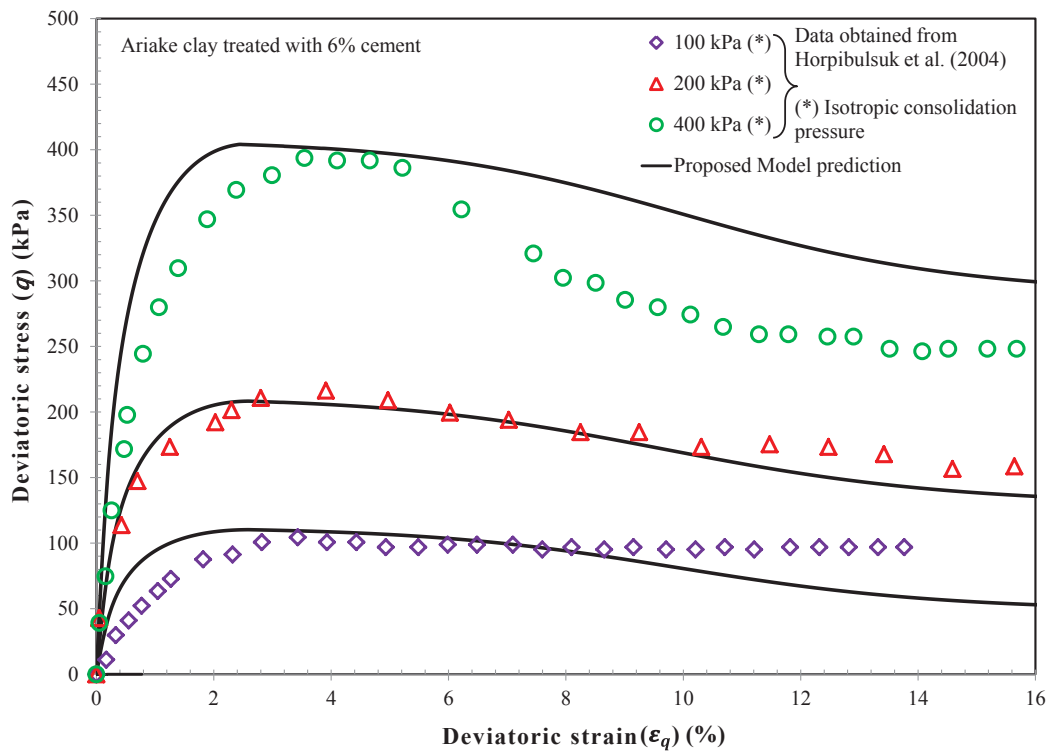


Figure 5.43: Predictions on the stress strain of the Ariake clay treated with 5% cement.

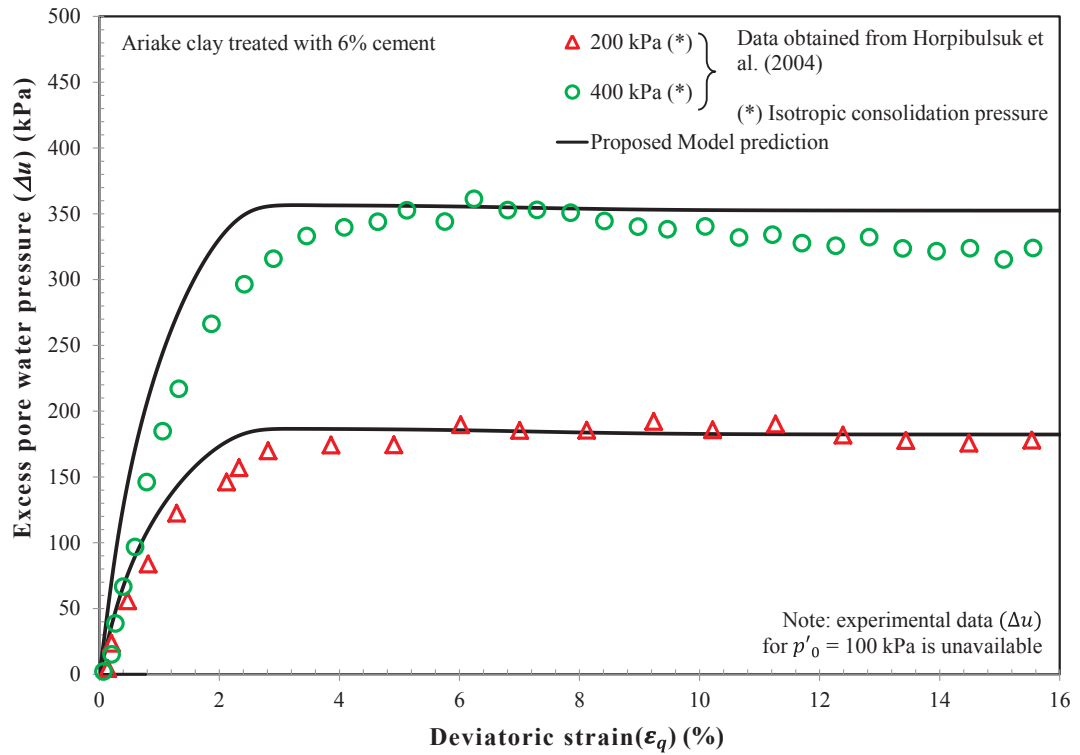


Figure 5.44: Predictions on the excess pore water pressure response of the Ariake clay treated with 6% cement

Kamruzzaman et al. (2009) performed a series of effective undrained triaxial tests on highly plastic Singapore marine clay admixed with 10% cement at different confining pressures ranging from 300 to 1000 kPa. The undrained stress paths, the stress-strain relationship and the excess pore water response of the cement treated Singapore clay are simulated in Figures 5.45 – 5.47, respectively. The proposed model predictions for the cement treated Singapore clay (at confining pressures of 300, 500 and 1000 kPa) are in very good agreement with measurements. Figure 5.45 showed that all the stress paths were observed to be higher than the critical state line indicating that part of cementation is still present in the soil structure at the shearing stage.

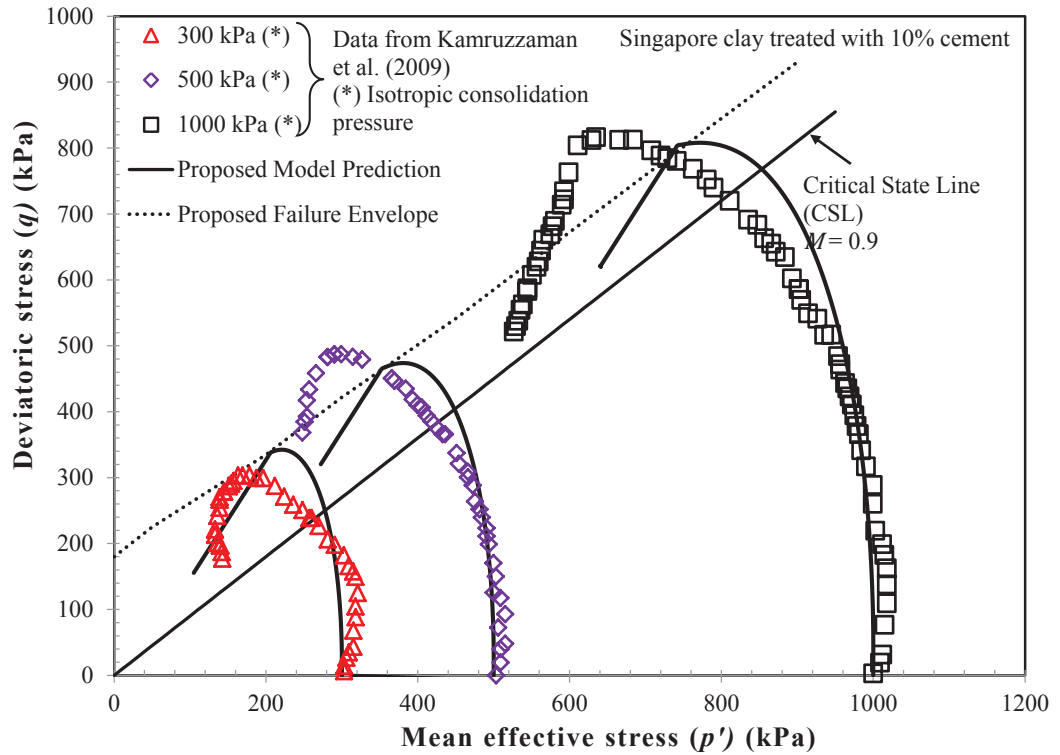


Figure 5.45: Predictions on the stress path curves of the Singapore clay treated with 10% cement.

Moreover, the reduction at the post peak stage of  $p'_0 = 1000$  kPa was more significant as compared to  $p'_0 = 300$  and  $500$  kPa in the same range of deviatoric strain indicating that the effect of cementation degradation is dramatic due to increasing mean effective yield stress, as shown in Figure 5.46. Although, there are some disparities between the predicted stress–strain relationship at the initial stages of loading and laboratory measurements, the predictions began to match up with the experimental data when the axial strain exceeds 2%, particularly at the post peak stage. However, the proposed model has over-predicted the post-peak shear strength of the 10% cement treated Singapore clay at high  $p'_0 = 1000$  kPa where the effect of plastic volumetric strain ( $\epsilon_p^p$ ) on the cementation degradation should be considered as explained above in case of treated Ariake clay. Overall, by combining the contribution of cementation to the shear strength ( $C_c$ ) and the effect of cementation degradation due to mean effective yield stress ( $p'_0$ ) and plastic deviatoric strain ( $\epsilon_q^p$ ) in the formulation of the modified mean effective stress ( $p'^*$ ) in Equation (3.48), the behaviour of the Singapore clay treated with 10% cement was simulated reasonably well.

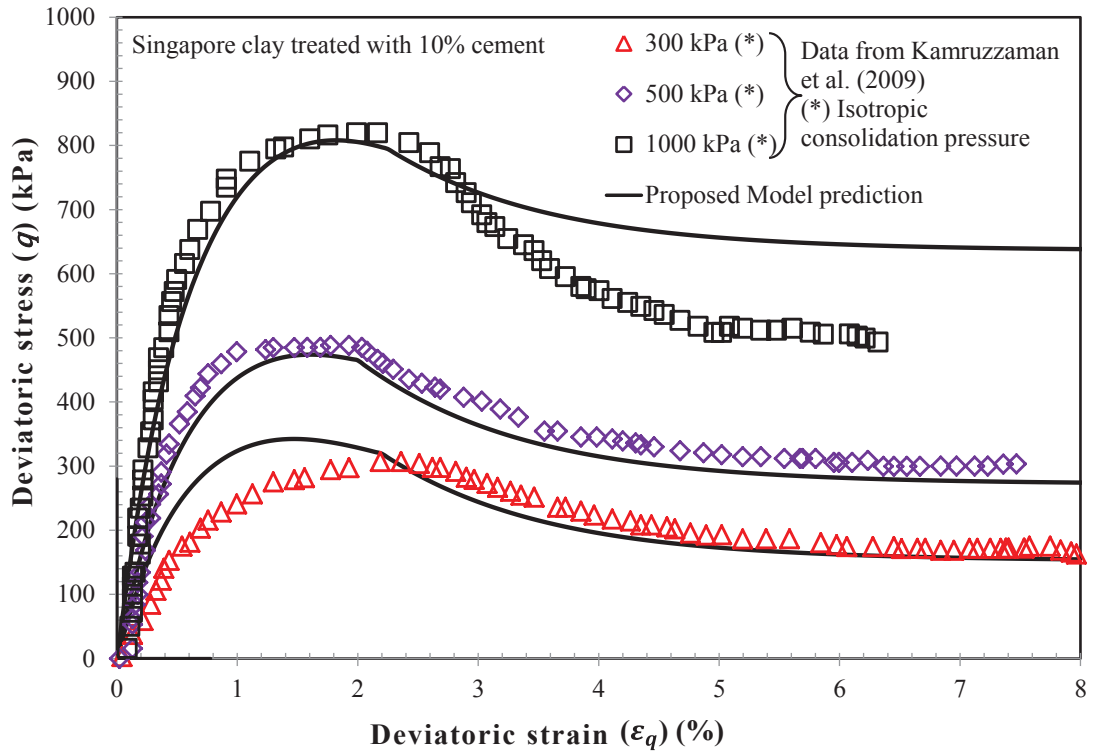


Figure 5.46: Predictions on the stress strain of the Singapore clay treated with 10% cement.

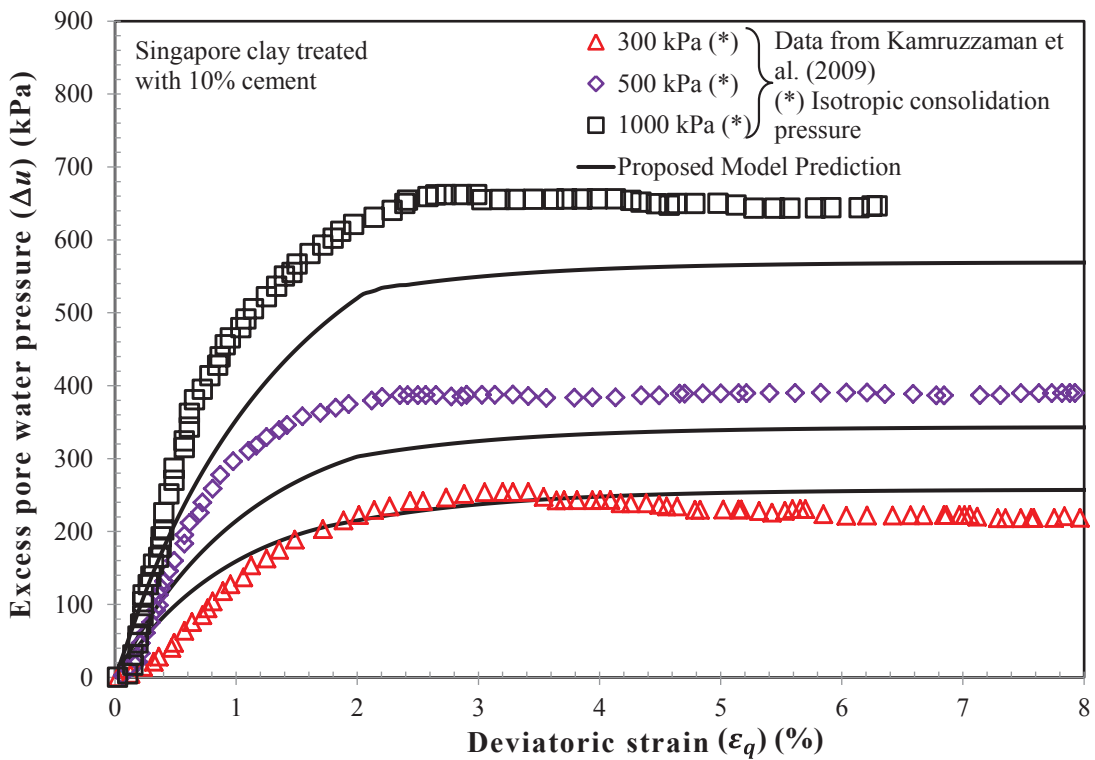


Figure 5.47: Predictions on the excess pore water pressure response of the Singapore clay treated with 10% cement

In summary, when the mean effective yield stress is on or outside the initial yield surface, the undrained effective stress path of cemented clays in  $p' - q$  plane initially rises upwards and bends towards to left and approaches the Critical State Line (CSL) of reconstituted cement-clay mixture indicating that plastic deformations occur as shown in the undrained stress paths of Aberdeen soil (Figure 5.38), Ariake clay (Figure 5.42 and Singapore clay (Figure 5.45). This behaviour of cement treated clay is similar to the normally consolidated soils, as observed by Horpibulsuk et al. (2010), Kasama et al. (2000), and Uddin et al. (1997). The undrained stress paths continue to pass the CSL and reach a peak strength state as the effect of cementation is still present. However, the beneficial contribution of cementation to the peak shear strength of the cement treated clay is reduced as the effective confining pressure increases, due to the breaking of cementation bonds during shearing as illustrated in Figures 5.39, 5.43 and 5.46. For high mean effective yield stress ( $p'_0 = 600$  kPa) in case of Aberdeen soil as shown in Figure 5.38 with low cement content (5%), the stress path reached a peak strength state which lied on the CSL as the effect of cementation was completely destroyed. In addition, the failure envelope of cement treated clay is clearly non-linear and gradually approaches the CSL of reconstituted soil-cement mixture as the mean effective yield stress increases as shown in Figure 5.38. When the peak shear strength is obtained, the cement treated clay sample undergoes softening process with significant breakage of cementation bonds. Moreover, the effect of cementation degradation at higher mean effective yield stress is more pronounced due to high volume change during consolidation. It can be noted that, when the effect of cementation is completely destroyed, the behaviour of the cement treated clay is similar to that of the un-treated clay.

The existing constitutive and numerical models do not capture the cementation degradation due to the applied mean effective stresses during isotropic consolidation, resulting in over estimating the peak shear strength of the cement treated soils and consequently the bearing capacity of foundations (i.e., aggressive design). In this study by introducing a nonlinear failure envelope capturing cementation degradation induced by the mean effective yield stress and the plastic deviatoric strain, more realistic behaviour of the cement treated soils is presented. Moreover, by introducing the effect of cementation degradation due to the applied mean effective stress and the shear strain

in the formulation of  $p''_{\Omega}$  in Equation (3.47), deformations are captured not only at the shearing stage, but also during the consolidation stage where other researchers have chosen to ignore this effect. In this study, the proposed model includes a non-associated plastic potential function to simulate the plastic deformations resulting in a realistic prediction of the peak shear strength and the associated deformation. Moreover, the plastic potential function is derived from energy dissipation equation which can be extended to simulate different types of soils or loadings. The existing models ignored the reduction in the cementation contribution due to cementation degradation by adopting a linear failure envelope while the model proposed in this study captures this behaviour of cement treated clays, thus provides a better agreement with experimental data.

## 5.4. Summary

In this chapter, the performance of the proposed models for the cement treated clay with or without fibre reinforcement has been evaluated by comparing the model predictions with the experimental triaxial test results conducted on the improved Ballina clay and Kaolin clay composite presented in Chapter 4. Furthermore, the existing case studies on the cement treated clay from the literature, namely the Singapore clay, the Ariake clay and the Aberdeen clay, were used to further verify the proposed model. The procedures for determining the model parameters were described in Section 5.2. It was suggested that, in order to determine the model parameters associated with the effect of cementation and its degradation, a set of undrained triaxial tests should be conducted on the cement treated clay without fibre reinforcement. Furthermore, the model parameters associated with fibre reinforcement should be estimated using the triaxial test results on the soil composite with cement and fibre.

The simulation results have been presented in the isotropic compression curve ( $e - \ln p'$  plane) stress path ( $p' - q$  plane), stress-strain curves ( $\varepsilon_q - q$  plane), and the excess pore water pressure response ( $\varepsilon_q - \Delta u$  plane). Overall, despite some limitations of the proposed model, the behaviour of cement treated clay with or without fibre

reinforcement can be successfully simulated by accurate estimation of the model parameters. Some conclusions can be drawn from the simulation results as follows:

- In the isotropic compressibility behaviour, the isotropic compression line (ICL) of the improved soil composite can be predicted in a similar way as the cement treated clay by assuming the effect of fibre reinforcement to be insignificant. Moreover, the isotropic behaviour of the cement treated clay depends mainly on the effect of cementation in elastic region while plastic deformation causes breaking of cementation bonds at the post-yield stage. At high stress level, significant reduction in void ratio occurs as the ICL of the cement treated clay approaches that of the reconstituted mixture. At this stage, the cement treated clay relies on the effect of fabric. By considering the effect of fabric change ( $\Delta s$ ) which increases with the cement content, the proposed model can simulate the isotropic compressibility of the cement treated clay with or without fibre reinforcement very well. Moreover, the rate of cementation degradation at the post yield stage can be captured using the parameter  $\beta$ . It can be noted that, higher values for  $\beta$  can be adopted to simulate lower degradation rate in higher cement contents.
- In the shearing stage, in both drained and un-drained conditions, accurate estimation of the parameter  $C_c$ , presenting the contribution of cement, can result to better prediction of the peak shear strength of the cement treated clay. It should be noted that the parameter  $C_c$  increases with cement content due to increasing initial mean effective yield stress ( $p'_{o,i}$ ) in higher cement content. Moreover, the behaviour of the cement treated clay in both pre and post peak states is influenced by the effect of cementation degradation which can be simulated by adopting the formulation of  $p''_{\Omega}$  in Equation (3.47).
- Furthermore, for the improved clay composite, the peak shear strength depends mainly on the effect of cementation ( $C_c$ ) while the contribution of the fibre ( $C_f$ ) is more effective in the residual strength state. At the post-peak state, the effect of cementation and fibre contribution reduce with increasing deviatoric strain ( $\varepsilon_q$ ). The simulation results showed that the peak and residual shear strengths of the improved soil composite can be captured considering the combined effect of cement and fibre, together with the cementation degradation and fibre failure mechanisms (in the formulations of  $p''_{\Omega}$  and  $p''_f$  in Equations (3.47) and (3.86), respectively).

- Moreover, the softening process in the behaviour of the cement treated soil with or without fibre reinforcement was smoothly simulated by assuming that the stress state of the sample remains on the failure line (in Equation (3.90)) with reduced effect of cementation and fibre failure ( $p''_{\Omega}$  and  $p''_f \approx 0$ ).
- Overall, by introducing the effect of cementation degradation (due to the mean effective stress and the deviatoric strain) and the effect of fibre failure (due to the deviatoric stress and strain) into the modified mean effective stress ( $p'^*$ ) (Equation (3.87)), the volumetric and deviatoric strains during the isotropic compression and shearing stages can be predicted accurately. Moreover, the peak shear strength and associated deformation at the post-peak state of cement treated clay with or without fibre reinforcement were predicted quite well by adopting the proposed model, including the non-associated flow rule and the plastic potential function, capturing the hardening and softening processes reasonably well.

# Chapter 6

## Conclusions and Recommendations

---

### 6.1. Summary

The main objective of this study has been to propose new constitutive models to simulate the behaviour of cement treated clay with or without fibre reinforcement. The proposed models have been validated against the experimental results conducted on the treated clay with various cement and fibre contents under different loading conditions. The summaries of the chapters are as follows:

- In Chapter 1, the introduction about the research topic on the behaviour of the cement treated clay with or without fibre reinforcement has been provided along with the problem statements, the objectives and the scope of the present study.
- Chapter 2 has provided a comprehensive literature review on the engineering properties of the cement treated clay with or without fibre under different loading conditions. The strength of the cement treated clay increases due to the formation of the cementation bonds within the soil-cement clusters as a result of chemical reactions between soil and cement. Factors influencing the engineering properties of the cement treated clay consists of cement content, curing time, water content and the type of clay. However, when the cement treated sample is loaded beyond the initial yield stress, plastic deformations occur causing significant breaking of cementation bonds. Moreover, the effect of increasing deviatoric (shear) strain

also contributes to a reduction in the strength at the post peak state as the treated sample undergoes softening process. When the effect of cementation is completely removed, the behaviour of the cement treated clay is similar to that of the un-treated clay. In addition, to improve the unfavourably brittle failure behaviour of the cement treated clay, the usage of fibre is recommended providing the bridging effect between the soil-cement clusters and the fibre. The shear strength, particularly the residual shear strength improves significantly owing to the inclusion of fibre. However, failure of fibre, including pull-out or breakage may occur due to the shear deformation, hence the effect of fibre reinforcement is diminished. Furthermore, the discussion on the existing constitutive models for the cement treated clay was provided in details, including their limitations. Although, some constitutive models were proposed for the fibre reinforced soil, to the best of the author's knowledge there is no constitutive model developed for the cement treated fibre reinforced clay.

- In Chapter 3, following the framework of the Critical State Soil Mechanics and on the basis of the Modified Cam Clay (MCC) model, the development of a new constitutive model and its extended version to simulate the behaviour of the cement treated clay with or without fibre reinforcement was provided in details. In these proposed models, the mean effective stress was modified to include the effect of cement ( $C_c$ ) and fibre ( $C_f$ ), together with the effect of cementation degradation ( $p''_{\Omega}$ ) and fibre failure ( $p''_f$ ) due to mean effective yield stress ( $p'_0$ ) and the deviatoric strain ( $\varepsilon_q^p$ ). It can be noted that, when the improved soil composite is subjected to high  $p'_0$  and large accumulation of  $\varepsilon_q^p$ , the effect of cementation and fibre reinforcement is diminished ( $p''_{\Omega}$  and  $p''_f \approx 0$ ), hence, the behaviour of the improved soil composite is similar to that of the un-treated clay. The special characteristics of the proposed models include the non-linear failure envelope and the non-associated plastic potential function developed from a modified plastic energy dissipation equation with the parameter  $\alpha$ . It can be noted that, when  $C_c$  and  $C_f = 0$  and the parameter  $\alpha$  is set to be zero, the proposed models return to the MCC model.

- Chapter 4 described the experimental program and reported the results for two types of clays, i.e. the natural Ballina clay and the artificial Kaolin clay, treated with various cement and fibre contents under different loading conditions. The sample preparation and the set-up of the testing apparatus were provided in this chapter. For the experimental program conducted on the cement treated clay, the Ballina clay was mixed with different cement contents (i.e. 10%, 12% and 15%) while the Kaolin clay was treated with 5% cement. Furthermore, to study the effect of the fibre reinforcement, 0.3% and 0.5% polypropylene fibre contents were added to 15% cement treated Ballina clay while Kaolin clay was improved with 5% cement and 0.1% and 0.5% fibre contents. Moreover, the results from the unconfined compression strength (UCS) tests, the Scanning Electron Microscopy (SEM) tests and the extensive triaxial tests were reported and discussed in details
- Chapter 5 has provided the predictions adopting the proposed models in Chapter 3 for the experimental results presented in Chapter 4. The detailed procedures to determine the model parameters were described in this Chapter. The performance of the proposed model for the cement treated clay was evaluated by comparing the model predictions with the experimental results conducted in this study and the existing case studies on the cement treated Singapore clay, Ariake clay and the Aberdeen clay available in the literature. Moreover, the extended version of the proposed model for the improved clay composite was validated against the un-drained triaxial test results on the improved Ballina clay composite and Kaolin clay treated with cement and fibre. The simulation results were provided in terms of isotropic consolidation curve, the stress path, the stress-strain relationship curves and the excess pore water pressure response. Overall, despite some disparities in the simulation results, the proposed models have captured the important features of the behaviour of the cement treated clay with or without fibre reinforcement, particularly the peak shear strength and the transition process from the peak to the residual strength state. By considering the combined effects of cement and fibre reinforcement, together with their degradations, the behaviour of the improved clay composite has been simulated successfully adopting the proposed model.

## 6.2. Conclusions

Cement stabilisation is an effective ground improvement method to enhance the properties of soft clay. The effect of cementation is to increase the shear strength of the soft clay due to the formation of cementation bonds and the soil-cement clusters. In fact, the unconfined compression strength (UCS) test results revealed significant increase in strength due to the effect of cementation. Moreover, the peak strength of the cement treated clay increased with cement content, given the same water content and curing time. In the isotropic compression test, the initial mean effective yield stress of the cement treated clay also increased with cement content which was observed to be higher than the corresponding values for the un-treated clay with the same void ratio. However, laboratory studies indicated that cementation degradation due to the mean effective stress and deviatoric strain influence the peak shear strength of cement treated clays such that during isotropic compression, as the mean effective yield stress increased beyond the initial yield stress, the effect of cementation decreased due to the degradation of cementation bonds, while the void ratio of cement treated clays decreased approaching the ICL of reconstituted soil due to a notable breakage of cementation bonds, particularly at high mean effective stresses. However, the fabric component of a cement treated clay structure may remain, indicating that the effect of fabric change may not be completely removed during isotropic compression. Moreover, the cementation bonds were progressively destroyed when the cement treated clays were subjected to shear deformation as major cracks formed within the samples. Following the softening process in the post peak state, the cementation bonds were removed even further as the sample approached the CSL of the reconstituted soil-cement mixture. Once the cement treated clays travelled on the CSL, the cementation bonds were completely removed, which resulted in only residual strength remaining.

Furthermore, similar to the behaviour of the cement treated clay, the combined effects of fibre reinforcement and cementation decreased as the improved soil composite was subjected to high mean effective stress during isotropic compression and shear deformation. The laboratory results confirmed that fibre reinforcement in isotropic compression had an insignificant effect, and similar to soil treated with cement only, the void ratio of composite soil decreased dramatically beyond the initial yield stress,

mainly due to cementation degradation. In addition, during shearing, the frictional resistance of the fibre was mobilised and the clusters of soil and cement were bridged; hence a peak shear strength higher than the corresponding values for the cement treated clay was obtained. The experimental results showed that the increase in the peak shear strength provided by the effect of fibre reinforcement depended on the type of the soft clay which could influence the interaction between the fibre and the soil-cement clusters. Furthermore, the fibre failure mode, including pull-out and rupture, was characterised by the critical mean effective stress ( $p_{crit}^*$ ), so when the composite soil is subjected to shearing at a mean effective stress lower than  $p_{crit}^*$ , the fibre is gradually pulled-out from the soil matrix as the interfacial forces between the fibre and clusters of soil and cement are less than the frictional resistance of the fibre. However, when shearing at higher mean effective stresses beyond  $p_{crit}^*$ , fibre rupture could occur before the peak shear strength is reached because the frictional resistance of the fibre may be exceeded, particularly at the shear bands. Thus, cementation plays an important role in the peak shear strength at this stage. Furthermore, a further reduction in the cementation bonds contributed to the reduction in the peak shear strength due to major cracks appeared after shear deformation. At the post peak state where large plastic deviatoric strains occurred, the softening behaviour included the cementation bonds being crushed and the fibre being either pulled out or ruptured. Furthermore, the experimental results also indicated that the effectiveness of the fibre decreased as the mean effective stress increased. Moreover, increasing the amount of fibre had a greater effect on ductility than the peak shear strength of the improved soil composite.

The effect of cementation and its degradation could be visually observed by the SEM studies. The cement treated clay showed a flocculated structure with clay clusters connected by the cementation bonds (shown as the precipitated crystals) due to the chemical reactions between the clay particles and cement. After shearing at high mean effective yield stresses, the cement treated clay depicted a more compacted structure with small void spaces because the structure was altered due to the mean effective stress and deviatoric strain. Moreover, there was no evidence of any precipitated crystals as the cementation bonds were completely destroyed at the ultimate stage. Additionally, SEM analysis of the improved clay composite showed some grooves on the surface of the fibre caused by shearing of the precipitated cementation products. The evidence of the precipitated crystals attached tightly to the fibre after shearing, shows that the

applied load were transferred effectively from the soil-cement clusters to the fibre body, consequently it led to an increase in strength and ductility.

In this study, a constitutive model was presented in light of the Critical State Framework and Cam Clay model families to describe the behaviour of cement treated clays under different loading conditions. Furthermore, the proposed model was extended to include the effect of fibre reinforcement on the behaviour of the improved soil composite. The models were formulated to include the modified mean effective stress ( $p'^*$ ) in a single equation to capture the beneficial contributions, and cementation degradation and fibre failure mechanisms, by considering the mean effective stress, the deviatoric stress, and the plastic deviatoric strain. Moreover, reductions in the contributions of cementation ( $p''_{\Omega}$ ) and fibre ( $p''_f$ ) were proposed in a single equation to describe the shear degradation in pre-and-post peak states. The characteristics of the proposed models include a non-linear failure envelope which progressively merges with the CSL of the reconstituted soil-cement mixture as the mean effective stress increases, to capture the effect of cementation and the rupture of fibre. A non-associated plastic potential function was also derived from the modified energy dissipation equation along with the elasto-plastic stress-strain relationship. Furthermore, the softening process of the cement treated clay with or without fibre at the post peak state can be simulated adopting the proposed models by assuming that the stress state of the treated sample remains on the failure line with a reduced effect of cementation and fibre ( $p''_{\Omega}$  and  $p''_f \rightarrow 0$ ). It can be noted that when fibre and cementation are absent ( $C_c$  and  $C_f = 0$ ), and the parameter  $\alpha = 0$  is adopted, both proposed models return to Modified Cam Clay model.

The experimental results, including the isotropic compression curve, the peak and the residual shear strength, and the excess pore water pressure, were reported in  $e - \ln p', p' - q, \varepsilon_q - q$  and  $\varepsilon_q - \Delta u$  planes. By accurate estimation of the model parameters, the peak and the residual shear strengths of the cement treated clay with or without fibre reinforcement could be captured and predicted well. Moreover, the isotropic compressibility of the improved soil composite could be predicted quite well, observed to follow the behaviour of the cement treated clay. Overall the model predictions had a satisfactory agreement with the experimental measurements, while capturing the combined effects of cementation and its degradation as well as fibre

failure. Accordingly, geotechnical practitioners may adopt the proposed models to predict the performance of cement treated clays with or without fibre reinforcement under various types of structural loads.

### **6.3. Recommendations for Future Studies**

- The proposed constitutive models in this study can be implemented in the commercially available software such as FLAC, ABAQUS to simulate field case studies and provide computed results for comparison with field measurements for further verification.
- A series of triaxial tests can be conducted on the fibre reinforced cement treated clay with different types of fibres (e.g. natural fibre and recycled carpet fibre), fibre length, water content and curing time to further understand the factors affecting the effect of fibre reinforcement.
- Usage of other additives to reduce the breakage of cementation bonds subjected to high loading can be investigated. Moreover, chemical treatment, for example asphalt emulsion, particularly for the natural fibre prior to mixing with cement and soil should be investigated to prevent fibre degradation with time due to surrounding environmental effects.
- An experimental program in the field should be designed and carried out to investigate the interaction between the improved clay composite and the surrounding soil. The results from the field tests can be used to further verify the proposed models which also present an opportunity for model improvements.
- The hardening effect of cementation can develop over a long period of time. Thus the strength of the cement treated clay increases with time. This is also applicable to the cement treated clay with fibre reinforcement. However, when the treated sample is subjected to a constant load over a prolonged period, the occurrence of creep may influence the strength of the improved clay. It is recommended to conduct an array of laboratory experiments to investigate the importance of creep and its mechanisms. Furthermore, an elastic-viscous-plastic constitutive model should be developed to include the time dependent stress-strain behaviour of the cement treated clay with or without fibre reinforcement.

- Behaviour of the cement treated soil with or without fibre reinforcement under dynamic and cyclic loading can be investigated experimentally. Moreover, constitutive model based on bounding surface or continuous plasticity theories can be developed for these loading conditions.
- The compatibility of the developed model with thermodynamic laws, particularly under unloading and reloading cycles, can be further investigated.
- Stabilising unsaturated soil with cement becomes increasingly popular. However, the knowledge on the behaviour of the unsaturated soil treated with cement remains very limited. Hence, experimental studies should be conducted to investigate the factors affecting the behaviour of the cement treated unsaturated soil which can be used to develop a new or modified constitutive model.

## References

- Australian Standard AS 5101.4: Methods for preparation and testing of stabilized materials - Unconfined compressive strength of compacted materials. Standards Australia, Sydney, 2008.
- Australian Standard AS 1289.6.4.2: Methods of testing soils for engineering purposes - Soil strength and consolidation tests - Determination of compressive strength of a soil - Compressive strength of a saturated specimen tested in undrained triaxial compression with measurement of pore water pressure. Standards Australia, Sydney, 1998.
- Australian Standard AS 1012.8.1: Methods of testing concrete - Method for making and curing concrete - Compression and indirect tensile test specimens. Standards Australia, Sydney, 2014.
- Allman, M. and Atkinson, J. 1992. Mechanical properties of reconstituted Bothkennar soil, *Géotechnique*, 42: 289-301.
- Anagnostopoulos, C. A., Tzetzis, D. and Berketis, K. 2014. Evaluation of the shear strength behaviour of polypropylene and carbon fibre reinforced cohesive soils, *Research Journal of Applied Sciences, Engineering and Technology*, 7: 4327-4342.
- Ando, Y., Tsuboi, H., Yamamoto, M., Harada, K. and Nozu, N. 1995. Recent soil improvement methods for preventing liquefaction, *Proceeding of Earthquake Geotechnical Engineering*: 1011-1016.
- Balasubramaniam, A., Kamruzzaman, A., Uddin, K., Lin, D., Phienwij, N. and Bergado, D. 1998. Chemical stabilization of Bangkok clay with cement, lime and flyash additives. *13th Southeast Asian Geotechnical Conference*. 253-258.
- Bardet, J. 1986. Bounding surface plasticity model for sands, *Journal of engineering mechanics*, 112: 1198-1217.
- Baudet, B. and Stallebrass, S. 2004. A constitutive model for structured clays, *Geotechnique*, 54: 269-278.
- Been, K., Jefferies, M. and Hachey, J. 1991. The critical state of sands, *Geotechnique*, 41: 365-381.
- Bergado, D., Anderson, L., Miura, N. and Balasubramaniam, A. 1996. Soft ground improvement in lowland and other environments. ASCE.

- Botero, E., Ossa, A., Sherwell, G. and Ovando-Shelley, E. 2015. Stress–strain behavior of a silty soil reinforced with polyethylene terephthalate (PET), *Geotextiles and Geomembranes*, 43: 363-369.
- Bousshine, L., Chaaba, A. and De Saxcé, G. 2001. Softening in stress–strain curve for Drucker–Prager non-associated plasticity, *International Journal of Plasticity*, 17: 21-46.
- Cai, Y., Shi, B., Ng, C. W. and Tang, C.-S. 2006. Effect of polypropylene fibre and lime admixture on engineering properties of clayey soil, *Engineering Geology*, 87: 230-240.
- Casagrande, M. D. T., Coop, M. R. and Consoli, N. C. 2006. Behavior of a fiber-reinforced bentonite at large shear displacements, *Journal of geotechnical and geoenvironmental engineering*.
- Chai, J. and Carter, J. P. 2011. *Deformation analysis in soft ground improvement*, Springer Science & Business Media.
- Chen, M., Shen, S.-L., Arulrajah, A., Wu, H.-N., Hou, D.-W. and Xu, Y.-S. 2015. Laboratory evaluation on the effectiveness of polypropylene fibers on the strength of fiber-reinforced and cement-stabilized Shanghai soft clay, *Geotextiles and Geomembranes*, 43: 515-523.
- Chew, S. H., Kamruzzaman, A. H. and Lee, F. H. 2004. Physicochemical and engineering behavior of cement treated clays, *Journal of geotechnical and geoenvironmental engineering*, 130: 696-706.
- Consoli, N., Casagrande, M. and Coop, M. 2007. Performance of a fibre-reinforced sand at large shear strains, *Geotechnique*, 57: 751-756.
- Consoli, N., Festugato, L. and Heineck, K. 2009a. Strain-hardening behaviour of fibre-reinforced sand in view of filament geometry, *Geosynthetics International*, 16: 109-115.
- Consoli, N., Montardo, J., Donato, M. and Prietto, P. 2004. Effect of material properties on the behaviour of sand—cement—fibre composites, *Proceedings of the ICE-Ground Improvement*, 8: 77-90.
- Consoli, N. C., Bassani, M. a. A. and Festugato, L. 2010. Effect of fiber-reinforcement on the strength of cemented soils, *Geotextiles and Geomembranes*, 28: 344-351.

- Consoli, N. C., Casagrande, M. D. and Coop, M. R. 2005. Effect of fiber reinforcement on the isotropic compression behavior of a sand, *Journal of geotechnical and geoenvironmental engineering*, 131: 1434-1436.
- Consoli, N. C., Prietto, P. D. and Ulbrich, L. A. 1998. Influence of fiber and cement addition on behavior of sandy soil, *Journal of geotechnical and geoenvironmental engineering*, 124: 1211-1214.
- Consoli, N. C., Prietto, P. D. M. and Ulbrich, L. A. 1999. The behaviour of a fibre-reinforced cemented soil, *Proceedings of the ICE-Ground Improvement*, 3: 21-30.
- Consoli, N. C., Vendruscolo, M. A., Fonini, A. and Dalla Rosa, F. 2009b. Fiber reinforcement effects on sand considering a wide cementation range, *Geotextiles and Geomembranes*, 27: 196-203.
- Consoli, N. C., Vendruscolo, M. A. and Prietto, P. D. M. 2003. Behavior of plate load tests on soil layers improved with cement and fiber, *Journal of geotechnical and geoenvironmental engineering*, 129: 96-101.
- Cotecchia, F. and Chandler, R. 2000. A general framework for the mechanical behaviour of clays, *Géotechnique*, 50: 431-447.
- Crouch, R. S., Wolf, J. P. and Dafalias, Y. F. 1994. Unified Critical-State Bounding-Surface Plasticity Model for Soil, *Journal of engineering mechanics*.
- Dafalias, Y. and Herrmann, L. 1982. Bounding surface formulation of soil plasticity, *Soil mechanics-transient and cyclic loads*, 10: 253-282.
- Das, B. and Dass, R. 1995. Lightly cemented sand in tension and compression, *Geotechnical & Geological Engineering*, 13: 169-177.
- Di Prisco, C. and Nova, R. 1993. A constitutive model for soil reinforced by continuous threads, *Geotextiles and Geomembranes*, 12: 161-178.
- Diambra, A. and Ibraim, E. 2014. Modelling of fibre-cohesive soil mixtures, *Acta Geotechnica*, 9: 1029-1043.
- Diambra, A., Ibraim, E., Russell, A. and Muir Wood, D. 2013. Fibre reinforced sands: from experiments to modelling and beyond, *International journal for numerical and analytical methods in geomechanics*, 37: 2427-2455.
- Diamond, S. and Kinter, E. B. 1965. Mechanisms of soil-lime stabilization, *Highway research record*: 83-102.

- Diamond, S., White, J. L. and Dolch, W. L. 1963. Transformation of Clay Minerals by Calcium Hydroxide Attack: Technical Paper.
- Divya, P., Viswanadham, B. and Gourc, J. 2013. Evaluation of Tensile Strength-Strain Characteristics of Fiber-Reinforced Soil through Laboratory Tests, *Journal of Materials in Civil Engineering*, 26: 14-23.
- Endo, M. 1976. Recent development in dredged material stabilization and deep chemical mixing in Japan. *Soils and Site Improvement-Lifelong Learning Seminar*.
- Fang, Z. 2006. Physical and numerical modelling of the soft soil ground improved by deep cement mixing method. The Hong Kong Polytechnic University.
- Fatahi, B., Khabbaz, H. and Fatahi, B. 2012. Mechanical characteristics of soft clay treated with fibre and cement, *Geosynthetics International* 19: 252-262.
- Fatahi, B., Le, T. M., Fatahi, B. and Khabbaz, H. 2013. Shrinkage properties of soft clay treated with cement and geofibers, *Geotechnical and Geological Engineering*, 31: 1421-1435.
- Fredlund, D. G. and Rahardjo, H. 1993. *Soil mechanics for unsaturated soils*, John Wiley & Sons.
- Freilich, J., Li, C. and Zornberg, G. 2010. Effective shear strength of fiber-reinforced clays. *9th international conference on geosyn, Brazil*.
- Gao, Z. and Zhao, J. 2012. Evaluation on failure of fiber-reinforced sand, *Journal of geotechnical and geoenvironmental engineering*, 139: 95-106.
- Gens, A. and Potts, D. 1988. Critical state models in computational geomechanics, *Engineering Computations*, 5: 178-197.
- Gray, D. H. and Ohashi, H. 1983. Mechanics of fiber reinforcement in sand, *Journal of Geotechnical Engineering*, 109: 335-353.
- Hamidi, A. and Hooresfand, M. 2013. Effect of fiber reinforcement on triaxial shear behavior of cement treated sand, *Geotextiles and Geomembranes*, 36: 1-9.
- Hayashi, H., Nishikawa, J. I., Ohishi, K. and Terashi, M. 2002. Field observation of long-term strength of cement treated soil, *Geotechnical Special Publication*, 1: 598-609.
- Heineck, K. S., Coop, M. R. and Consoli, N. C. 2005. Effect of microreinforcement of soils from very small to large shear strains, *Journal of geotechnical and geoenvironmental engineering*, 131: 1024-1033.

- Hejazi, S. M., Sheikhzadeh, M., Abtahi, S. M. and Zadhoush, A. 2012. A simple review of soil reinforcement by using natural and synthetic fibers, *Construction and Building Materials*, 30: 100-116.
- Horpibulsuk, S. 2001. Analysis and assessment of engineering behavior of cement stabilized clays. *PhD Dissertation*, Saga University.
- Horpibulsuk, S., Liu, M. D., Liyanapathirana, D. S. and Suebsuk, J. 2010. Behaviour of cemented clay simulated via the theoretical framework of the structured cam clay model, *Computers and Geotechnics*, 37: 1-9.
- Horpibulsuk, S., Miura, N. and Bergado, D. T. 2004. Undrained shear behavior of cement admixed clay at high water content, *Journal of geotechnical and geoenvironmental engineering*, 130: 1096-1105.
- Horpibulsuk, S., Rachan, R., Suddeepong, A., Liu, M. D. and Du, Y. J. 2013. Compressibility of lightweight cemented clays, *Engineering Geology*, 159: 59-66.
- Huang, J. and Airey, D. 1998. Properties of artificially cemented carbonate sand, *Journal of geotechnical and geoenvironmental engineering*, 124: 492-499.
- Ismail, M., Joer, H., Randolph, M. and Meritt, A. 2002. Cementation of porous materials using calcite, *Geotechnique*, 52: 313-324.
- Jasperse, B. H. and Ryan, C. R. 1992. Stabilization and fixation using soil mixing. *Grouting, Soil Improvement and Geosynthetics*. ASCE, 1273-1284.
- Jiang, H., Cai, Y. and Liu, J. 2010. Engineering properties of soils reinforced by short discrete polypropylene fiber, *Journal of materials in civil engineering*, 22: 1315-1322.
- Kamruzzaman, A. H., Chew, S. H. and Lee, F. H. 2006. Microstructure of cement-treated Singapore marine clay, *Proceedings of the ICE-Ground Improvement*, 10: 113-123.
- Kamruzzaman, A. H., Chew, S. H. and Lee, F. H. 2009. Structuration and Destructuration Behavior of Cement-Treated Singapore Marine Clay, *Journal of geotechnical and geoenvironmental engineering*, 135: 573-589.
- Kaniraj, S. R. and Havanagi, V. G. 2001. Behavior of cement-stabilized fiber-reinforced fly ash-soil mixtures, *Journal of geotechnical and geoenvironmental engineering*, 127: 574-584.

- Kasama, K., Ochiai, H. and Yasufuku, N. 2000. On the stress-strain behaviour of lightly cemented clay based on an extended critical state concept, *Soils and Foundations*, 40: 37-47.
- Kavvadas, M. and Amorosi, A. 2000. A constitutive model for structured soils, *Geotechnique*, 50: 263-273.
- Kitazume, M., Nakamura, T., Terashi, M. and Ohishi, K. 2002. Laboratory tests on long-term strength of cement treated soil, *Geotechnical Special Publication*, 1: 586-597.
- Kolovos, K. G., Asteris, P. G., Cotsovos, D. M., Badogiannis, E. and Tsivilis, S. 2013. Mechanical properties of soilcrete mixtures modified with metakaolin, *Construction and Building Materials*, 47: 1026-1036.
- Kumar, R., Kanaujia, V. K. and Chandra, D. 1999. Engineering behaviour of fibre-reinforced pond ash and silty sand, *Geosynthetics International*, 6: 509-518.
- Lade, P. V. and Overton, D. D. 1989. Cementation effects in frictional materials, *Journal of Geotechnical Engineering*, 115: 1373-1387.
- Lea, F. M. 1956. *The chemistry of cement and concrete*, E. Arnold.
- Lee, F. H., Lee, Y., Chew, S. H. and Yong, K. Y. 2005. Strength and modulus of marine clay-cement mixes, *Journal of geotechnical and geoenvironmental engineering*, 131: 178-186.
- Leroueil, S. and Vaughan, P. 1990. The general and congruent effects of structure in natural soils and weak rocks, *Geotechnique*, 40: 467-488.
- Li, C. 2005. Mechanical response of fiber-reinforced soil. *3184844 Ph.D.*, The University of Texas at Austin.
- Li, J. and Ding, D. 2002. Nonlinear elastic behavior of fiber-reinforced soil under cyclic loading, *Soil Dynamics and Earthquake Engineering*, 22: 977-983.
- Ling, H. I. and Tatsuoka, F. 1994. Performance of anisotropic geosynthetic-reinforced cohesive soil mass, *Journal of Geotechnical Engineering*, 120: 1166-1184.
- Liu, M. D. and Carter, J. P. 2002. A structured Cam Clay model, *Canadian Geotechnical Journal*, 39: 1313-1332.
- Liu, M. D. and Carter, J. P. 2003. Volumetric deformation of natural clays, *International Journal of Geomechanics*, 3: 236-252.
- Liu, M. D., Carter, J. P. and Desai, C. S. 2003. Modeling compression behavior of structured geomaterials, *International Journal of Geomechanics*, 3: 191-204.

- Lo, S. and Wardani, S. 1999. Deformation Behaviour of Cement-flyash Stabilised Silt. *Proceedings 8th Australia New Zealand Conference on Geomechanics: Consolidating Knowledge*. Australian Geomechanics Society, 761.
- Lo, S. and Wardani, S. P. 2002. Strength and dilatancy of a silt stabilized by a cement and fly ash mixture, *Canadian Geotechnical Journal*, 39: 77-89.
- Locat, J., Bérubé, M.-A. and Choquette, M. 1990. Laboratory investigations on the lime stabilization of sensitive clays: shear strength development, *Canadian Geotechnical Journal*, 27: 294-304.
- Lorenzo, G. A. and Bergado, D. T. 2004. Fundamental parameters of cement-admixed clay-new approach, *Journal of geotechnical and geoenvironmental engineering*, 130: 1042-1050.
- Lorenzo, G. A. and Bergado, D. T. 2006. Fundamental characteristics of cement-admixed clay in deep mixing, *Journal of materials in civil engineering*, 18: 161-174.
- Maher, M. and Ho, Y. 1993. Behavior of fiber-reinforced cemented sand under static and cyclic loads, *Geotechnical Testing Journal*, 16.
- Maher, M. and Ho, Y. 1994. Mechanical properties of kaolinite/fiber soil composite, *Journal of Geotechnical Engineering*, 120: 1381-1393.
- Maher, M. H. and Gray, D. H. 1990. Static response of sands reinforced with randomly distributed fibers, *Journal of Geotechnical Engineering*, 116: 1661-1677.
- Michalowski, R. L. and Cermák, J. 2003. Triaxial compression of sand reinforced with fibers, *Journal of geotechnical and geoenvironmental engineering*, 129: 125-136.
- Michalowski, R. L. and Čermák, J. 2002. Strength anisotropy of fiber-reinforced sand, *Computers and Geotechnics*, 29: 279-299.
- Mitchell, J. K. and Soga, K. 1976. *Fundamentals of soil behavior*, Wiley New York.
- Miura, N., Horpibulsuk, S. and Nagaraj, T. 2001. Engineering behavior of cement stabilized clay at high water content, *Soils and Foundations*, 41: 33-45.
- Moses, G. G., Rao, S. N. and Rao, P. N. 2003. Undrained strength behaviour of a cemented marine clay under monotonic and cyclic loading, *Ocean engineering*, 30: 1765-1789.
- Mroz, Z., Norris, V. and Zienkiewicz, O. 1981. An anisotropic, critical state model for soils subject to cyclic loading, *Geotechnique*, 31: 451-469.

- Neff, T. 1996. Underground Engineering for the Central Artery/Tunnel Project, *Civil Engineering Practice-Boston*, 11: 7-10.
- Novello, E. and Johnston, L. 1995. Geotechnical materials and the critical state, *Geotechnique*, 45: 223-235.
- Panda, A. P. and Rao, S. N. 1998. Undrained strength characteristics of an artificially cemented marine clay, *Marine georesources & geotechnology*, 16: 335-353.
- Park, S.-S. 2009. Effect of fiber reinforcement and distribution on unconfined compressive strength of fiber-reinforced cemented sand, *Geotextiles and Geomembranes*, 27: 162-166.
- Park, S.-S. 2011. Unconfined compressive strength and ductility of fiber-reinforced cemented sand, *Construction and Building Materials*, 25: 1134-1138.
- Perić, D. and Ayari, M. A. 2002. On the analytical solutions for the three-invariant Cam clay model, *International Journal of Plasticity*, 18: 1061-1082.
- Porbaha, A. 1998. State of the art in deep mixing technology. Part I: Basic concepts and overview, *Ground Improvement*, 2: 81-92.
- Porbaha, A., Shibuya, S. and Kishida, T. 2000. State of the art in deep mixing technology. Part III: Geomaterial characterization, *Proceedings of the ICE-Ground Improvement*, 4: 91-110.
- Prevost, J. H. 1982. Two-surface versus multi-surface plasticity theories: A critical assessment, *International Journal for Numerical and Analytical Methods in Geomechanics*, 6: 323-338.
- Prusinski, J. and Bhattacharja, S. 1999. Effectiveness of Portland cement and lime in stabilizing clay soils, *Transportation Research Record: Journal of the Transportation Research Board*: 215-227.
- Ranjan, G., Vasan, R. and Charan, H. 1996. Probabilistic analysis of randomly distributed fiber-reinforced soil, *Journal of Geotechnical Engineering*, 122: 419-426.
- Roscoe, K., Schofield, A. and Thurairajah, A. 1963. Yielding of clays in states wetter than critical, *Geotechnique*, 13: 211-240.
- Roscoe, K. H. and Burland, J. B. 1968. On the generalised stress-strain behaviour of "wet" clay, *Engineering Plasticity*: 535-609.
- Rotta, G., Consoli, N., Prietto, P., Coop, M. and Graham, J. 2003. Isotropic yielding in an artificially cemented soil cured under stress, *Geotechnique*, 53: 493-501.

- Sariosseiri, F. 2008. Critical state framework for interpretation of geotechnical properties of cement treated soils. *Ph.D. Dissertation*, Washington State University.
- Sariosseiri, F. and Muhunthan, B. 2009. Effect of cement treatment on geotechnical properties of some Washington State soils, *Engineering Geology*, 104: 119-125.
- Sasanian, S. 2011. The Behaviour of Cement Stabilized Clay At High Water Contents. *Dissertation*, The University of Western Ontario.
- Schofield, A. and Wroth, P. 1968. *Critical State Soil Mechanics*, London, McGraw-Hill.
- Shao, W., Cetin, B., Li, Y., Li, J. and Li, L. 2014. Experimental investigation of mechanical properties of sands reinforced with discrete randomly distributed fiber, *Geotechnical and Geological Engineering*, 32: 901-910.
- Shen, W. Q., Shao, J. F., Kondo, D. and Gatmiri, B. 2012. A micro–macro model for clayey rocks with a plastic compressible porous matrix, *International Journal of Plasticity*, 36: 64-85.
- Suebsuk, J., Horpibulsuk, S. and Liu, M. D. 2010. Modified Structured Cam Clay: A generalised critical state model for destructured, naturally structured and artificially structured clays, *Computers and Geotechnics*, 37: 956-968.
- Suebsuk, J., Horpibulsuk, S. and Liu, M. D. 2011. A critical state model for overconsolidated structured clays, *Computers and Geotechnics*, 38: 648-658.
- Tan, T. S., Goh, T. L. and Yong, K. Y. 2002. Properties of Singapore marine clays improved by cement mixing, *ASTM geotechnical testing journal*, 25: 422-433.
- Tang, C.-S., Shi, B. and Zhao, L.-Z. 2010. Interfacial shear strength of fiber reinforced soil, *Geotextiles and Geomembranes*, 28: 54-62.
- Tang, C., Shi, B., Gao, W., Chen, F. and Cai, Y. 2007. Strength and mechanical behavior of short polypropylene fiber reinforced and cement stabilized clayey soil, *Geotextiles and Geomembranes*, 25: 194-202.
- Tatsuoka, F., Uchida, K., Imai, K., Ouchi, T. and Kohata, Y. 1997. Properties of cement-treated soils in Trans-Tokyo Bay Highway project, *Proceedings of the ICE-Ground Improvement*, 1: 37-57.
- Topolnicki, M. 2004. In situ soil mixing, *Ground Improvement*: 331-428.
- Tremblay, H., Leroueil, S. and Locat, J. 2001. Mechanical improvement and vertical yield stress prediction of clayey soils from eastern Canada treated with lime or cement, *Canadian Geotechnical Journal*, 38: 567-579.

- Tsoi, W. Y. 2005. Constitutive model development for lightly cemented scrap rubber tire chips. *3193990 Ph.D.*, Hong Kong University of Science and Technology (Hong Kong).
- Uddin, K., Balasubramaniam, A. S. and Bergado, D. T. 1997. Engineering behavior of cement-treated Bangkok soft clay, *Geotechnical Engineering*, 28: 89-119.
- Wood, M. 1990. *Soil behaviour and critical state soil mechanics*, Cambridge university press.
- Xiao, H. and Lee, F. 2008. Curing time effect on behavior of cement treated marine clay, *Proceedings of World Academy of Science, Engineering and Technology (PWASET)*, 33: 2070-3740.
- Yang, Y., Wang, G., Xie, S., Tu, X. and Huang, X. 2013. Effect of mechanical property of cemented soil under the different pH value, *Applied Clay Science*, 79: 19-24.
- Yapage, N. and Liyanapathirana, D. 2012. Implementation of an elasto-plastic constitutive model for cement stabilized clay in a non-linear finite element analysis, *Engineering Computations*, 30: 74-96.
- Yasufuku, N., Ochiai, H. and Kasama, K. 1997. The dissipated energy equation of lightly cemented clay in relation to the critical state model. *Proceedings 9th International Conference on Computer Methods & Advances in Geomechanics*. 917-922.
- Yetimoglu, T. and Salbas, O. 2003. A study on shear strength of sands reinforced with randomly distributed discrete fibers, *Geotextiles and Geomembranes*, 21: 103-110.
- Yin, J.-H. 2001. Stress-strain-strength characteristics of soft Hong Kong marine deposits without or with cement treatment, *Lowland Technology International*, 3: 1-13.
- Yin, J. and Lai, C. 1998. Strength and stiffness of Hong Kong marine deposits mixed with cement, *Geotechnical Engineering*, 29: 29-43.
- Yin, Z.-Y., Chang, C. S., Hicher, P.-Y. and Karstunen, M. 2009. Micromechanical analysis of kinematic hardening in natural clay, *International Journal of Plasticity*, 25: 1413-1435.
- Yu, H.-S. 2006. *Plasticity and geotechnics*, Springer.

- Yuanming, L., Yugui, Y., Xiaoxiao, C. and Shuangyang, L. 2010. Strength criterion and elastoplastic constitutive model of frozen silt in generalized plastic mechanics, *International Journal of Plasticity*, 26: 1461-1484.
- Zhu, Q. Z., Shao, J. F. and Mainguy, M. 2010. A micromechanics-based elastoplastic damage model for granular materials at low confining pressure, *International Journal of Plasticity*, 26: 586-602.
- Zornberg, J. 2002. Discrete framework for limit equilibrium analysis of fibre-reinforced soil, *Geotechnique*, 52: 593-604.

## APENDIX A

### Derivation of Plastic Potential Function for the Cement Treated Clay

Expanding and simplifying Equation (3.21) results in:

$$(qd_\varepsilon^p)^2 = (Md_\varepsilon^p)^2(p' + \xi p'_\Omega)^2 - 2qd_\varepsilon^p d_v^p(p' + \xi p'_\Omega) \left(\frac{\alpha+1}{A}\right) \quad (A-1)$$

Dividing both sides by  $d_\varepsilon^p$ :

$$d_\varepsilon^p [q^2 - M^2(p' + \xi p'_\Omega)^2] A = -2q(p' + \xi p'_\Omega)(\alpha + 1)d_v^p \quad (A-2)$$

Rearranging Equation (A-2) to obtain the flow rule:

$$\frac{d_v^p}{d_\varepsilon^p} = \frac{[q^2 - M^2(\xi p'_\Omega + p')^2] A}{-2q(\alpha + 1)(p' + \xi p'_\Omega)} \quad (A-3)$$

Substitutes the modified stress ratio  $\left(\eta^* = \frac{q}{p' + \xi p'_\Omega}\right)$  into Equation (A-3), the flow rule is taking the form of:

$$\frac{d_v^p}{d_\varepsilon^p} = \frac{A(\eta^{*2} - M^2)}{-2\eta^*(\alpha + 1)} \quad (A-4)$$

Using the normality condition as follows:

$$\frac{d_v^p}{d_\varepsilon^p} = -\frac{dq}{dp'} \quad (A-5)$$

Combining Equations (A-4) and (A-5) results in:

$$-\frac{dq}{dp'} = \frac{A(\eta^{*2} - M^2)}{2\eta^*(\alpha + 1)} \quad (A-6)$$

Substituting Equation (3.14) in the modified stress ratio  $\left(\eta^* = \frac{q}{p' + \xi p'_\Omega}\right)$  results to:

$$\eta^* = \frac{q}{p' + \frac{c}{M} \left[ 1 + \left( \frac{p'_0 - p'_{0,i}}{\beta} \right) \right] e^{-\left( \frac{p'_0 - p'_{0,i}}{\beta} \right)}} \quad (A-7)$$

The equation for the partial derivatives of Equation (A-7) with respect to  $q$  and  $p'$  is expressed as follows:

$$d\eta^* = \frac{\partial \eta^*}{\partial p'} dp' + \frac{\partial \eta^*}{\partial q} dq \quad (A-8)$$

Evaluating the derivative of Equation (A-7) with respect to  $p'$  results in:

$$\frac{\partial \eta^*}{\partial p'} = \frac{-qA}{\left\{ p' + \frac{c}{M} \left[ 1 + \left( \frac{p'_0 - p'_{0,i}}{\beta} \right) \right] e^{-\left( \frac{p'_0 - p'_{0,i}}{\beta} \right)} \right\}^2} \quad (A-9)$$

Evaluating the derivative of Equation (A-7) with respect to  $q$  results in:

$$\frac{\partial \eta^*}{\partial q} = \frac{1}{p' + \frac{c}{M} \left[ 1 + \left( \frac{p'_0 - p'_{0,i}}{\beta} \right) \right] e^{-\left( \frac{p'_0 - p'_{0,i}}{\beta} \right)}} \quad (A-10)$$

Substituting Equations (A-9) and (A-10) in Equation (A-8) leads to:

$$\frac{dq}{dp'} = \left\{ p' + \frac{c}{M} \left[ 1 + \left( \frac{p'_0 - p'_{0,i}}{\beta} \right) \right] e^{-\left( \frac{p'_0 - p'_{0,i}}{\beta} \right)} \right\} \frac{d\eta^*}{dp'} + \eta^* A \quad (A-11)$$

Substituting the flow rule presented in Equation (A-6) into Equation (A-11) and then rearranging in the following form:

$$\frac{dp' A}{\left\{ p' + \frac{c}{M} \left[ 1 + \left( \frac{p'_0 - p'_{0,i}}{\beta} \right) \right] e^{-\left( \frac{p'_0 - p'_{0,i}}{\beta} \right)} \right\}} = - \frac{2\eta^*(\alpha+1)d\eta^*}{M^2 + 2\eta^{*2}\alpha + \eta^{*2}} \quad (A-12)$$

Integrating Equation (A-12) using the boundary conditions ( $p' = p'_0$  when  $q = 0$ ) results in the plastic potential function as follows:

$$g = q^2(1 + 2\alpha) + p'^{*2} M^2 \left[ 1 - \left( \frac{p'_{*0}}{p'^*} \right)^{\frac{(2\alpha+1)}{\alpha+1}} \right] \quad (A-13)$$

## APENDIX B

### Derivation of Plastic Potential Function for the Fibre Reinforced Cement Treated Clay

Expanding and simplifying Equation (3.63) results in:

$$\frac{(q d_\varepsilon^p)^2}{(p' + \xi p'_\Omega + p'_f)^2} - (M d_\varepsilon^p)^2 = - \frac{\{2\eta^*(\alpha+1)(1-\eta^*B) + B[\eta^{*2}(1+2\alpha) + M^2]\}}{1+A} d_\varepsilon^p d_v^p \quad (B-1)$$

Dividing both sides by  $d_\varepsilon^p$ :

$$\frac{(q^2 d_\varepsilon^p)}{(p' + \xi p'_\Omega + p'_f)^2} - (M^2 d_\varepsilon^p) = - \frac{[2\eta^*(\alpha+1)(1-\eta^*B) + B[\eta^{*2}(1+2\alpha) + M^2]]}{1+A} d_v^p \quad (B-2)$$

Rearranging Equation (B-2) and substitutes the modified stress ratio  $\eta^*$  (in Equation (3.66), the flow rule is taking the form of:

$$\frac{d_v^p}{d_\varepsilon^p} = - \frac{(\eta^{*2} - M^2)(1+A)}{2\eta^*(\alpha+1)(1-\eta^*B) + B[\eta^{*2}(1+2\alpha) + M^2]} \quad (B-3)$$

Using the normality condition as follows:

$$\frac{d_v^p}{d_\varepsilon^p} = - \frac{dq}{dp'} \quad (A-5 \text{ bis.})$$

Combining Equations (B-3) and (A-5 bis.) results in:

$$- \frac{dq}{dp'} = - \frac{(\eta^{*2} - M^2)(1+A)}{2\eta^*(\alpha+1)(1-\eta^*B) + B[\eta^{*2}(1+2\alpha) + M^2]} \quad (B-4)$$

The equation for the partial derivatives of the modified stress ratio

$\left(\eta^* = \frac{q}{(p' + \xi p'_\Omega + p'_f)^2}\right)$  with respect to  $q$  and  $p'$  is expressed as follows:

$$d\eta^* = \frac{\partial \eta^*}{\partial p'} dp' + \frac{\partial \eta^*}{\partial q} dq \quad (B-5)$$

Evaluating the derivative of Equation (B-5) with respect to  $p'$  results in:

$$\frac{\partial \eta^*}{\partial p'} = \frac{-q(1+A)}{(p' + \xi p'_{\Omega} + p'_f)^2} \quad (B-6)$$

Noted that, the term  $A$  refers to the derivative of  $p'_{\Omega}$  with respect to  $p'$  which can be found in Equation (3.71)

Evaluating the derivative of Equation (B-5) with respect to  $q$  results in:

$$\frac{\partial \eta^*}{\partial q} = \frac{(p' + \xi p'_{\Omega} + p'_f) - qB}{(p' + \xi p'_{\Omega} + p'_f)^2} \quad (B-7)$$

Noted that, the term  $B$  refers to the derivative of  $p'_f$  with respect to  $q$  which can be found in Equation (3.73)

Substituting Equations (B-5) and (B-7) into Equation (B-5) leads to:

$$\frac{dq}{dp'} = \frac{d\eta^*(p' + \xi p'_{\Omega} + p'_f)^2 + q(1+A)dp'}{[(p' + \xi p'_{\Omega} + p'_f) - qB]dp'} \quad (B-8)$$

Substituting the flow rule presented in Equation (B-4) into Equation (B-8) and then taking integration using the boundary conditions ( $p' = p'_0$  when  $q = 0$ ), the results can be expressed as:

$$\left(\frac{1+\alpha}{2\alpha+1}\right) \ln[M^2 + \eta^{*2} + 2\alpha\eta^{*2}] = -\ln(p' + \xi p'_{\Omega} + p'_f) \quad (B-9)$$

Rearranging Equation (B-9) results in the plastic potential function as follows:

$$g = q^2(1 + 2\alpha) + (p' + \xi p'_{\Omega} + p'_f)^2 M^2 \left[ 1 - \left(\frac{p'^*_0}{p' + \xi p'_{\Omega} + p'_f}\right)^{\left(\frac{2\alpha+1}{\alpha+1}\right)} \right] \quad (B-10)$$